LEABHARLANN CHOLÁISTE NA TRÍONÓIDE, BAILE ÁTHA CLIATH | TRINITY COLLEGE LIBRARY DUBLIN
Ollscoil Átha Cliath | The University of Dublin

Terms and Conditions of Use of Digitised Theses from Trinity College Library Dublin

Copyright statement

All material supplied by Trinity College Library is protected by copyright (under the Copyright and Related Rights Act, 2000 as amended) and other relevant Intellectual Property Rights. By accessing and using a Digitised Thesis from Trinity College Library you acknowledge that all Intellectual Property Rights in any Works supplied are the sole and exclusive property of the copyright and/or other IPR holder. Specific copyright holders may not be explicitly identified. Use of materials from other sources within a thesis should not be construed as a claim over them.

A non-exclusive, non-transferable licence is hereby granted to those using or reproducing, in whole or in part, the material for valid purposes, providing the copyright owners are acknowledged using the normal conventions. Where specific permission to use material is required, this is identified and such permission must be sought from the copyright holder or agency cited.

Liability statement

By using a Digitised Thesis, I accept that Trinity College Dublin bears no legal responsibility for the accuracy, legality or comprehensiveness of materials contained within the thesis, and that Trinity College Dublin accepts no liability for indirect, consequential, or incidental, damages or losses arising from use of the thesis for whatever reason. Information located in a thesis may be subject to specific use constraints, details of which may not be explicitly described. It is the responsibility of potential and actual users to be aware of such constraints and to abide by them. By making use of material from a digitised thesis, you accept these copyright and disclaimer provisions. Where it is brought to the attention of Trinity College Library that there may be a breach of copyright or other restraint, it is the policy to withdraw or take down access to a thesis while the issue is being resolved.

Access Agreement

By using a Digitised Thesis from Trinity College Library you are bound by the following Terms & Conditions. Please read them carefully.

I have read and I understand the following statement: All material supplied via a Digitised Thesis from Trinity College Library is protected by copyright and other intellectual property rights, and duplication or sale of all or part of any of a thesis is not permitted, except that material may be duplicated by you for your research use or for educational purposes in electronic or print form providing the copyright owners are acknowledged using the normal conventions. You must obtain permission for any other use. Electronic or print copies may not be offered, whether for sale or otherwise to anyone. This copy has been supplied on the understanding that it is copyright material and that no quotation from the thesis may be published without proper acknowledgement.

Molecular Engineering of Conjugated Organic Molecule and Carbon Nanotube Assemblies- a Linear and Nonlinear Spectroscopic Study

Éimhín Máire Caitríona Ní Mhuircheartaigh

B.Sc., P.Grad.Dip.

A thesis submitted to the University of Dublin in
fulfillment of the requirement for the degree of

Doctor of Philosophy

School of Physics,
University of Dublin, Trinity College.

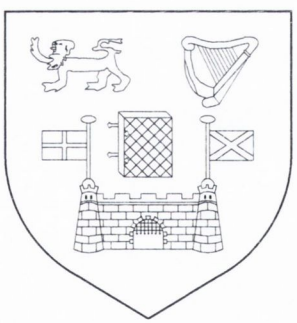

May 2007

TRINITY COLLEGE
21 NOV 2007
LIBRARY DUBLIN
THESIS
8275

Declaration

I declare that the work in this thesis has not been previously submitted as an exercise for a degree to this or any other university.

The work described herein is entirely my own, except for the assistance mentioned in the acknowledgements and the collaborative work mentioned in the list of publications.

I agree that Trinity College Library may lend or copy this thesis on request.

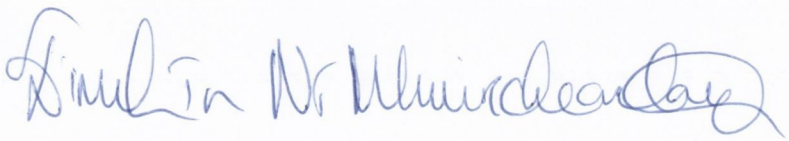

Éimhín Ní Mhuircheartaigh

May 2007

Summary

Single walled carbon nanotubes (SWNTs) possess unique structural, mechanical and electronic properties, and are thus promising materials for a host of future applications. However, their potential is limited in that they are insoluble in aqueous and organic solutions and satisfactory control over nanotube location and orientation has yet to be achieved. SWNT solubility has recently been achieved by functionalizing them covalently and non-covalently. Non- covalent functionalization is of particular interest as it provides a method of handling the nanotubes chemically without altering the electronic structure of the SWNT themselves.

This thesis aims to gain a better understanding of the physics behind non- covalent SWNT interactions with a variety of conjugated organic molecules, with a view to ultimately aiding the development and optimization of a technique for isolating individual SWNT in solution, in addition to the development of novel nanomaterials with superior optical properties. In order to broaden the understanding of the physical processes governing SWNT interactions in solution, a number of conjugated molecules related structurally to the polymer PmPV (poly[metaphenylenevinylene-co-2,5-dioctyloxy-para-phenylenevinylene]) are investigated in order to study the importance of the molecular structure of the dispersant.

Due to their high degree of conjugation, it was expected that molecules from the porphyrin family would also interact strongly with carbon nanotubes through Van der Waals interactions. Porphyrins are an enormously important family of functional dyes with a variety of unique photophysical, chemical and biological properties. The nature and strength of non- covalent interactions existing between a series of non- planar conjugated tetraphenylporphyrin (TPP) derivatives and carbon nanotubes in solution is investigated experimentally using a number of linear and nonlinear optical techniques. These are compared with experimental findings for planar porphyrin systems. Additional complementary molecular dynamics studies were found to strongly agree with all experimental observations for these porphyrin systems. The importance of porphyrin conformation to these interactions is systematically investigated through use of a series of non- planar TPP derivatives. Convincing evidence of binding between SWNT and some of these porphyrins is presented,

with a non- planar macrocycle found to increase the likelihood of non- covalent binding onto nanotubes. Nonlinear optical studies showed that the optical limiting behaviour of the TPP derivatives deteriorated with increasing porphyrin non- planarity, but that formation of nanotube composites dramatically improved the optical limiting properties of all molecules studied. It also provided further evidence of interaction between the SWNT and the porphyrin molecules. The significant photoluminescence quenching behaviour reported in literature for porphyrin composite solutions was found to be at least partly caused by photoluminescence and excitation self- absorption, and is therefore an artefact of the system.

It was also found that porphyrin molecules are protonated in a number of common chlorinated organic solvents upon sonication. Regardless of the functional molecule, sonication is a key step in the dispersion of SWNT when making composite solutions. Extreme care must therefore be taken when working with carbon nanotube composite solutions in halogenated solvents as protonation of acid sensitive molecules may take place, changing their physicochemical properties.

This thesis is dedicated to John Mc Carthy and Mary, Seán, Eoin, Cian, Orla, Aogán and especially Colm Ó Muircheartaigh.

In memory of Éanna Bean Uí Mhuircheartaigh

Acknowledgments

First and foremost, I would like to thank Prof. Werner Blau for his expert supervision for the duration of my PhD. His approachability, optimism and above all scientific brilliance are phenomenal, and I am grateful to him for giving me the opportunity to carry out this work. Thanks is owed also to Dr. Silvia Giordani, who supervised my research on a day to day basis. It was an honour to learn from such a talented researcher, and I am grateful for your help, support and guidance over the past three years.

I am grateful to everyone else who gave me help and guidance. Many thanks to the various members of Group BU who made my journey through Trinity a little easier. In particular I'd like to thank everyone in my office — Sharon, Rory, Umar and Chris. I would like to express deepest thanks and appreciation for technical and administrative support to Jeanette Cummins and John Kelly. For provision of materials and scientific expertise thank you Anna Drury, Dr. Silvia Giordani, Dr. Manuel Ruether, and Prof. Mathias Senge. For expertise in using LaTeX and other technical issues, thanks Paul Mc Nicholas and Sharon King. For proofreading thanks to Mam, Silvia, Werner, Adam and Anna.

Special thanks is also owed to Doireann, Caoimhe, Ronan, Shane and Susan O'Reilly, Karl O'Hanlon, Paula Kirwin, Tony Buckley, Gina Fitzgerald, Andrew O' Brien, Aengus Concannon, Big Mike, JD, Martina, Marisa Phelan, Kate O'Connor, Elena Mc Philbin, Adrian Flynn, James 'twinkletoes' Williams, Laura Thornton, Jenny, Judith, Roisin, Triona, Aindiu Mac an Bhaird, Peter Gall, Brenda Finnegan, Dervla O' Donnell, Conor O' Regan, Micheal Langan and Gearoid O' Sullivan, Sharon and Paul. Thank you!

A million thank you's are owed to my family both immediate and extended. I particularly wish to mention my parents, Mam and Dad who have always supported me over the years, in spite of everything I put them through, and my siblings Eoin, Cian, Orla, Aogan and Colm to whom this thesis is dedicated. And last, but not least, I wish to thank my fiancé John, without whose help none of this would be possible. Go raibh maith agat. Ní neart go cur le chéile. ××

Financial support for the duration of this thesis by Intel Ireland, the Trinity College Dublin Postgraduate award and Science Foundation Ireland is gratefully acknowledged.

Contents

List of Figures ix

List of Tables xvii

1 Introduction 1
- 1.1 Scientific Background . . . 1
- 1.2 Thesis Outline . . . 5

2 Materials and Optics Background 11
- 2.1 Organic Materials . . . 11
  - 2.1.1 Basic Concepts of Organic Materials . . . 11
  - 2.1.2 Photophysics . . . 15
- 2.2 Specific Materials Studied . . . 19
  - 2.2.1 Porphyrin Molecules . . . 19
  - 2.2.2 Polymers and Oligomers . . . 23
  - 2.2.3 Carbon Nanostructures . . . 26
- 2.3 Nonlinear Optical Phenomena . . . 34
  - 2.3.1 Nonlinear Refraction . . . 35
  - 2.3.2 Nonlinear Absorption . . . 36
- 2.4 Organic Materials as Optical limiters . . . 37

3 Characterization of Non-Covalently Functionalized Carbon Nanotubes 41
- 3.1 Characterization Techniques . . . 41
  - 3.1.1 Absorption Spectroscopy . . . 41
  - 3.1.2 Fluorescence Spectroscopy . . . 44
  - 3.1.3 Z-scan Technique Overview . . . 44

4 Characterization of Carbon Nanotube Interactions with Conjugated Polymers and Organic Molecules 51
- 4.1 Carbon Nanotube Bundles . . . 51
  - 4.1.1 Photoluminescence Quenching Model . . . 52
  - 4.1.2 Absorption Spectroscopy Studies of Carbon Nanotube Composites formed with Conjugated Polymers and Molecules . . . 70
- 4.2 Nonlinear Optical Extinction in Polymer/CNT systems . . . 77

4.2.1 PmPV 78
4.2.2 PFO 79
4.3 Conclusions 79

5 Linear Optical Characterization of Carbon Nanotube:Porphyrin systems 85
5.1 Introduction to Carbon Nanotube:Porphyrin Systems 85
5.1.1 Solubilization Studies 86
5.1.2 Donor-Acceptor Nanohybrids for Photovoltaic Applications 91
5.1.3 Carbon Nanotube De-Bundling 102
5.2 Linear Optical Properties of Planar Porphyrin Systems and their Carbon Nanotube Composites 103
5.2.1 Experimental Section 104
5.2.2 Results and Discussion 104
5.3 Linear Optical Properties of Nonplanar Tetraphenylporphyrin Derivatives and their Carbon Nanotube Composites 110
5.3.1 Experimental Section 112
5.3.2 Results and Discussion 113
5.3.3 Inner Filter Effect and Non-Covalent Binding of Porphyrins to Nanotubes 116
5.4 Sonication-Induced Degradation of Chlorinated Solvents leading to Protonation of Porphyrin-Nanotube Composites. 127
5.4.1 Experimental Section 128
5.4.2 Results and Discussion 129
5.4.3 Effect of Carbon Nanotubes on Porphyrin Protonation 136
5.5 Conclusions 143

6 Nonlinear Optical Characterization of Carbon Nanotube:Porphyrin systems 153
6.1 Introduction to Nonlinear Optical Properties of Porphyrins and their Carbon Nanotube Composites. 153
6.2 Experimental Section 157
6.2.1 Results and Discussion 158
6.3 Molecular Simulation 178
6.3.1 Simulation Setup 179
6.3.2 Results and Discussion 179
6.4 Conclusions 181

7 Conclusions 191

List of Figures

1.1 The ideal response of an optical limiting material 5

2.1 Bonding structure of ethylene with p_z orbitals (A) and pi bonds resulting from the combination of these adjacent p_z orbitals (B) 13
2.2 Chemical structure of repeat unit of polyacetylene 14
2.3 An extensive π- system is formed in polyacetylene by the overlapping of the p_z orbitals 14
2.4 Chemical structure of repeat unit of poly(para-phenylene vinylene) (PPV) . 14
2.5 The p_z orbitals which overlap to form the π orbitals in the PPV molecule . 15
2.6 Jablonski Diagram. 16
2.7 Chemical structure of protoporphyrin IX molecule 20
2.8 Chemical structure of tetraphenylporphryin molecule 21
2.9 UV-Visible absorption spectrum of Tetraphenylporphyrin (TPP) in the solvent Dimethylformamide (DMF) 22
2.10 The four orbital model. The LUMO and LUMO+1 orbitals are the degenerate e_g orbitals 23
2.11 Nanotubes are formed by rolling up a graphene sheet into a cylinder and capping each end with half of a fullerene molecule. Shown here is a (5, 5) armchair nanotube (top), a (9, 0) zigzag nanotube (middle) and a (10, 5) chiral nanotube. The diameter of the nanotubes depends on the values of n and m. 28
2.12 The unit cell of the carbon nanotube 29
2.13 Transitions possible between mirror image singularities in CNT DOS 31
2.14 Absorption spectra of fullerene nanotubes in SDS-D_2O suspension. The top trace D is typical of tubes prepared in suspension without centrifugation. The broadened and redshifted absorption features show that most nanotubes in the sample are aggregated in small bundles. Trace C is from individual SDS micelle coated nanotubes after addition of PVP. Traces B and A are from samples of individual nanotubes separated and solubilized by SDS micelles. Nanotubes in sample A have a smaller average diameter than in B because they were grown under a higher CO pressure. 32

2.15 Emission spectrum (red) of individual fullerene nanotubes suspended in SDS micelles in D_2O excited by 8 ns, 532-nm laser pulses, overlaid with the absorption spectrum (blue) of the sample in this region of first van Hove band gap transitions. The detailed correspondence of absorption and emission features indicates that the emission is band gap photoluminescence from a variety of semiconducting nanotube structures. 33

3.1 Schematic for the Open Aperture Z-scan technique 45
3.2 Experimental Setup for the Open Aperture Z-scan technique (*Image from Ph.D. Thesis, James J. Doyle, Trinity College Dublin, 2007*) 48

4.1 Singlewalled Carbon Nanotube bundle 52
4.2 Repeat unit chemical structure of poly(metaphenylenevinylene-co-2,5-dioctyloxy-para-phenylenevinylene) (PmPV) 56
4.3 Photoluminescence spectra of a solution of PmPV and corresponding PmPV:SWNT (1:1) composite solution (4×10^{-3} kg m^{-3}, $CHCl_3$, 25^oC) 56
4.4 Plot of the fraction of free polymer as a function of concentration, determined from PL studies at 454nm for a 2:1 PmPV molecules:HiPCO single walled nanotubes composite solutions. The solid line is a theoretical fit to Equation 4.3 in the low concentration regime. 57
4.5 Plot of the characteristic concentration as a function of concentration, determined from PL studies for 2:1 PmPV molecules:HiPCO single walled nanotubes composites. 58
4.6 The repeat unit chemical structure of poly(9,9-di-n-octylfluorenyl-2,7'-diyl) (PFO) 59
4.7 Plot of the fraction of free polymer as a function of concentration, determined from PL studies for a 1:1 PFO molecules:HiPCO single walled nanotubes composite solutions. 60
4.8 Molecular structure of pDSB molecule. 62
4.9 Absorption spectra of a solution of pDSB and the corresponding SWNT 2:1 composite solution ($4x10^{-2}$ kg m^{-3} pDSB, $CHCl_3$, 25^oC) 62
4.10 Plot of absorbance as a function of concentration for (1:1) pDSB:SWNT composites. 63
4.11 Plot of absorbance as a function of concentration for pDSB solutions. . . . 63
4.12 Plot of absorbance as a function of concentration for (2:1) pDSB:SWNT composite solutions. 64
4.13 Emission spectra of a solution of pDSB and the corresponding pDSB: SWNT (2:1) composite solution (pDSB concentration, C_{pDSB}= $4x10^{-5}$ kg m^{-3}, $CHCl_3$, 25^oC) 65
4.14 Plot of the fraction of free molecules as a function of concentration, determined from PL studies for a 2:1 pDSB molecules:HiPCO single walled nanotubes composite solutions. Note that for all concentrations the partial nanotube concentration, c_{SWNT}, equals half of the partial polymer concentration as the ratio of pDSB:SWNT = 2 : 1. The solid line is a fit to Equation 4.3 in the low concentration regime. 66

4.15 Plot of the characteristic concentration as a function of concentration, determined from PL studies for 2:1 pDSB molecules:HiPCO single walled nanotubes composites. 67
4.16 A comparison of the characteristic concentrations of two molecule:SWNT composite systems as a function of nanotube concentration shows differences between the PmPV and pDSB molecule composites. 68
4.17 Chemical structure of 1,4-bis-octyloxy-2,5-bis [2-(4-styryl-phenyl)-vinyl]-benzene (PVB) molecule. 69
4.18 Chemical structure of pDNB molecule or 2,5- dioctyloxy-1,4-dinaphthylvinylbenzene. 70
4.19 PmPV n=18 fraction before centrifugation showing Van Hove peaks in the 300-800nm region of the spectrum. 72
4.20 PmPV n=7 fraction after centrifugation showing Van Hove peaks in the 300-800nm region of the spectrum. This proves binding of the molecule onto the surface of the carbon nanotubes in solution. 73
4.21 PVB after centrifugation showing Van Hove peaks in the 300-800nm region of the spectrum. 74
4.22 PmPV n=18 fraction analysis: (A) Absorbance per unit length measured at λ = 660 nm, A_{660}/l, before and after centrifugation as a function of initial nanotube concentration. (B) Absorption coefficient at λ = 660 nm before centrifugation found by dividing A_{660}/l by the initial nanotube concentration, C_I. (C) Fraction of the nanotube mass contained in large aggregates as a function of initial concentration. 76

5.1 TEM (transmission electron microscopy) image shows adhesion of organic porphyrin molecules to the outside of Nanocyl double wall nanotubes (DWNT). As can be seen in the micrograph above, the double wall nanotubes consisted of between two- and five- or six- walled multiwalled nanotubes. The image above was taken for a 2:1 ZnTPP:DWNT composite at a high concentration of 0.02 kg/m^3 in chloroform. 105
5.2 The absorption spectrum of TPP before (solid line) and after (dashed line) sonication for 30 seconds (3.3μM, $CHCl_3$, 25^{o}C) 106
5.3 Photoluminescence spectrum of sonicated TPP (gray line) and the corresponding sonicated TPP:SWNT (1:1) composite solutions at a concentration of 6.5 μM upon excitation at 446 nm. All spectra were taken in quartz cuvettes of 1 cm pathlength. 107
5.4 Absorption spectra of TPP (solid lines) and corresponding TPP:SWNT (1:1) composite solutions (dashed lines) before (black lines) and after (red lines) sonication (35.1 μM, DMF, 25^{o}C). Spectra were taken in quartz cuvettes of 1 mm pathlength. 109
5.5 Photoluminescence spectrum of TPP and corresponding TPP:SWNT (1:1) composite solutions in DMF at 7.6μM. PL spectra obtained are identical, with quenching observed for the composite only at concentrations above 2.4μM. 110

5.6 The plot of emission as a function of concentration shows that the presence of nanotubes does not delay the onset of aggregation- induced quenching at higher concentrations. All spectra were taken in quartz cuvettes of 1 cm pathlength. 111

5.7 Structure of series of nonplanar tetraphenylporphryin derivative molecules . 112

5.8 Normalised UV-VIS absorption spectra of TPP, DETPP, tTETPP, cTETPP, HETPP and OETPP and their (1:1) SWNT composites (0.001mg/ml, DMF, 25°C). 114

5.9 The VIS-NIR absorption spectra of DETPP, its (1:1) SWNT composite and a dispersion of SWNT alone in DMF show the characteristic Q Bands and Van Hove peaks, and show the absorption spectrum of the composite solution is intermediate between that of the porphyrin and the SWNT with characteristics of both. 116

5.10 Photoluminescence spectra of porphryins examined in DMF showed porphyrin emission exhibiting both a redshift and a reduction in intensity with increasing nonplanarity, with the exception of OETPP which did not display any fluoresce at any concentration studied. 117

5.11 Plot of the ratio of composite to porphyrin emission for DETPP as a function of concentration appears to show PL quenching (solid line a theoretical fit to data proposed by Coleman et al.) 118

5.12 Plot of DETPP emission intensity at 654 nm as a function of concentration show quenching observed for the composite only at concentrations above 0.0004 mg/ml, after the onset of concentration-induced PL quenching. . . 119

5.13 Both emission bands were much lower in intensity for higher concentration solutions of DETPP for spectra normalised at 693 nm- an effect consistent with the inner filter effect. All spectra were taken in quartz cuvettes of 1 cm pathlength. 120

5.14 The PL quenching behaviour of tTETPP appeared to be in conservative agreement with the binding model at concentrations sufficiently dilute display an appreciable level of emission quenching 121

5.15 The PL intensity is directly proportional to the concentration of the tTETPP molecule over the concentration range studied 4.9×10^{-6} to 0.0025 mg/ml . . 122

5.16 Plot of porphyrin (solid circles) and composite (open circles) emission upon photoexcitation in the Soret band region at 424 nm (top) and the Qband region at 596 nm (middle) for tTETPP as a function of concentration for high concentration solutions. Concentration- induced self absorption is greatly reduced by altering the excitation wavelength. All spectra were measured in a 2mm quartz cuvette. 123

5.17 PL emission of TPP and its 10:1 SWNT composite upon photoexcitation in the Soret band region at 417 nm (top) and the Q band region at 590 nm (centre) as a function of concentration for high concentration solutions. Also shown is the ratio of composite to porphyrin emission as a function of concentration upon excitation at 417 nm (black) and 590 nm (red). The 2 mm cuvette was used for all solutions at concentrations higher than 0.001 mg/ml. 124

5.18 PL intensity as a function of concentration for 5:1 porphyrin:SWNT solutions for OEP shows enhanced luminescence for composites. These solutions were photoexcited at the Soret band wavelength of 396 nm (Top) and Q band wavelength of 529 nm (Bottom) 126

5.19 PL intensity as a function of concentration for 5:1 porphyrin:SWNT solutions for TPP shows enhanced luminescence for composites. These solutions were photoexcited at the Soret band wavelength of 417 nm (Top) and Q band wavelength of 590 nm (Bottom) 127

5.20 Absorption spectra of (a) a solution of TPP before sonication, (b) after sonication for 1 minute (c) after addition of 150 equivalents of HCl and of (d) a composite solution of TPP and SWNTs (4.5 μM, $CHCl_3$, 25^{o}C). 129

5.21 Absorption spectra of TPP upon addition of 0, 25, 50, 75, 100, 125, 150 equivalents of HCl (4.5 μM, $CHCl_3$, 25^{o}C) The spectral changes represent protonation equilibrium between two forms of porphyrin. 132

5.22 Absorption spectra of AZ in $CHCl_3$ (a) before and (b) after sonication for 1 minute. 134

5.23 Emission spectra of sonicated TPP (a) without SWNT (grey line) and (b) with SWNT (black line) upon excitation at 446 nm μM, $CHCl_3$, 25^{o}C). . . 135

5.24 Emission spectra of (a) a solution of TPP before sonication, (b) after sonication for 1 minute (c) after addition of 150 equivalents of HCl and of (d) a composite solution of TPP and SWNTs. Excitation at the corresponding Soret band in all cases (6.5 μM, $CHCl_3$, 25^{o}C). 136

5.25 Absorption changes of TPP (4.5 μM, CH_2Cl-CH_2Cl, 25^{o}C) before (black line) and after tip sonication for 30 seconds (red line), 1 minute (green line) and 2 minutes (blue line). 137

5.26 Absorption changes of TPP (4.5μM, $C_6H_4Cl_2$, 25^{o}C) before (black line) and after tip sonication for 15 seconds (red line), 30 seconds (green line) and 1 minute (blue line). 138

5.27 Absorption spectra of TPP (4.5μM, CH_2Cl_2, 25^{o}C) before and after tip sonication for 30, 60 and 90 minutes remained unchanged. 139

5.28 Absorption spectra of a solution of TPP after sonication for 1 minute in (a) DCM, (b) DCE (c) DCB (4.5μM, 25^{o}C) 140

5.29 Absorption spectra of a solution of TPP before sonication (black line), after sonication for 30 seconds (red line) and of a composite solution of TPP and SWNTs after sonication for 30 seconds (grey line). (4.5 μM, $CHCl_3$, 25^{o}C) 141

5.30 Absorbance of protonated TPP upon titration with HCl for (a) porphyrin (filled squares) and (b) composite (empty squares) solutions 4.5 μM, $CHCl_3$, 25^{o}C) 142
5.31 Titration of TPP with HCl in DMF shows an isosbestic point at 425.3 nm . 143
5.32 Titration of the TPP composite with HCl in DMF also shows an isosbestic point at 425.3 nm 144
5.33 Titration of TPP with HCl in DMF 145
5.34 Titration of TPP with TFA in DMF 146
5.35 Titration of TPP with Citric Acid in DMF 147
5.36 Titration of TPP with Ascorbic Acid in DMF 148

6.1 Plot of normalised transmission vs. distance from focus for TPP and composite solutions at low concentration and low energy. Concentrations were 21 μM for the TPP solution and 2.7 μM for the composite solution with on-focus intensities of 0.138 and 0.194 GW/cm^2 for the TPP and composite solutions respectively 159
6.2 Plot of normalised transmission vs. distance from focus for TPP and composite solutions at low concentration and high energy. Concentrations were 21 μM for the TPP solution and 2.7 μM for the composite solution with on-focus intensities of 1.23 and 1.80 GW/cm^2 for the TPP and composite solutions respectively. Thermal degradation of the TPP sample is evident at these intensities, although conditions were chosen to minimize this effect. . 160
6.3 Plot of normalised transmission vs. distance from focus for TPP and composite solutions at high concentration and low energy. Concentrations were 98 μM for the TPP solution and 7.6 μM for the composite solution with on-focus intensities of 0.136 and 0.188 GW/cm^2 for TPP and composite solutions respectively 161
6.4 Plot of normalised transmission vs. distance from focus for TPP and composite solutions at high concentration and high energy. Concentrations were 98 μM for the TPP solution and 7.6 μM for the composite solution with on-focus intensities of 1.16 and 1.58 GW/cm^2 for TPP and composite solutions respectively 162
6.5 Plots of effective β_I against the on- focus beam intensity I_0 for TPP (Black Square), TPP:SWNT (Open Square), ZnTPP (Black Circle), ZnTPP:SWNT (Open Circle) solutions (12.7 μM, TPP (Black Triangle), TPP:SWNT (Open Triangle) solutions (21.5 μM) and a 0.01mg/ml SWNT suspension (Red Star). Solid lines indicate $CHCl_3$ solutions and dotted lines indicate DMF solutions. 163
6.6 Plots of normalized transmission against pulse energy density for solutions A-F. Symbols used are as described in Figure 6.5. The composite solutions (open symbols) were found to be much better optical limiters than both the porphyrin solutions (filled symbols) and SWNT alone (Red star). 165

6.7 Plots of normalized transmission against pulse energy density for TPP (Black Triangle), TPP:SWNT (Open Triangle), PP(ix) (Black Diamond), PP(ix):SWNT (Open Diamond) solutions (21.5 μM, DMF, 25^{o}C) and a 0.01mg/ml SWNT suspension (Red Star). All plots shown were observed at an on- focus beam intensity, I0, of approximately 0.2 GW cm^{-2} 166

6.8 Normalised transmission vs. distance from focus for porphyrin and composite solutions at low energies for DETPP. Porphyrin and composite solutions were at concentrations of 0.01 mg/ml, with on-focus intensities of 0.12 GW/cm^2 for porphyrin solutions and 0.25 GW/cm^2 for composite solutions 168

6.9 Normalised transmission vs. distance from focus for porphyrin and composite solutions at low energies for tTETPP. Porphyrin and composite solutions were at concentrations of 0.01 mg/ml, with on-focus intensities of 0.13 GW/cm^2 for porphyrin solutions and 0.16 GW/cm^2 for composite solutions 169

6.10 Normalised transmission vs. distance from focus for porphyrin and composite solutions at low energies for cTETPP. Porphyrin and composite solutions were at concentrations of 0.01 mg/ml, with on-focus intensities of 0.14 GW/cm^2 for porphyrin solutions and 0.24 GW/cm^2 for composite solutions 170

6.11 Normalised transmission vs. distance from focus for porphyrin and composite solutions at low energies for HETPP. Porphyrin and composite solutions were at concentrations of 0.01 mg/ml, with on-focus intensities of 0.25 GW/cm^2 for porphyrin solutions and 0.23 GW/cm^2 for composite solutions 171

6.12 Normalised transmission vs. distance from focus for porphyrin and composite solutions at low energies for OETPP. Porphyrin and composite solutions were at concentrations of 0.01 mg/ml, with on-focus intensities of 0.23 GW/cm^2 for porphyrin solutions and 0.19 GW/cm^2 for composite solutions 172

6.13 The higher final transmittance compared with the initial transmittance indicates the destruction of molecules present in the solution. Porphyrin and composite solutions were at concentrations of 0.01mg/ml, with on-focus intensities of 1.63575 GW/cm^2 for porphyrin solutions and 0.19 GW/cm^2 for composite solutions. 173

6.14 Plots of the nonlinear absorption coefficient, β_I at an on- focus beam intensity I_0 of 0.2 GW /cm^2 in DMF as a function of Non planarity. With 1=TPP, 2=DETPP, 3= tTETPP, 4= cTETPP, 5= HETPP and 6= OETPP. 174

6.15 Plots of the effective Im$\chi^{(3)}$ at an on- focus beam intensity I_0 of 0.2 GW /cm^2 in DMF as a function of Non planarity. With 1=TPP, 2=DETPP, 3= tTETPP, 4= cTETPP, 5= HETPP and 6= OETPP. 175

6.16 Optical limiting behaviour of porphyrin solutions is shown in these plots of normalised transmission vs pulse energy density. All plots are for on- focus beam intensity I_0 of approximately 0.2 GW /cm^2. 177

6.17 Superior optical limiting behaviour of porphyrin composites is clearly to be seen by comparing these plots of normalised transmission vs pulse energy density to those in Figure 6.16. All plots are for on- focus beam intensity I_0 of approximately 0.2 GW /cm^2. 178

6.18 (A) Simulation initial conditions are shown for the HETPP-SWNT-DMF system. While there are 20 HETPP molecules, only 4 HETPP molecules, a single DMF (yellow) molecule and the SWNT are actually rendered using effective Van der Waals diameters. The box is infact repeated in all directions periodically, to simulate a bulk solvent, and an infinitely long SWNT (B) The DETPP- SWNT- DMF solvent system. The prounced tendencies of DETPP to aggregate on, and close to the SWNT is evident (C) The TPP-CNT-dmf solvent system. There is no tendency for TPP to aggregate on or close to the CNT. 180

List of Tables

6.1 Optical Coefficients measured for the Planar Porphyrin systems studied. . . 164
6.2 Optical Coefficients measured for the Nonplanar Porphyrin systems studied 176
6.3 Summary of porphyrin aggregation behaviour. N denotes the number of porphyrin molecules in contact with the SWNT, and M denotes the largest porphyrin derivative self-aggregate 181

Chapter 1

Introduction

1.1 Scientific Background

The semiconductor industry, encompassing all types of electronics technologies, has enjoyed a phenomenal rate of progress over the last few decades. Due to the myriad applications offered by modern electronics, it has gradually permeated all areas of our modern day lives. This relatively recent expansion of the electronics industry is primarily due to advances in the field of inorganic semiconductors, and the traditionally silicon- based complementary metal-oxide-semiconductor (CMOS) processes and integrated circuit (IC) devices. However, the extensive development of the field of organic electronics is also partly responsible for the continued expansion of this sector. Indeed, inorganic devices are starting to be replaced by organic devices in many areas, and this trend is expected to continue as advances continue to be made. When the first semiconducting polymer, polyacetylene[1], was developed in 1974 the potential of organic systems for electronic applications was realized. This polymer was found to rival traditional inorganic semiconductors, with enhanced conductivity readily achieved through oxidation with an element such as iodine[2], analogous to doping in silicon. Once a promising material is identified and characterized for any technology, the first step to industrial implementation is the development of functional devices. The first polymeric device- the organic LED- was developed by J.H. Burroughs and co- workers in 1990[3], subsequently leading to the development of organic photodiodes[4], photovoltaic cells[5], field

effect transistors[6] and optically pumped lasers.[7]

Despite these recent advances in the field of organic electronics, however, it is now accepted that the limitations of current electronics technologies are rapidly being approached. In order to maintain the recent rate of progress, device dimensions must be further reduced and processing speeds increased. However, these parameters have already been optimized almost to the limits of physical possibility within current inorganic semiconductor technology. Nanotechnology is hoped to address some of these difficulties, with the possible incorporation of novel nanoscale silicon and germanium materials into current processes seen as one approach to the problem of miniaturization. The compatibility of these materials with the inorganic semiconductors currently in use is one enormous advantage, and research has been undertaken to characterize the novel properties and electronic structures of these quantum confined materials.[8] However, the incorporation of new materials with novel electronic properties into existing CMOS processes must also be investigated in order to facilitate the future optimization of device fabrication. In this, organic materials may once again be of use.

Another boost to the fledgling field of organic electronics was the discovery of a third allotrope of carbon, the C_{60} molecule also known as Buckminster Fullerene by H.E. Kroto, R.F. Curl, and R.E. Smalley in 1986.[9] Carbon nanotubes are a member of this family of nanoscale molecules, and are of great interest for several reasons. Subsequent studies found that the C_{60} molecule was only one of a family of such carbon molecules. Multi-Walled Carbon Nanotubes(MWNT),[10] the long, multiple concentric cylindrical fullerenes were initially discovered in 1991 by S. Iijima who subsequently also discovered Single-Walled Carbon Nanotubes (SWNT).[11] The unique dimensions and unusual electron conduction mechanism exhibited by carbon nanotubes make them ideal nanoscale components of electrical circuits. Nanotube based transistors have been developed that operate at room temperature and that are capable of single electron digital switching.[12] The first working, integrated silicon circuit successfully incorporating carbon nanotubes in its design was made in 2004.[13] Despite these successes, however, many challenges lie ahead before successful implementation and commercialization of these carbon nanotube- silicon hybrid circuits may be realized, with regulation of nanotube conductivity remaining a major challenge. The tendency of nan-

otubes to bundle together through attractive Van der Waals forces and the consequent difficulty in isolating individual nanotubes is also a major problem for device fabrication and processing. Some degree of carbon nanotube functionalization is therefore required- either covalent or non- covalent- in order to achieve some degree of control over the manipulation of individual nanotubes. Non-covalent functionalization of carbon nanotubes is superior to covalent functionalization, as it preserves the unique electronic structure that makes carbon nanotubes a key material for nanoelectronic applications in the first place. Therefore the non-covalent functionalization of carbon nanotubes with conjugated organic molecules studied in this thesis is an area of enormous potential importance in the future of electronics, and understanding the interactions between these molecular systems and the properties of their composites may form a basis for the engineering of the molecular electronic materials of tomorrow.

Indeed, it is possible that nanoelectronics may not be the ultimate solution should these problems prove insurmountable, and scientists are increasingly looking to provide other solutions to meet our future information and communication needs. The emerging field of photonics may provide an answer to these problems. Photonics is the technology concerned with the generation and control of all forms of electromagnetic energy whose quantum unit is the photon. In the same way that electronics may be defined as the acquisition, manipulation, storage and transmission of information using electricity, so photonics is the control, manipulation, transfer and storage of information using light. One clear advantage photonics offers over electronics is the possibility of processing data at the speed of light.

With the advent of the laser and the subsequent development of the theory of nonlinear optics, one of the principle prerequisites for photonics implementation was satisfied- the existence of appropriate optical techniques. In order to realize photonics technology in everyday life, suitable optical materials must be identified and fully characterized in order to fabricate optical circuits and devices analogous to those utilized in modern electronics. Novel materials capable of facilitating efficient nonlinear optical interactions must be identified, and subsequently used in the fabrication of useful optical devices. Potential organic molecular optical switches which behave in the way as transistors- the building blocks of

integrated circuit devices- have already been identified and characterized.[14,15] However, much work remains to be done before this becomes a viable technology. Due to their easily polarized electronic $\pi-$ orbitals, conjugated organic materials are extremely promising candidates for future photonics applications, and current research is focussing on the design and optimization of these materials for laser- induced nonlinear optical behaviour. The field of organic materials for photonic applications encompasses a wide range of interesting materials including the familiar polymers or plastics, the naturally occurring porphyrins and the related phthalocyanine family, in addition to fullerenes and carbon nanotubes. Organic materials produce large and ultrafast nonlinear responses due to their ability to support considerable nonlinear optical interactions, and are architecturally flexible and readily and cheaply fabricated.

Organic molecules possessing macrocycles have conjugated organic structures and can be considered as two-dimensionally delocalized π-electron systems. Porphyrins may therefore be considered a two-dimensional system based on a planar configuration whereas carbon nanotubes are one-dimensional systems exhibiting quantum wire- type dimensionality. The effects of a systematic variation in porphryin structure on its optical properties are investigated in this thesis, and subsequent changes in the noncovalent interaction between these two different organic systems are probed. The nonlinear optical response of these novel hybrid nano-dimensional materials is also investigated here, with a view to ultimately gaining information about material optimization for optical device fabrication.

With the development and implementation of high intensity laser light sources and the various photonics technologies, a need has arisen for the protection of delicate optical sensors (including the human eye) from accidental irradiation by the high intensity lasers employed by this technology. Hence the field of optical limiting has enjoyed much attention of late. Optical limiting is a process whereby nonlinear optical processes such as nonlinear scattering and reverse saturable absorption (RSA) result in the suppression of high intensity incident irradiation once it exceeds a threshold intensity. High transmission of low photonic energy ambient light irradiation is allowed by optical limiting materials. This need for the development of optical limiters has further increased interest in novel nonlinear optical mechanisms and devices using organics, fullerenes, semiconductors and other materials.[16]

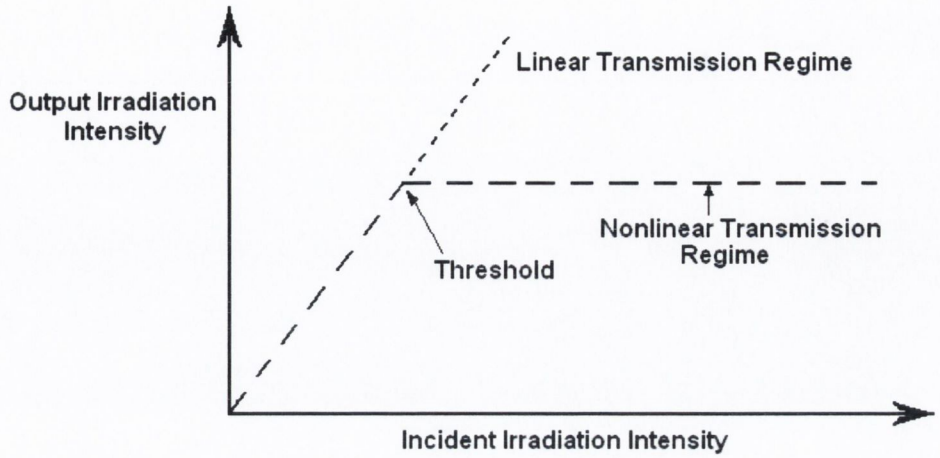

Figure 1.1: The ideal response of an optical limiting material

The ideal response of an optical limiter is shown in Figure 1.1, and displays linear transmission at low incident irradiation intensities. At a characteristic threshold intensity the material enters the nonlinear regime, and the dissipative nonlinearities of the material cause the transmitted intensity to remain constant for all incident light at energies higher than this threshold. An optical limiter would be analogous to an electronic fuse- designed so that this threshold energy would be lower than the intensity required to damage the sensor being protected.

1.2 Thesis Outline

In this thesis, the non-covalent interaction of carbon nanotubes with a number of conjugated organic molecules is investigated, and the linear and nonlinear optical properties of these composite systems are characterized. The organic moieties studied are of two distinct categories, namely highly conjugated molecules related in structure to the polymer PmPV, and members of the porphyrin family largely consisting of tetraphenylporphyrin derivatives.

The structure of this thesis will be as follows: Chapter two introduces the background theory to the materials used, providing a basic introduction to organic materials.

This will be followed by a description of the possible photophysical processes typically observed from such organic systems. A detailed introduction to the specific materials studied in this thesis is given. The chapter concludes with a general introduction to nonlinear optical phenomena, and the optical limiting behaviour specifically exhibited by organic materials.

Chapter three will be concerned with a description of the various experimental techniques employed in the linear and nonlinear optical characterization of the materials investigated in this thesis. The principle techniques employed in this thesis are absorption spectroscopy, fluorescence spectroscopy and the z-scan technique.

Chapter four will deal with the characterization of carbon nanotube interactions with conjugated organic molecules and polymers. This chapter consists of two sections. Firstly, a simple adsorption/desorption equilibrium model developed by Coleman et al.[17] is introduced, which describes a method of monitoring the carbon nanotube dispersion capability of conjugated polymers and their short chain analogues based on photoluminescence quenching behaviour observed for such carbon nanotube composites in solution. This model allows calculation of the concentration at which individual SWNTs are observed for each system. A number of carbon nanotube composite systems are characterized and the results presented in this chapter. In the second part of this chapter, detailed absorption spectroscopy studies are undertaken on those molecules which, during the photoluminescence studies, appeared to interact strongly with carbon nanotubes in solution. A detailed picture of non-covalent interaction between carbon nanotubes and organic molecules is built up using centrifugation to remove the large nanotube aggregates formed at higher concentrations and confirm the binding between them at lower concentrations.

In Chapter five, the interactions of carbon nanotubes with molecules from the porphyrin family are characterized using linear optical spectroscopy techniques. Porphyrins are a family of highly conjugated organic molecules, and are thus expected to interact strongly with nanotubes through Van der Waals interactions. This chapter begins with a review of all literature available concerning carbon nanotube/porphyrin composites. The experimentally determined linear optical properties of planar porphyrin systems and their composites are then presented. The chapter also contains an investigation of the linear optical properties of nonplanar tetraphenylporphyrin derivatives and their composites. The

principal aim of this chapter is to determine the nature of the interaction that exists between conjugated porphyrin molecules and carbon nanotubes, and to investigate what effect- if any- the planarity of the porphryin macrocycle has on this interaction. The spectroscopic changes upon sonication and laser irradiation of tetraphenylporphyrin composite solutions in a range of chlorinated solvents are also investigated in this chapter. These changes are subsequently attributed to the protonation of the porphyrin core nitrogen atoms when sonication- induced degradation of the solvent molecules produces hydrochloric acid as a byproduct. The effect of the presence of carbon nanotubes on the rate of porphyrin protonation is also presented. The implications of these results are that extreme care must be taken when working with carbon nanotube composite solutions in chloroform as protonation of acid sensitive molecules may take place, changing their physicochemical properties.

In Chapter six, the nonlinear optical properties of these carbon nanotube/ porphryin composites are characterized using the z-scan technique. This chapter begins with a literature review of papers describing the nonlinear optical properties of porphyrins and carbon nanotube/porphyrin composites. The experimentally determined nonlinear optical properties of the porphyrin systems and their composites are then presented. The principal aim of this chapter is to further examine the nature of the interaction that exists between porphyrin molecules and carbon nanotubes, and to investigate the consequences of porphryin macrocycle planarity on the optical limiting behaviour of these systems with a view to creating efficient light attenuation materials. A molecular dynamics simulation carried out by colleagues in Trinity College Dublin is also described, where the tendency exhibited by these tetraphenylporphyrin derivatives to aggregate close to a nanotube surface in the same solvent was investigated. These complementary molecular dynamics studies were found to strongly agree with the experimental observations.

Finally, a summary of the work presented herein is given in Chapter seven, thus concluding the thesis.

Bibliography

1. Shirakawa, H., Ito, T., and Ikeda, S. *Polymer Journal, 4, 460* (1973).

2. Chiang, C., Fincher, C., Park, Y., Heeger, A., Shirakawa, E., Lown, E., Gau, S., and Mac Diarmuid, A. *Physical Review Letters, 39C, 1098* (1977).

3. Burroughs, J., Bradley, D., Brown, A., Marks, R., Mackey, K., Friend, R., Burns, P., and Holmes, A. *Nature, 347, 539* (1990).

4. Halls, J., Walsh, C., Greenham, N., Marseglia, E., Friend, R., Moratti, S., and Holmes, A. *Nature, 376, 498* (1995).

5. Halls, J., Baigent, D., Cacialli, F., Greenham, N., Friend, R., Moratti, S., and Holmes, A. *Thin Solid Films, 276, 13* (1996).

6. Burroughs, J., Jones, C., and Friend, R. *Nature, 335, 137* (1988).

7. Tessler, N., Denton, G., and Friend, R. *Nature, 382, 695* (1996).

8. Audoit, G., Ni Mhuircheartaigh, E., Lipson, S., Morris, M., Blau, W., and Holmes, J. *Journal Of Materials Chemistry, 15 (45), 4809-4815* (2005).

9. Kroto, H., Heath, J., O'Brien, S., Curl, R., and Smalley, R. *Nature, 318, 162* (1985).

10. Iijima, S. *Nature, 354, 56* (1991).

11. Iijima, S. and Ichihashi, T. *Nature, 363, 603* (1993).

12. Postma, H., Teepen, T., Yao, Z., Grifoni, M., and Dekker, C. *Science 293, 76-79* (2001).

13. Tseng, Y., Xuan, P., Javey, A., Malloy, R., Wang, Q., Bokor, J., and Dai, H. *Nano Letters 4(1),123-127* (2004).

14. Raymo, F., Giordani, S., White, J., and Williams, D. *Journal of Organic Chemistry, 68, 4158-4169* (2003).

15. Raymo, F. and Giordani, S. *Proceedings of the National Academy of Sciences USA (Supramolecular Chemistry and Self-assembly Special Feature Article), 99, 4941-4944* (2002).

16. Tutt, L. and Boggess, T. *Progress In Quantum Electronics, 17, 299-338* (1993).

17. Coleman, J., Fleming, A., Maier, S., O'Flaherty, S., Minett, A., Ferreira, M., Hutzler, S., and Blau, W. *Journal of Physical Chemistry B 108, 3446-3450* (2004).

Chapter 2

Materials and Optics Background

2.1 Organic Materials

2.1.1 Basic Concepts of Organic Materials

Organic materials is a term used to describe all chemical compounds of carbon and hydrogen, which may contain any number of other elements, such as nitrogen, oxygen, halogens, and more rarely phosphorus or sulfur. Because of their unique properties, an extremely large variety of multi-carbon compounds exist with myriad applications. They are important constituents of many products (paints, plastics, food, explosives, drugs, petrochemicals, and many others) and they form the basis of all life processes. They encompass a vast range of materials, from methane to polymers, fullerenes and nanotubes, large macrocyclic molecules such as phthalocyanines and porphyrins and most biological materials. The materials used in this thesis consist of conjugated polymers and oligomers, porphyrins and carbon nanotubes.

Carbon is a unique element, as it can form a variety of different bond arrangements due to a process called orbital hybridization. In chemistry, hybridization is the concept of mixing atomic orbitals to form new hybrid orbitals suitable for the qualitative description of atomic bonding properties.[1] Carbon's ground-state configuration is $1s^2\ 2s^2\ 2p_x^1\ 2p_y^1$ (or $1s^2\ 2s^2\ 2p^2$). Therefore, the valence bond theory would predict, based on the existence of two half-filled π-type orbitals that carbon would be expected to exhibit a valence of

two, and would form two covalent bonds leading to structures such as CH_2. However, for a tetrahedrally coordinated carbon (e.g. methane, CH_4), the carbon should have 4 orbitals with the correct symmetry to bond to the 4 hydrogen atoms. Due to the small difference in energy levels between the 2s and 2p electronic orbitals compared with the binding energy of chemical bonds, the wave functions of these four electrons can mix to create new mathematical functions known as hybridised orbitals. In the case of carbon attempting to bond with four hydrogens, four orbitals are required. Therefore, the 2s orbital mixes with the three 2p orbitals to form four sp^3 hybrids. In methane, four sp^3 hybridised orbitals are overlapped by hydrogen's 1s orbital, yielding four sigma (σ) bonds of equal length and strength. In carbon, three possible hybridizations are possible: sp, sp^2 and sp^3, where the superscript indicates the number of 2p electrons involved. This linear combination of s and p atomic orbitals forms molecular orbitals that are directed along certain directions. In sp^3 hybridization, the bonds are along the four directions connecting the center of a regular tetrahedron to its four corners, with a bonding angle of approximately 109.5^o. In sp^2 hybridization, the bonds are along the sides of a hexagon and make angles of 120^o with each other. Similarly sp bonding gives rise to chain structures.

The properties of an organic molecule are strongly dependent on the type of carbon hybridization present. For sp^3 bonded molecules all the electrons are tightly bound in high energy σ bonds and a large amount of energy is therefore required to excite these electrons. Hence, such molecules tend to be relatively inert. In sp^2 hybridization, only three valence electrons are involved in bonding, with the fourth electron remaining in the original unhybridized p_z orbital. These p_z orbitals are arranged in a dumbbell shape out of plane and form lower energy π bonds. When two or more such sp^2 hybridized carbon atoms bond, the π-electron orbitals overlap to form extensive delocalized molecular orbitals. This occurs for molecules such as ethylene, shown in Figure 2.1, where the delocalization of the electrons in p_z orbitals results in an effective electron cloud equally probable above and below the plane of the molecule. Due to the low energy and extensive delocalization of these π-bonds, much less energy is required to excite them. Large perturbation of the molecular orbital can therefore be readily achieved through excitations of the π-electrons, inducing a large polarization in the molecule. If the ethylene molecule is polymerized, the saturated

(i.e. non-conjugated) polymer polyethylene is obtained. For such non-conjugated systems, the electrons are highly localized between the carbon atoms and are not free to participate in the conduction process. These highly localized electrons yield the large bandgap observed for these materials. Therefore polyethylene is known to have a large bandgap, and may be considered an electronically insulating material.

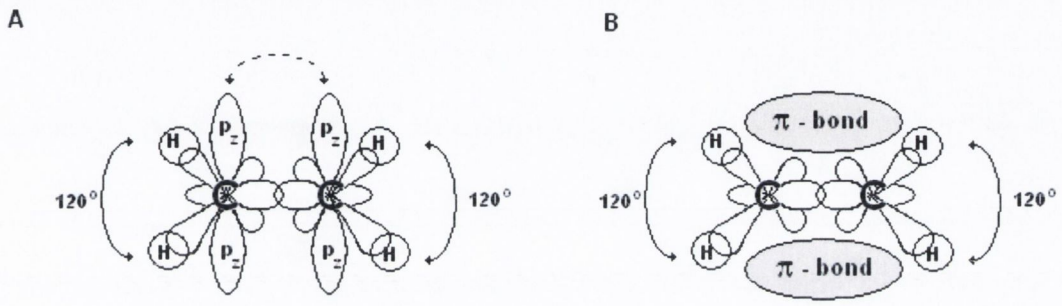

Figure 2.1: Bonding structure of ethylene with p_z orbitals (A) and pi bonds resulting from the combination of these adjacent p_z orbitals (B)

Conjugated organic molecules- such as those investigated in this thesis- are molecules in which sp^2 bonding is predominant and have alternating single and multiple carbon bonds. These molecules therefore exhibit π-bonding which lends itself to excellent nonlinear optical performance in organic materials. Conjugated polymers possess extended π -systems due to alternating single and multiple bonds containing delocalized electrons such as that shown above for ethylene and may be considered intrinsic semiconductors. Such conjugation may be extended to a large number of alternating single and multiple bonds in large molecules such as polymer chains, and the π- electrons may subsequently be delocalized over the entire molecule. For polymers this means that the π-electrons tend to delocalize over a number of repeat units of the polymer. Two polymers which might be considered typical conjugated polymers are polyacetylene and poly(para-phenylene vinylene) (PPV). Potential applications for conjugated polymers include light-emitting devices (LEDs) for use in flat-screen displays, solar cells and optoelectronic devices such as waveguides. Polyacetylene is the simplest conjugated polymer and its chemical structure is shown in Figure 2.2. The

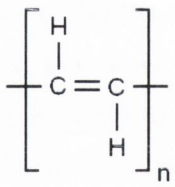

Figure 2.2: Chemical structure of repeat unit of polyacetylene

continuous π- system formed by the overlapping of p_z orbitals is illustrated in Figure 2.3, and the resultant cloud of delocalized electrons along the polymer backbone shown.

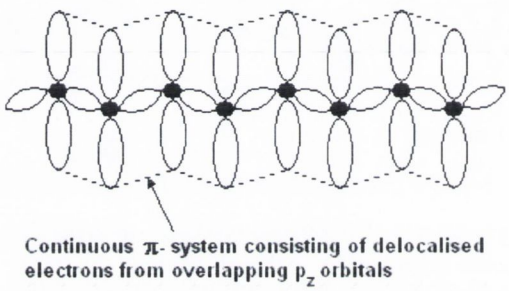

Figure 2.3: An extensive π- system is formed in polyacetylene by the overlapping of the p_z orbitals

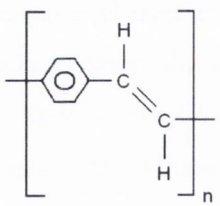

Figure 2.4: Chemical structure of repeat unit of poly(para-phenylene vinylene) (PPV)

The chemical structure of PPV may be seen in Figure 2.4, illustrating the electron delocalization over the conjugation length of this polymer. The main polymer studied in this thesis, PmPV, is related to PPV with alternating para and meta linkages on each benzene ring. The overlap of the p_z orbitals (Figure 2.5) again leads to the formation of a delocalized

electron cloud over the conjugation length of the polymer. These π- electrons are bound very weakly to particular atoms in the polymer chain, and are therefore highly mobile and free to move over

Figure 2.5: The p_z orbitals which overlap to form the π orbitals in the PPV molecule

2.1.2 Photophysics

Photophysical processes involve photoexcitation and subsequent relaxation of a molecular entity by electromagnetic radiation, leading from one state to another through both radiative and radiationless transitions, with no chemical change involved. Such processes include absorption, vibrational relaxation, photoluminescence, phosphorescence, intersystem crossing and internal conversion. Once a molecule has absorbed energy in the form of electromagnetic radiation, there are a number of routes by which it can return to ground state (the statistically most common energy state for room temperature chemical species). These electronic levels and photophysical processes in organic materials can be represented schematically in a Jablonski diagram such as that shown in Figure 2.6. A Jablonski diagram illustrates the electronic states of a molecule and the transitions between them. The states are arranged vertically by energy and grouped horizontally by spin multiplicity, with singlet states denoted as S_n, and triplet states T_n. These electronic states are vibrationally broadened to form bands. Radiative transitions are indicated by straight arrows and nonradiative transitions by wavy arrows. The vibrational ground states of each electronic level are indicated with thick lines, the higher vibrational states with thinner lines. Radiative transitions involve the absorption or emission of a photon. Nonradiative transitions arise through several different mechanisms, all differently labelled in the diagram.

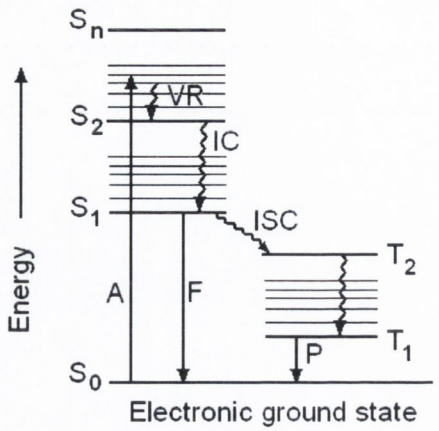

Figure 2.6: Jablonski Diagram.

Absorption (A)

Absorption is the process by which the energy of a photon is taken up by an atom or molecule whose valence electrons make a transition between two electronic energy levels. The photon is destroyed in the process. The absorbed energy can be lost by heat and radiation. The absorbance of an object quantifies how much light is absorbed by it. This may be related to other properties of the object through the Beer-Lambert law.

At room temperature, there is an extremely high probability that a given molecule is in the lowest vibrational level of its ground state, and a low probability that it is in higher vibrational levels of the ground state, as described by the Boltzmann distribution. Therefore the majority of ground state excitations excite a molecule from the lowest vibrational level of its ground state into a vibrational level in its first or second excited state. As the excitation typically occurs from the ground state only, the absorption spectrum may give us information about the energy distributions for the first and second excited states. Excited state absorption is also possible, upon excitation of a molecule which is already in an excited state, and is one of the dominant processes responsible for optical limiting. Extremely high irradiation intensities are required to promote electrons out of excited singlet and triplet states, as the population of the ground state of the molecule in question must be suitably depleted in order for nonlinear processes to take place. The energy of the incident photons

must also correspond to the energy difference between the excited state and some other higher energy level.

Fluorescence (F)

Fluorescence, or photoluminescence occurs when a molecule or quantum dot relaxes to its ground state after being electronically excited from the ground state to the next electronic level of higher energy, S_1. It may be described by the following equation:

$$S_1 = S_0 + h\nu$$

where $h\nu$ is a generic term for photon energy where: h = Planck's constant and ν= frequency of the light emitted.

Photoluminescence is a radiative relaxation process that occurs once a molecule has been photoexcited, and subsequently undergone a vibrational energy relaxation to the ground state of the excited electronic level. This can only occur if both states have the same multiplicity, e.g. between two singlet or triplet states, and typically occurs on a timescale of less than 100ns. As emission takes place from the lowest levels of the first excited state to the various vibrational levels of the ground state, the photoluminescence spectrum yields much information about the vibrational energy distribution of the ground state. As the molecules relax nonradiatively prior to photoemission, the energy of the emitted photons is always lower than that of the excitation energy. This red shift in the emission spectrum relative to the absorption spectrum is known as the Stokes shift.

Various rules govern fluorescence behaviour, such as the Kasha rule which dictates that in complex molecules, all emission occurs from the lowest excited electronic state of a given multiplicity and is independent of the wavelength of exciting radiation.

The fluorescence quantum yield gives the efficiency of the fluorescence process. It is defined as the ratio of the number of photons emitted to the number of photons absorbed. The maximum fluorescence quantum yield is 1.0 (100%), where every photon absorbed results in a photon emitted. Compounds with quantum yields of 0.10 are still considered quite fluorescent. Most substances have very weak fluorescence ($\psi \leq 10^{-3}$). Free base porphyrins have large quantum yields, with values of 0.11 and 0.03 reported

for tetraphenylporphyrin and the metalloporphyrin tetraphenylporphyrin zinc respectively in the solvent dichloromethane.[2] There are many other processes that may compete with radiative relaxation such as intersystem crossing, internal conversion and various quenching mechanisms.

Vibrational Energy Relaxation (VR)

Relaxation of the excited state to its lowest vibrational level is labelled VR in the Jablonski diagram. Vibrational energy relaxation is a process in which the population distribution of molecules in vibrational quantum states of a high energy level caused by an external perturbation returns to the Maxwell-Boltzmann distribution. It occurs over a lifetime of approximately 10^{-13} s. This process involves the dissipation of energy from the molecule to its surroundings, and thus it cannot occur for isolated molecules.

Internal Conversion (IC)

A second type of nonradiative transition is internal conversion (IC), which occurs when a vibrational state of an electronically excited state can couple to a vibrational state of a lower electronic state. Internal conversion is defined as a transition from one set of excited electronic levels to another set which have the same spin multiplicity. An example of IC would be from the second singlet state to the first singlet state. This is a form of radiationless de-excitation, and is an isoenergetic process.

Intersystem Crossing (ISC)

Intersystem crossing (ISC) is a nonradiative transition to a state with a different spin multiplicity, such as from a singlet to a triplet state. While both IC and ISC are radiationless methods of de-excitation, the molecular spin state for internal conversion remains the same, whereas it changes for intersystem crossing. Intersystem crossing is very important for many members of the porphyrin family, facilitating processes such as excited state absorption, thus yielding efficient optical limiting materials. This type of nonradiative transition can be important for nonlinear excited state absorption from the triplet state under high input fluences. If the energy from absorbed photons undergoes intersystem crossing into a state

of higher spin multiplicity such as a triplet state, the energy becomes trapped in the triplet state as radiative transition back to the lower singlet energy states is quantum mechanically forbidden. It therefore takes place on a very long timescale and is known as phosphorescence. Such spin forbidden transitions such as phosphorescence and intersystem crossing are made possible through spin- orbit coupling.

Phosphorescence (P)

Phosphorescence is a type of photoluminescence which occurs from the lowest lying vibrational level of the triplet state. This radiative relaxation process differs to fluorescence in that the transitions involved require a change in multiplicity. The molecule undergoes transitions from a triplet state where two electrons are unpaired to a singlet state where the electrons are fully paired. Thus phosphorescence typically occurs on a timescale ranging from 10^{-4} to 10^{4} s as a consequence of this spectroscopic requirement. The emission is generally weak as the long lifetime ensures that competing processes may quench the triplet exciton.

2.2 Specific Materials Studied

2.2.1 Porphyrin Molecules

A porphyrin is a heterocyclic macrocycle made from 4 pyrrole subunits linked on opposite sides (α – position) through 4 methine bridges (=CH-).[3] The extensive conjugated system makes the compound chromatic, hence the name porphyrin, from a Greek word for purple. The macrocycle has 22 π electrons, 18 of which are active in the conjugated system. In organic chemistry, it is possible to predict whether a planar ring molecule will have aromatic properties by following Huckel's rule, the quantum mechanical basis for which was first worked out by physical chemist Erich Huckel in 1931. A cyclic ring molecule follows Huckel's rule if its number of π electrons equals 4n + 2 where n is zero or any positive. As they follow Huckel's rule, porphyrins have aromatic properties. The chemical structure of the planar molecule protoporphyrin (IX) is shown in Figure 2.7.

Porphyrins and porphyrin- type molecules are abundant in nature, and they play

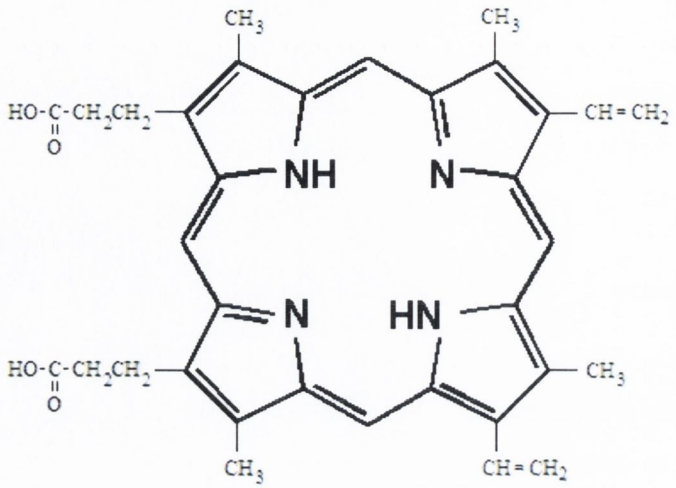

Figure 2.7: Chemical structure of protoporphyrin IX molecule

important roles in a large number of different naturally occurring processes such as the energy transfer processes photosynthesis and the coordination of oxygen in heme and myoglobin molecules, resulting in the transport of oxygen from the lungs to muscles.

Porphyrin molecules have been studied extensively. Such research includes their use as model systems for photoinduced electron transfer, or solar energy conversion in artificial photosynthesis experiments and for general electron and energy transfer studies,[4] for photodynamic therapy studies[5] and as sensitisers for various photoactive switches and supramolecular devices.[6,7] With myriad substitution and metal binding possibilities, the porphyrin structure lends itself to incredible diversity enabling us to tune properties such as solubility, redox potentials, excited state energies and lifetimes through slight alteration of the molecular structure. The porphyrin macrocycle can accommodate a variety of substitutions including peripheral and axial, linking the molecules to electron and energy donors and acceptors without dramatic alteration of the physical, chemical and optical properties. In Figure 2.8, the chemical structure of the planar porphyrin tetraphenylporphyin (TPP) may be seen. In this thesis, the importance of macrocycle planarity to porphyrin optical properties was investigated through a systematic study of a series of tetraphenylporphyrin derivatives. These TPP derivatives contained an increasing number of ethyl- substitutions

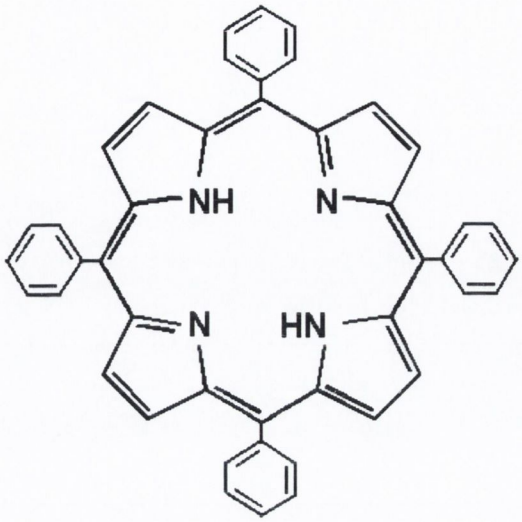

Figure 2.8: Chemical structure of tetraphenylporphryin molecule

on the macrocycle, which led to a distortion of the macrocycle due to steric crowding. The complete series is illustrated in Figure 5.7 in Chapter 5 of this thesis.[1] A number of different metal cations can also be substituted into the macrocycle cavity, coordinating to the four central nitrogen atoms to form metalloporphyrins. Different metal cations each introduce new properties to the molecule, and thus the porphyrin photophysical and photochemical properties can be finely tuned.[8] Included in this thesis is a case study of a series of tetraphenyl porphyrin derivative molecules which differ only in their degree of porphyrin macrocycle nonplanarity. A large number of macrocyclic substituents (ethyl groups) are successively attached to the basic tetraphenyl porphyrin macrocycle and the influence of the steric crowding caused by these substituents- and the consequent distortion of the typically planar macrocycle- on the noncovalent molecular interactions with carbon nanotubes is investigated optically in this work. Porphyrins are classified as being regular or irregular by the ground state absorption spectra. The absorption spectrum of a regular porphyrin is determined essentially by the π orbitals of the porphyrin macrocycle, whereas an irregular porphyrin displays absorption features with contributions also from its metal d- orbitals. In regular porphyrins, such as those studied, the absorption spectrum is characterised by

[1]These images shown in Figure 5.7 are shown courtesy of Dr. Donal Mac Kernan

a strong transition centred around 420 nm, often denoted as the B or the Soret band and weaker transitions in 500 – 650 nm range often denoted as the Q bands. In the free base porphyrins, the Q bands can be seen as four distinct bands. If a closed shell metal ion, like Zn^{2+} is coordinated to the porphyrin, two of the states corresponding to transitions in the free base porphyrin become degenerate, and the absorption from these transitions overlap. Thus, the absorption of the Q bands will be reduced to two bands for metallated porphyrins.

A typical linear absorption spectrum for the unsubstituted free base tetraphenylporphyrin is shown below in Figure 2.9. For clarity, the Q band region is magnified by a factor of 5, displaying the four Q bands characteristic of free base porphyrins.

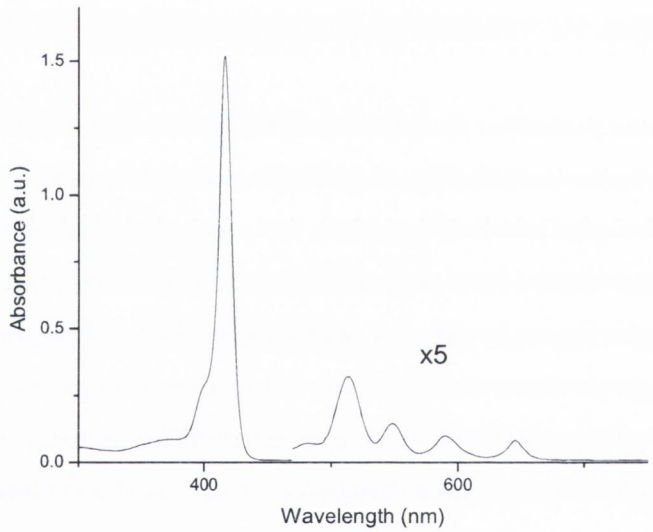

Figure 2.9: UV-Visible absorption spectrum of Tetraphenylporphyrin (TPP) in the solvent Dimethylformamide (DMF)

The absorption spectra in the visible range have been successfully described by a four orbital model. The four orbitals involved are the HOMO−1, HOMO (Highest Occupied Molecular Orbital), LUMO (Lowest Unoccupied Molecular Orbital) and LUMO+1 which are π and π^* orbitals from the porphyrin structure. The Soret band consists of transitions involving the a_{1u} and the e_g orbitals while the Q bands are described by transitions involving

the a_{2u} and the e_g orbitals (See Figure 2.10 below).

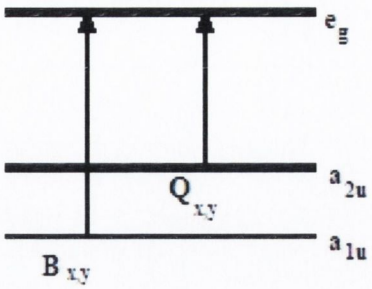

Figure 2.10: The four orbital model. The LUMO and LUMO+1 orbitals are the degenerate e_g orbitals

Binding of a (closed shell) metal does not give rise to new transitions, but interaction with the metal d orbitals will cause a shift of the π orbitals on the porphyrin ring. The a_{1u} MO (molecular orbital) has nodes on the nitrogens, and does not interact directly with the metal orbitals, while the a_{2u} MO will be shifted by interaction with metal orbitals. Thus, metalation of the porphyrin will change the Q bands by degeneration of the two bands and also by a change of the energy. Further, the intensity of the Q transition can be correlated with the interaction with the bound metal. The four methine carbons in the porphyrin skeleton are denoted meso positions, and the a_{1u} orbital has nodes at these positions while the a_{2u} orbital places considerable electron density here. Hence, substitutions on the meso positions are likely to affect the absorption spectrum mostly in the Q bands. The β carbons at the pyrrole rings have more charge in the a_{1u} orbital than in the a_{2u}, and therefore the absorption spectrum is expected to be changed in the Soret band upon substitution on the pyrrole rings.

2.2.2 Polymers and Oligomers

Both polymers and oligomers are one- dimensional macromolecules, constructed from many repetition units which are known as monomers. Monomers are small units consisting mainly of carbon, oxygen and hydrogen atoms which form the building blocks for chains of oligomers and polymers.

The electronic characteristics of the resulting chain are determined by the number

of repeated monomer units, and the resulting molecule is known as an oligomer (for more than two and less than approximately 15 repetition units), or a polymer (for long chains). The line between an oligomer and a polymer is very poorly defined. Long undisturbed chains of perfect repetition are rare, so very often the transition from oligomers to polymers is set for 10-15 repetition units for a molecule. The key difference between them is that for polymers, the states are assumed close enough to be approximated with a bandstructure. In contrast, this assumption cannot be made for oligomers, as distinct energy levels still exist.

Conjugated polymers are characterised by their highly delocalized electronic states.[9] Band theory states that in order for electronic conduction to occur in a material, a continuous system of strongly interacting atomic orbitals is necessary, leading to the formation of band-like electronic states, and an insufficient number of electrons must be present to fill these bands. For traditional conductors such as metals, the atomic orbitals of each atom overlap with each other in the solid state in such a way as to create a number of continuous energy bands comprised of closely spaced energy states. Thus, the electrons are delocalized throughout the entire array of atoms. Between these energy bands is the band gap- a range of energies forbidden to the electrons. The highest occupied energy band is referred to as the valence band whereas the lowest unoccupied band is called the conduction band. If the valence band is only partially filled, the electrons in this band may move under an applied electric field, resulting in metal like conduction. If the valence band is completely filled, conduction can only occur when electrons are promoted into the conduction band across the band gap, leaving a hole in the valence band and adding free electrons to the empty conduction band.

The bandwidth, or the spread of energy levels available to the electrons within each band is determined by the strength of the interaction between the overlapping orbitals which in turn establishes the extent of delocalization that is possible for a given system. The greater the degree of electron delocalisation, the larger the bandwidth, and the higher the mobility of the carriers within the band.

It is therefore clear that electronic conduction is optimised for a continuous system of overlapping atomic orbitals which establishes the delocalized electronic states needed for

ease of electronic movement in an electric field.

For saturated polymers however, the molecular orbitals responsible for bonding the carbon atoms of the chain together are sp^3 hybridized sigma orbitals. In such bonds, the electrons involved in bonding are strongly localized between the carbon atoms that they hold together and cannot contribute to the conduction process without potentially altering the molecular structure of the polymer. In terms of a simple band theory, this type of bonding produces a large energy gap between the highest occupied energy band (which is completely filled) and the lowest unoccupied energy band imparting to the material the characteristics of a good electrical insulator. (e.g. a saturated polymer like polyethylene)

A conducting polymer therefore requires the existence of a bonding system that provides a continuous system of atomic orbitals that can approach each other closely enough to allow the formation of delocalized electronic states, such as the pi bonds formed in molecules containing conjugated unsaturated bonds.

As previously mentioned, a conjugated polymer consists of an approximately planar sequence of alternating single and multiple bonds along its backbone. In such a system, each carbon atom is fitted with a p_z orbital which is oriented perpendicular to the polymer backbone and capable of overlapping with its neighbours. These dumbbell shaped p_z orbitals are arranged out of plane and form low energy π- bonds. When a large number of these sp^2 hybridized carbon atoms bond in a polymer chain, extensive delocalized molecular orbitals are formed where the π-electron orbitals overlap. This electronic delocalization results in an electron cloud forming above and below the plane of the polymer chain along its conjugation length.

Although the chain efficiently lowers its energy by means of alternating short and long bonds, this in fact limits the extent of electronic delocalization possible along the polymer backbone. Adding additional conjugated bonds to the chain will not produce a corresponding increase in the length over which the electrons are delocalized as this value is determined by bond alternation effects. For most bond alternating polymer chains the maximum extent of delocalization is obtained when about 15-20 multiple bonds are linked together.

Due to the low energy and extensive delocalization of these π bonds, much less

energy is required to excite them. These electrons are highly mobile and loosely bound to a particular atom, and are therefore free to move over the conjugation length of the polymer. As each bond consists of two overlapping orbitals, which can each accommodate two electrons, it follows that each bond can accommodate four electrons, two in each energy level, of opposite spins. Each level contains only two electrons, and is therefore only half-filled. For conjugated polymers, with overlapping pi bonds, the result is a half-filled band. This is similar to a metallic electron structure, where energy levels alter to form a tightly spaced band, due to the Pauli Exclusion Principle. Large molecular orbital perturbations may easily be achieved through excitations of the π-electrons, inducing a large polarization in the molecule.

Upon interaction with a photon of light of the appropriate energy, an electron in the ground state undergoes a $\pi - \pi^*$ transition whereby it is promoted from the HOMO to the LUMO. The probability of transition between two states is proportional to the overlap of ground and excited state wavefunctions. As electronic transitions occur about 100 times faster than vibrational excitations (10^{-15} s compared to (10^{-13} s) the nuclei do not have a chance to change configuration over the time scale of the electronic transition. This is known as a vertical Franck-Condon transition. Following this transition, the nuclei are not at their equilibrium position and so must vibrationally relax to their lowest energy state. This is possible because the lifetime of a singlet excitation is about ten times longer than the timescale of vibrational relaxation. Upon subsequent radiative relaxation of the electron into the ground state the nuclei must once again vibrationally relax into the lowest vibrational state. Photoemission is therefore always at an energy lower than that of absorption. The difference in energy between absorption and emission is known as the Stokes shift.

2.2.3 Carbon Nanostructures

Physical Properties

Since their discovery,[10] carbon nanotubes (CNTs) have attracted huge scientific interest due to their unique electrical, mechanical and optical properties. CNTs constitute ideal low dimensional materials with characteristics such as diameter dependent band gap and the

presence of singularities in the density of states (DOS) ensuring that CNTs are promising materials for a host of applications. Over the past decade some of their properties have been harnessed by industry, such as the production of high strength lightweight composite materials. There remains, however, a multitude of possibilities for these materials. An ideal nanotube can be thought of as a hexagonal network of carbon atoms that has been rolled up to make a cylinder. These tubular carbon molecules have diameters typically ranging from 1nm to approximately 50nm and lengths on the order of tens of μm's, with each end "capped" with half of a fullerene molecule.

There are two main types of CNTs: multi-walled carbon nanotubes (MWNTs) and single walled carbon nanotubes (SWNTs). Single-wall nanotubes can be thought of as the cylindrical fundamental building blocks of both multi-wall nanotubes and of carbon nanotube ropes, which are ordered arrays of single-wall nanotubes. SWNTs consist of a single graphene sheet wrapped up to form a tube. MWNTs were discovered first in 1991[10] and were seen to consist of multiple concentric shells of these single wall nanotubes, composed entirely of sp^2 hybridised carbon bonds.

There are many different ways this wrapping can be accomplished. In principle the ends of any vector connecting two crystallographic equivalent points can be joined to form a CNT. Any such vector, C, is a linear combination of the two lattice translation vectors, a_1 and a_2. The integer indices (n,m) provide a crystallographic description of the CNT. Three types of single wall nanotube are possible- armchair, zigzag and chiral nanotubes- which differ in the angle at which the two-dimensional graphene sheet is rolled up and wrapped around onto itself.[11] A diagram of the three different nanotube types is shown in Figure 2.11.[12]

Of these, zigzag and armchair nanotubes have particularly high symmetry. For zigzag nanotubes, the rows of the lattice structure are perpendicular to the nanotube axis. These nanotubes have chiral vectors of the form (n, 0). On the other hand, for armchair nanotubes, which have (n, n) chiral vectors, the rows of the lattice structure lie in the same direction as the nanotube axis. These different types are most easily explained in terms of the unit cell of a carbon nanotube. A general carbon nanotube may be specified in terms of the tubule diameter dt and the chiral angle θ which are shown in the diagram below. As

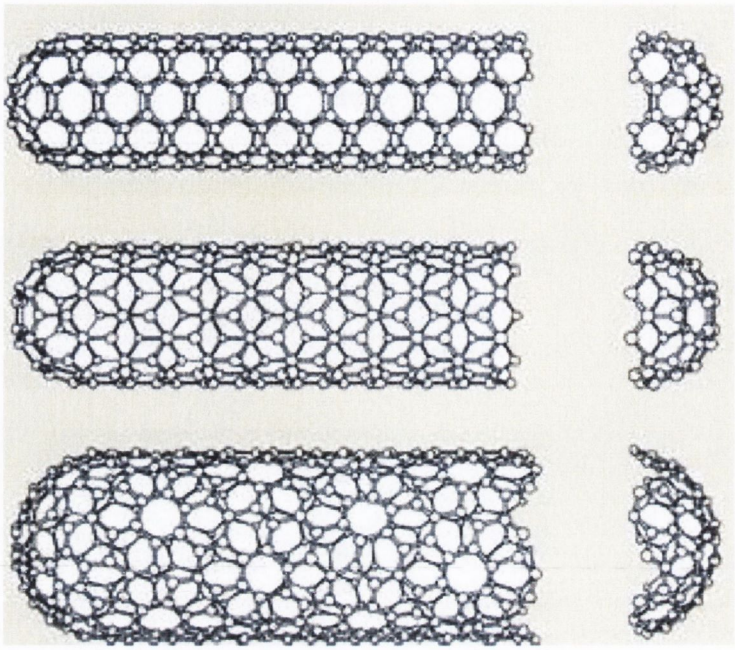

Figure 2.11: Nanotubes are formed by rolling up a graphene sheet into a cylinder and capping each end with half of a fullerene molecule. Shown here is a (5, 5) armchair nanotube (top), a (9, 0) zigzag nanotube (middle) and a (10, 5) chiral nanotube. The diameter of the nanotubes depends on the values of n and m.

previously mentioned, the chiral vector C_h is defined in terms of the integers (n,m) and the basis vectors a_1 and a_2 of the honeycomb lattice by the relationship

$$C_h = na_1 + ma_2 \tag{2.1}$$

The integers (n,m) uniquely determine d_t and θ. The length L of the chiral vector C_h is directly related to the tube diameter dt. The chiral angle theta between the C_h direction and the zigzag direction of the honeycomb lattice (n,0) is related to the integers (n,m) by the following equations:

$$\sin\theta = \frac{\sqrt{3}m}{2\sqrt{n^2 + m^2 + nm}} \tag{2.2}$$

$$\cos\theta = \frac{2n + m}{2\sqrt{n^2 + m^2 + nm}} \tag{2.3}$$

$$\tan\theta = \frac{\sqrt{3}m}{2n+m} \tag{2.4}$$

where the chiral angle is given by θ and all SWNTs have θ values of between 0 and 30^o.

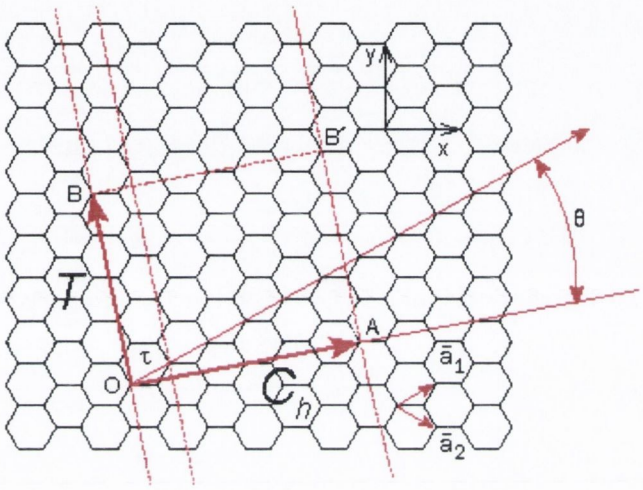

Figure 2.12: The unit cell of the carbon nanotube

The unit cell of the carbon nanotube is shown in Figure 2.12 as the rectangle bounded by the vectors C_h and T, where T is the 1D translation vector of the nanotube. (Picture and caption from Physics World website).[13] The vector T is normal to C_h and extends from the origin to the first lattice point B in the honeycomb lattice.

Electronic Properties

The remarkable electrical properties of CNTs, specifically SWNTs, stem from the unusual electronic structure of graphene. Its band structure is quite unusual, as it has conducting states at the Fermi energy, but only at specific points along certain directions in reciprocal space, namely at the corners of the first Brillouin Zone. For this reason, it is known as a zero band gap semiconductor.

As SWNTs display quantum confinement of electrons normal to the CNT axis,

the band structure of single walled nanotubes can be derived directly from that of graphene by imposing strict periodic boundary conditions for translations by the chiral vector that defines the nanotube, permitting only certain wave vectors, k to exist in the circumferential direction. These periodic boundary conditions around the circumference of the nanotube are a result of the perfect rotational symmetry of the (defect free) graphene nanotubes. Consequently, the electronic density of states (DOS) must also have this periodicity. This is known as the Born- von Karmen boundary condition, and all allowed electronic states obey this condition. The allowed k values are then quantized in the direction perpendicular to the Chiral vector C such that $k.C = 2\pi n$,where n is an integer. Applying this model to the electronic structure of the nanotube, it is clear that it is strongly dependent on the circumference of the nanotube and therefore on (n,m) of the chiral vector. If allowed states exist at the Fermi energy, the nanotube will be metallic; conversely if a bandgap exists at the Fermi level, it will be semiconducting.

In general, an (n,m) nanotube will have a band gap unless $\frac{n-m}{3} = p$, where p is an integer. It is then immediately evident that one third of all possible chiral vectors (or possible nanotubes) are metallic, and that all armchair nanotubes (n=m) are metallic. In fact, the bandgap in SWNTs is inversely proportional to the tube diameter and is given by

$$E_g = \frac{2r_{C-C}\gamma_0}{d} \tag{2.5}$$

This is consistent with the curvature of the lattice inducing a strain in the graphene sheet, resulting in the electronic bandgap. As the tube diameter increases and the curvature consequently decreases, the strain is lowered and the bandgap reduces. Thus, where the diameter tends to infinity, the result is a flat semiconducting graphene sheet with zero bandgap, otherwise known as graphite.

Another notable feature of the electronic structure of nanotubes which is generally observed in SWNTs due to the confinement of the electronic wavevectors is the presence of van Hove singularities in the density of states on the tube. These are a direct consequence of the one dimensional nature of the nanotube and may be attributed to the confinement of the electronic wave vectors parallel to the nanotube axis. In the density of states they appear as sharp spikes arranged symmetrically about the Fermi level. The electronic transitions

which are possible between mirror image singularities for various nanotubes are indicated in Figure 2.13 below:

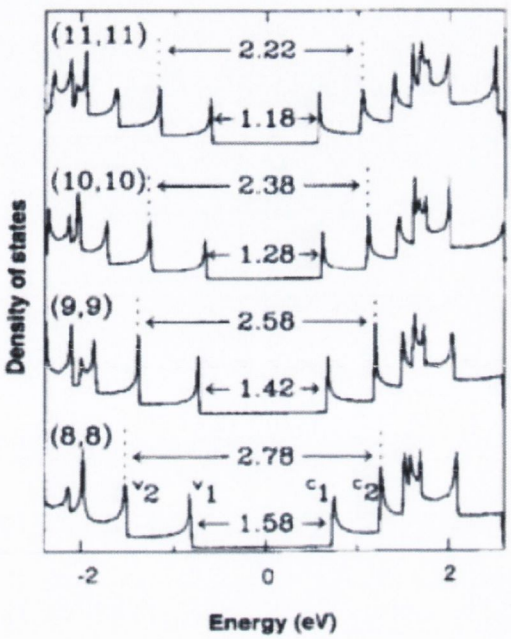

Figure 2.13: Transitions possible between mirror image singularities in CNT DOS

The dependence of the nanotube chiral vector on the positioning of the singularities about the bandgap is illustrated in this figure. The evolution of the singularities with tube size is also indicated with the inverse relationship between band gap and tube diameter evident.

Multi- walled nanotubes (MWNT) consist of many concentric singlewalled cylinders, which may interact with each other and greatly complicate their electronic structure. The DOS of a MWNT is much more complex than that of its SWNT counterparts, however it is generally thought that the outer shell dominates the electronic structure, as it is this that interacts with the ambient environment in which the tube resides.[14]

Optical Properties of Carbon Nanotubes

The electronic absorption spectrum of individual single walled carbon nanotube samples yields a range of peaks across the UV-Vis- NIR corresponding to the individual transitions between the various Van Hove singularities in the density of states (DOS). A typical spectral structure is shown below in Figure 2.14, which has been interpreted as a superposition of distinct electronic transitions from a variety of fullerene nanotubes isolated within columnar SDS micelles.[15]

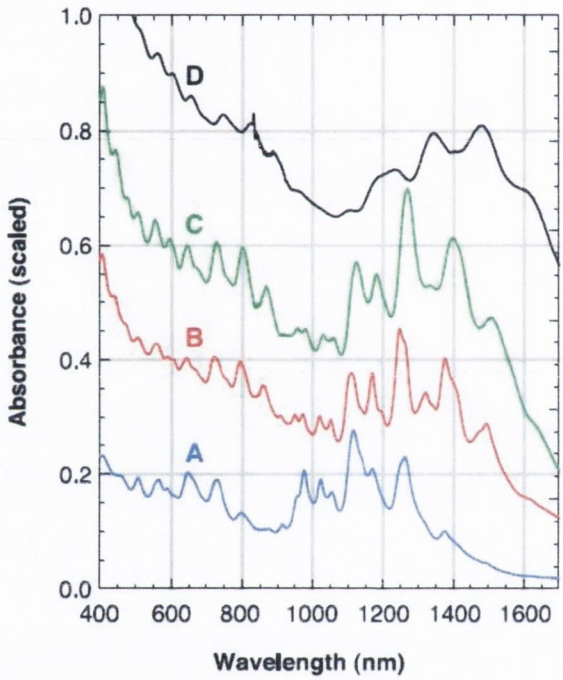

Figure 2.14: Absorption spectra of fullerene nanotubes in SDS-D_2O suspension. The top trace D is typical of tubes prepared in suspension without centrifugation. The broadened and redshifted absorption features show that most nanotubes in the sample are aggregated in small bundles. Trace C is from individual SDS micelle coated nanotubes after addition of PVP. Traces B and A are from samples of individual nanotubes separated and solubilized by SDS micelles. Nanotubes in sample A have a smaller average diameter than in B because they were grown under a higher CO pressure.

Theory predicts that the electronic structure of a single-walled carbon nanotube, including semiconducting versus metallic character, depends on the diameter and chiral

wrapping angle describing its construction from a graphene sheet.[16] Quasi one-dimensionality causes the electronic density of states to have a series of sharp van Hove maxima at energies dependent mainly on tube diameter. The optical absorption spectrum of a particular tube is expected to be dominated by a series of relatively sharp interband transitions, at energies denoted E_{11}, E_{22}, etc., associated with those van Hove singularities.[17]

The spectra shown in Figure 2.14 are consistent with this expectation, with the first van Hove transitions, E_{11}, of the direct band gap semiconducting tubes falling in the 800- to 1600-nm wavelength range, slightly overlapping the 550- to 900-nm region of their E_{22} transitions. The lowest energy van Hove transitions of the metallic tubes appear between ≈400 and 600 nm. It was found that the spectrum of aggregated nanotubes in SDS micelles, showed features red-shifted and broadened relative to those observed for individual nanotubes. This broadening was attributed to interactions between bundled tubes in side-by-side Van der Waals contact.[18]

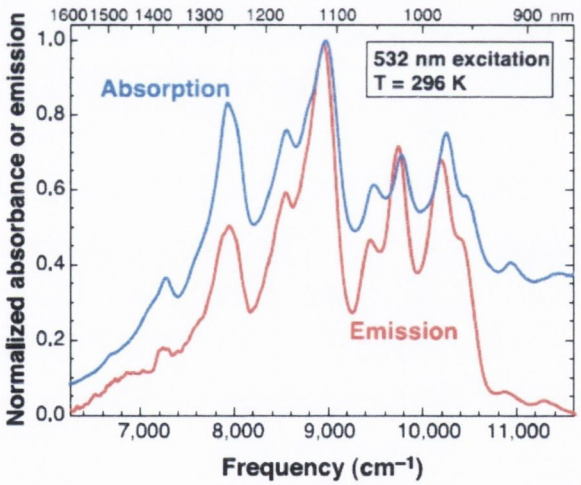

Figure 2.15: Emission spectrum (red) of individual fullerene nanotubes suspended in SDS micelles in D_2O excited by 8 ns, 532-nm laser pulses, overlaid with the absorption spectrum (blue) of the sample in this region of first van Hove band gap transitions. The detailed correspondence of absorption and emission features indicates that the emission is band gap photoluminescence from a variety of semiconducting nanotube structures.

O' Connell et al. also reported a bright, structured photoluminescence displayed in the near infrared from individual fullerene nanotube samples. Figure 2.15 shows the spectrum of this emission from nanotubes in SDS micelles in D_2O after pulsed laser excitation at 532 nm. A striking correspondence of this photoluminescence spectrum was noted with the absorption spectrum of the same sample. It was found that each absorption component in the spectral region of E_{11}- the first van Hove band gap transition for semiconducting nanotubes- present in the emission spectrum, red-shifted by only $\approx$45 cm^{-1} (= 0.01 eV). Therefore the emission was assigned to semiconducting nanotubes.

2.3 Nonlinear Optical Phenomena

The optical response of matter to an incident electromagnetic field manifests itself as an induced polarisation in the material. This polarisation characterizes the response of the material's electric dipoles upon interaction with an oscillating electric field. Under low intensity irradiation the rules of linear optics apply, and materials tend to respond harmonically - i.e. the electric dipoles oscillate at the same frequency as the applied field. However, under high intensity irradiation the electric field can cause large oscillations in the electronic dipoles which become hyperpolarized and facilitate multiphoton interactions. Therefore an anharmonic response of materials observed at high incident optical intensities can be identified with observable physical phenomena such as the emission of radiation at frequencies which are higher harmonics of the incident electromagnetic radiation.

The polarisation vector $\underline{P}$ therefore represents the optical response of any given material. Upon irradiation at low intensities this polarisation is linearly dependent on the electric field strength, $\underline{E}$, and has the form

$$\underline{P} = \underline{P}_0 + \epsilon_0 \chi^{(1)} \underline{E} \tag{2.6}$$

where $\underline{P}_0$ is the static polarisation and $\epsilon_0 \chi^{(1)} \underline{E}$ is known as the linear polarisation ($\underline{P}_{linear}$) where ϵ_0 is the permittivity of free space and $\chi^{(1)}$ represents the material's linear susceptibility and is a second rank tensor describing the linear optical properties of the material such as absorption and emission and reflection. Under the condition of incident light of high

intensity, the linear approximation is no longer accurate, and a series expansion is required to express the induced polarization:

$$\underline{P} = \underline{P}_0 + \epsilon_0(\chi^{(1)}\underline{E} + \chi^{(2)}\underline{E}^2 + \chi^{(3)}\underline{E}^3 + ...) \tag{2.7}$$

where $\chi^{(m)}$ denote the m^{th} order optical susceptibilities. Expressions with m > 1 constitute the nonlinear optical regime and indicate the involvement of multiphoton interactions. The polarization induced varies with some power of the incident field intensity.

The symmetry relationship $\underline{P}(\underline{E})=\underline{P}(-\underline{E})$ means that even order susceptibilities do not feature in materials with centrosymmetry as is the case for the materials studied here. As $\chi^{(2)}$ does not feature, the next highest term is $\chi^{(3)}$, the third order susceptibility, which has no symmetry restrictions.

2.3.1 Nonlinear Refraction

In the linear regime, the refractive index of a material may be expressed as

$$n_0^2 = 1 + \chi^{(1)} \tag{2.8}$$

Upon the incorporation of the third order contribution, this becomes:

$$n^2 = 1 + \chi^{(1)} + \chi^{(3)}\underline{EE} \tag{2.9}$$

This refractive index, n may also be expressed in the form

$$n = n_0 + n_2 I \tag{2.10}$$

The nonlinearity displayed by the refractive index of a medium manifests itself in a phenomenon called self-focusing. This mechanism is the basis for the z-scan technique which is utilized to measure the nonlinear response of samples throughout this thesis. When an optical beam of non-uniform intensity distribution- such a gaussian shaped laser beam- propagates through a material, self-focusing is observed. For samples where n_2 is positive, the refractive index of the material is much higher for the centre of the beam due to its intensity dependence. The sample consequently behaves as a positive lens, causing the

beam to focus. This phenomenon is the basis of the Z-scan experiment, which is detailed in Chapter 3.

The expression

$$n_2 = \frac{3Re\chi^{(3)}}{4\epsilon_0 c n_0^2} \tag{2.11}$$

describes the relationship between the nonlinear refractive index and the real part of the third order susceptibility.

2.3.2 Nonlinear Absorption

The third order optical susceptibility of a material is a complex entity. While the real part is related to the refractive index of the medium as discussed above, the imaginary part involves the modification of the material's absorption coefficient. The absorption coefficient is linearly dependent upon the incident intensity, and may be expressed in a form similar to that used to describe the refractive index:

$$\alpha = \alpha_0 + \beta I \tag{2.12}$$

where β is the nonlinear absorption coefficient of the material. At higher incident intensities, absorption can either increase or decrease, depending on the sign of the nonlinear absorption coefficient.

Saturable absorption is the phenomenon observed in the event of a negative β value. This leads to a decrease in the absorption coefficient of a material under high intensity irradiation. Materials which have large absorption cross sections in the ground state may behave as saturable absorbers if the population rate of the excited state exceeds the rate of return to the ground state. At higher incident excitation intensities where the photon and population densities become comparable, the absorption coefficient is depleted manifesting itself in a corresponding increase in the transmission observed for the sample. As the excited states become populated, the ground state absorption cross section is reduced because of the decline in the ground-state population. Consequently, the transmission ultimately increases with incident intensity indicating that the ground state absorption has bleached.

Conversely, for Reverse Saturable Absorption (RSA) which is the opposite of saturable absorption, the transmission decreases with increasing incident intensity. This was

initially discussed in 1967[19] and occurs when the excited state absorption cross section is greater than that of the ground state.

Materials which display this nonlinear absorption characteristic are known as optical limiters and may be used to protect sensitive optical sensors and optics from exposure to dangerously high light intensities. Nonlinear scattering and RSA are the two mechanisms responsible for optical limiting behaviour, and are of great commercial importance. One potential application for this effect is sensor protection where the amount of light that can be passed through the protecting medium is limited.

2.4 Organic Materials as Optical limiters

The recent development of readily synthesized and architecturally flexible organic materials have accelerated progress in Nonlinear Optical (NLO) materials over the past decade.[20,21] Consequently, organic materials have emerged as a highly promising family of materials for NLO applications. Their advantages include an ultra fast nonlinear response, a high capacity for multiphoton interactions and hence a large nonlinear optical response, high optical damage thresholds, design flexibility and ease of fabrication. The NLO response of many organic materials is extremely rapid because the effects occur primarily through electronic polarization. This is particularly relevant in systems with π-conjugation as their highly delocalized electronic structure is conducive to facile polarization.

Porphyrins are among the most versatile of organic materials for nonlinear optics, and as such have recently been the focus of intense research activity.[22,23,24,25] Their highly conjugated macrocycle is a structure known to give large optical nonlinearities. Generally, an optimal NLO material has a high dissipative optical nonlinearity, an inherently fast response time, a large dynamic range and a broadband spectral response. In this context aromatic tetrapyrroles such as porphyrins and phthalocyanines are extremely useful and versatile organic nanomaterials. Their immense flexibility allows the manipulation of χ^3 by chemical substitution and provides the possibility of tailoring the nonlinear optical response to a target application. It has been shown that single- and multi- walled carbon nanotubes in suspension also behave as excellent optical limiters. This nonlinear behaviour has been

shown to arise from strong nonlinear scattering due to the creation of new scattering centers by ionized carbon microplasmas and solvent microbubbles.

Improved optical nonlinear behaviour is therefore to be expected from carbon nanotube composite solutions formed with conjugated organic molecules, with an additional scattering component expected to enhance the nonlinear optical limiting behaviour of the molecules. In particular, the optical properties of carbon nanotubes functionalized both covalently and non- covalently with porphyrin molecules are of great interest in both the linear and nonlinear regimes, as their NLO response may potentially be readily tuned. For this reason, we present in this thesis a complete optical characterization of a number of noncovalently- functionalized carbon nanotube composite systems.

Bibliography

1. Website:. *http://en.wikipedia.org/wiki/Carbon (accessed on 1/11/2006)* .

2. Anannarukan, W., Tantayanon, S., Zhang, D., Aleman, E., Modarelli, D., and Harris, F. *Polymer 47, 49364945* (2006).

3. Website:. *http://en.wikipedia.org/wiki/Porphyrin (accessed on 1/11/2006)* .

4. Wasielewski, M. *Chemical Reviews, 92, 435-461* (1992).

5. Ali, H. and van Lier, J. *Chemical Reviews, 99, 2379-2450* (1999).

6. Hayes, R., Wasielewski, M., and Gosztola, D. *Journal of the American Chemical Society, 122, 5563-5567* (2000).

7. Debreczeny, M., Svec, W., Marsh, E., and Wasielewski, M. *Journal of the American Chemical Society, 118, 8174-8175* (1996).

8. Fajer, J., Borg, D., Forman, A., Dolphin, D., and Felton, R. *Journal of the American Chemical Society, 92(II), 3451-3459* (1970).

9. Geoffrey J. Ashwell, E. *"Molecular Electronics", Research Studies Press Ltd. (Pub.)* (find out year).

10. Iijima, S. *Nature, 354, 56* (1991).

11. Website:. *http://physicsweb.org/articles/world/11/1/9 (accessed on 20/10/2006)* .

12. Website:. *http://physicsweb.org/articles/world/11/1/9/1/world%2D11%2D1%2D9%2D2 (accessed on 1/11/2006)* .

13. Website:. *http://physicsweb.org/articles/world/11/1/9/1/world%2D11%2D1%2D9%2D1(accessed on 1/11/2006)* .

14. Brennan, M. *"Ph.D. Thesis, School of Physics, Trinity College Dublin* (2001).

15. O'Connell, M., Bachilo, S., Huffman, C., Moore, V., Strano, M., Haroz, E., Rialon, K., Boul, P., Noon, W., Kittrell, C., Ma, J., Hauge, R., Weisman, R., and Smalley, R. *Science, 297, 593-596* (2002).

16. Saito, R., Dresselhaus, G., and Dresselhaus, M. *"Physical Properties of Carbon Nanotubes" (Imperial College Press, London)* (1998).

17. Saito, R., Dresselhaus, G., and Dresselhaus, M. *Physical Review B, 61, 2981* (2000).

18. Reich, S., Thomsen, C., and Ordejon, P. *Physical Review B, 65, 155411* (2002).

19. Guiliano, C. and Hess, L. *"IEEE Journal of Quantum Electronics, QE-3, 338* (1967).

20. Baldwin, G. C. *"An Introduction to Nonlinear Optics", Plenum Press, New York* (1969).

21. Prasad, P. N. and Williams, D. J. *"Introduction to Nonlinear Optical Effects in Molecules and Polymers", Wiley, New York* (1990).

22. Saleh, B. E. A. and Teich, M. C. *"Fundamentals of Photonics", Wiley, New York* (1991).

23. Ashwell, G. J. and Bloor, D. *"Organic Materials for Nonlinear Optics III", Royal Society of Chemistry, Boston"* (1993).

24. Chemla, D. S. and Zyss, J. *"Nonlinear Optical Properties of Organic Molecules and Crystals Vol. I-II", Academic Press, Orlando"* (1987).

25. Notaras, E. G. A., Fazekas, M., Ni Mhuircheartaigh, E., Senge, M., and Blau, W. *Advanced Materials (In Press)* (Submitted 2006).

Chapter 3

Characterization of Non-Covalently Functionalized Carbon Nanotubes

3.1 Characterization Techniques

The two principle optical characterization techniques utilized in these studies were absorption and luminescence spectroscopy. These are highly versatile techniques, which yield information about the various electronic transitions possible in an organic material and its local environment through examination of optical excitations and de-excitations of the material, and are of great value in analytical chemistry. In order to alter the distribution of electrons in an organic molecular system, energies in the region of several electron volts are required.[1] Photons absorbed or emitted in such processes lie in the visible region of the electromagnetic spectrum. Hence, a wide range of colours is observed for organic materials.

3.1.1 Absorption Spectroscopy

UV-visible absorption spectroscopy involves passing a monochromatic beam of light through a sample and recording its linear absorbance as a function of wavelength over a range extending from the infrared to the ultraviolet region of the electromagnetic spectrum. The resultant spectrum obtained corresponds to electronic excitations between the energy levels of the lowest energy molecular orbitals of the system. The uncertainty caused by lamp

intensity variations at different frequencies is eliminated by comparison of the detected absorption with a blank reference sample in a double beam arrangement. When a beam of light passes through a material, a photon of the appropriate energy may interact with the material, leading to the promotion of an electron into a state of higher energy. This involves absorption of the photon and a reduction in detected beam intensity is subsequently detected. Information about the electronic structure of the material may be deduced through measurement of the light absorbed at a particular wavelength.

At room temperature, the electrons in a molecule at thermal equilibrium typically reside in the lowest vibrational level of the ground state (S_{00}). Almost all excitation transitions therefore occur from this level. As photoexcitation occurs from S_{00} into the excited state vibrational levels, an absorption spectrum yields information on the vibrational energy distribution of the first excited state.

UV-Visible spectroscopy is particularly useful in the identification of conjugated organic systems, as transitions involving lone pairs and π orbitals are of great importance in this technique. In such molecules, $\pi - \pi^*$ transitions are the primary cause of UV-Visible absorption, as the energy gap between the highest occupied molecular orbital (HOMO) and the lowest unoccupied molecular orbital (LUMO) in the ground state is in the near UV to infrared range of the electromagnetic spectrum. The greater the degree of conjugation in a molecule, the smaller the HOMO-LUMO gap and therefore the lower the frequency and higher the wavelength of the corresponding absorption peak observed. The energy required to excite electrons from σ bonds is much higher in the near to far ultraviolet, and so these are unaffected by the measurements performed here. Photoexcitation of these bonds often irreversibly changes the molecular structure, resulting in photo-degradation of the molecule. Each specific part of a molecule is excited at a different frequency, allowing UV-Visible spectroscopy to be used as a diagnostic tool to determine the effect of environmental changes such as concentration-dependent self-aggregation and molecular interaction with solvents and other moities such as carbon nanotubes in solution.

When light passes through a sample, the reduction detected in transmitted beam intensity, dI, is directly proportional to the sample thickness and the incident light intensity, I.

$$dI = -\alpha I dz \tag{3.1}$$

This is known as the Beer-Lambert law and means that the linear absorption coefficient (α) of the material remains constant under low intensity irradiation (i.e. in the linear optical regime). Integrating with limits on dz over the thickness of the material (going from z = 0 to L, where L is the pathlength through the sample) and the limits on dI going from $I = I_{initial}$ to $I_{transmitted}$ gives an expression for the light intensity as a function of thickness.

$$I = I_{initial} e^{-\alpha L} \tag{3.2}$$

It is therefore evident that for a particular frequency, the amount of light absorbed over a specified distance is dictated by the parameter α of the sample. The spectrometer actually measures the absorbance, and so this intrinsic parameter is calculated by dividing the absorbance measured by the pathlength through the sample. Considering that the transmission may be described by $T = I_{transmitted}/I_{initial}$, the Beer-Lambert equation may now be rewritten as

$$T = e^{-\alpha_0 L} = e^{-\sigma_0 N L} \tag{3.3}$$

where σ_0 is the absorption cross section of the ground state to the first excited singlet state transition, and N represents the total number density of absorbing species, which for low excitation density is equal to cN_A where c is concentration and N_A is Avogadro's Number.

Upon passing through a medium, a light beam may also be attenuated by scattering, whereby inhomogenities in the sample cause the light to diffract, changing direction. If a photon's direction is sufficiently altered, it is scattered out of the beam path, and subsequently is not detected. Scattering effects are usually confined to photon energies lower than the band gap and may be neglected in the region of electronic transitions.

3.1.2 Fluorescence Spectroscopy

Fluorescence spectroscopy is a useful technique which is complementary to absorption spectroscopy, since while absorption spectroscopy probes the energies of excitations to higher states, fluorescence spectroscopy probes the energies at which these higher states relax radiatively back to the ground state. Radiation at a fixed wavelength (often the absorption band maximum) is used to photoexcite the material, and the variation in emitted light intensity is recorded as a function of wavelength.

Upon absorption of a photon, a π-electron in a conjugated organic molecule is promoted into a higher vibrational level of the first excited state. This is an unstable excited state, and the electron subsequently may lose this excess energy in a number of ways, both radiative and non-radiative in which the energy is lost as photons and vibrational phonons respectively. Neglecting intersystem crossing and internal conversion, the electron falls very rapidly through the vibrational manifold to the lowest energy level of that excited state. The electron subsequently radiatively decays from the lowest vibrational level in the first excited state to the vibrational levels of the ground state.

As radiative relaxation always takes place from only one level in the excited state to the vibrational levels in the ground state, information on the vibrational energy level distribution of the ground state may be deduced from the resultant photoluminescence spectrum. The emission spectrum is invariably red shifted relative to the absorption spectrum of the molecule. This red shift is termed the Stokes shift and is caused by the molecule losing energy through thermal relaxation after the initial photoexcitation.

3.1.3 Z-scan Technique Overview

The Z-scan technique was first described in 1990 by Mansoor Sheik-Bahae, Ali A. Said, Tai-Huei Wei, David J.Hagan and E.W. Van Stryland[2] and has since become a standard tool in the field of nonlinear optics, aiding a facile determination of the sign of the nonlinearity and both real and imaginary third order susceptibility coefficients. It is a sensitive single-beam technique for measuring both the nonlinear refractive index and nonlinear absorption coefficient for a wide variety of materials. The nonlinear response of the sample under

study induces changes in beam curvature, which is then readily translated into detectable transmittance changes. The Z-scan principle involves traversing the sample under study along the path of a tightly focused Gaussian beam thereby subjecting it to a large range of intensities.

A schematic of an open aperture Z-scan experimental arrangement is shown below in Figure 3.1. When the incident irradiation intensity rises above a threshold value, nonlinear optical behaviour may be induced in a sample. The transmitted power is measured as a function of sample position in the far field, using two detectors, one apertured and one unperturbed. The apertured detector is sensitive to the nonlinear refractive index of the sample, which is related to the real $\chi^{(3)}$ response. This setup is referred to as 'closed z-scan'. In the absence of an aperture, transmittance changes due only to nonlinear absorption are detected, and this is referred to as 'open z-scan'.

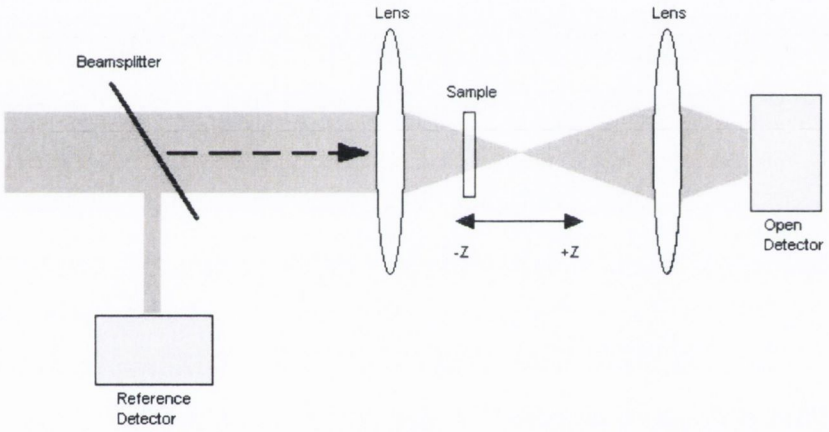

Figure 3.1: Schematic for the Open Aperture Z-scan technique

Closed Aperture Z-scan Measurement of Refractive Nonlinearities

During the closed aperture Z-scan measurement, the transmittance of a nonlinear medium is measured through a finite aperture in the far field as a function of the sample position z measured with respect to the focal plane using a single Gaussian laser beam in a tight focus geometry. Assuming a material with a negative nonlinear refractive index and a

thickness smaller than the diffraction length of the focused beam (a thin medium), this can be regarded as a thin lens of variable focal length.[2] Starting the scan from a distance far away from the focus (negative z), the beam irradiance is low and negligible nonlinear refraction occurs; hence, the transmittance remains relatively constant. The beam irradiance increases as the sample approaches the focus, leading to self-lensing in the sample. A negative self-lensing prior to focus will tend to collimate the beam, causing a beam narrowing at the aperture which results in an increase in the measured transmittance. As the scan in z continues and the sample passes the focal plane to the right (positive z), the same self-defocusing increases the beam divergence, leading to beam broadening at the aperture, and thus a decrease in transmittance. This suggests that there is a null as the sample crosses the focal plane. This is analogous to placing a thin lens at or near the focus, resulting in a minimal change of the far-field pattern of the beam. The Z-scan is completed as the sample is moved away from focus (positive z) such that the transmittance becomes linear since the irradiance is again low.

A prefocal transmittance maximum (peak) followed by a postfocal transmittance minimum (valley) is, therefore, the Z-scan signature of a negative refractive nonlinearity. Positive nonlinear refraction, following the same analogy, gives rise to an opposite valley-peak configuration. It is an extremely useful feature of the z-scan method that the sign of the nonlinear index is immediately obvious from the data, and as we will show in the following section, the magnitude can also be easily estimated using a simple analysis for a thin medium.

Open Aperture Z-scan Measurement of Absorptive Nonlinearities

In the above discussion, the effects arising from nonlinear absorption are completely neglected. Qualitatively, multiphoton absorption suppresses the peak and enhances the valley, while saturation produces the opposite effect. The sensitivity to nonlinear refraction is entirely due to the aperture, and removal of the aperture completely eliminates the effect. However, in this case, the z-scan will still be sensitive to nonlinear absorption. Nonlinear absorption coefficients can be extracted from such open aperture experiments.

The open aperture Z-scan corresponds to the measurement of the total transmit-

tance through the sample in the absence of an aperture in front of the detector. It is only sensitive to the nonlinear absorption corresponding to the imaginary component of the nonlinearity. Both saturable and reverse saturable nonlinear absorption exist, depending on the sign of the nonlinear absorption coefficient β of the material being studied.

In order to measure the nonlinear absorption behaviour of a system, a z-scan with a fully open aperture is used, which detects the total transmittance through the sample and is not sensitive to nonlinear refraction in the sample with only the imaginary component of the materials nonlinearity detected. The intensity dependent absorption coefficient at first approximation varies linearly with the incident intensity I_0 as

$$\alpha(I) = \alpha_0 + \beta I_0 \tag{3.4}$$

For RSA (reverse saturable absorption) and TPA (two-photon absorption) $\beta > 0$ and the absorption coefficient is therefore described by Equation 3.4 with β positive. In this case the transmittance as a function of position z, $T_{op}(z)$ has been calculated[2] and is equal to

$$T_{op}(z) = T_0 \sum_{m=0}^{\infty} [-q_0(z,o)]^m/(m+1)^{3/2} \tag{3.5}$$

where T_0 is the linear transmittance at low intensity and is equal to $e^{-\alpha_0 L}$, and

$$q_0(z,0) = \beta I_0(t=0) L_{eff}/(1+z^2/z_0^2), \tag{3.6}$$

where $L_{eff} = (1-e^{-\alpha_0 L})/\alpha_0$. However, Equation 3.5 is only true while

$$|q_0(z=0,0)| < 1. \tag{3.7}$$

The calculation of the $Im\chi^{(3)}$ value involved computing the β values which are calculated from the fitting of Equation 3.5 to the open Z-scan curves. Imaginary $\chi^{(3)}$ ($Im\chi^{(3)}$) is then given by

$$Im\chi^{(3)}(esu) = \frac{10^{-6}}{480\pi^2} c n_0^2 \beta \tag{3.8}$$

Experimental Setup

The schematic for the Z-scan apparatus used is illustrated in Figure 3.1 and in Figure 3.2 below (Image from Ph.D. Thesis, James J. Doyle, Trinity College Dublin, 2007[3]). Measurements performed during the optical limiting experiments described in this thesis were taken using the open aperture of this setup with 6 ns pulses from a Q switched nanosecond Nd:YAG laser system. This laser was operated at a slow repetition rate of 10 Hz in order to minimise thermal effects. The laser beam was spatially filtered with an aperture, removing the higher order modes and yielding a more Gaussian profile, and then tightly focused with a 9 cm focal length lens.

The output of the laser in the mode of operation used was 532 nm pulses. As the fundamental mode of the Nd:YAG laser outputs photons of wavelength 1064 nm, frequency doubling was employed to obtain the required wavelength. During this process two 1064 nm photons are absorbed simultaneously by a doubling crystal in a two- photon absorption process and reemitted as a single photon with double the energy, double the frequency and half the wavelength. Thus the reemitted photon is at a wavelength of 532 nm. All measurements were performed in quartz cells of 1cm pathlength.

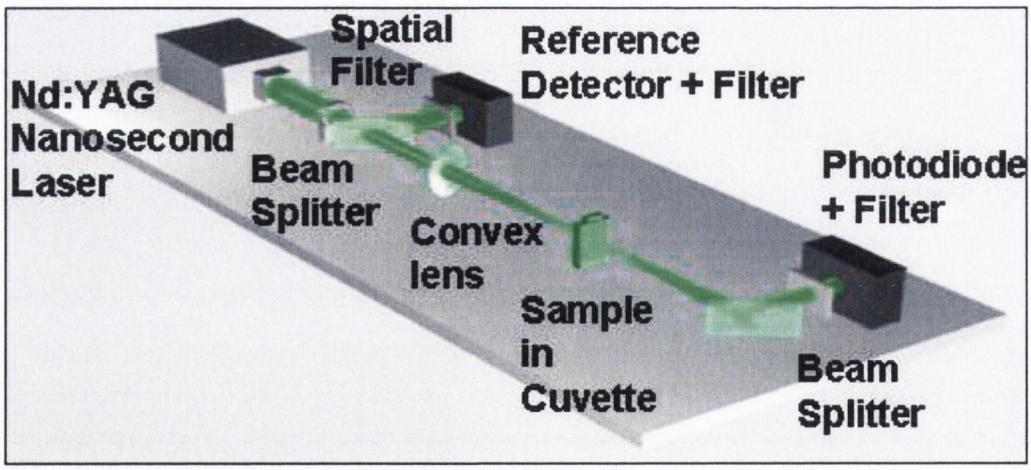

Figure 3.2: Experimental Setup for the Open Aperture Z-scan technique (*Image from Ph.D. Thesis, James J. Doyle, Trinity College Dublin, 2007*)

Bibliography

1. W., A. P. *"Physical Chemistry", Oxford University Press* (1990).

2. Sheik-Bahae, M., Said, A., Wei, T., Hagan, D., and Van Stryland, E. *IEEE Journal of Quantum Electronics. 26(4), 760* (1990).

3. Doyle, J. J. *Ph.D. Thesis, Trinity College Dublin* (2007).

Chapter 4

Characterization of Carbon Nanotube Interactions with Conjugated Polymers and Organic Molecules

4.1 Carbon Nanotube Bundles

SWNT do not typically exist as isolated entities, instead forming nanotube bundles or ropes, as illustrated in Figure 4.1 (Image taken from literature[1]). To form these bundles, SWNT are attracted to each other by Van der Waals forces which are formed between the π clouds surrounding two adjacent nanotubes. These nanotubes consequently pack tightly together in a trigonal lattice, forming nanotube bundles, resulting in nanotube insolubility in common organic solvents such as chloroform and toluene.

SWNT dispersion in solution therefore involves nanotube debundling. An ideal dispersant would maintain the superior electrical and mechanical properties which lend such promise to nanotubes as potential future materials. Dispersion by means of non-covalent nanotube functionalization is ideal for this purpose, as the SWNT extended π-system remains unaffected and the unique nanotube properties are not compromised.

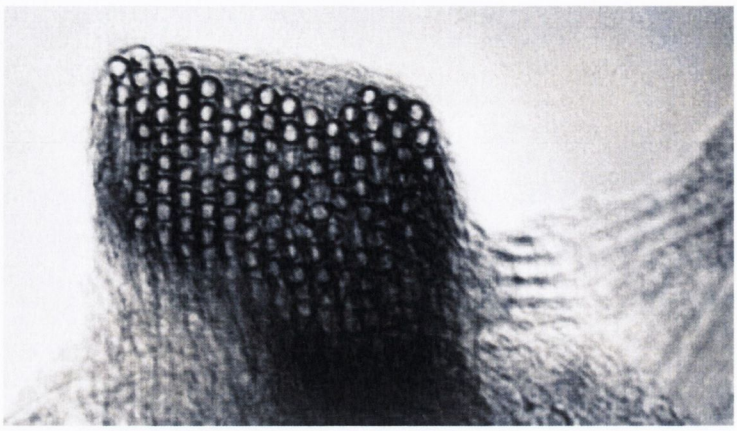

Figure 4.1: Singlewalled Carbon Nanotube bundle

In this thesis, the interaction of SWNTs with conjugated luminescent molecules is investigated. This non-covalent functionalization is achieved through Van der Waals interactions between the extended π-systems of the nanotubes and the conjugated organic molecule in question.

4.1.1 Photoluminescence Quenching Model

Recently Coleman et al.[2] have modelled and performed measurements on a system consisting of polymer- single walled carbon nanotubes dispersed in solution as a function of concentration. In the system examined, the composites were prepared with the polymer and nanotube masses in equal proportions. The level of polymer coating the carbon nanotubes was therefore low. Certain amounts of the polymer in such a system will bind to the nanotubes and the remaining polymer will explore the solution through thermal diffusion. At equilibrium, this system will undergo continuous transitions of adsorption and desorption of the polymer to the nanotubes or nanotube bundles. The photoluminescence (PL) efficiency of the bound polymer molecules is expected to be low as any photo- generated singlet excitons preferentially decay non- radiatively through the fast vibrational manifold of the nanotubes, so the polymer bound to the nanotubes will not fluoresce whereas the free polymer molecules will. Thus any observed PL from the polymer / SWNT composite solutions is due to the free polymer only. If one therefore measures the photoluminescence

intensity of two polymer solutions at equivalent concentrations,one with SWNTs and the other without, the ratio of these photoluminescence intensities is a measure of the fraction of free polymer in the solution. A subsequent plot of the fraction of free polymer as a function of concentration shows itself to be highly nonlinear, implying complicated behaviour occurs during the adsorption- desorption process as a function of concentration. At very low concentrations the plot approaches 1, indicating that most molecules are unbound at low concentrations.

This behaviour was accurately modelled by Coleman et al. by considering the adsorption- desorption kinetics as a function of concentration. They considered that at thermal equilibrium, the adsorption rate of polymer molecules to the nanotubes should be equal to the desorption rate. However, the adsorption rate is primarily dependent upon spatial considerations, such as the likelihood of a free polymer molecule encountering a dispersed SWNT bundle, while the desorption rate is dependent upon the Van der Waals binding energy of the polymer molecule to the carbon nanotube.

The adsorption rate $(-dN/dt)$ was thus derived as:

$$-\frac{dN}{dt} = \frac{24DR}{\pi}\frac{N_F}{V}\int_{z=-A}^{z=-A}\int_{\rho=R}^{\rho=A}\int_{u=-l/2}^{u=l/2}\frac{\rho^2 d\rho du dz}{(\rho^2+(u-z)^2)^{5/2}} = \frac{24DR}{\pi}\frac{N_F}{V}f \tag{4.1}$$

where f is the value of the triple integral and A is the spatial extent of the volume of solution per bundle; $V_{\text{bun}} = 2\pi A^3$. $\frac{N_F}{V}$ is the number of free molecules per unit volume, D is the diffusion coefficient for the polymer molecules and R is the radius of the nanotube bundle.

For extended polymer molecules on graphite surfaces, desorption has been shown to follow first order kinetics, and so the desorption rate $(-dN/dt)$ was derived as being:

$$-\frac{dN}{dt} = v\frac{N_B}{V}\frac{m_{bun}}{C_{NT}}e^{-\frac{E_B}{kT}} \tag{4.2}$$

where $\frac{N_B}{V}$ is the number of bundles per unit volume, m_{bun} is the bundle mass and E_B is the polymer- nanotube binding energy.

At equilibrium, the adsorption rate equals the desorption rate, so by equating Equations 4.1 and 4.2 above and noting that $m_{bun} = \rho_{bun}R^2 l$ and the bundle surface area,

$A_{bun} = 2\pi Rl$, we get

$$\frac{N_B}{N_F + N_B} = \frac{1}{1 + C_{NT}/C_0} \tag{4.3}$$

where

$$C_0 = \frac{\pi^2 \nu \rho_{bun} A_{bun} e^{-\frac{E_B}{kT}}}{48Df} \tag{4.4}$$

where C_0 is a characteristic concentration, ρ_{bun} is the bundle mass density, N_F is the number of free molecules, N_B is the number of bound molecules and so $\frac{N_F}{N_F+N_B}$ is the fraction of free polymer.

Coleman et al. described the fraction of free polymer as a function of concentration in the composite solutions with Equation 4.3 above. If the characteristic concentration, C_0, were constant, the fraction of free polymer would be expected to decrease monotonically with increasing concentration. Their experimental results showed that this was clearly not the case. As the polymer- nanotube binding energy is expected to be constant, Coleman thus surmised that the bundle surface area must in fact vary with concentration.

This theory was tested by transformation of their experimental data to represent C_0 as a function of nanotube concentration, using Equation 4.3. These data showed that C_0 decreased consistently as the concentration was decreased, before saturating at a minimum value at low concentrations. As C_0 is directly proportional to A_{bun}, this suggested that as the concentration is decreased, the bundles spontaneously break up. As they reach a minimum size, this suggests that individual nanotubes are stable in low concentration solutions.

Results and Discussion

As single-wall carbon nanotubes (SWNT) almost always exist in the form of rope-like bundles, their applications are severely restricted. Using the simple adsorption/desorption equilibrium model described above, the dispersing capability of polymers and their short chain analogues can be qualitatively investigated, and the concentration at which individual SWNTs are observed for each system may be calculated. A number of carbon nanotube com-

posite systems were characterised, using the spectroscopic techniques previously described. The organic molecules employed in the investigation of non-covalent functionalization of SWNT included the polymers PmPV and PFO, and the molecules 2,5- dioctyloxy-1,4- distyrylbenzene molecule (pDSB), 1,4-bis-octyloxy-2,5-bis [2-(4-styryl-phenyl)-vinyl]-benzene (PVB) and 2,5- dioctyloxy-1,4-dinaphthylvinylbenzene (pDNB) in addition to various short fractions of PmPV.

Experimental Procedures

The purified nanotubes used in these studies were prepared by the HiPCO process,[3] supplied by Carbon Nanotechnologies Inc. (lot # PO289) and used without further treatment. The HPLC- grade chloroform used was purchased from Aldrich. Sonication was performed using a high power ultrasonic tip, model GEX600 (120W, 60kHz). Two identical chloroform solutions of each molecule were prepared and pure HiPCO SWNTs were then added to one solution, such that the molecule -SWNT mass ratio was 2:1. Both of these high concentration stock solutions were subsequently sonicated for 2 minutes using a high-power sonic tip (200 Watts at 20%). Each solution was serially diluted approximately twenty times to yield a wide concentration range for the series of solutions ($C_{CNT} = 10^{-2}\text{kg/m}^3 - 10^{-8}\text{kg/m}^3 \text{and} C_{\text{Molecule}} = 2x10^{-2}\text{kg/m}^3 - 2x10^{-8}\text{kg/m}^3$). In between dilutions, each solution was again sonicated for 1 minute and all solutions were finally left for 24 hours to come to equilibrium. No sedimentation was observed over this period.

Polymers Studied

Polymer 1:Poly(metaphenylenevinylene-co-2,5-dioctyloxy-para-phenylenevinylene) (PmPV)

In recent years, significant research has been carried out in Trinity College Dublin focussing on nanotube composites of the polymer Poly(metaphenylenevinylene-co-2,5-dioctyloxy-para-phenylenevinylene) (PmPV).[4,5] PmPV is a derivative of poly(p-phenylenevinylene) (PPV), a conjugated, electronically active polymer which is well known for its use in organic LEDs.[6] The molecular structure for this molecule is given below in Figure 4.2.

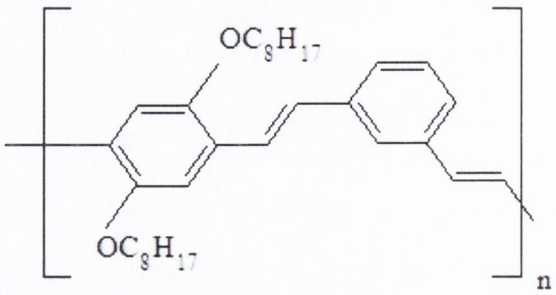

Figure 4.2: Repeat unit chemical structure of poly(metaphenylenevinylene-co-2,5-dioctyloxy-para-phenylenevinylene) (PmPV)

The absorption spectrum for PmPV has been well characterized in the past[7] and consists of two absorption bands centred at 330 nm and 400 nm respectively. In our case, the second absorption peak was found to be at 398 nm, and this wavelength was consequently used as the excitation wavelength in obtaining emission spectra for all solutions studied.

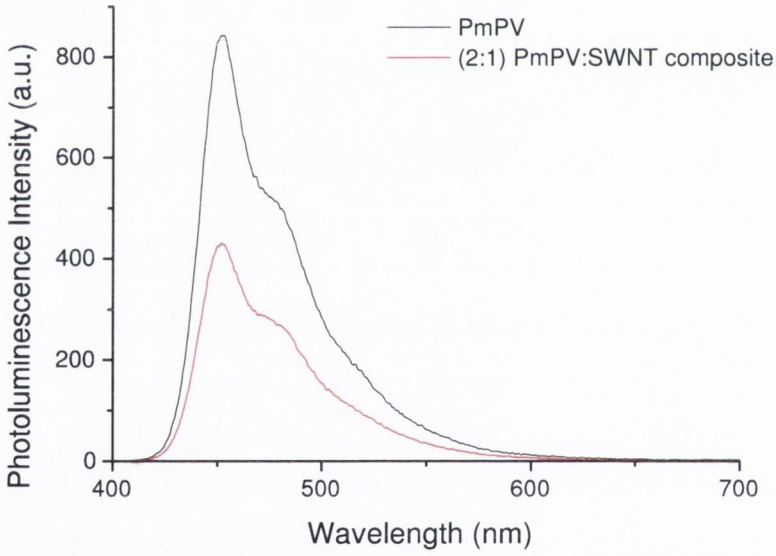

Figure 4.3: Photoluminescence spectra of a solution of PmPV and corresponding PmPV:SWNT (1:1) composite solution (4×10^{-3} kg m^{-3}, $CHCl_3$, 25^{o}C)

An example of typical emission spectra from a PmPV solution and it's corre-

sponding PmPV:SWNT (1:1) composite is shown above (Figure 4.3). These spectra show the photoluminescence observed from the solutions upon excitation at the absorption peak of 398nm. The PL spectra are identical in profile for both solutions, with the composite PL quenched with respect to that of the polymer, as expected upon interaction with the carbon nanotube moieties.

Adsorption/Desorption PL studies

Figure 4.4 below is a plot of the fraction of free polymer against concentration, determined from photoluminescence studies for a 2:1 ratio of PmPV molecules to HiPCO single walled nanotubes. The fraction of free polymer was calculated in the usual way from the ratio of the photoluminescence intensity for a composite solution at the PL maximum of 454nm, to the photoluminescence intensity for the equivalent polymer solution at the same wavelength.

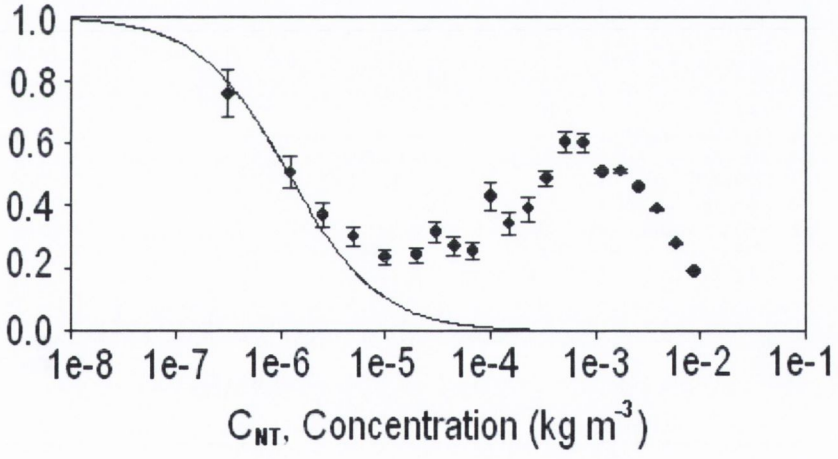

Figure 4.4: Plot of the fraction of free polymer as a function of concentration, determined from PL studies at 454nm for a 2:1 PmPV molecules:HiPCO single walled nanotubes composite solutions. The solid line is a theoretical fit to Equation 4.3 in the low concentration regime.

The nonlinear plot obtained for the 2 : 1 PmPV molecules:HiPCO SWNT compos-

ite is as predicted by the adsorption/desorption model for the low concentration solutions. The solid line is a fit to Equation 4.3 in the low concentration region using the saturation value of $C_0 = 1.2x10^{-6}kgm^{-3}$, and is in excellent agreement with the experimental results for the low concentration solutions. It was not possible to measure more dilute solutions due to the very low signal to noise ratio (SNR) of the PL observed at these lower concentrations. For very low intensity emission spectra, the noise encountered in the observed PL can render the measurements unreliable.

The characteristic concentration (C_0) for this polymer- nanotube system was subsequently plotted as a function of concentration, again using Equation 4.3. This data is presented in Figure 4.5 below:

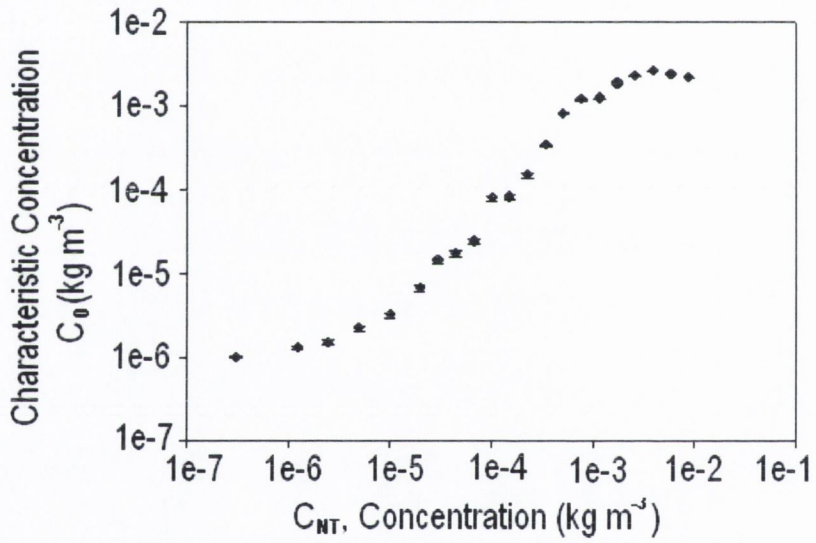

Figure 4.5: Plot of the characteristic concentration as a function of concentration, determined from PL studies for 2:1 PmPV molecules:HiPCO single walled nanotubes composites.

These data show that C_0 decreases consistently as the concentration is decreased before saturating at C_0= c. $1x10^{-6}$ kg m^{-3}. As the surface area of the nanotube bundles, A_{bun} is directly proportional to the characteristic concentration C_0, the variation in A_{bun} as a function of nanotube concentration should mirror the variation in characteristic concen-

tration for a given concentration range. This is consistent with the bundles spontaneously breaking up as the concentration is decreased. The data obtained indicate that individual nanotubes are stable in solution with PmPV below a concentration of approximately $1x10^{-5}$ mg/ml for 2:1 PmPV:SWNT composite solutions.

Polymer 2: Poly(9,9-di-n-octylfluorenyl-2,7'-diyl) (PFO)

The polymer poly(9,9-di-n-octylfluorenyl-2,7'-diyl) (PFO) is a commercially available polymer, and its repeat unit chemical structure is depicted in Figure 4.6. All UV -Visible

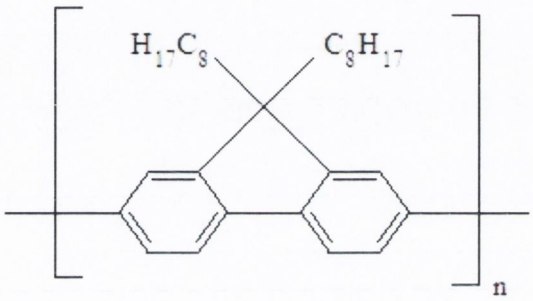

Figure 4.6: The repeat unit chemical structure of poly(9,9-di-n-octylfluorenyl-2,7'-diyl) (PFO)

absorption spectra obtained for the PFO solutions with and without nanotubes present showed an absorbance peak at 388 nm over the concentration range $2x10^{-4}$ -$2.5x10^{-2}$ kg m^{-3}. Emission spectra for the PFO and corresponding PFO:SWNT (1:1) composite solutions showed that the PL spectra are identical for both solutions, with the composite PL quenched with respect to that of the polymer. This is as predicted for a luminescent polymer upon interaction with carbon nanotubes, and indicates that the PFO system will follow the photoluminescence pattern predicted by the binding model.

Adsorption/Desorption PL studies

The plot of the composite to polymer PL ratio as a function of nanotube concentration for PFO yielded a surprising result, as it did not follow the emissive behaviour predicted by the binding model, despite exhibiting quenched luminescence for all composite solutions

(Figure 4.7). In principle, the adsorption- desorption binding model proposed by Coleman

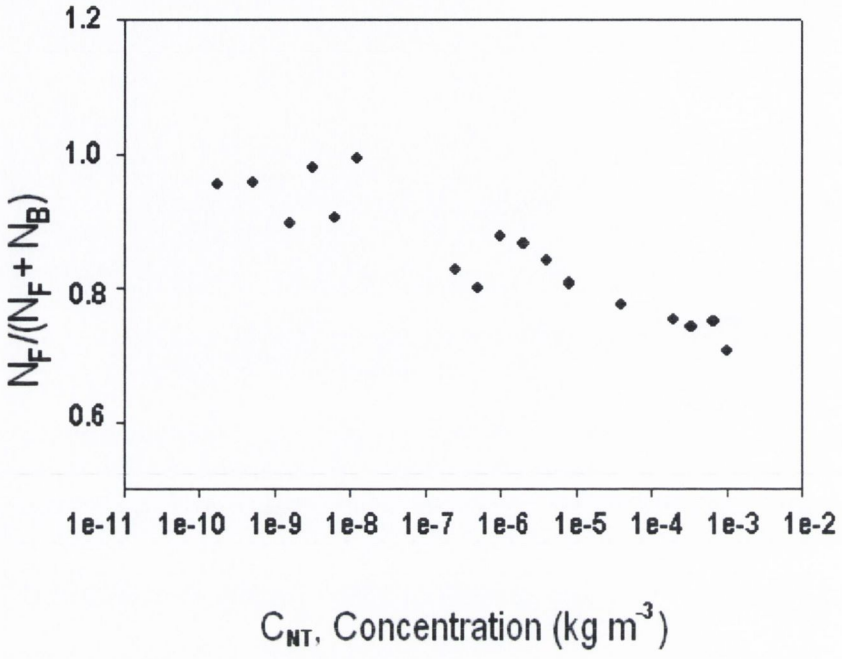

Figure 4.7: Plot of the fraction of free polymer as a function of concentration, determined from PL studies for a 1:1 PFO molecules:HiPCO single walled nanotubes composite solutions.

et al. is generic, and can be used to monitor dispersions of any metallic nanomaterials in suitable, luminescent organic solutions. However, Coleman's binding model failed to accurately describe the behaviour of SWNT composites with the light emitting polymer PFO (poly(9,9-di-n-octylfluorenyl-2,7'-diyl)), as the ratio of free polymer to polymer bound to nanotubes did not follow the expected nonlinear variation predicted by the model for either (1:1) or (2:1) PFO:SWNT solutions.

A significant difference between the PmPV and PFO polymers is that PmPV has been used to purify multiwalled carbon nanotubes, selectively suspending MWNTs relative to graphitic impurities. This preferential dispersion of carbon nanotubes in solution causes the graphitic impurities present to sediment out from the almost pure PmPV-nanotube suspension. This suspension is then decanted from the settled solid, yielding a highly pure MWNT suspension which is stable over periods of months.[8,9] In contrast, for similar

PFO-MWNT composite solutions, it has been shown that at least 10% by mass of the non-polymer material is graphitic impurities in nanoparticle form, with the number density of nanoparticles far exceeding that of the nanotubes for a given composite.[10]

It is therefore likely that a large number of the PFO polymer chains for our 1:1 and 2:1 PFO:SWNT solutions are bound to graphitic impurities instead of carbon nanotubes. It is understandable, therefore, that luminescence quenching behaviour from these impurity-bound chains may be different to that observed from polymer chains bound to carbon nanotubes. Thus, it is hardly surprising that the binding model is inaccurate in describing the luminescence behaviour from these systems.

Molecules Studied

The short conjugated molecules studied in this thesis were intentionally designed to be similar in structure to the PmPV polymer which was found to be an excellent SWNT dispersant. It was possible to produce much purer samples of these molecules than of the crude PmPV polymer and the PmPV fractions. These short molecules are all completely delocalized and were therefore predicted to adhere non-covalently to the nanotube surfaces. These short molecules all contained para linkages, whereas PmPV contains meta linkages.

Molecule 1: 2,5- dioctyloxy-1,4- distyrylbenzene molecule (pDSB)

The molecule 2, 5- dioctyloxy-1,4-distyrylbenzene (pDSB) is a short-chain analogue of the well known polymer Poly(p-phenylenevinylene) (PPV), and was synthesised in- house. The molecule has a very long π conjugation length as it is conjugated throughout the molecule, and so a high degree of interaction was expected between it and the carbon nanotubes. Successful dispersion of SWNTs in chloroform was achieved upon formation of composites with pDSB.[11] The structure of the pDSB molecule is shown below in Figure 4.8.

This molecule was found to be highly fluorescent, with negligible evidence of self-aggregation observed for the concentration range studied. As can be seen from Figure 4.9 below, the absorption spectrum for both the pDSB solution and the equivalent 2:1 pDSB:SWNT composite solution yielded an identical absorption profile for both solutions, with the absorption slightly quenched for the composite solution. This serves as evidence

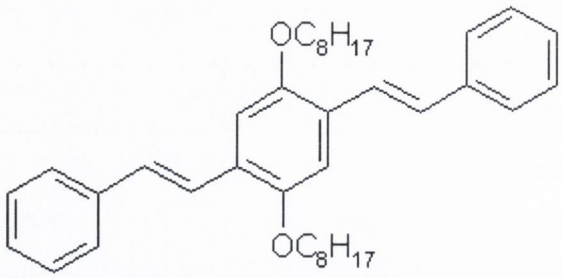

Figure 4.8: Molecular structure of pDSB molecule.

that the electronic properties of the pDSB molecules are not changed upon interaction with the carbon nanotubes.

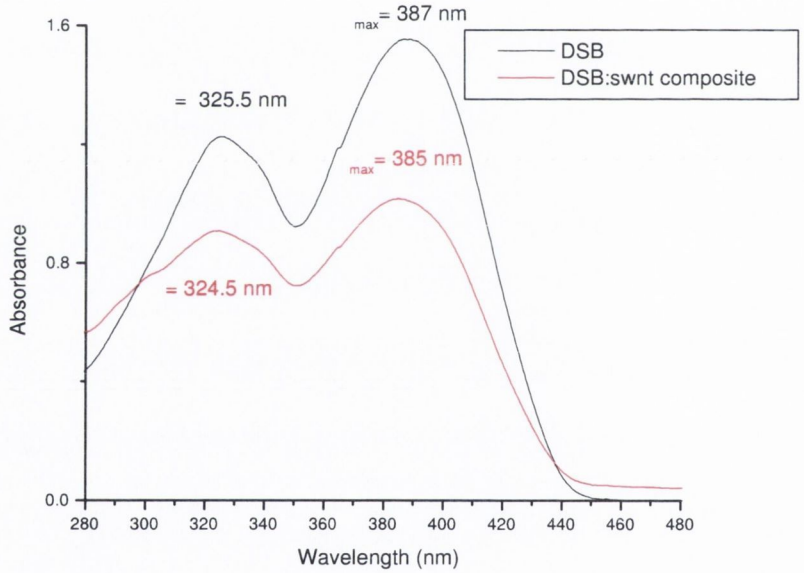

Figure 4.9: Absorption spectra of a solution of pDSB and the corresponding SWNT 2:1 composite solution ($4x10^{-2}$ kg m^{-3} pDSB, $CHCl_3$, 25^oC)

Plots of absorbance as a function of concentration for pDSB:SWNT composites and their equivalent pDSB solutions showed that the pDSB molecule obeyed the Beer Lambert law for the concentration range used, even after interaction with the nanotubes

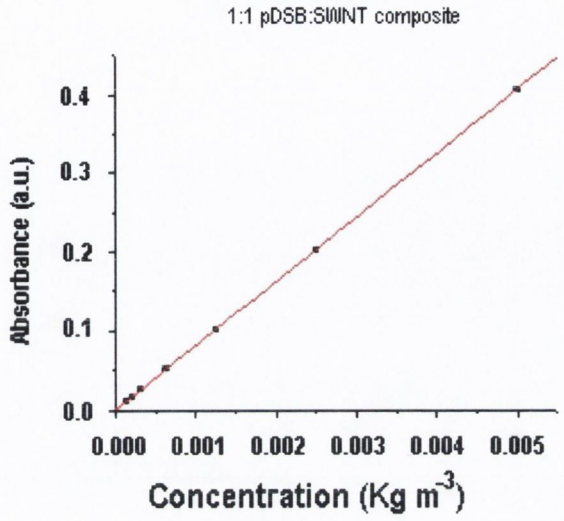

Figure 4.10: Plot of absorbance as a function of concentration for (1:1) pDSB:SWNT composites.

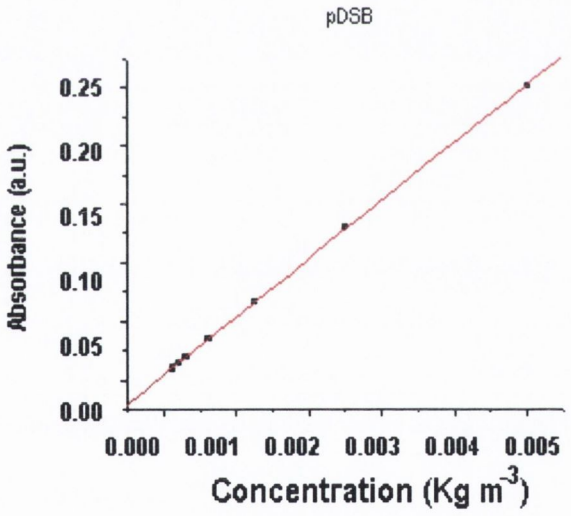

Figure 4.11: Plot of absorbance as a function of concentration for pDSB solutions.

(Figure 4.10). The coefficient of linear absorption is reduced for the composite solutions,

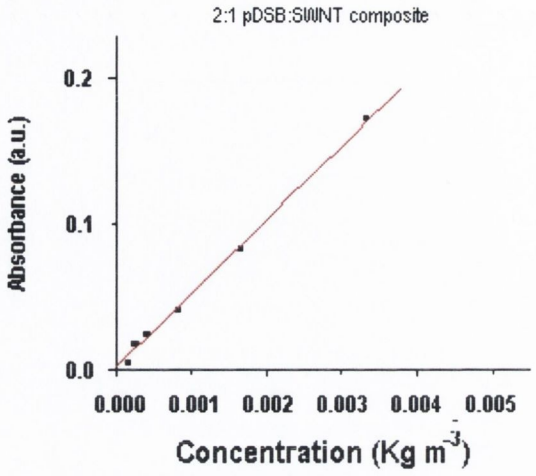

Figure 4.12: Plot of absorbance as a function of concentration for (2:1) pDSB:SWNT composite solutions.

however, and this is shown by the slopes of the plots in Figure 4.10). The 2:1 pDSB:SWNT composite solutions were investigated as with twice as many fluorescing pDSB molecules as fluorescence quenching nanotubes, it was possible to observe the luminescence behaviour for much lower concentrations with an improved signal to noise ratio.

Photoluminescence emission spectra observed from pDSB and pDSB: SWNT (2:1) composite solutions show identical PL profiles, with maxima at a wavelength of 446nm for both solutions (Figure 4.13). This demonstrates efficient quenching of photoluminescence brought about by introduction of the nanotubes into the system as a result of non radiative recombination of the photogenerated excitons through the fast vibrational manifold of the nanotubes.

Figure 4.14 is a plot of the fraction of free polymer against concentration, determined from photoluminescence studies for a 2:1 ratio of pDSB molecules to HiPCO single walled nanotubes. The fraction of free polymer was calculated from the ratio of the photoluminescence intensity for a composite solution to the photoluminescence intensity for the equivalent polymer solution, as described above. The plot of the fraction of free molecules

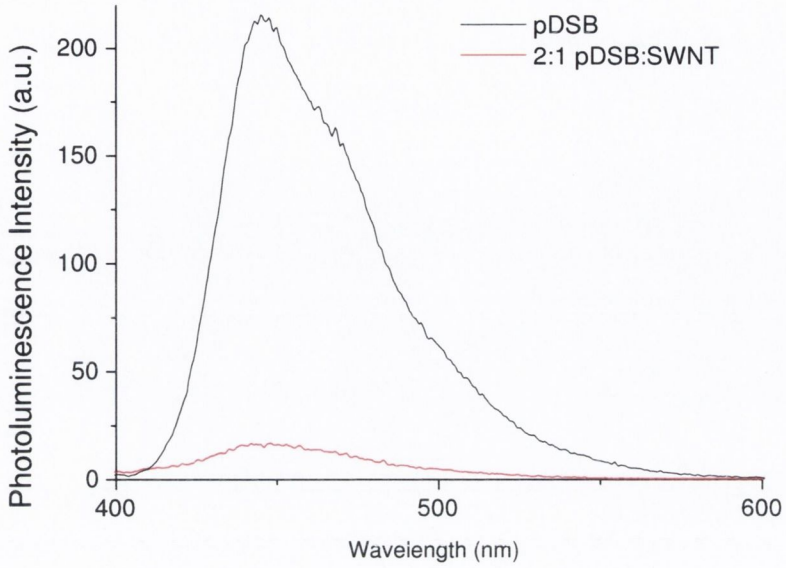

Figure 4.13: Emission spectra of a solution of pDSB and the corresponding pDSB: SWNT (2:1) composite solution (pDSB concentration, C_{pDSB}= 4x10^{-5} kg m^{-3}, $CHCl_3$, 25^{o}C)

as a function of concentration for a 2:1 pDSB molecules:HiPCO single walled nanotubes composite is shown above in Figure 4.14. The solid line is a fit to Equation 4.3 in the low concentration region using the saturation value of C_0= 9x10^{-9} kg m^{-3}, and is in excellent agreement with the experimental results for the low concentration solutions, showing that this function fits the experimental data extremely well.

The shape of this highly nonlinear plot is exactly as predicted by the adsorption/desorption model and the validity of the proposed binding model is further reinforced upon transformation of the data in Figure 4.14 to represent the characteristic concentration (C_0) as a function of concentration using Equation 4.3. This data is presented in Figure 4.15. Again C_0 decreases consistently as the concentration is decreased before saturating at $C_0 = c.1x10^{-8}kgm^{-3}$. As C_0 α A_{bun} this indicates that the bundle surface area decreases as the concentration is decreased before saturating at a minimum value, suggesting that as the concentration is decreased the bundles spontaneously break up. As they reach a minimum size, this indicates that individual nanotubes are stable in this solution below a

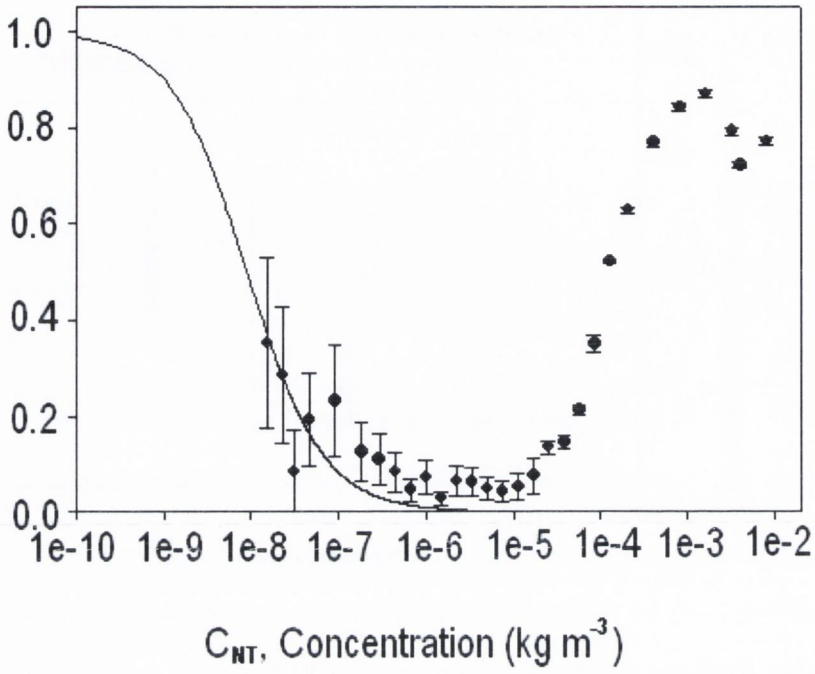

Figure 4.14: Plot of the fraction of free molecules as a function of concentration, determined from PL studies for a 2:1 pDSB molecules:HiPCO single walled nanotubes composite solutions. Note that for all concentrations the partial nanotube concentration, c_{SWNT}, equals half of the partial polymer concentration as the ratio of pDSB:SWNT = 2 : 1. The solid line is a fit to Equation 4.3 in the low concentration regime.

concentration of approximately 1×10^{-6} kg m^{-3}. If one compares the variation in characteristic concentration as a function of nanotube concentration for PmPV composites with that observed for the pDSB composites, it is immediately apparent that there are some differences between the two systems

As the characteristic concentration is directly proportional to the nanotube bundle area, it would appear that the carbon nanotube bundles are of smaller dimensions for the PmPV solutions than for the equivalent pDSB:SWNT solutions at high concentrations. As the composite solutions become more dilute, and the nanotube concentration decreases, both solutions begin to plateau at a concentration of 10^{-5} kg m^{-3}. The levelling off of

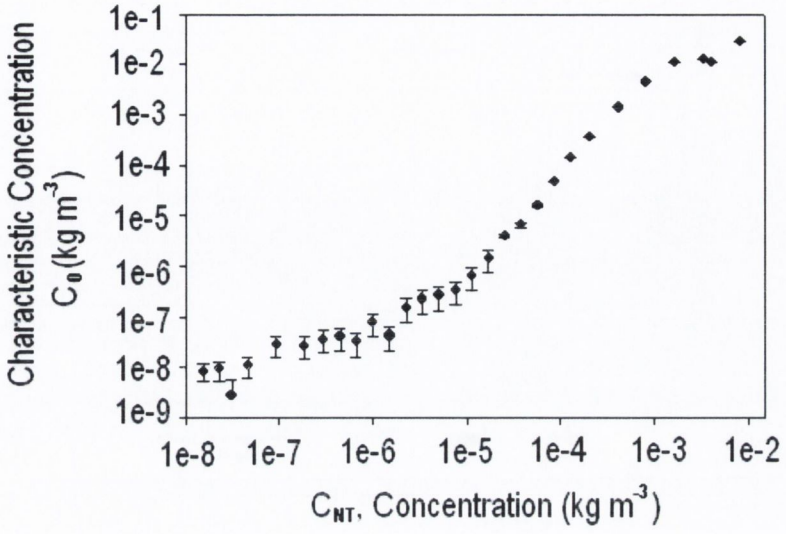

Figure 4.15: Plot of the characteristic concentration as a function of concentration, determined from PL studies for 2:1 pDSB molecules:HiPCO single walled nanotubes composites.

the characteristic concentration for low concentration solutions is known to be indicative of minimum bundle surface area being reached as a result of bundle breakup, this means that individual nanotubes are stable in both of these solutions below 10^{-5} kg m^{-3}.

As can be seen from Equation 4.4, C_0 is directly proportional to A_{bun} and $e^{-E_B/kT}$. As A_{bun} is assumed constant for individual single wall nanotubes, and the saturation value for C_0 differs by a factor of 100 for the two systems (with $C_0 = 10^{-8}$ kg m^{-3} and $C_0 = 10^{-6}$ kg m^{-3} for the pDSB and PmPV composites respectively), it may therefore be concluded that the pDSB molecule- nanotube binding energy is clearly higher than the PmPV- nanotube binding energy. This result is not at all surprising, as it is possible for the pDSB molecule to get much closer to the nanotube to which it is binding than a PmPV polymer chain could, since the pDSB molecule has no side chains to obstruct binding to the nanotube.

Recently, theoretical investigations into the interaction between conjugated polymers and carbon nanotubes have been reported.[12] The calculations by Panhuis et al. indi-

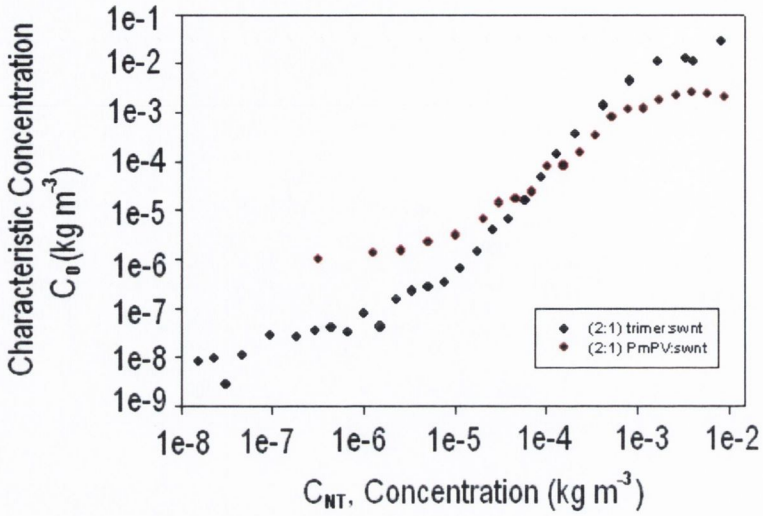

Figure 4.16: A comparison of the characteristic concentrations of two molecule:SWNT composite systems as a function of nanotube concentration shows differences between the PmPV and pDSB molecule composites.

cated an extremely strong noncovalent binding energy of circa 80 meV per carbon atom of PmPV bound to a SWNT. If one considers this atomic binding energy with the binding energy per molecule determined by Coleman et al.[2] of circa 1.06eV per molecule, this implies that approximately 14 carbon atoms per polymer molecule are binding to the nanotube. Given that the optimised structure of the polymer exhibits a rigid straight backbone, one would thus expect that the polymer chain crosses the nanotube allowing the electrostatic bonding of the 14 or so atoms, and the remaining sections of the polymer chain reside in the solution where they are free to form solvation shells to successfully disperse the nanotube.

Given the superior nanotube dispersion properties exhibited above by the polymer PmPV and its shorter analogue, pDSB, these dispersion studies were extended by Cuniffe et al.[13] in Trinity College Dublin to include the short conjugated molecules 1,4-bis-octyloxy-2,5-bis [2-(4-styryl-phenyl)-vinyl]-benzene (PVB) and 2,5- dioctyloxy-1,4-dinaphthylvinyl benzene (pDNB) which are both very similar to PmPV in chemical structure. In addition to this, gel permeation chromatography (GPC) a technique also known as size exclusion

chromatography (SEC) was used by them to separate a crude sample of the PmPV polymer used in the study above into different fractions, which were subsequently studied individually for their dispersion properties. GPC is a technique which separates molecules according to their size, and yielded fractions with PDIs of 1-1.9.

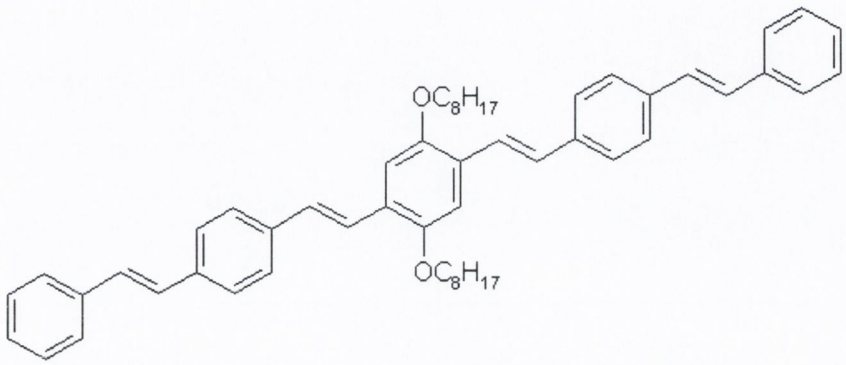

Figure 4.17: Chemical structure of 1,4-bis-octyloxy-2,5-bis [2-(4-styryl-phenyl)-vinyl]-benzene (PVB) molecule.

The 1,4-bis-octyloxy-2,5-bis [2-(4-styryl-phenyl)-vinyl]-benzene (PVB) molecule is a short conjugated molecule with 5 benzene rings, which is very similar in structure to the shortest PmPV fraction which has 5 repeating units, but it has para linkages as opposed to the PmPV meta linkages. This molecule was used as a comparison to the shortest PmPV fraction, and its structure is shown in Figure 4.17. The molecule 2,5- dioctyloxy-1,4-dinaphthylvinylbenzene or pDNB was also studied as it is very similar to the molecule pDSB in structure, as can be seen from Figure 4.18.

The crude polymer PmPV was found to consist of 19 repeating units, with a weight average molecular weight (M_w)of 48,533, a number average molecular weight (M_n) of 8,785 and a polydispersivity index (PDI) of 5 showing the broad range of polymer chain lengths present. This PmPV polymer was fractionated using GPC, which yielded different fractions with chain lengths of 5, 7, 18, 36, 44 and 51 repeat units. SWNTs were found to debundle upon formation of composites with all of the PmPV fractions studied.[13] All fractions were found to follow the Beer-Lambert law over the concentration range studied, with no evidence of self aggregation observed for any concentrations studied. In contrast, the 1,4-bis-octyloxy-2,5-bis [2-(4-styryl-phenyl)-vinyl]-benzene (PVB) molecule displayed evidence

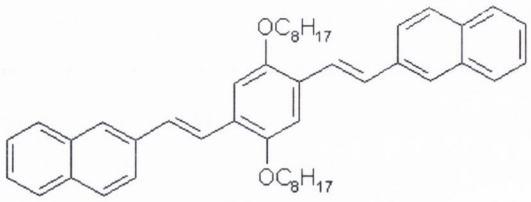

Figure 4.18: Chemical structure of pDNB molecule or 2,5- dioctyloxy-1,4-dinaphthylvinylbenzene.

of self- aggregation for concentrations of 0.01 mg/ml and above. This meant that this molecule was unsuitable for use in monitoring SWNT dispersions using the PL quenching technique, in spite of its structural similarity to the shortest PmPV fraction. This difference between the two molecules' behaviour may arise from the meta linkages in the PmPV and the para linkages in the 1,4-bis-octyloxy-2,5-bis [2-(4-styryl-phenyl)-vinyl]-benzene (PVB) molecule. Shorter chain PmPV fractions were shown to be the most effective at SWNT de-bundling. This is consistent with the entire polymer chain being capable of binding to the nanotube surface via the $\pi - \pi$ bonds for short chains, thus interrupting the Van der Waals forces existing between adjacent nanotubes, while the longer chains may only attach over part of their lengths and therefore prohibit the dispersion of SWNT with the remainder of the chain.

4.1.2 Absorption Spectroscopy Studies of Carbon Nanotube Composites formed with Conjugated Polymers and Molecules

The Effects of Centrifugation

Recently, large-scale debundling of single-walled nanotubes has been achieved by Giordani and co-workers in Trinity College, Dublin through successive dilution of nanotube dispersions in the solvent N-methyl-2-pyrrolidone (NMP).[14] This article reported the existence of some very large (100s of micrometers) nanotube aggregates at high concentrations, which were subsequently removed by mild centrifugation (5000 rpm or 4000g for 90 min). By measurement of the absorbance before and after centrifugation as a function of concentration the relative aggregate and dispersed nanotube concentrations were successfully monitored.

Using procedures developed in this study, an investigation was undertaken of the molecules and selected PmPV fractions studied in Section 4.1.1 above in order to confirm that molecules remain bound to the nanotube surface following such mild centrifugation, and that nanotube de- bundling occurs at low concentrations, in agreement with the PL studies previously described. In the case where binding does not occur, the nanotubes are removed from the solution during this procedure, with no Van Hove peaks present or observed in the absorption spectrum of the supernatant. Conversely, in the case of strong non- covalent binding occurring between the SWNT and the conjugated organic molecules examined, the dispersed nanotubes will remain in solution, with only the large aggregates observed for high concentrations being removed after centrifugation.

Experimental Procedure:

Dispersions of pristine HiPCO nanotube composites were made up with each organic molecule such that the molecule-SWNT mass ratio was 1:1, with a maximum nanotube concentration of 0.05 mg/ml. An identical 0.05 mg/ml solution of the molecule was also made up for comparison purposes. Chloroform ($CHCl_3$) was the solvent used in each case. These initial stock solutions were subsequently sonicated for 2 minutes each using a high-power ultrasonic tip processor (120W, 60 kHz). To produce the dilution series, the initial dispersion was then serially diluted to produce a range of dispersions with concentrations from 0.05 to approximately 0.0008 mg/ml. After each dilution the dispersions were sonicated for 2 min by tip. All dispersions were subsequently centrifuged at 5000 rpm (4000g) for 90 min to remove any large aggregates. UV-vis- NIR absorption measurements were made before and after centrifugation using a Perkin-Elmer Lambda 900 UV-vis-NIR spectrometer.

Results and Discussion:

After the initial dilution and sonication procedure, it became evident that the nanotubes were aggregating in the higher concentration dispersions, with significant quantities of nanotube aggregates observed in these samples. No evidence of nanotube aggregation appeared to be present at lower-concentrations. Prior to centrifugation, a UV-vis-NIR absorption spectrum was taken of each dispersion, in order to quantify the aggregates observed. Fol-

lowing mild centrifugation at 5000 rpm for 90 minutes, the aggregates had clearly been removed from the dispersions forming a sediment at the bottom of each sample vial. Even to the naked eye, it was clear that the amount of nanotubes removed from each dispersion was dependent on its initial concentration, with a large quantity of removed nanotube aggregates observed for the high concentration solutions, and none observed for the lowest concentrations. In each case, the supernatant was carefully removed, and UV-Vis-NIR spectra were measured again. Spectra from both before and after centrifugation were compared.

Absorption spectroscopy studies were undertaken on a representative group of PmPV polymer fractions with chain lengths of 7, 18 and 51 repeat units, all of which appeared from Cuniffe's PL studies to interact as predicted by the binding model. All of these polymer fractions yielded absorption spectra with Van Hove singularities present over the concentration range studied. Figure 4.19 is typical of the pre-centrifugation absorption

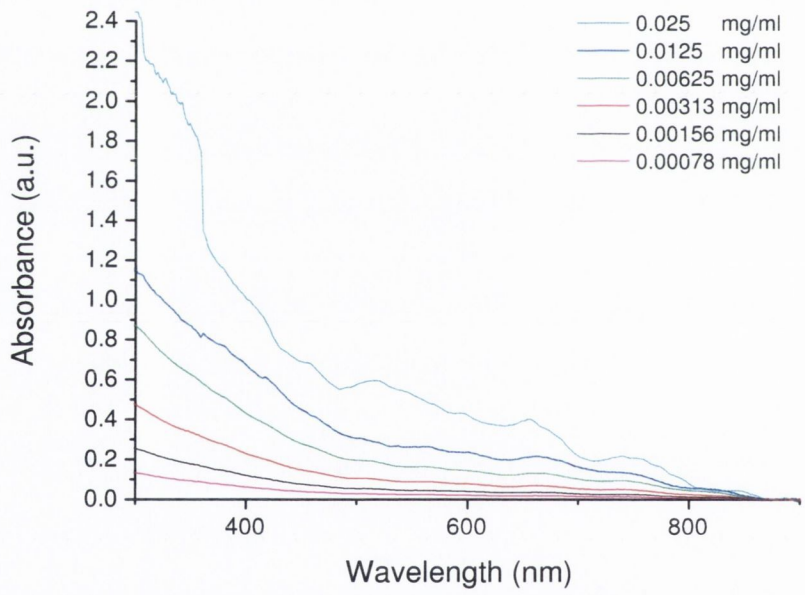

Figure 4.19: PmPV n=18 fraction before centrifugation showing Van Hove peaks in the 300-800nm region of the spectrum.

spectra measured for all samples, with the carbon nanotube Van Hove peaks clearly in

evidence for all concentrations studied. These Van Hove peaks in the post- centrifugation spectra confirm binding to the carbon nanotubes in solution. The UV-Vis-NIR absorption spectra recorded after mild centrifugation are shown in Figure 4.20 for the short PmPV fraction consisting of seven repeating units. These post- centrifugation absorption spectra

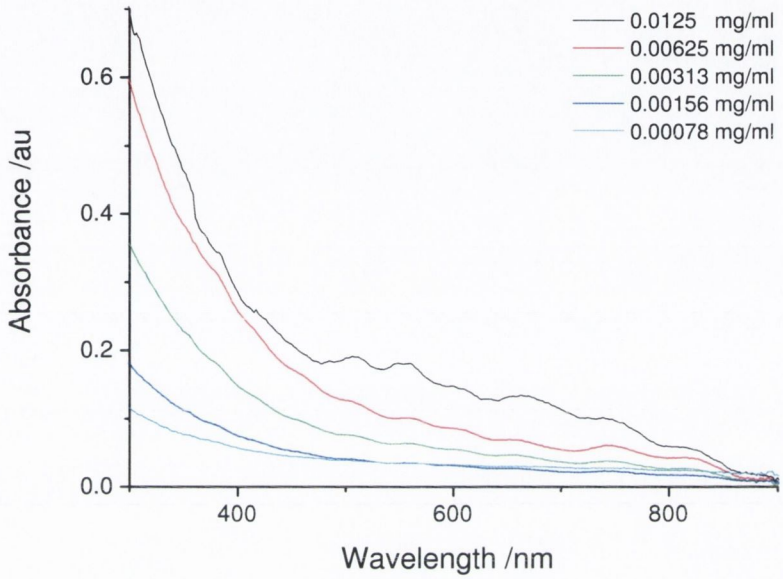

Figure 4.20: PmPV n=7 fraction after centrifugation showing Van Hove peaks in the 300-800nm region of the spectrum. This proves binding of the molecule onto the surface of the carbon nanotubes in solution.

therefore confirm the fact that this short PmPV fraction (with 7 repeating units) does in fact bind to the nanotubes, holding them in solution. In fact, binding was confirmed in this way between the carbon nanotubes and all PmPV polymer fractions of chain length 7, 18 and 51 repeat units.

The short conjugated molecules PVB and pDNB were also examined in this way, to confirm their binding to the nanotubes. The absorption spectra measured for the PVB-nanotube composites before and after centrifugation are shown below. As previously mentioned in Section (4.1.1), the PVB molecule is extremely similar structurally to the shortest PmPV (n=5) fraction studied by Cuniffe et al.[13] for it's PL quenching behaviour. How-

ever, the PVB molecule contains para linkages instead of the meta linkages found in the polymer. PVB was found to be unsuitable for use in monitoring SWNT dispersion using the photoluminescence quenching technique described, as self aggregation was evident for concentrations greater than 0.01 mg/ml. This does not necessarily mean that binding did not take place between the PVB molecules and the SWNT, and the centrifugation method was used in order to investigate this. Van Hove peaks were observed in both the pre- and post- centrifugation spectra, confirming the fact that PVB does in fact bind to the nanotubes, holding them in solution. It would therefore appear that although the PVB molecules contain para linkages whereas the polymer fraction contains meta linkages, this does not appear to affect non-covalent binding onto the SWNT surface. This was also

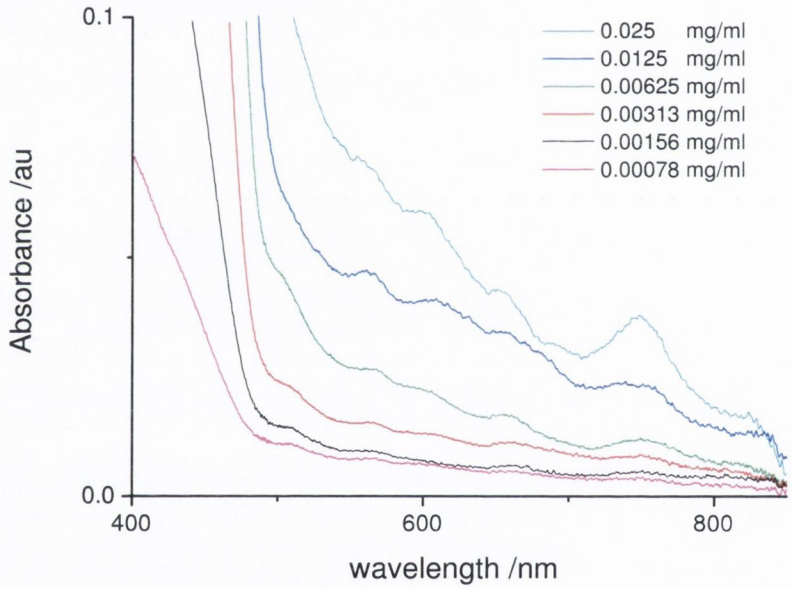

Figure 4.21: PVB after centrifugation showing Van Hove peaks in the 300-800nm region of the spectrum.

found to be the case for the pDNB-SWNT composite solutions, where the existence of non-covalent binding between these molecules and SWNT in solution was also investigated using the centrifugation method. The pDNB molecule is also related structurally to the

conjugated polymer PmPV containing para linkages instead of the polymer meta linkages. Photoluminescence quenching studies undertaken by Cuniffe et al. also indicated binding between these molecules and the SWNT. Once again, the presence of Van Hove peaks in both the pre- and post- centrifugation spectra confirmed the fact that the pDNB molecule does in fact bind to the nanotubes, holding them in solution.

It has therefore been shown that molecules which are similar in structure to the polymer PmPV bind noncovalently to SWNT in solution, irrespective of whether they contain para linkages or meta linkages. The nanotube composites formed are stable following mild centrifugation, with the presence of nanotubes in solution confirmed post- centrifugation by absorption spectroscopy.

Further evidence for the nanotube de-bundling implied by PL studies for the PmPV polymer was provided by employing a technique developed by Giordani et al.[14] for the mid-length PmPV fraction with 18 repeating units. This fraction was chosen as the crude polymer PmPV was found to consist of 19 repeating units (with M_w = 48,533, M_n = 8,785 and PDI = 5). The value A_{660}/l was obtained by dividing the absorbance measured for each sample at $\lambda = 660nm$ (A_{660}) by the cell length which was equal to 1 cm (or 0.01m). A_{660}/l was found to scale approximately linearly with the initial concentration, C_I, over the entire concentration range prior to centrifugation. This can be seen from Figure 4.22(A) where the dotted line fit to the data yields a value for the extinction coefficient of 2101.1 mL $mg^{-1}m^{-1}$. To investigate the SWNT absorption coefficient, the data in Figure 4.22(A) for the precentrifuged samples were divided by the initial nanotube concentration to give a plot of α_{660} before centrifugation as a function of initial concentration as shown in Figure 4.22(B). The plot of α_{660} before centrifugation as a function of initial concentration shown in Figure 4.22(B) clearly revealed variations in the SWNT absorption coefficient α_{660} as a function of concentration with α_{660} found to decrease to relatively low values at high concentrations. At C_I = 0.025 mg/ml, α_{660} = 1561.2 mL mg^{-1} m^{-1} and again increases gradually, approaching 2400 mL mg^{-1} m^{-1} as C_I approaches 0.00078 mg/ml. This behaviour is in striking agreement with that experienced for the same range for SWNT in NMP, indicating that nanotube debundling is taking place at these concentrations. Post- centrifugation A_{660}/l values are lower compared to the pre- centrifugation measurements over the

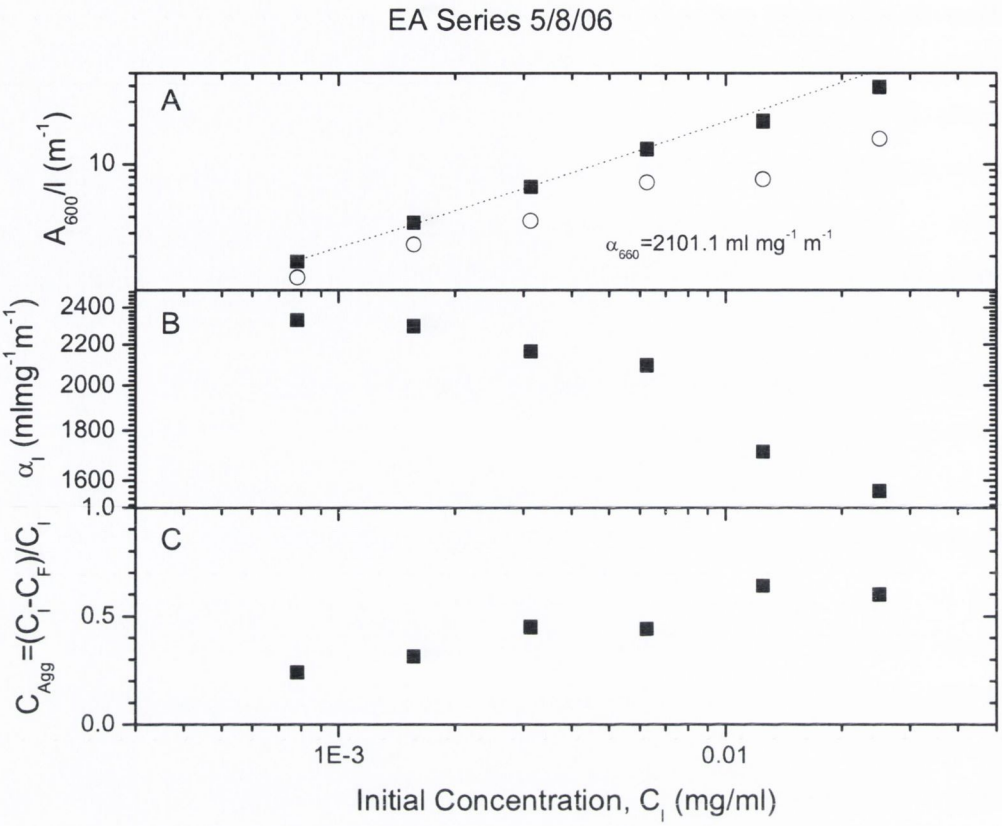

Figure 4.22: PmPV n=18 fraction analysis: (A) Absorbance per unit length measured at $\lambda = 660$ nm, A_{660}/l, before and after centrifugation as a function of initial nanotube concentration. (B) Absorption coefficient at $\lambda = 660$ nm before centrifugation found by dividing A_{660}/l by the initial nanotube concentration, C_I. (C) Fraction of the nanotube mass contained in large aggregates as a function of initial concentration.

entire concentration range studied, confirming the removal of nanotube aggregates during centrifugation. This information may be used in conjunction with α_{660} to calculate the true concentration after centrifugation, C_{NT}. In addition, the mass fraction of aggregates, χ_{agg}, may also be calculated using the following equation developed by Giordani et al.:

$$\chi_{agg} = \frac{A_{660,I} - A_{660,F}}{A_{660,I}} \tag{4.5}$$

For the n=18 PmPV fraction studied, the mass fraction of aggregates is plotted as a function of initial concentration in Figure 4.22(C). The true concentration after centrifugation, C_{NT} was found to range from 5.92x10^{-4} to 0.01005 mg/ml for composites with initial concentrations of 7.82x10^{-4} to 0.025 mg/ml respectively. This represents a mass fraction of aggregates, χ_{agg} of between approximately 24% and 64% respectively, as illustrated as a function of initial concentration in Figure 4.22(C) above.

These results are consistent with the findings of Giordani et al.[14] for SWNT dispersions in NMP, where this behaviour was found to represent the concentration range over which debundling is observed. As hypothesized in their study, this increase in absorption coefficient at low concentration may be associated with the increased presence of small bundles and individual nanotubes as opposed to larger bundles at higher concentrations. Our calculated values of α_{660} are in conservative agreement with those reported by Giordani et al.[14] and Landi et al.[15] who both measured values of between 3000 and 3500 mL $mg^{-1}m^{-1}$ at 660nm and 700 nm respectively for dispersions of SWNTs in various amide solvents. As our PL studies in Section 4.1.1 indicated that the onset of carbon nanotube debundling occurred for the polymer PmPV over the same concentration range (Figures 4.4 and 4.5), this absorption spectroscopy study provided further evidence of the efficiency of PmPV as a nanotube dispersant, and provides complementary evidence of the accuracy of the PL binding model for such conjugated systems.

In conclusion, using PmPV fractions of varying lengths, and some short conjugated molecules of a similar chemical structure it was found to be possible to routinely prepare good quality SWNT dispersions. While at higher concentrations ($C_I > 0.02$ mg/ml) these dispersions contain some large aggregates, these can be removed by mild centrifugation. UV-vis-NIR absorbance spectroscopy was used to monitor these dispersions before and after centrifugation, using a technique developed by colleagues in Trinity.

4.2 Nonlinear Optical Extinction in Polymer/CNT systems

Nonlinear extinction coefficients were calculated by O'Flaherty et al.[10] in Trinity College, Dublin for PmPV-MWNT and PFO-Carbon nanostructures composites, by performing an

intensity dependent open aperture z-scan investigation as described in Section 3.1.3 and Chapter 6 of this thesis. Their findings are briefly summarized in this section. The distinction made in this study between carbon nanotube and carbon nanostructure composites for PmPV and PFO respectively, is derived from the fact that while PFO was found to bind to both MWNT and graphitic particles, PmPV is known to successfully disperse carbon nanotubes in solution allowing other graphitic particles to form a sediment below the almost pure PmPV-MWNT suspension.

In these studies, the effective nonlinear absorption coefficient β_I replaces the nonlinear absorption coefficient β, signifying an additional scattering or possible higher order absorption contribution to the nonlinear optical response. The magnitude of the dissipation quantified by β_I, determined from the fitting of Equation 6.1 to the open aperture scans was determined as a function of the focal intensity for all samples.

A decrease in transmittance about the focus, typical of an induced positive nonlinear extinction of incident light, was exhibited by all open aperture z-scans performed with the exception of the pure PFO sample which exhibited no dissipation of the incident light for all incident intensities. The intensity dependence of β_I was investigated, and found to be approximately constant for both polymers, implying that the effective extinction coefficient may be accurately described for these systems using only third order nonlinearities. The PmPV composites with 0% and 1.1% MWNT mass fractions were found to exhibit different lower intensity type behaviour from all other materials in the PmPV series, with β_I increasing as a function of I_0. All other materials displayed an approximately constant β_I over this region, suggesting some type of unsaturated nonlinearity for lower intensities.

4.2.1 PmPV

Optical limiting and nonlinear transmission studies of these polymer systems were undertaken, with the normalized nonlinear transmission plotted against incident pulse energy density measured using the open aperture zscan technique. The PmPV-MWNT composites were investigated for a range of samples with 0, 0.013, 0.025, 0.036 and 0.059 MWNT mass content (i.e. $0 - 5.9\%$ MWNT by weight). All samples displayed optical limiting, or positive nonlinear extinction for high incident energy densities. The nonlinear dissipation

of the incident laser pulses was found to manifest itself in two distinct operating regimes, with the nonlinear responses of the samples with MWNT mass content lower than 0.036 dominated by the polymer response, whereas the higher MWNT mass content samples exhibited MWNT dominant behaviour. For the MWNT dominant regime, the onset of nonlinear optical activity was observed at energy densities about one order of magnitude lower (below $\approx 1 Jcm^{-2}$) than the polymer matrix dominating regime which were found to be nonlinearly active only above $\approx 10 Jcm^{-2}$. A critical inclusion of $(3.1 + / - 0.6)\%$ by mass MWNT was found to be required for MWNT dominant behaviour, below which the polymer matrix dominated the response.

4.2.2 PFO

All PFO carbon nanotube composite samples exhibited positive optical limiting about the focal point of the lens, while the pure PFO sample which exhibited no dissipation of the incident light for all incident intensities. The onset of optical limiting for all composite samples was found to be similar in all cases, occurring at approximately $0.3 Jcm^{-2}$, indicating that the limiting is directly caused by the carbon nanostructures in all cases. The magnitude of the nonlinear effect was found to increase systematically when the mass fraction of the nanostructures was increased from 0.011 to 0.038, saturating for mass fractions in excess of this range. In contrast to the PmPV and PmPV-MWNT samples, a polymer nonlinear response was not observed for PFO. Hence only one nonlinear regime was observed which was attributed to the carbon nanostructures.

4.3 Conclusions

In this chapter, the characterization of carbon nanotube interactions with conjugated organic polymers and molecules is described. A simple adsorption/desorption equilibrium model is introduced, which describes a method of monitoring the carbon nanotube dispersion capability of conjugated polymers and their short chain analogues based on photoluminescence quenching behaviour observed for such carbon nanotube composites in solution. A number of different carbon nanotube composite systems were characterized

using this model and the results presented in this chapter. Firstly, the interaction between carbon nanotubes and two different conjugated polymers was studied. These polymers were poly(metaphenylenevinylene-co-2,5-dioctyloxy-para-phenylenevinylene), known as PmPV and poly(9,9-di-n-octylfluorenyl-2,7'-diyl) or PFO. PmPV/SWNT composites were found to behave in excellent agreement with the binding model as a function of concentration, whereas PFO did not. Therefore, molecules related structurally to PmPV were also predicted to follow a similar noncovalent binding behaviour. Thus the molecule pDSB (2,5- dioctyloxy-1,4- distyrylbenzene molecule) which is a short-chain analogue of the well known polymer Poly(p-phenylenevinylene) was investigated. Successful dispersion of SWNTs in chloroform was achieved upon formation of composites with pDSB, and luminescence quenching behaviour indicated that the pDSB molecule- nanotube binding energy is in fact higher than the PmPV- nanotube binding energy. Following on from these successful PL binding studies with PmPV and pDSB, Cuniffe et al[13] extended the PL studies to investigate nanotube dispersions with two other short molecules structually similar to PmPV- pDNB and PVB- as well as some fractions of varying lengths of the crude PmPV polymer. PVB was found to be unsuitable for use in monitoring SWNT dispersion using the photoluminescence quenching technique described, as self aggregation was evident. The PL work undertaken by Cuniffe indicated a strong interaction between carbon nanotubes and all of the other molecules and PmPV fractions studied, with superior nanotube dispersion achieved using shorter molecules.

In the second part of this chapter, detailed absorption spectroscopy studies were undertaken on molecules and a selection of the PmPV polymer fractions which appeared from Cuniffe's PL studies to bind noncovalently onto the surface of SWNT in solution. It was confirmed using centrifugation and absorption spectroscopy techniques that noncovalent binding did exist between SWNT and PmPV fractions with 7, 18 and 51 repeat units. The same absorption study was conducted on the PVB molecule, which is extremely similar structurally to the shortest PmPV (n=5) fraction studied by Cuniffe et al. but contains para linkages instead of the meta linkages found for the polymer. Interestingly, this molecule was found to bind to the nanotubes. Similarly, pDNB was also found to bind non-covalently to carbon nanotubes in chloroform. It has therefore been shown that mole-

cules which are similar in structure to the polymer PmPV bind noncovalently to SWNT in solution, irrespective of whether they contain para linkages or meta linkages. The nanotube composites formed are stable following mild centrifugation, with the presence of nanotubes in solution confirmed post- centrifugation by absorption spectroscopy. A detailed picture of non-covalent interaction between carbon nanotubes and organic molecules was therefore built up using centrifugation to remove any large nanotube aggregates formed at higher concentrations and confirm the existence of non-covalent binding between them at lower concentrations. Absorption spectroscopy also proved a complementary technique for providing evidence of the nanotube de-bundling implied by PL studies for the PmPV polymer. A technique developed by Giordani et al.[14] was employed to monitor composites of the mid-length PmPV fraction with 18 repeating units as a function of concentration. The increase in the pre-centrifugation SWNT absorption coefficient at low concentration was found to be consistent with debundling of the SWNT in solution, and may be associated with the increased presence of small bundles and individual nanotubes as opposed to larger bundles at higher concentrations.[14]

The nonlinear optical (NLO)properties of the composites formed by the polymers PFO and PmPV with carbon nanotubes were not measured in this thesis as they had previously been investigated separately in our group by O' Flaherty and co- workers.[10] For completeness, a brief summary of their findings was included in this chapter.

Bibliography

1. Thess, A., Lee, R., Nikolaev, P., Dai, H. J., Petit, P., Robert, J., Xu, C. H., Lee, Y. H., Kim, S. G., Rinzler, A. G., Colbert, D. T., Scuseria, G. E., Tomanek, D., Fischer, J. E., and Smalley, R. E. *Science, 273, 5274, 483* (1996).

2. Coleman, J., Fleming, A., Maier, S., O'Flaherty, S., Minett, A., Ferreira, M., Hutzler, S., and Blau, W. *Journal of Physical Chemistry B 108, 3446-3450* (2004).

3. Nikolaev, P., Bronikowski, M., Bradley, R., Rohmund, F., Colbert, D., Smith, K., and Smalley, R. *Chemical Physics Letters 313, 9197* (1999).

4. Davey, A., Drury, A., Maier, S., Byrne, H., and Blau, W. *Synthetic Metals 103, 2478-2479* (1999).

5. Drury, A., Maier, S., Davey, A., Dalton, A., Coleman, J., Byrne, H., and Blau, W. *Synthetic Metals 119, 151-152* (2001).

6. Burroughes, J., Bradley, D., Brown, A., Marks, R., Mackay, K., Friend, R., Burns, P., and Holmes, A. *Nature, 347, 539-541* (1990).

7. Dalton, A. e. a. *Journal of Photochemistry and Photobiology A: Chemistry 144, 31- 41* (2001).

8. Murphy, R., Coleman, J., Cadek, M., McCarthy, B., Bent, M., Drury, A., Barklie, R., and Blau, W. *Journal of Physical Chemistry B, Vol. 106, No. 12, 3087- 3091* (2002).

9. Coleman, J., Dalton, A., Curran, S., Rubio, A., Davey, A., Drury, A., McCarthy, B., Lahr, B., Ajayan, P., Roth, S., Barklie, R., and Blau, W. *Advanced Materials, 12, No. 3* (2000).

10. O'Flaherty, S. *Ph.D. Thesis, Trinity College Dublin* (2003).

11. Giordani, S., Bergin, S., Drury, A., Ní Mhuircheartaigh, S., Coleman, J., and Blau, W. *AIP Conference Proceedings, Volume 786, pp. 232-235* (2005).

12. Panhuis, M., Maiti, A., Dalton, A., van den Noort, A., Coleman, J., McCarthy, B., and Blau, W. *Journal of Physical Chemistry B 107, 478-482* (2003).

13. Cuniffe, G. *Undergraduate Final Year Thesis, Trinity College Dublin* (2006).

14. Giordani, S., Bergin, S., Nicolosi, V., Lebedkin, S., Kappes, M., Blau, W., and Coleman, J. *Journal of Physical Chemistry B, 110(32), 15708-15718* (2006).

15. Landi, B. J., Ruf, H. J., Worman, J. J., and Raffaelle, R. P. *Journal of Physical Chemistry B, 108, 17089* (2004).

Chapter 5

Linear Optical Characterization of Carbon Nanotube:Porphyrin systems

5.1 Introduction to Carbon Nanotube:Porphyrin Systems

Since their initial discovery in 1991, carbon nanotubes have attracted much attention in various fields of nanoscience and nanotechnology due to their unique structural and electronic properties. Considerable attention has been focused on the preparation of soluble carbon nanotubes with great interest focused on noncovalent sidewall-functionalized soluble carbon nanotubes which would enable further physical, chemical and biological applications of carbon nanotubes to be developed. As previously described, porphyrins are an enormously important family of functional dyes with a variety of unique photophysical, chemical and biological properties. Although it has been known for some time that both acyclic and cyclic oligomers of (metallo) porphyrins form strong complexes with fullerenes in organic solvents, it has only been in the last few years that metalloporphyrins have been shown to dissolve SWNTs in aqueous solutions and in organic solvents ranging from dimethylformamide to chloroform. In fact, the initial finding on the dissolution of single walled carbon nanotubes (SWNTs) in organic solutions by zinc protoporphyrin IX molecules and

the subsequent separation of the SWNTs- porphyrin hybrid nanomaterials from the solutions was only reported in 2003 by Hiroto Murakami and T. N., Naotoshi Nakashima.[1] Atomic force microscopic investigation revealed that both individually dissolved nanotubes and bundles of nanotubes coexisted in the solution. The solid purified SWNTs (p- SWNTs) -porphyrin nanomaterials were readily separated from the p-SWNTs- porphryin soution and this nanomaterial was re- dissolvable in Dimethylforamide (DMF). Measurements of its fluorescence spectrum gave evidence for the interaction between the nanotube sidewall and porphyrin molecules in solution. This observed interaction between SWNTs and porphyrin molecules signalled the emergence of a rapidly expanding field of research, and many subsequent studies were consequently undertaken. The research in this field typically falls into two categories: studies investigating carbon nanotube solubilization, and donor-acceptor studies which have the aim of searching for long-lived charge separated states that could be used in the field of photovoltaics. A summary of all available published literature in both fields of research is presented in Sections 5.1.1 and 5.1.2.

5.1.1 Solubilization Studies

In order to effectively utilize SWNTs as building blocks for nanotechnology, nanotubes have been covalently and noncovalently functionalized in a number of ways to render them soluble in aqueous and organic solutions and to gain precise control over nanotube orientation and location. There are two general strategies for gaining spatial control of SWNTs. In the direct growth strategy, nanotube length, location and orientation can be controlled using pre- patterned catalyst and chemical vapour deposition (CVD). In the post growth strategy, nanotubes can be aligned by various methods including biomolecular recognition, manipulation by an atomic force microscopic (AFM) tip, application of an electric field or a magnetic field, deposition on chemically patterned surfaces, alignment by gasflow or dip coating washing. For many applications, it is important that the inherent functionality of the carbon nanotubes not be altered or destroyed by high temperature CVD covalent chemical functionalization steps or various applied fields. For this reason, the dissolution of SWNTs by the water soluble porphyrin [meso-(tetrakis-4- sulfonatophenyl) porphine dihydrochloride] was investigated by Chen and Collier.[2] The porphyrin/SWNT solutions

prepared were also found to be stable for weeks without covalent chemical functionalization of the tubes or the use of surfactants. These solutions were characterized by taking UV visible absorption and fluorescence spectroscopic measurements as a function of pH, which showed that the free base form of the porphyrin selectively interacted with the nanotubes and was mainly responsible their solubility in water. Interaction with the SWNTs inhibited the protonation of the free base to the diacid. Under mildly acidic conditions J-aggregates form on the nanotubes. The fluorescent properties of the free base and diacid forms of H_2TPPS^{4-} were not significantly perturbed by the nanotubes but emission from the J aggregates was completely quenched. Crucially, it was found that this solubilization procedure allowed alignment of the SWNTs by combing the nanotubes from the aqueous solution onto clean polydimethylsiloxane (PDMS) stamps, followed by transfer printing of the tubes from PDMS to silicon or glass surfaces. In another approach to the problem of nanotube solubility, the dynamic chemistry that occurs readily between cis- protected Pd^{II} and Pt^{II} complexes and linear divalent ligands such as metalloporphyrins carrying 4 pyridyl groups at two of their diametrically disposed meso positions was exploited.[3] The porphyrin molecules and the Pd^{II} complex were left to self assemble under thermodynamic control allowing the formation of multiply charged acyclic and cyclic oligomers. Introduction of SWNTs into this allowed them to be solubilized in aqueous acetonitrile solution. Ultrasonication of SWNT samples in the presence of porphyrins alone led to no apparent solubilisation in (1:1) $MeCN/H_2O$ but instead resulted in the adsorption of the porphyrins onto the surfaces of the SWNTs as seen through the visual inspection with the naked eye and more precisely using UV/vis spectroscopy. Under the same conditions similar results were observed when SWNTs were treated with the free palladium complex, i.e. SWNTs were not solubilized and only the presence of the palladium complex was detected in solution by UV visible spectroscopy. However, when self assembly was performed with sonicated samples of SWNTs with equimolar mixtures of porphyrins and palladium complex, the SWNTs were solubilized. Electrical measurements were also conducted on these composites. Although porphyrins and metalloporphyrins in general have been shown to interact strongly with SWNTs they cannot disperse SWNTs efficiently in aqueous solutions because of their limited solubility in water. Whereas the porphyrins and metalloporphyrins alone cannot

solubilize SWNT in the aqueous solution, the self assembled oligomer formed in the presence of a free palladium complex was found to create the required hydrophilic encapsulation for nanotubes to maintain their solubility in water. The supramolecular electronic effects that the individual components of their acyclic and/or cyclic complexes impart upon a single semiconducting SWNT were also probed within a nanotube field-effect transistor device.

Single walled nanotubes SWNTs produced via various techniques are generally mixtures of metallic and semiconducting SWNTs which correspond to different electrical conductivities and other related properties. These properties are important to a variety of technological applications of SWNTs including for example, the electrical conductivity and charge dissipation in polymeric/carbon nanocomposites and thin films. The enrichment of metallic over semiconducting SWNTs or vice versa in a nanotube sample toward a complete separation of the two different kinds of SWNTs has also attracted much attention, with the selectivity of a derivatized porphyrin toward semiconducting SWNTs in noncovalent interactions reported by H. Li and co-workers.[4] This resulted in significantly enriched semiconducting SWNTs in the solubilized sample and predominantly metallic SWNTs in the residual solid sample, which was verified using Raman, NIR absorption and bulk conductivity characterization. It was concluded that the porphyrin ring probably bound to the SWNT surface leaving long alkyl chains to wiggle around in solution. Such a picture was supported by high resolution Transmission Electron Microscopy (TEM) results which showed soft materials on the surfaces of individual nanotubes. The interactions of THPP with SWNT were found to be specific to the porphyrin free base and were hindered upon the chelation of a metal cation. For example, the Zn THPP was used in place of THPP under the same experimental conditions but no interaction leading to the solubilization of SWNTs was observed.

Stable porphyrin/single-walled nanotube (SWNT) composites were also synthesized by condensation of tetraformylporphyrins and diaminopyrenes on SWNTs.[5] The degree of interaction between SWNTs and porphyrin was evaluated by UV-vis and fluorescence spectra, and by chemical removal of porphyrin from SWNTs. In the composites, the Soret and Q-bands of porphyrin moieties were significantly broadened and their fluorescence was almost quenched. Apparent extinction coefficients at the Soret bands of the composites

were decreased to ca. 20%. Three tetraformylporphyrins were prepared, with a variety of substituents, namely carboxylic acid (1a), oligoether (1b), and alkyl groups (1c). These substituents were selected in order to compare the effect of different functional groups. Since both porphyrin and pyrene are known to interact with CNTs, condensation of tetraformylporphyrins and diaminopyrenes on the surface of the CNT was expected to proceed, causing it to become wrapped by an imine polymer. Absorption spectra and UV-Visible-near IR of the composites showed that the characteristic semiconducting bands I (SI) and II (SII) of SWNTs around 1600 and 900 nm, remained unperturbed even after composite formation in all cases. Resonance Raman signals corresponding to the composite's radial breathing mode (RBM) around 100-350 cm^{-1} and the G-line at 1590 cm^{-1} were also the same as those of pure SWNTs. In contrast, the porphyrin absorption spectra were significantly changed, with broad Soret bands observed for composites formed both in the presence and absence of aminopyrene with peak maxima red shifting by 5 nm and 1 nm respectively to 425 nm and 421 nm from the porphyrin Soret band at 420 nm. In the Q-band region, the four characteristic Q-bands of free-base porphyrin were only slightly red shifted upon interaction with nanotubes, while the Q-bands of the aminopyrene composite exhibited markedly lower intensities. Fluorescence spectra of free-base tetraformylporphyrins were compared with those of the composite formed with and without aminopyrene. The porphyrin fluorescence intensity decreased to 37% and 2% of that of the free base for composites formed in the absence and presence of aminopyrene, respectively. This suggests that the polymer-wrapping procedure using diaminopyrenes is important in enabling a strong interaction with SWNTs. Acid hydrolysis results- carried out to estimate the amount of porphyrin in the composites- suggested that the strength of the interaction with SWNTs decreased from 1a (strongest) to 1c (weakest) (where porphyrin substituents were carboxylic acid (1a), oligoether (1b), and alkyl groups (1c) respectively) which agreed with the degree of fluorescence quenching. Atomic Force Microscopy (AFM) and High Resolution Transmission Electron Microscopy (HRTEM) studies also supported the polymer wrapping theory.

Protonated porphyrins provide a convenient way to construct ordered molecular assemblies. SWNT-driven aggregation of protonated porphyrin to produce supramolecular assemblies in the form of macroscopic bundles with specific spectroscopic fingerprints

has also been reported.[6] The $\pi - \pi$ interaction between porphyrins and SWNTs plays an important role to influence the orientation of protonated porphyrins, inducing J- and H-type aggregation effects on the SWNTs surface. The interaction of 5,15-bis(3,5-di-tert-butylphenyl) porphyrin (H_2P) with SWNT was investigated in this report. The unusual molecular aggregation phenomenon driven by SWNTs was found to further assemble in the form of linear bundles. This simple method of designing supramolecular assembly could pave the way for developing light harvesting assemblies and optoelectronic devices. To facilitate $\pi - \pi$ interaction of protonated porphyrin and SWNTs, these experiments were conducted in acidified Tetrahydrofuran (THF). The binding of SWNTs with the protonated form (H_4P^{2+}) in acidified THF solution was found to be quite strong and yielded better solubility and stability of the suspension than one obtained with the unprotonated form, in agreement with previous reports. In the absence of acid, the interaction between H_2P and SWNTs was rather weak, and no ordered assembly structure in the TEM was observed. TEM images of SWNTs and porphyrin composites prepared in THF with and without acidification show fully grown rod structures 40-60 nm in diameter and 0.5-3.0 μm in length for the protonated porphyrin composites. Judging from the molecular size of porphyrins and SWNTs, it is evident that H_4P^{2+}-bound SWNTs undergo linear assembly to yield large rodlike structures. The reproducibility of obtaining rods of similar shape shows the importance of SWNTs in driving the supramolecular assembly into well-defined cylindrical structures.

Fuyong Cheng and Alex Adronov investigated the noncovalent functionalization and solubilization of carbon nanotubes by using a highly soluble, conjugated Zn-Porphyrin polymer.[7] The synthesis of the highly stable and soluble Zn-porphyrin polymer with three hexadecyl branches linked via robust ether bonds to the aryl substituents on both of the porphyrin meso positions was described in this report. This conjugated porphyrin polymer was found to be capable of strong supramolecular interactions with SWNTs resulting in the formation of very stable and highly soluble polymer-SWNT nanocomposites, although it was composed of Zn-porphyrins rather than free-base porphyrins. It was found that addition of trifluoroacetic acid (TFA) to the polymer-nanotube solution greatly enhanced the supramolecular interaction in THF. The polymer-nanotube assembly process was found to

induce a coplanarization in the polymer repeat units, causing enhanced conjugation and a 127 nm bathochromic shift of the Q-band absorption. It was found that mixing and sonication of the polymer and the SWNTs in THF resulted in no observable nanotube solubility, consistent with previous observations of Sun and co-workers. It was postulated that coordination of THF to the Zn-porphyrin repeat units prohibits the polymer from closely interacting with the carbon nanotube surface. However, when the same experiment was conducted in acidified THF, containing 5% trifluoroacetic acid (TFA) (v/v), a high degree of nanotube solubility was observed, reaching close to 1 mg/ml. A very dark and stable solution was obtained after sonication for 5 minutes, leaving practically no observable insoluble nanotube residue. This solution remained stable upon standing for several weeks, with no sedimentation even after centrifugation for 20 min at 5000 rpm, indicating that the multivalent polymer-nanotube interaction is very strong, and allows the retention of significant amounts of polymer bound to the nanotube surface even after excess unbound polymer has been removed. The exact role of TFA in promoting supramolecular interactions between SWNTs and the zinc-porphyrin polymer is not fully understood and is currently under investigation. In addition, AFM studies indicated exfoliation of nanotube bundles creating long strands from multiple nanotubes. The high nanotube solubility in these composites coupled with the broad absorption spectrum observed, ranging from the UV to the near-IR, was also found to be conducive to potential future applications in the development of light-harvesting photovoltaic systems and other optoelectronic devices.

5.1.2 Donor-Acceptor Nanohybrids for Photovoltaic Applications

Nanoscale carbon materials are an attractive platform for applications in optoelectronics and photovoltaics. The presence of extended, delocalized π electron systems makes these carbon materials very useful for managing charge transfer and charge transport when combined with photoexcited electron donors such as metalloporphyrins. The long-lived intermediate electronic state that is accessed upon irradiation of porphyrins by visible light is what makes them unique. It is this photoexcited porphyrin state that initiates an electron-transfer process within the grana of the chloroplast in chlorophyll. Nature's process of electron transport has been mimicked in the form of an electron donor/acceptor (D/A) pair

utilizing porphyrin derivatives combined with a complementary electron-accepting species. Charge-separated states have been studied by forming composites between porphyrin derivatives and carbon-based nanostructures such as C_{60} [8,9,10,11] and, more recently, single-wall nanotubes (SWNTs). These states have extremely long lifetimes with reported durations in excess of 300 μs for porphyrin/fullerene[11] and 10 μs for porphyrin/SWNT dyads. A variety of spectroscopic studies performed in solution indicate that a photoinduced electron transfer (PET) occurs from the porphyrin to the carbon-based species. In a report by David S. Hecht and co-workers, it was demonstrated that a porphyrin derivative can be combined with SWNTs to mimic part of the natural process of photosynthesis or, more specifically, the use of a light harvesting material to initiate an electron transfer.[12] Single-wall carbon nanotube (SWNT) field effect transistors (FETs), functionalized noncovalently with a zinc porphyrin derivative, were used to directly detect a photoinduced electron transfer (PET) within a donor/acceptor (D/A) system. However, unlike photosynthesis, in this system the absorption of light was found to initiate the transfer of holes rather than electrons from the porphyrin so that the SWNTs act as the electron donor and the porphyrin molecules as the electron acceptor. The magnitude of the PET was found to be a function of both the wavelength and intensity of applied light, with a maximum value of 0.37 electrons per porphyrin for light at 420 nm and 100 W/m^2. A complete understanding of the photophysics of this D/A system is necessary, as it may form the basis for applications in artificial photosynthesis and alternative energy sources such as solar cells. The direction and magnitude of the PET in these systems may be controllable, and different porphyrin derivatives and SWNT functionalization methods are currently being investigated by these authors. The combination of a light-absorbing molecule having tunable absorption bands with a complementary material having high mobility can potentially act as a photosensitive wire able to move photoexcited charges away from the recombination centers. Such a device that exhibits these properties has promising applications in tunable light detection as in artificial eyes and, in the near future, as a photovoltaic device.

Quenching via excited state energy transfer in dye- functionalized carbon nanotubes represents a potentially significant competing pathway to the desired photosynthetic process, and is subsequently an impediment towards their usage as an alternative

to nanoparticles in photovoltaic devices. In an early paper, Huaping Li and co-workers successfully synthesized SWNT covalently functionalized with porphyrin molecules in order to investigate and understand the photophysical properties of these composites.[13] Steady state and time resolved fluorescence measurements showed that the excited state energy transfer quenching of porphyrin fluorescence by SWNT is dependent on the length of the tether linking the porphyrin moiety to the nanotube, with no quenching of fluorescence quenching observed for samples with a shorter tether. The derivatized porphyrins containing a terminal hydroxyl group used in the functionalization of SWNT were (1) 5-(p-hydroxyhexyloxyphenyl)-10, 15, 20-tris(p-hexadecyloxyphenyl)-21H,23H-porphine and (2) 5-(p-hydroxymethylphenyl)-10,15,20-tris(p-hexadecyloxyphenyl)-21H,23H-porphine. The nanotube- porphyrin samples were observed directly by TEM imaging, and soft material was observed to be attached to individual nanotubes at high resolutions, which was attributed to the tethered porphyrin functionalities. The room temperature UV-Vis spectra of the porphyrin (1) composite was similar to that of the porphyrin, and the profile of the photoluminescence was also identical to the porphyrin with the quantum yield only 70% of that of the porphyrin alone. This reduced fluorescence quantum yield upon attachment to SWNT was not attributed to intramolecular quenching associated with the excited state porphyrin to nanotube electron transfer due to its insensitivity to changes in the polarity of the medium. Therefore intramolecular excited state energy transfer was found to be the most likely mechanism. In the case of porphyrin (2), the fluorescence quenching was successfully suppressed due to the length of the tether being very short and therefore prohibiting the porphyrin ring from taking a position facing the nanotube surface. This means that chromophore decorated SWNTs can be prepared without altering the photoexcited state properties of the chromophores, lending itself to interesting applications. For example, the porphyrin (2) composites could serve as a sensitive fluorescent probe as each nanotube is attached with a large number of porphyrin molecules.

An interest in the photophysical properties of SWNT derivatives obtained by covalent and noncovalent functionalization, with the aim of searching for long-lived charge separated states that could be used in the field of photovoltaics was also shared by Mercedes Alvaro et al.[14] It is well known that metalloporphyrins interact with pyridyl nitrogens

through an apical coordinative bond between the porphyrin transition metal atom and the pyridyl ligand. A highly soluble SWNT derivative functionalized at the tips with pentyl esters and on the walls by pyridyl isoxazoline groups was prepared and characterized. TEM images were obtained showing the short length of the tubes and the solution ^{1}H NMR showed the presence of corresponding adducts. Raman spectroscopy showed the expected peaks for the organic groups and confirmed the occurrence of a high degree of lateral functionalization. This pyridylfunctionalized SWNT (Py- SWNT) formed complexes with a zinc porphyrin (ZnPor) in a way parallel to that of a pyridyl-derivatized C_{60}. The occurrence of this complex was clearly revealed by optical spectroscopy and by the shifts in CV potentials of ZnPor in the presence of Py- SWNT, similar but larger than for the corresponding fullerene analogues. Steady-state fluorescence and nanosecond transient spectroscopy indicated an energy transfer quenching of the ZnPor singlet excited state by Py-SWNT and no evidence for the occurrence of electron transfer.

The immobilization of an octasodium salt of a porphyrin and the related zinc complex as electron donors onto electron accepting SWNTs was investigated by Guldi et al.,[15] and showed through static and time resolved fluorescence data and transient absorption data that the SWNTs serve as the electron acceptor component in donor acceptor materials. Such arrangements might lead to novel, highly efficient photoelectrochemical cells for applications such as photochemical water splitting and the reduction of CO_2 to fuels. A further report by this group (2005) investigated the supramolecular association of pristine SWNTs with linearly polymerized porphyrin polymers en route to versatile donor- acceptor ensembles.[16] TEM confirmed the successful non-covalent solubilization of SWNTs and their presence in solution. Also a certain degree of de bundling was noted upon formation of SWNT- poly (H_2P) and confirmed further with AFM which showed some individual SWNT present. Excited state interactions were tested in SWNT- poly(H_2P) by means of steady state and time resolved fluorescence. Excitation at the Q-band wavelength of 518 nm showed strong H_2P emission quenching for the composite solutions relative to a H_2P reference.

Covalent functionalization of carbon nanotubes through surface modification with porphyrins was addressed by Baskaran et al.[17] In this communication, supramolecular struc-

tures consisting of porphyrins covalently grafted to carbon nanotubes were synthesized and their photoinduced electron transfer properties studied. The absorption and fluorescence of these complexes demonstrated that the carbon nanotubes serve as an efficient electron acceptor and paved the way to construct novel photovoltaic devices and light harvesting systems using various porphyrin functionalized carbon nanotubes.

Fuyong Cheng and co-workers recently reported that a novel triply fused Zn^{II}-porphyrin trimer formed extremely strong and nearly irreversible supramolecular interactions with SWNTs, resulting in stable solutions of porphyrin-nanotube complexes in THF.[18] The motivation for this work included the recent report of triply fused porphyrin dimers covalently derivatized with two C_{60} molecules, resulting in a dyad structure capable of undergoing up to fifteen reversible electron transfer steps.[19,20] This behaviour implied possibly intriguing donor-acceptor ensembles formed non-covalently between the trimer and nanotubes. No increase in nanotube solubility was observable upon introduction to the porphyrin monomer, indicating that no significant interaction between the monomer and the SWNTs existed. In contrast, use of a solution of the triply fused dimer in acidified THF resulted in the initial formation of a homogeneous solution, which was stable enough for characterization by UV/Vis/ NIR absorption spectroscopy. However, upon standing for several hours, the SWNTs were observed to precipitate, indicating that the solubilizing influence of the triply fused dimer could not overcome the inter-nanotube Van der Waals attraction that causes SWNTs to aggregate into bundles. When the trimer was used, a very stable, dark solution was obtained after sonication for 5 min. This solution remained stable upon standing indefinitely, with no sedimentation even after centrifugation for 20 min at 5000 rpm. This stability indicated that the interaction strength between the trimer and the nanotube sidewall prevented nanotube re-bundling after formation of the nanotube-trimer complex. Bathochromic shifts in the UV-Vis and UV-vis-NIR absorption spectra upon oligoporphyrin complexation to SWNTs indicate electronic interactions between the porphyrins and the nanotubes, possibly signifying a porphyrin- to-nanotube charge transfer. With the triply fused oligomers, negligible absorption of the free dimer and trimer was detected in equilibrium with the nanotube-bound oligoporphyrins. This indicates that the triply fused oligoporphyrins form extremely strong complexes with SWNTs. AFM was

used to further characterize the composite solutions. The height profile of most features shown is consistently in the 2-4 nm range, indicating that large nanotube bundles must have been exfoliated into either individual nanotubes or very small bundles that are coated with porphyrin trimer molecules. It was also found that the porphyrin coating on the nanotubes is relatively uniform, with practically no observable uncoated SWNTs, again demonstrating the exceptionally strong nature of the SWNT-trimer interaction allowing for complete coverage of the nanotube surface.

Dirk M. Guldi et al also reported on donor-acceptor nanoensembles of solubilized carbon nanotubes.[21] In this study, the coulomb complex formation of a water-soluble SWNT grafted with poly(sodium 4-styrenesulfonate) (SWNT-PSS) and an octapyridinium free base porphyrin salt H_2P^{8+} en route to versatile donor-acceptor ensembles was presented along with the proof for an intra-ensemble charge separation in SWNT-PSS^{n-}/ H_2P^{8+} that lived for tens of microseconds. First insight into the electrostatic binding of SWNT-PSS^{n-} and H_2P^{8+} came from TEM. One drop of dilute aqueous solution containing equivalent amounts of SWNT-PSS^{n-} and H_2P^{8+} (0.1%) was cast onto a copper grid. For SWNT-PSS^{n-} thick bundles and ropes were evident, while for SWNT-PSS^{n-} / H_2P^{8+} thinner bundles surrounded by dark areas were observed, most likely deriving from electrostatic interactions. Absorption spectroscopy of the titration of dilute aqueous solution of H_2P^{8+} with SWNT-PSS^{n-} showed a clean conversion from H_2P^{8+} to SWNT-PSS^{n-}/ H_2P^{8+}, observed through an isosbestic point at 424 nm, with red shift of the Soret- and Q-bands. When SWNT-PSS^{n-} was added to H_2P^{8+}, the fluorescence also underwent several key changes. The fluorescence intensities decrease exponentially and converge to a final plateau value. The decrease in H_2P^{8+} fluorescence with SWNT-PSS^{n-} is as large as thirtyfold. Secondly, the intensity of the fluorescence peaks at 651 and 711 nm shift progressively to the red with final maxima at 654 and 715 nm. This trend mirrors the changes in the ground state absorption spectra. Thirdly, the H_2P^{8+} fluorescence lifetime (i.e., 10.2 ns), which in the absence of SWNT-PSS^{n-} is best fitted by a mono-exponential rate law, is replaced by a bi-exponential decay. In the presence of SWNT-PSS^{n-} a long- (10.2 ns) and a short-lived component (0.3 ns) are observed. The long-lived component relates to free H_2P^{8+} that is not associated with any SWNT-PSS^{n-}, while the short-lived component is attributed to

the deactivation within the SWNT-PSS^{n-}/ H_2P^{8+} nanoensemble.

Covalently porphyrin-functionalized single-walled carbon nanotubes were also optically examined by Zhen Guo et al.[22] and their donor- acceptor properties investigated. Novel covalently porphyrin-functionalized single-walled carbon nanotubes (SWNTs) were synthesized by the reaction of SWNTs with in situ generated porphyrin diazonium compounds. The resulting nanohybrid was characterized by spectroscopic (UV-Vis-NIR, FTIR (Fourier Transform InfraRed) and Raman) and microscopic (TEM and AFM) methods. The Raman and absorption spectroscopy data showed that the electronic properties of the modified tubes were mostly retained, without damaging their one-dimensional electronic properties. The fluorescence from the porphyrin moiety was almost completely quenched by SWNTs, indicating that the unique direct linkage mode facilitated the effective energy and electron transfer between the excited porphyrin moiety and the extended π -system of SWNTs. This novel nanohybrid material also exhibited excellent optical limiting properties, which will be discussed further in Chapter 6. The stability of SWNTs-TPP was further confirmed by the titration of hydrochloric acid to accelerate the colloid coagulation. When 2 ml of 0.46 N HCl solution was added to the solution of the mixture of SWNTs/TPP, visible black deposits appeared immediately, and the absorption spectrum became 'bumpy' because of the scattering caused by these particles. When adding HCl to a solution of SWNTs-TPP, no visible particles were observed even after all the porphyrin had been completely protonated. Solutions used for optical limiting measurements also showed the same results. Clearly, porphyrins covalently attached to SWNTs-TPP helped to disperse the SWNTs in the solvent and sustain the stability of the resulting colloid to environmental changes. SWNTs-TPP were found to show much better optical limiting properties compared with the benchmark material (C_{60}) and the individual components (TPP and SWNTs). Considering the donor-acceptor property of this nanohybrid in the excited state, the much enhanced optical limiting performance of SWNTs-TPP was attributed to the charge-separated excited state produced by photoinduced electron transfer from the electron-donating TPP moiety to the electron-accepting SWNTs.

Another report by Guldi and co-workers[23] focused on the potential of SWNT as building blocks for solar-energy conversion. SWNT are attractive platforms for photovoltaic

applications as they are good electron acceptors, and at the same time one-dimensional nanowires. Therefore, they are ready to accept electrons, which are then transported with high efficiency. In light of this feature, the combination of SWNT with donor groups signifies an innovative concept to 1) harvest solar energy and 2) convert it into useful electricity. Based on these principles, a SWNT-based solar cell should work efficiently. In this study, the systematic and molecularly controlled integration/organization of SWNT, together with porphyrin systems, into nanostructured devices is explored. The rich and extensive absorptions, typical of porphyrinoid systems, make an efficient use of light. The new system gives rise to promising monochromatic solar-energy conversion efficiencies- up to 8.5% internal photoconversion efficiencies (IPCE). The favorable charge-separation features of SWNT-PSS^{n-}/H_2P^{8+} and SWNT/pyrene^{+}/ZnP^{8-} nanohybrids are promising for the construction of photoactive electrode surfaces in addition to the combination of the electron-accepting character of SWNT with ZnP, which acts as an excited state electron donor. In testing these novel SWNT architectures in photoelectrochemical devices, they were integrated sequentially onto solid substrates using the electrostatic interactions between SWNT-PSS^{n-}/ZnP^{8+} and SWNT/pyrene^{+}/ZnP^{8-}. Conventional spectrophotometry was used to assess the adhesion of the individual building blocks to the surface, and this was subsequently verified by AFM. It was also demonstrated that solar-energy conversion devices could be assembled through the successful incorporation of SWNT hybrids-noncovalently linked SWNT/pyrene^{+} and covalently linked SWNT-PSS^{n-}–onto semitransparent ITO electrodes. A cell containing a single layer of SWNT/pyrene^{+} and single layer of ZnP^{8-} led to promising monochromatic conversion efficiencies of up to 4.2% (that is, with a +200 mV bias).

Guldi and co-workers also reported on a set of new cationic metalloporphyrins, FeP^{8+} and CoP^{8+} and their systematic integration into novel SWNT ensembles.[24] Stable dispersions of SWNT/pyrene^{-} were prepared by stirring, sonicating, and centrifuging 10 mL of a sodium tetraborate decahydrate buffer (pH 9.2) pyrene solution (1 mM) with 1 mg of purified SWNT. Bathochromic shifts (of approximately 2 nm) in the absorption spectra of these SWNT/pyrene complexes suggested mutually interacting π-systems indicating Van der Waals interactions between SWNT and each of the four pyrene moieties employed in

these studies. It was previously shown that in covalently linked SWNT/pyrene nanohybrids intramolecular fluorescence quenching prevails. The quenching is attributed to intramolecular transduction of singlet excited energy- from the high-energy pyrene singlet excited state to the low-energy manifold of SWNT. In line with this conclusion, strong fluorescence quenching was observed for all the new SWNT/ pyrene$^-$ ensembles. Time-resolved fluorescence decay measurements indicated that the residual fluorescence is largely due to non-immobilized pyrene$^-$. Electrostatic interactions between negatively charged SWNT/ pyrene$^-$ and positively charged metalloporphyrins MP^{8+} (where M = Zn, H_2, Fe, and Co) were tested in a series of investigations. These include microscopy (i.e., transmission electron microscopy (TEM) and atomic force microscopy (AFM)) and spectroscopy (i.e., absorption and fluorescence spectroscopy). Absorption spectroscopy was used to assess the interaction between SWNT/pyrene$^-$ and ZnP^{8+}. ZnP^{8+} solutions were titrated with several concentrations of SWNT/pyrene$^-$, which resulted in notable red-shifts of the Soret- and Q-band features of ZnP^{8+} and the presence of two isosbestic points at 426 and 437 nm. The Soret transition at the endpoint of the titration was found to have a slightly larger half-width and a slightly lower extinction. These changes were also noted in the absence of SWNT proving that electrostatic forces are selective tools for associating SWNTs with ZnP, and not observed at all for negatively charged porphyrins which are repelled by SWNT/ pyrene$^-$. The integration of SWNTs, water soluble pyrene$^-$, and a series of water-soluble porphyrins into functional nanohybrids was accomplished through a combination of associative Van der Waals and electrostatic interactions. The SWNT functioned as an electron acceptor, while MP^{8+} metalloporphyrins were employed as excited-state electron donors. Crucial for the binding studies were SWNT/pyrene$^-$ templates that bear carboxylate or sulfonate appendages. These negatively charged groups function (i) as promoters for suspending SWNT samples in aqueous media and (ii) as anchors for interaction with one or several pyridinium headgroups present in the different MP^{8+}. Spectroscopic and microscopic methods were then used to characterize the resulting SWNT/pyrene$^-$ and SWNT/pyrene$^-$/ MP^{8+}. All the novel nanohybrids formed stable suspensions in aqueous media allowing steady-state and time-resolved work. A key feature of the SWNT/ pyrene$^-$ and SWNT/ pyrene$^-$ / MP^{8+} systems is that an efficient debundling was achieved, which in

some cases gave isolated nanohybrid structures. Transient absorption and fluorescence measurements demonstrated that SWNT serve as the electron acceptor component in SWNT/ pyrene^{-} / MP^{8+} (i.e., H_2P^{8+} and ZnP^{8+}). Intrahybrid electron transfer was found to occur on the 200-300 ps time scale and evolve from the photoexcited H_2P^{8+} and ZnP^{8+}). to SWNT. This event leads to the reduction of the electron-accepting SWNT and oxidation of the electron-donating MP^{8+}). The radical ion pairs are long-lived and benefit from charge recombination dynamics that are located in the Marcus inverted region.

A combination of both covalent and non-covalent approaches have also been recently utilized by this group to form donor-acceptor hybrid structures.[25] SWNT were grafted with poly(4-vinylpyridine), PVP, to form DMF-soluble SWNT-PVP. The pyridine moieties present in SWNT-PVP favor the axial coordination of a strong donor in the excited state, zinc tetraphenylporphyrin (ZnP). Two regions of transitions are discernable in the absorption spectra, namely the UV transitions corresponding to the polymer and the characteristic van Hove singularities of SWNT (bandgap transitions in semiconducting and metallic SWNT) in the visible and near-infrared. The presence of van Hove singularities indicates only minor modification of the electronic structure had occurred during the free-radical polymerization preparation of SWNT-PVP. SWNT-PVP can be fully dispersed in DMF, yielding suspensions that are stable for months. The complexation of ZnP with SWNT-PVP, was confirmed by spectroscopic fluorescence and absorption titration experiments. With increasing SWNT-PVP concentration the ZnP absorption features (Soret and Q-band) revealed bathochromic shifts of up to around 2 nm. These shifts were further accompanied by small but notable broadenings and isosbestic points at around 422 and 429 nm. The presence of the isosbestic points implies a clean conversion from ZnP to SWNT-PVP/ZnP. The same bathochromic shifts in the Soret band developed when just PVP or pyridine were mixed with ZnP. The shifts observed, though small, indicate a ligand-exchange reaction. The fluorescence emission experiments with ZnP allow a distinction between coordinating SWNT-PVP or PVP. In particular, when adding SWNT-PVP, the ZnP fluorescence quantum yields dropped exponentially This behavior was assigned to static electron-transfer quenching within a SWNT-PVPZnP complex. Redshifts of the fluorescence maxima were also observed. In contrast, a reference experiment using PVP gave no appreciable fluores-

cence quenching due to the lack of any electron-accepting character of PVP.

For comparison purposes, upon titration of SWNT-PVP with free-base tetraphenylporphyrin no absorption spectrum shift was observed, confirming the absence of coordination. However, a moderate H_2P fluorescence quenching of less than 20% was observed, which suggested some other pathways of excited-state deactivation. It should be noted that for SWNT-PVPZnP under comparable conditions the quenching is more than 65%. To investigate the SWNT-H_2P interactions, similar concentrations of pristine SWNT, suspended in DMF, were added to H_2P and/or ZnP, giving identical results of no shift in absorption and about 20% fluorescence quenching. It is reasonable to deduce $\pi - \pi$ interactions to be responsible for the residual fluorescence quenching. Transient absorption studies indicated that an intracomplex electron transfer, evolving from the photoexcited ZnP to the electron-accepting SWNT-PVP, governs the photoexcited-state deactivation of SWNT-PVP/ZnP. Therefore fluorescence and transient absorption measurements provided kinetic and spectroscopic evidence of a transfer of charge density for this composite, where a consequence of strong donor-acceptor coupling is the rapid formation of microsecond-lived radical- ion-pair states.

In a recent communication a purely non-covalent immobilization of free base and zinc tetraphenylporphyrins onto the SWNT surface for novel electron donor-acceptor nanohybrid structures was explored by G. M. Aminur Rahman et al from the same group.[26] The absorption features were compared in the pristine solutions and in the corresponding SWNT suspensions, and at first glance appeared to be identical. A closer inspection of the absorption spectra revealed a broadening of the Soret band and an apparent red-shift, especially for SWNT/H_2P. Both features reflect notable electronic communication between the two $\pi-$ systems of SWNT and H_2P. The weaker interactions observed for SWNT/ZnP, were attributed to an appreciable interference between the zinc metal and the SWNT surface and SWNT/H_2P suspensions appear more stable than SWNT/ZnP. AFM investigations showed the nanotubes in SWNT/ZnP to be more aggregated than SWNT/H_2P, consistent with the zinc located in the center of the porphyrin decreasing the interactions between the nanotube and the porphyrin π systems. In other words, ZnP is not able to fully exfoliate and/or stabilize individual SWNT in DMF solutions. In the excited state, mutual electronic

interactions between ZnP or H_2P and SWNT were deduced from fluorescence spectroscopy, where SWNT/ZnP or SWNT/H_2P suspensions were compared with DMF solutions of just ZnP or H_2P. Porphyrin fluorescence was appreciably reduced in both SWNT cases with quenching factors of around 2.6 (SWNT/ZnP) and 5.9 (SWNT/H_2P) deduced. Transient absorption measurements were performed on the systems, in which charge transfer features persistent on the time scale of hundreds of nanoseconds were observed due to these electronic interactions.

Nikos Tagmatarchis reported in an earlier paper on supramolecular methods utilized to immobilize a positively charged water-soluble pyrene derivative to purified single-walled carbon nanotube (SWNT), which was further coupled by attractive electrostatic interactions to an oligoanionic porphyrin.[27] Electron transfer from the photoexcited states were probed by fluorescence and transient absorption spectroscopy measurements. Strong, slightly red-shifted, $\pi - \pi^*$ transitions of pyrene$^+$ were observed in the UV-Vis region in addition to the characteristic van Hove singularities corresponding to the S_{11}, S_{22} and M_{11} semiconducting and metallic SWNT which were present in the Vis-NIR region. The red-shift supports the electronic communication between the two different ring systems while the presence of the Van Hove peaks shows that the novel electronic properties of SWNT remained virtually unchanged upon the Van der Waals complexation of the pyrene$^+$ derivative. TEM was used to image the SWNT, SWNT/pyrene$^+$ and SWNT/pyrene$^+$/H_2P^{8-} where the porphyrins were readily observed, and were found to cause exfoliation of nanotube bundles. The strong fluorescence emission at 655 and 715nm of photoexcited H_2P^{8-} was quenched upon addition of SWNT/ pyrene$^+$, with an exponential decrease solely dependent on the concentration of the added SWNT/pyrene$^+$. It was concluded that the excited-state quenching process in the (SWNT/pyrene$^+$)/H_2P^{8-} nanoensemble involved either electron or hole transfer, i.e. oxidation of the porphyrin moiety and reduction of the SWNT unit.

5.1.3 Carbon Nanotube De-Bundling

As discussed in Chapter 4 of this thesis, disentanglement of carbon nanotube ropes through controlled nanotube de-bundling is necessary in order to realize functional SWNT-based nanocomposites and devices. This was achieved in Chapter 4 by chemical modification

of SWNT surfaces through non-covalent interaction with conjugated organic molecules, such as the polymer PmPV and structurally related short chain molecules. Similarly, porphyrin/carbon nanotube composites have also attracted growing interest as a powerful means to disperse and debundle SWNT, with the ultimate aim of isolating significant populations of individual SWNT at high concentrations. It is noteworthy that much of the literature reviewed above characterizing various porphyrin/nanotube systems reports evidence of carbon nanotube bundle exfoliation upon formation of these composites.[7,16,18,24,26,27]

5.2 Linear Optical Properties of Planar Porphyrin Systems and their Carbon Nanotube Composites

Single walled carbon nanotubes (SWNTs) therefore possess unique structural, mechanical and electronic properties, and are thus promising materials for future device fabrication. However, their potential is limited in that they are insoluble in aqueous and organic solutions and satisfactory control over nanotube location and orientation has yet to be achieved. As discussed, SWNT solubility has recently been achieved by functionalizing them covalently and noncovalently. Noncovalent functionalization is of particular interest as it provides a method of handling the nanotubes chemically without altering the electronic structure of the nanotubes themselves, and this has been achieved in a number of ways, as described in Chapter 4. Porphyrins are an important family of conjugated organic molecules, whose members include many important biochemical compounds such as haemoglobin and chlorophyll, and have applications in many industries including medicine, optics and electronics. Porphyrins are used in cancer photodynamic therapy, sensitisers for photoactive switches, artificial photosynthesis studies and electronics. By functionalizing SWNTs with porphyrins, it is also hoped that the nanotubes may acquire many of the intrinsic porphyrin properties such as luminescence and biocompatibility. Thus, the optical properties of carbon nanotubes noncovalently functionalized with porphyrin molecules are of great interest in both the linear and nonlinear regimes. In this chapter, a report on the photophysical properties of planar and nonplanar porphyrin molecules and their non-covalent SWNT composites is presented. In addition to this, discrepancies in optical absorption and fluorescence spectra reported by

others are clarified for the first time.

5.2.1 Experimental Section

The purified SWNTs used in this work were prepared by the HiPCO process, supplied by Carbon nanotechnologies inc and used without further treatment. The porphyrin molecules used were purchased from Aldrich. Two identical sets of solutions of each porphyrin were made with concentrations ranging from approximately 1 -200 μM in chloroform and dimethylformamide. Pure HiPCO SWNT was added to one porphyrin solution at each concentration such that the porphyrin- SWNT mass ratio was 1:1.

All photoluminescence measurements in this thesis were carried out using an LS-55 Perkin-Elmer luminescence spectrometer with an excitation wavelength equal to the absorption maximum of the porphyrin in question for each solvent. The linear absorption spectra were recorded using a Shimadzu UV3100 UV-Vis-NIR spectrometer. All optical measurements were performed in 1 cm pathlength quartz cells.

5.2.2 Results and Discussion

Dispersions containing the HiPCO SWNT alone were found to be completely insoluble in $CHCl_3$, and fell out of solution at all concentrations within minutes. Limited solubility was observed for SWNT in DMF for concentrations below 0.01 g l^{-1}. In both solvents it was found that tetraphenylporphyrin (TPP) and its zinc metalloporphyrin derivative (Zn-TPP) could dissolve SWNT. No precipitation was noticed in the TPP:SWNT and ZnTPP:SWNT solutions even after several months of storage.

Due to their high degree of conjugation, porphyrin molecules are expected to bind non-covalently to carbon nanotubes through Van der Waals interactions, as previously observed in the literature. These non-covalently functionalized porphyrin- carbon nanotube composites were observed with TEM (Figure 5.1) where the amorphous ZnTPP molecules can clearly be seen adhering to the nanotube surface.

A slow aggregation of the TPP:SWNT composite solutions was noticed when the concentration of the dispersion was greater than 59 μM. The TPP and Zn- TPP molecules in chloroform both displayed typical absorption spectra, with Soret bands observed at 418

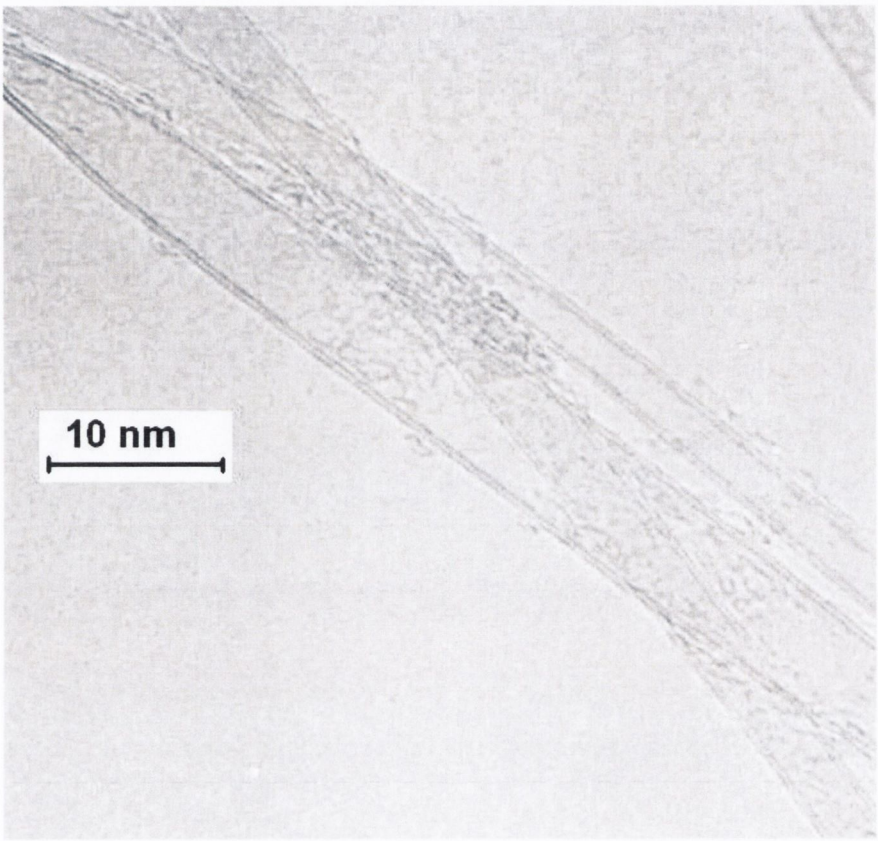

Figure 5.1: TEM (transmission electron microscopy) image shows adhesion of organic porphyrin molecules to the outside of Nanocyl double wall nanotubes (DWNT). As can be seen in the micrograph above, the double wall nanotubes consisted of between two- and five- or six- walled multiwalled nanotubes. The image above was taken for a 2:1 ZnTPP:DWNT composite at a high concentration of 0.02 kg/m^3 in chloroform.

and 422 nm respectively. However upon introduction of energy into the system in the form of sonication- or intense irradiation during z- scan- the Soret band split (Figure 5.2), with a second absorption band appearing at the longer wavelength of 446 nm. Introduction of the nanotubes into this system did not affect the positions of these peaks. However, as sonication was necessary in order to disperse the nanotubes throughout the solution, the composite solutions always yielded this second red shifted absorption peak. The absorption spectrum of the unsonicated form is characterized by four Q bands localized at 515.5, 550, 591 and 646 nm, whereas upon sonication the Q Bands shift to two strong maxima at 610 and 661 nm. The green solution obtained in these conditions did not show any sign of

aggregation even after several weeks. It was found that sonodegradation of $CHCl_3$ during sample preparation yielded HCl, which subsequently caused protonation of the core nitrogen atoms. Therefore, chloroform was found to be unsuitable for monitoring carbon nanotube composites in solution. This behaviour was investigated and is described in detail in Section 5.4 of this thesis.

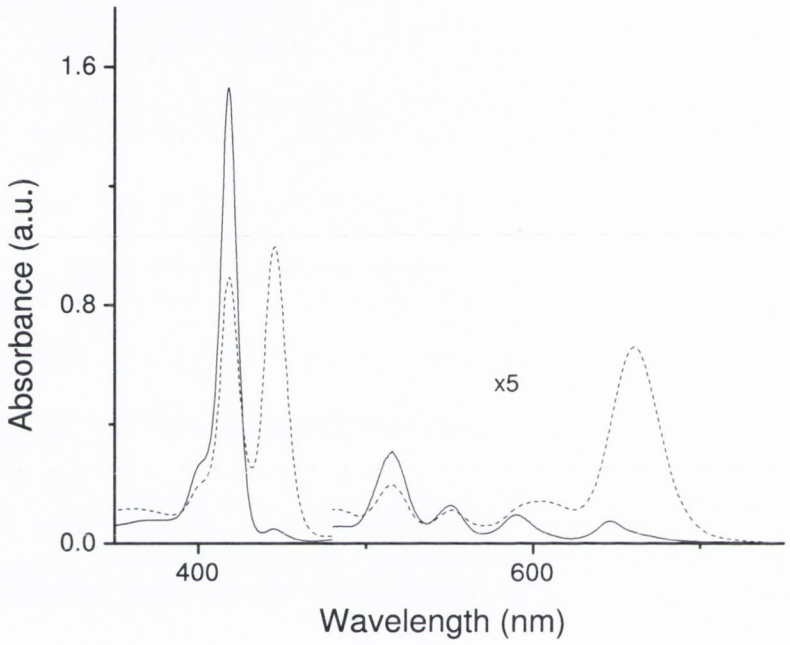

Figure 5.2: The absorption spectrum of TPP before (solid line) and after (dashed line) sonication for 30 seconds (3.3μM, $CHCl_3$, 25^{o}C)

Once the absorption and the concentration were measured, the ground state absorption cross- section σ_g was found from the relationship $\alpha_g = N\sigma_g$, where α_g is the ground state absorption coefficient and N is the molecular concentration. The values obtained for σ_g at 532 nm were 6.51 x 10^{-16} cm^2 for the bi- protonated TPP form and 7.137 x 10^{-16} cm^2 for the deprotonated one at a concentration of 35.1 μM. This is in conservative agreement with reported values of 0.8 x 10^{-17} cm^2 and 2.1 x 10^{-17} cm^2 for bi- protonated and deprotonated meso-tetra(sulfonatophenyl) porphyrin ($TPPS_4$) solutions respectively. Addi-

tion of 10μL of triethylamine again completely reversed the protonation process, restoring the deprotonated normal absorption spectrum for the TPP solutions. This confirms the equilibrium nature of the protonation mechanism.

Two characteristic emission peaks at 650 and 715 nm were observed for unsonicated (and therefore deprotonated) TPP samples in $CHCl_3$ with the luminescence maximum observed at 650 nm. This is typical of porphyrin emission spectra. After sonication, the emission spectrum obtained from the same solution upon excitation at the same wavelength appeared very different. The fluorescence spectra for excitation at the Soret band of each solution, as depicted in Figure 5.3 below, present a single maximum at 686 nm for the bi protonated TPP solutions.

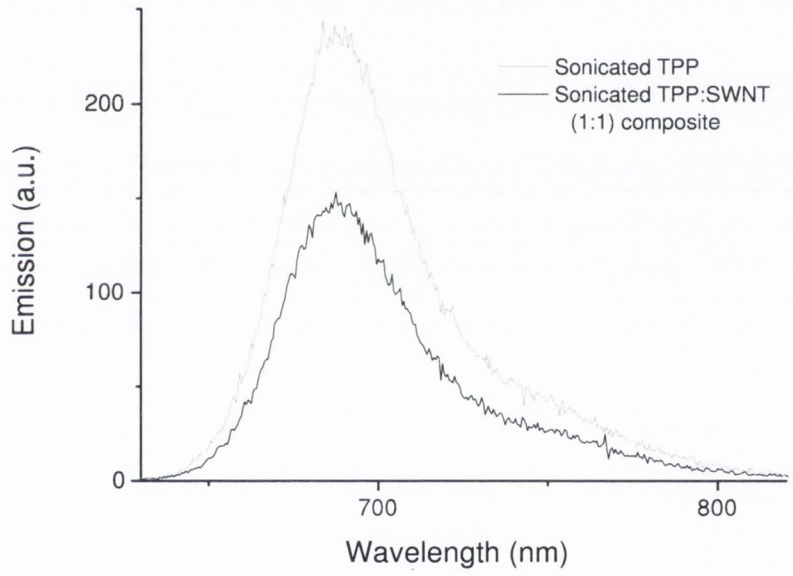

Figure 5.3: Photoluminescence spectrum of sonicated TPP (gray line) and the corresponding sonicated TPP:SWNT (1:1) composite solutions at a concentration of 6.5 μM upon excitation at 446 nm. All spectra were taken in quartz cuvettes of 1 cm pathlength.

The two characteristic sharp emission bands of the TPP solution had been replaced by a single, broad emission band, centred at a wavelength of 685 nm as can be seen in Figure 5.3. Upon formation of a (1:1) composite with the SWNT, the emission was unchanged,

and was typical of that observed from the protonated porphyrin. Negligible quenching was observed for composite solutions at concentrations below 6.5 μM. Emission spectra for solutions of Zn- TPP with and without HiPCO SWNT over the same concentration range displayed a similar red shift of 44.5 nm of the peak emission band from 603.5 nm to 648 nm upon sonication. Fluorescence was quenched in the Zn porphyrins relative to their free base counterparts. The low quantum yields for Zn- porphyrins reflect a high efficiency of nonradiative decay processes for metalloporphyrins which is to be expected since this photochemistry arises only from high- lying excited states.

Dimethylformamide (DMF) was chosen instead as a suitable solvent for our nanotube composite solutions, as it was capable of dissolving the porphyrin molecules, and was not found to sono-degrade. UV-Visible absorption spectra taken for TPP solutions in DMF, with and without nanotubes present, are shown in Figure 5.4 and display a normal absorption spectrum, with a Soret band observed at 416 nm. Neither the intensity nor the position of this band was found to be altered upon solution irradiation or sonication, and the introduction of nanotubes into the system does not affect the absorption bands.

Two characteristic porphyrin photoluminescence bands were observed in the 600 to 750 nm region from the TPP and composite solutions in DMF (Figure 5.5). Sonication and irradiation did not alter the emission spectrum of TPP in DMF which displayed peaks at 650 and 717 nm.

The emission spectrum is identical in the presence of nanotubes, with some quenching observed for the composite solutions. This quenching may be indicative of efficient energy transfer between the porphyrin molecules and the nanotube. However, negligible quenching was observed for composite solutions below a concentration of approximately 2.5 μM for both TPP and ZnTPP, and as the quenching coincided with the onset of aggregation in the solutions, it could not conclusively be attributed to energy transfer to the nanotubes. An appreciable reduction in the porphyrin fluorescence for SWNT composites with both TPP and ZnTPP in DMF has been reported, with quenching factors of around 2.6 (SWNT/ZnTPP) and 5.9 (SWNT/TPP) observed. In fact, we found the quenching factor to be concentration dependent, with values ranging from 1.27 to 12.6 observed for TPP concentrations of 2.8μM and 59μM respectively, and values of 1.26 to 5.6 obtained for

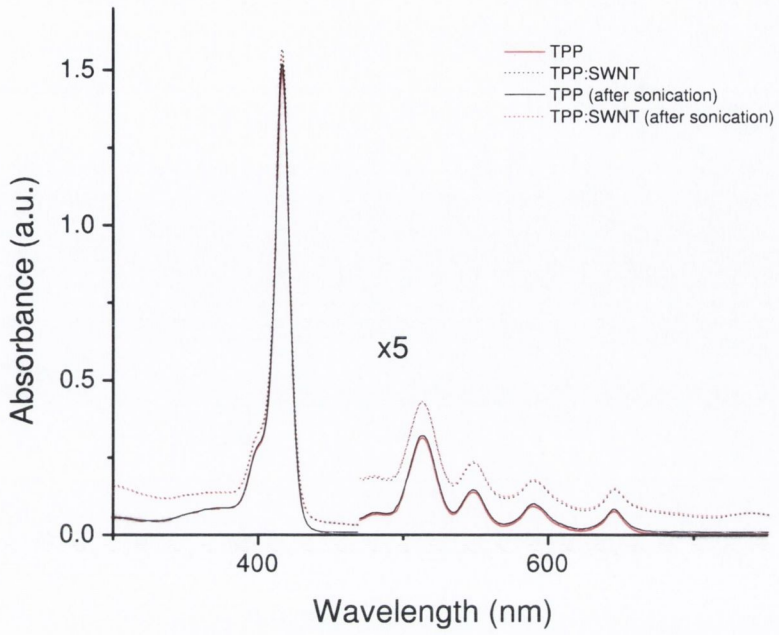

Figure 5.4: Absorption spectra of TPP (solid lines) and corresponding TPP:SWNT (1:1) composite solutions (dashed lines) before (black lines) and after (red lines) sonication (35.1 μM, DMF, 25°C). Spectra were taken in quartz cuvettes of 1 mm pathlength.

2.5μM and 53μM ZnTPP solutions. The introduction of nanotubes into the system did not affect the onset of what appeared to be porphyrin aggregation for either molecule, which occurred for concentrations above 2.4μM (Figure 5.6).

Although the energy transfer efficiency for TPP and ZnTPP composite solutions was found to be doubtful, the enhanced solubility of SWNT in both DMF and $CHCl_3$ was not. This is particularly noticable for composites in $CHCl_3$, in which SWNT are usually completely insoluble. Therefore, although potential applications as donor-acceptor nanoensembles for photovoltaics may be in question for these planar porphyrins, the enhanced nanotube solubility of their composites still merits current and future investigation.

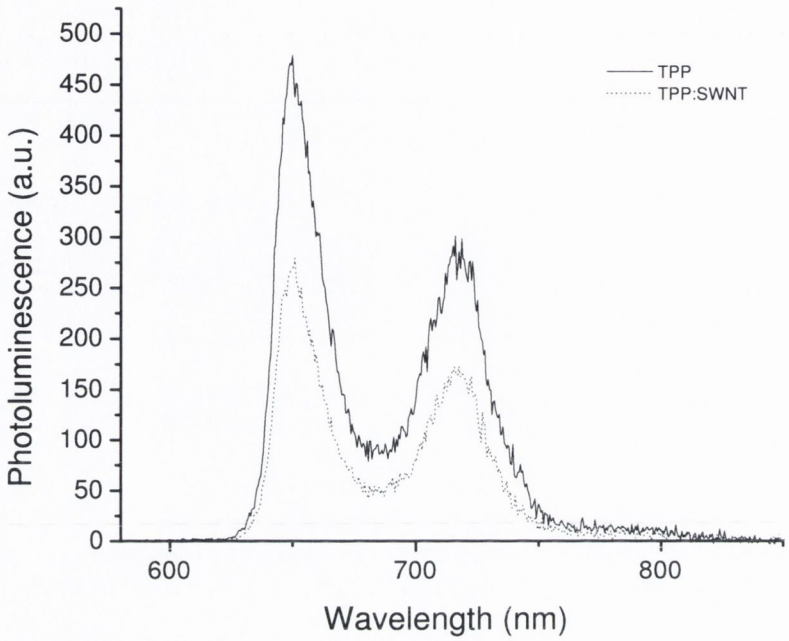

Figure 5.5: Photoluminescence spectrum of TPP and corresponding TPP:SWNT (1:1) composite solutions in DMF at 7.6μM. PL spectra obtained are identical, with quenching observed for the composite only at concentrations above 2.4μM.

5.3 Linear Optical Properties of Nonplanar Tetraphenylporphyrin Derivatives and their Carbon Nanotube Composites

Natural cofactors are often found to be tetrapyrroles, due to the high versatility of these organic structures. The functional variety afforded by this class of compound is related to the flexibility of their molecular conformations, as the physicochemical properties of such molecules may be tuned through manipulation of the macrocycle. In recent years, porphyrins with such nonplanar macrocyclic conformations have thus attracted considerable attention in an attempt to understand the relationship between conformational distortion and photophysical properties. Through functionalization with porphyrins, it is hoped that the superior physicochemical properties of the porphyrin moiety may be achieved by the

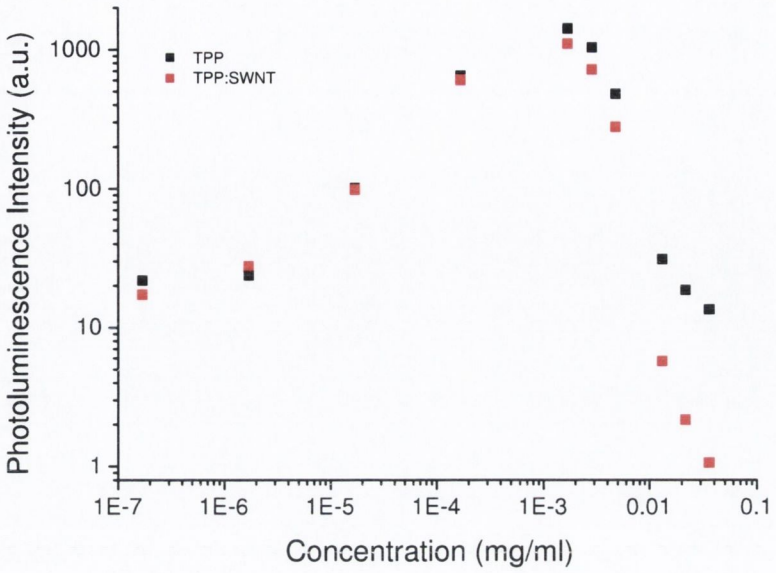

Figure 5.6: The plot of emission as a function of concentration shows that the presence of nanotubes does not delay the onset of aggregation- induced quenching at higher concentrations. All spectra were taken in quartz cuvettes of 1 cm pathlength.

nanotubes. Non-covalent interactions between SWNT and nonplanar porphyrins are therefore of great importance in determining what correlation, if any, exists between the degree of macrocycle nonplanarity and the strength of the subsequent binding for these nanotube composites. In other words, it is possible that the planarity of the TPP and ZnTPP porphryin macrocycles examined lead to a geometric incompatibility between these molecules and the curved surface of the carbon nanotubes they attempt to bind to. For this reason, a series of six ethyl- substituted tetraphenylporphyrins were synthesised by Prof. Mathias Senge in the School of Chemistry in Trinity College Dublin, using a technique previously reported[28] with intermediate graded degrees of distortion due to -ethyl- substituted pyrrole rings ranging from that of tetraphenylporphyrin (H_2TPP) to the standard nonplanar porphyrin 2,3,7,8,12,13,17,18-octaethyl-5,10,15,20-tetraphenylporphyrin (H_2OETPP). The complete series is illustrated in Figure 5.7. [1]

[1]These images shown in Figure 5.7 are shown courtesy of Dr. Donal Mc Kernan

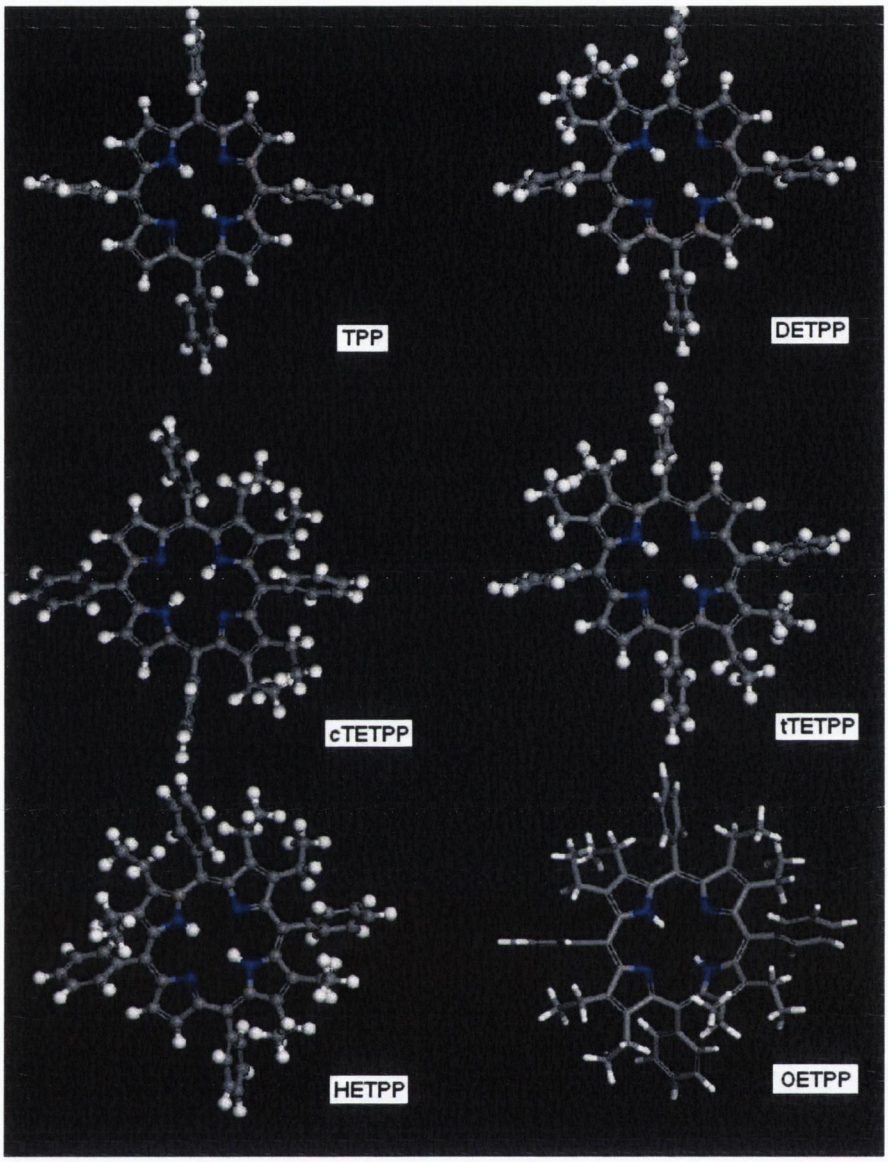

Figure 5.7: Structure of series of nonplanar tetraphenylporphryin derivative molecules

5.3.1 Experimental Section

The purified SWNTs used in this work were prepared by the HiPCO process, supplied by Carbon Nanotechnologies Inc. and used without further treatment. The nonplanar tetraphenylporphyrin (TPP) derivatives were prepared by colleagues in the School of Chem-

istry, Trinity College Dublin, using methods described elsewhere.[28] The TPP molecules used were purchased from Aldrich. Two identical sets of solutions of each porphyrin were made with concentrations ranging from approximately 1 -500 μM in dimethylformamide (DMF). Pure HiPCO SWNT was added to one porphyrin solution at each concentration yielding solutions with porphyrin- SWNT mass ratios of 1:1, 5:1 and 10:1. Photoluminescence measurements were again carried out using an LS-55 Perkin-Elmer luminescence spectrometer and the linear absorption spectra were recorded using a Shimadzu UV3100 UV-Vis-NIR spectrometer as before. Measurements were performed in quartz cells of either 1 cm or 2 mm path length.

5.3.2 Results and Discussion

In order to study the correlation between macrocycle nonplanarity for porphyrin molecules and their noncovalent interactions with carbon nanotubes, a series of porphyrins with graded degrees of macrocycle distortion were synthesized via mixed condensation of pyrrole, diethylpyrrole and benzaldehyde as previously described.[28] The behaviour of the nanotube composites formed with these nonplanar porphyrins was compared with that of the more planar molecule tetraphenylporphyrin (TPP).

Limited solubility was observed for the HiPCO SWNT solely in DMF for concentrations below 0.01 g L^{-1}. It was found that TPP and its nonplanar derivatives 2,3- diethyl- 5,10,15,20- tetraphenylporphyrin (DETPP), 2,3,12,13- tetraethyl- 5,10,15,20- tetraphenylporphyrin (tTETPP), 2,3,7,8- tetraethyl- 5,10,15,20- tetraphenylporphyrin (cTETPP), 2,3, 7,8,12,13- hexaethyl- 5,10,15,20- tetraphenylporphyrin (HETPP) and 2,3,7,8,12,13,17,18- octaethyl- 5,10,15,20- tetraphenyl porphyrin (OETPP) could all dissolve SWNT. Crystallographic studies have previously shown that the macrocycle distortion in the solid state for these molecules increases gradually in the order TPP < DETPP < tTETPP < cTETPP < HETPP < OETPP. Negligible precipitation was noticed in these composite solutions even after several months of storage.

Porphyrin molecules are expected to bind non-covalently to carbon nanotubes through Van der Waals interactions as a result of their high degree of conjugation. Several reports of such non-covalently functionalised carbon nanotube systems have been described

in Section 5.1, and adhesion of Zn-TPP molecules to the surface of carbon nanotubes observed with TEM (Figure 5.1) provides some evidence of interaction between the two moieties in solution, even for the planar porphyrins investigated above which did not appear to bind particularly strongly to the nanotube surface. A slow aggregation of the porphyrin:SWNT composite solutions was noticed when the concentration of the dispersion was greater than 59 μM for solutions where the porphyrin: nanotube mass ratio was 1:1, and approximately 100 μM for the 5:1 and 10:1 porphyrin: nanotube solutions. This confirmed that non-covalent porphyrin interaction enhanced the solubility of carbon nanotubes in DMF.

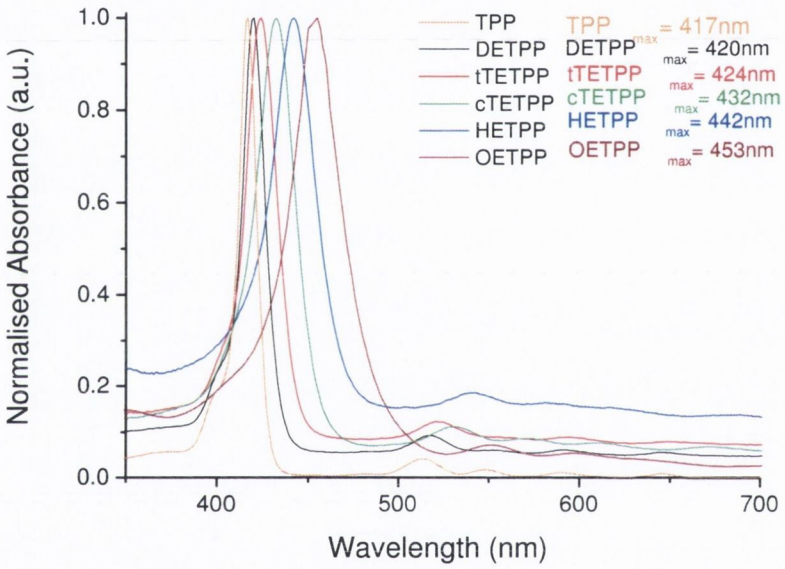

Figure 5.8: Normalised UV-VIS absorption spectra of TPP, DETPP, tTETPP, cTETPP, HETPP and OETPP and their (1:1) SWNT composites (0.001mg/ml, DMF, 25^{o}C).

The TPP derivative molecules in dimethylformamide all displayed typical absorption spectra, with Soret bands observed ranging between 417 nm and 453 nm (Figure 5.8). The absorption maximum, or Soret band, of each porphyrin was found to shift to a lower energy with increasing porphyrin non-planarity relative to the TPP molecule. The Soret bands were observed at 417, 420, 424, 432, 442 and 453 nm for TPP, DETPP, tTETPP,

cTETPP, HETPP and OETPP respectively. The porphyrin nonplanarity results from a gradual distortion of the porphyrin macrocycle due to steric crowding with each additional ethyl group added. These absorption band red shifts are characteristic of non-planar porphyrins, where the degree of non-planarity of a molecule is often determined by examination of such spectral shifts.[29,30,31]

Upon interaction with the carbon nanotubes, the composite Visible-NIR absorption spectra are intermediate between the spectrum of the SWNT suspension and the porphyrin spectrum, with Q bands and Van Hove peaks present, but slightly shifted in some cases (HETPP and OETPP) for the 1:1 composite solutions. For the 5:1 and 10:1 composites, no change in the absorption spectrum was observed, with the composite displaying peaks originating from both the individual porphyrin molecules and the carbon nanotube Van Hove absorption peaks at 377, 409, 451, 504, 559, 602 and 658 nm. Further evidence of increased nanotube solubility in the presence of the porphyrins was confirmed by the intensity increase of the Van Hove peaks for the composite solutions using UV-Visible-Near IR absorption spectroscopy (Figure 5.9)

The fluorescence spectra upon excitation at the Soret band of each solution, as depicted in Figure 5.10 below, present two emission peaks characteristic of porphyrin photoluminescence for the two most planar samples, TPP and DETPP. The emission deviates from this pattern with increasing macrocycle distortion, with one broad peak observed for tTETPP, cTETPP, and HETPP displaying PL which is barely resolved into two peaks. As the porphyrin macrocycle becomes more perturbed, the luminescence becomes increasingly less intense, with no fluorescence observed for OETPP at all concentrations studied.

The emission wavelengths were also found to red shift with increasing macrocycle non planarity.[32,33] It was not possible to determine if this was true for the non-fluorescent molecule OETPP. The Stokes shift also increased with increasing molecule non planarity, with values of 232, 232, 246, 269 and 308 nm for TPP, DETPP, tTETPP, cTETPP, and HETPP respectively. Upon formation of a (1:1) composite with the SWNT, the emission profile was unchanged for all porphyrins studied.

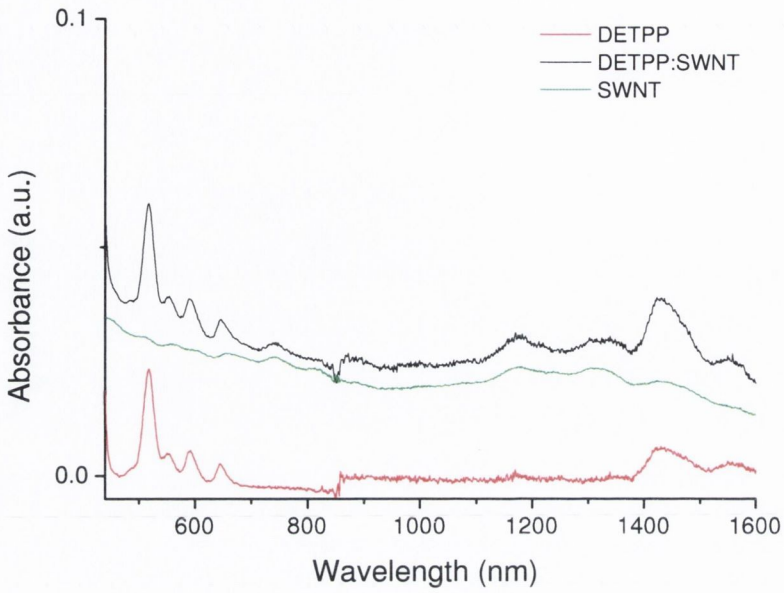

Figure 5.9: The VIS-NIR absorption spectra of DETPP, its (1:1) SWNT composite and a dispersion of SWNT alone in DMF show the characteristic Q Bands and Van Hove peaks, and show the absorption spectrum of the composite solution is intermediate between that of the porphyrin and the SWNT with characteristics of both.

5.3.3 Inner Filter Effect and Non-Covalent Binding of Porphyrins to Nanotubes

Previously, it was found that both TPP and its metalloporphyrin derivative Zn- TPP displayed negligible quenching for (1:1) composite solutions at concentrations below 6.5 μM, with self-aggregation of the solutions appearing evident at higher concentrations where strong PL quenching was observed for the composite solutions. In the context of this thesis, aggregation is defined as a generic term which describes any interaction between individual molecules which in turn affects the electronic structure of the individual molecule (including $\pi - \pi$ stacking and other nonpolar interactions). These findings were consistent with the literature, where strong photoluminescence quenching of composite solutions was attributed to evidence of non-covalent binding of porphyrin molecules to carbon nanotubes. Such studies were typically performed at only one concentration, at the same high concentrations where

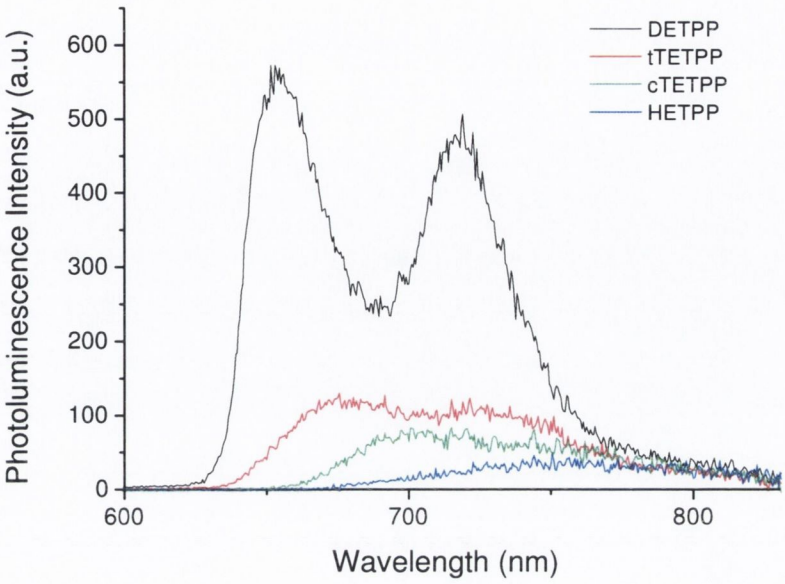

Figure 5.10: Photoluminescence spectra of porphryins examined in DMF showed porphyrin emission exhibiting both a redshift and a reduction in intensity with increasing nonplanarity, with the exception of OETPP which did not display any fluoresce at any concentration studied.

we had also found strong quenching.

In this section, evidence is presented that this reported photoluminescence behaviour for porphyrin composite solutions is not a real effect, and is in fact the result of a common photoluminescence phenomenon. These findings imply that many of the optical findings which support non-covalent porphyrin functionalization reported in the literature may be artefacts and not actually attributable to either energy transfer or photoinduced electron transfer from the bound porphyrins to the SWNT as suggested. Under commonly used experimental conditions, the observed fluorescence signal from a solution can be found to decrease relative to its concentration, as the solution becomes increasingly concentrated. This decrease is due, in part, to an attenuation of the excitation beam in regions of the solution in front of the point from which the fluorescence is collected by the detector, and to absorption of the emitted fluorescence within the solution . This effect is known as the

Inner Filter effect, as defined by Parker and Rees (1962).[34]

The variation in photoluminescence (PL) intensity was studied as a function of concentration for composite solutions over a wide concentration range. Assuming non-covalent binding of the porphyrins onto the carbon nanotube surface through Van der Waals interactions, the photoluminescence of the composite solutions is expected to be quenched relative to that of the same concentration of porphyrin, consistent with the model developed by Coleman et al.[35] which accurately described non-covalent nanotube interactions with the conjugated polymer poly[m-phenylenevinylene-co-(1,5- dioctyloxy-2,6-naphthylene vinylene (pmNV) and some of the oligomers and polymers introduced in Chapter 4. Due to constant porphyrin adsorption/desorption from the nanotubes, the extent of this photoluminescence quenching is predicted to be highly nonlinear with concentration approaching 1 at very low concentrations.

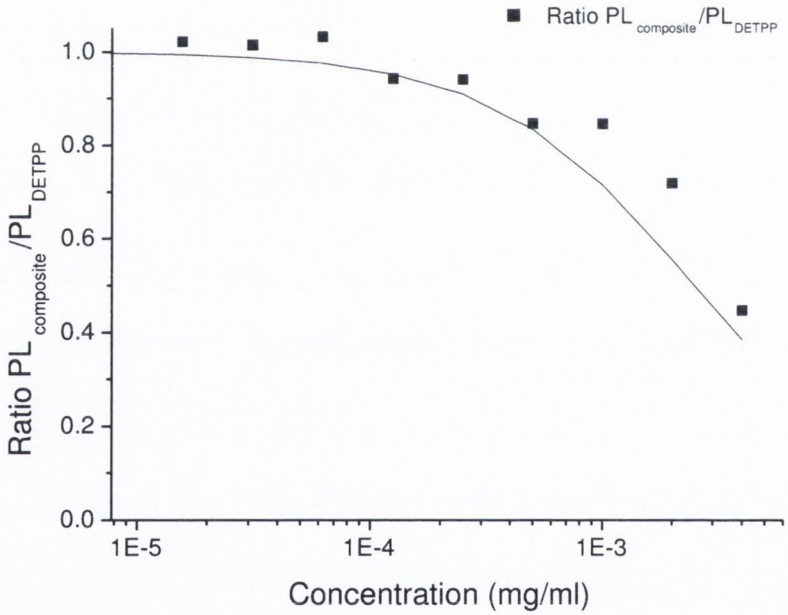

Figure 5.11: Plot of the ratio of composite to porphyrin emission for DETPP as a function of concentration appears to show PL quenching (solid line a theoretical fit to data proposed by Coleman et al.)

Concentration- dependent PL studies were performed upon the series of tetraphenylporphyrin derivatives and their 1:1, 5:1 and 10:1 composites formed with SWNT in order to determine the extent of the non-covalent binding. For the 1:1 DETPP:SWNT solutions, quenching behaviour was observed for the composite solutions for concentrations greater than approximately $1x10^{-4}$mg/ml with an appreciable reduction in the porphyrin fluorescence for SWNT composites observed. This data initially appeared to be in tenuous agreement with the binding model proposed by Coleman et al., with very weak interaction indicated between the nanotubes and the porphyrin solutions. However, this occurred at the onset of the concentration-dependent emission quenching, similar to the behaviour previously found for TPP and Zn-TPP (Figures 5.11 and 5.12).

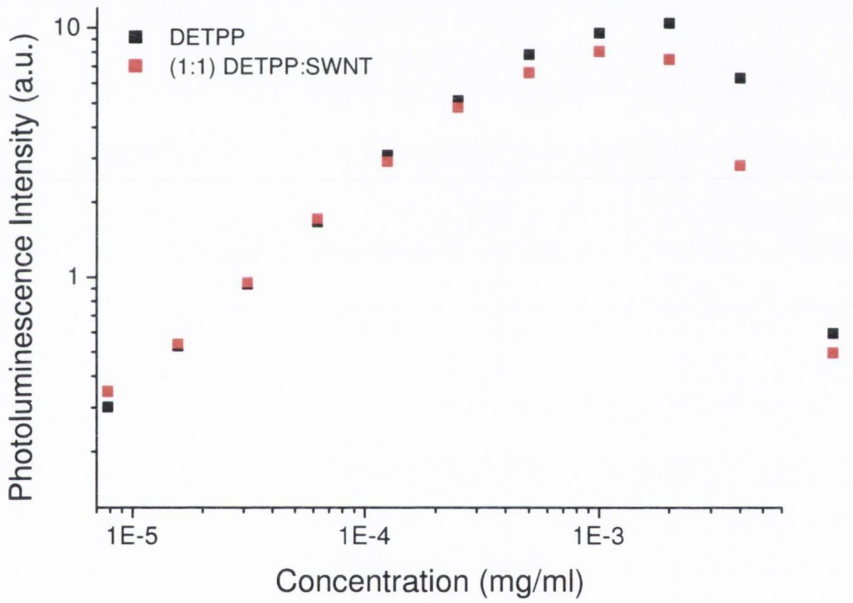

Figure 5.12: Plot of DETPP emission intensity at 654 nm as a function of concentration show quenching observed for the composite only at concentrations above 0.0004 mg/ml, after the onset of concentration-induced PL quenching.

The PL behaviour of DETPP displayed only 15% quenching at sufficiently dilute concentrations where emission intensity was directly proportional to concentration (i.e. for

concentrations $< 5x10^{-4}$mg/ml). Negligible quenching was observed in this concentration range for cTETPP and HETPP. It was also observed that both emission bands, particularly the more intense band at 654 nm, were much lower in intensity at higher concentration solutions for spectra normalised at 693 nm (Figure 5.13). This effect became more marked with increasing concentration, consistent with the inner filter effect. Only (1:1) composite

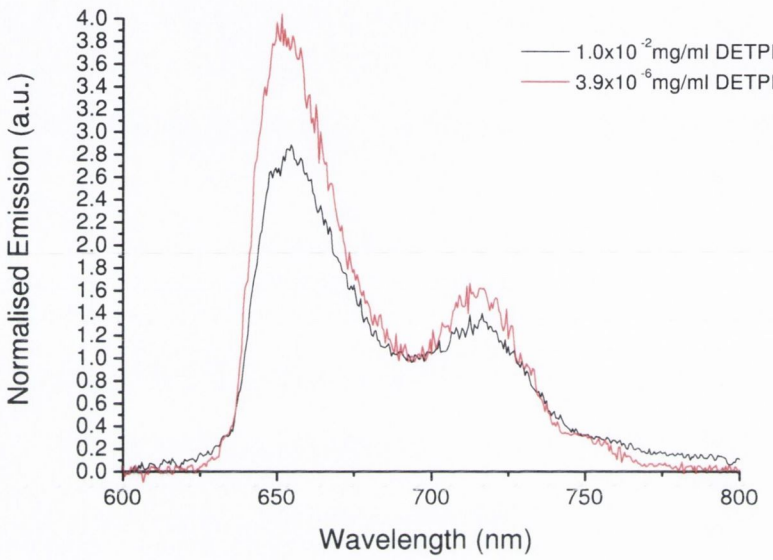

Figure 5.13: Both emission bands were much lower in intensity for higher concentration solutions of DETPP for spectra normalised at 693 nm- an effect consistent with the inner filter effect. All spectra were taken in quartz cuvettes of 1 cm pathlength.

solutions of one of the porphyrin molecules studied- tTETPP- appeared to display an appreciable level of emission quenching, in conservative agreement with the binding model (Figure 5.14) at these dilute concentrations. It is worth noting that OETPP was non-fluorescent, and so it was not possible to probe the interaction of this molecule with SWNT using this technique. Figure 5.15 displays the linear relationship of the photoluminescence intensity as a function of concentration for this concentration range. No aggregation or inner filter effects are apparent at these concentrations, and so the binding model may be applied to this system.

Two steps were taken in order to examine the role of the inner filter effect in our

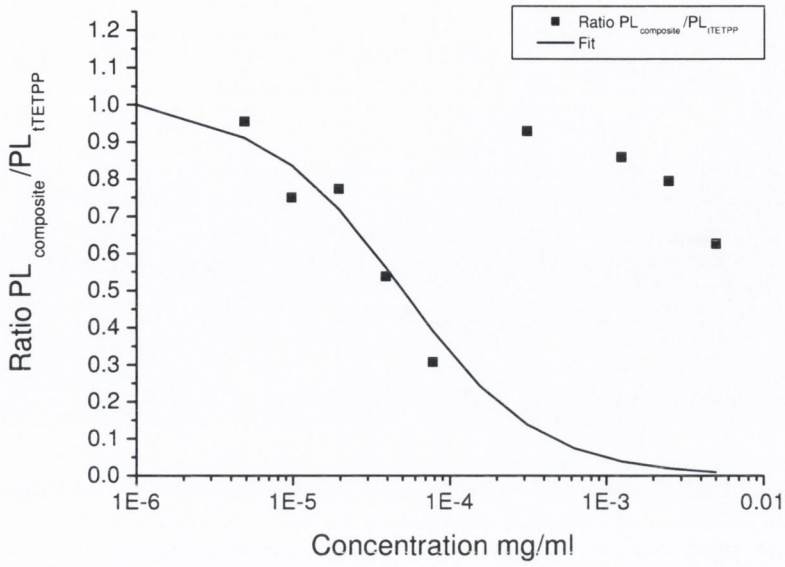

Figure 5.14: The PL quenching behaviour of tTETPP appeared to be in conservative agreement with the binding model at concentrations sufficiently dilute display an appreciable level of emission quenching

studies. Firstly, as one characteristic of the inner filter effect is that fluorescence emission spectra excited in regions of high absorbance are suppressed, the effects on the PL of exciting at different wavelengths was examined. Secondly, it is well documented that the cell geometry is of great importance in the inner filter effect. In order to minimize this phenomenon at high concentrations, our 1 cm path length quartz cuvette was replaced with a 2 mm quartz cuvette, which was mounted in a specially designed holder within the fluorimeter.

The ratio of porphyrin to SWNT was also increased (to 5:1 and 10:1 porphyrin:nanotube), enabling us to investigate the effects of much higher porphyrin concentrations, as nanotubes were found to fall out of solution for 1:1 composites at concentrations of greater than approximately 0.01 mg/ml. Maximum concentrations of 0.04375 mg/ml and 0.175 mg/ml of porphyrin were achieved for the 5:1 and 10:1 composites respectively, which are equivalent to 0.00875 mg/ml and 0.0175 mg/ml of SWNT. This indicates that the maximum possible

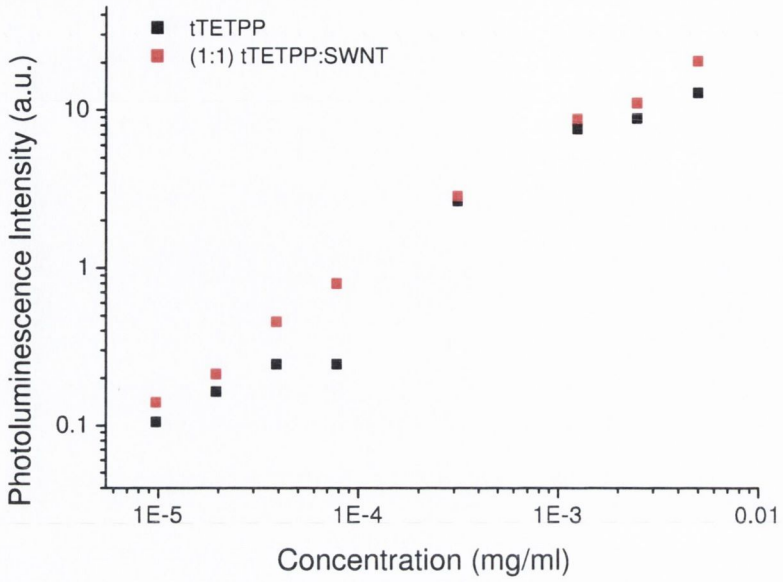

Figure 5.15: The PL intensity is directly proportional to the concentration of the tTETPP molecule over the concentration range studied $4.9\text{x}10^{-6}$ to 0.0025 mg/ml

concentration of nanotubes in solution is approximately constant, irrespective of how many porphyrin molecules are available to aid solubilization.

The influence of the inner filter effect was immediately apparent upon examination of composite solutions containing 10:1 porphyrin:SWNT when both steps were taken to minimize this effect. In order to improve the signal to noise ratio of the PL spectra obtained, the normal 1 cm path length quartz cuvette was used for measurements of solutions containing less than 0.001mg/ml of the fluorescent porphyrin molecules. For the higher concentration solutions, the 2mm path length quartz cuvette was used. Additionally, the solutions were all photoexcited at a number of wavelengths, namely in the Soret band of the porphyrin in question, in the Q-bands of the porphyrin, and in a region of no absorbance. The difference in the emission for higher concentration solutions was significant (Figure 5.16). It is apparent that the inner filter effect is responsible for much of the PL quenching observed for composite solutions at high concentration, as this effect was greatly enhanced in the presence of SWNT. This is probably due to the combination of light being

scattered by the nanotubes in addition to the self-absorption of the porphyrin molecules present. Hence, strong apparent composite PL quenching was observed for all molecules studied when appropriate precautions were not taken to counter the effects of the inner filter effect.

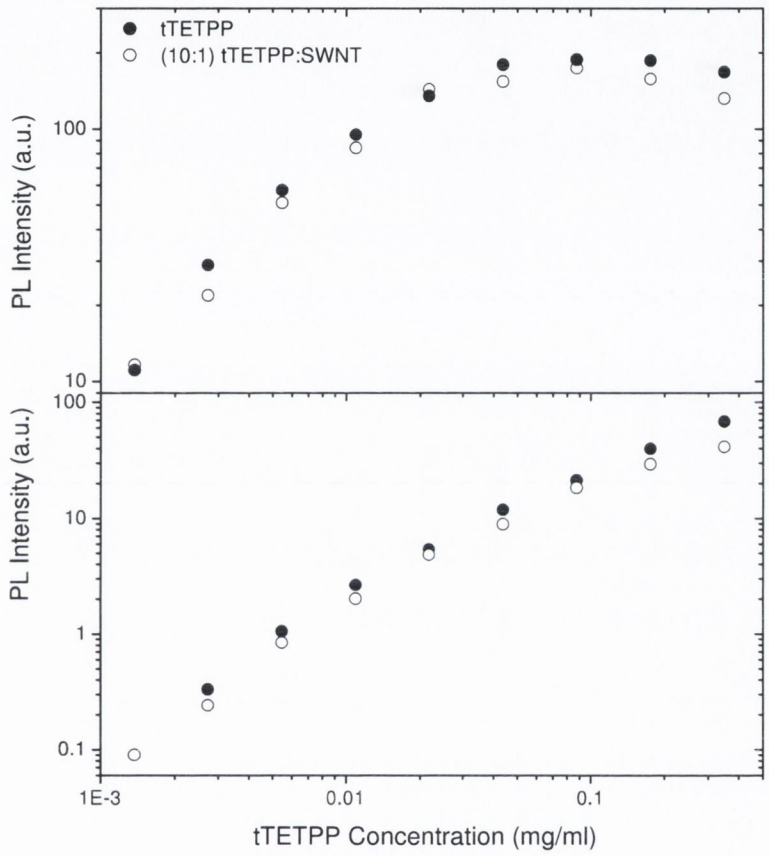

Figure 5.16: Plot of porphyrin (solid circles) and composite (open circles) emission upon photoexcitation in the Soret band region at 424 nm (top) and the Qband region at 596 nm (middle) for tTETPP as a function of concentration for high concentration solutions. Concentration- induced self absorption is greatly reduced by altering the excitation wavelength. All spectra were measured in a 2mm quartz cuvette.

Taking this into account, PL studies of all molecules were conducted. Plots of TPP and its 10:1 composite emission upon photoexcitation in the Soret band region at 417

nm (top) and the Q band region at 590 nm (bottom) for TPP as a function of concentration for high concentration solutions are shown in Figure 5.17. Also shown is the ratio of composite to porphyrin emission as a function of concentration upon excitation at both wavelengths. The 2mm cuvette was used for all solutions at concentrations higher than 0.001mg/ml. It is evident that negligible quenching is found for the composite solutions upon excitation at both wavelengths. This is in direct contrast to our previous studies with 1:1 TPP:swnt composites, where 92% 'quenching' was observed for composites at a concentration of 0.036mg/ml. As this result was consistent with those reported in the literature, it is likely that many other published reports have failed to correct for the inner filter effect.

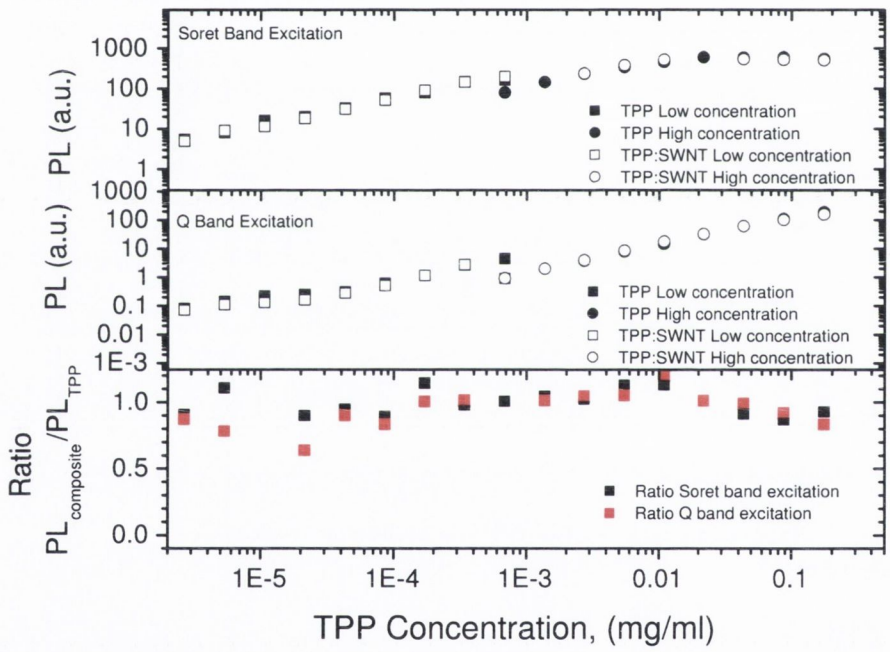

Figure 5.17: PL emission of TPP and its 10:1 SWNT composite upon photoexcitation in the Soret band region at 417 nm (top) and the Q band region at 590 nm (centre) as a function of concentration for high concentration solutions. Also shown is the ratio of composite to porphyrin emission as a function of concentration upon excitation at 417 nm (black) and 590 nm (red). The 2 mm cuvette was used for all solutions at concentrations higher than 0.001 mg/ml.

Some quenching was in fact found for the 10:1 tTETPP composites. However, the quenching remained approximately constant over the concentration range 0.001- 0.175mg/ml, yielding a median quenching of 25.2%. No quenching whatsoever was evident for (10:1) solutions of cTETPP and DETPP . For comparison purposes, (10:1) solutions of the planar molecule octaethylporphyrin (OEP) were also studied, and no change was noted in the PL intensity levels upon addition of nanotubes, except that the luminescence was possibly slightly enhanced.

A series of (5:1) porphyrin:SWNT solutions were also examined for the planar molecules TPP and OEP. Once again, the inner filter effect was found to have a significant impact, even after taking the precautions mentioned above. In both cases, the composite luminescence appeared to be enhanced relative to that of the same concentration of porphyrin. As the interaction of the porphyrin molecules with nanotubes is expected to quench the emission intensity, if anything, it is clear that the system is not as straightforward as initially thought. One possible explanation for this behaviour is that the porphyrin molecules self- aggregate in DMF, and that interaction with the nanotubes prevents this aggregation from occurring. It would appear that although these molecules do not bind to the nanotube surface in a way which facilitates photoinduced electron transfer, the noncovalent interactions between them are stronger than the attractive forces between adjacent porphyrin molecules. Interestingly, (1:1) Zn-TPP:SWNT solutions also yielded composite luminescence which was approximately 17% higher than those of the porphyrin solutions for concentrations lower than $1.7\text{x}10^{-4}$mg/ml. Our results for (1:1) TPP:SWNT were inconclusive at these concentrations under identical experimental conditions.

The absence of PL quenching observed for the (10:1) composite solutions of these molecules is also consistent with this theory. With a greater mass of porphyrins than nanotubes present in these solutions by an order of magnitude, it is clear that this quantity of nanotubes has no measurable impact on the degree of self-aggregation. With fewer SWNT present in solution, fewer sites for porphyrin aggregation are provided, and consequently the SWNT have less effect on the porphyrins present in solution.

The ratio of composite to porphyrin PL as a function of concentration is shown below (Figure 5.19) for the 5:1 TPP:SWNT solutions. This figure clearly shows that the

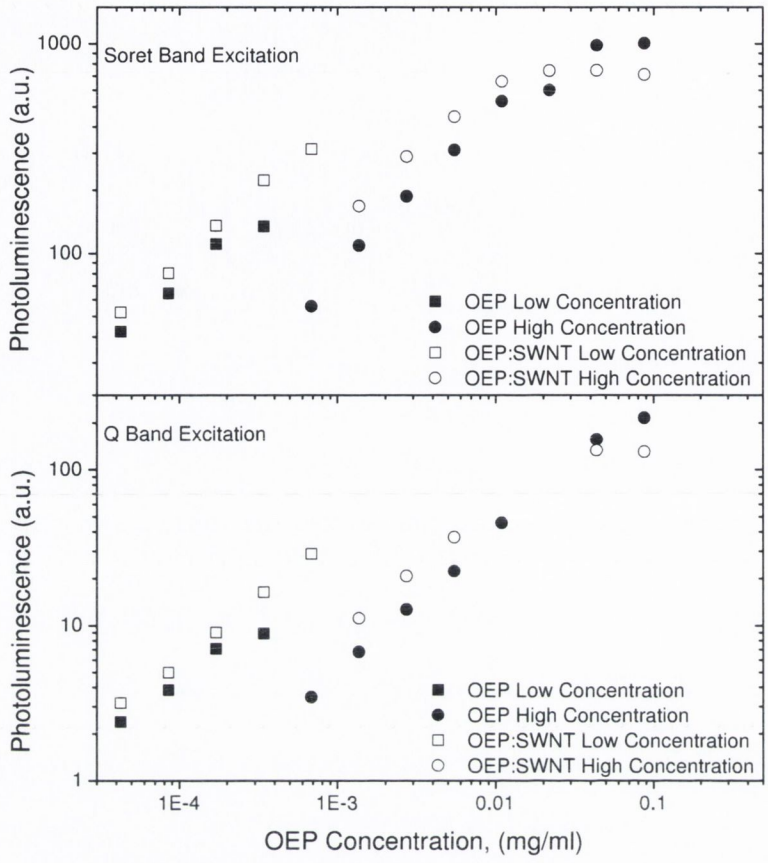

Figure 5.18: PL intensity as a function of concentration for 5:1 porphyrin:SWNT solutions for OEP shows enhanced luminescence for composites. These solutions were photoexcited at the Soret band wavelength of 396 nm (Top) and Q band wavelength of 529 nm (Bottom)

composite luminescence is approximately double that of the its corresponding TPP solution over the concentration range studied. These results are consistent with those of a complementary molecular dynamics simulation carried out by colleagues in Trinity College, Dublin, where a pronounced tendency to aggregate both onto the SWNT surface and onto each other was exhibited by these porphyrin molecules. These results are presented in brief in Chapter 6.

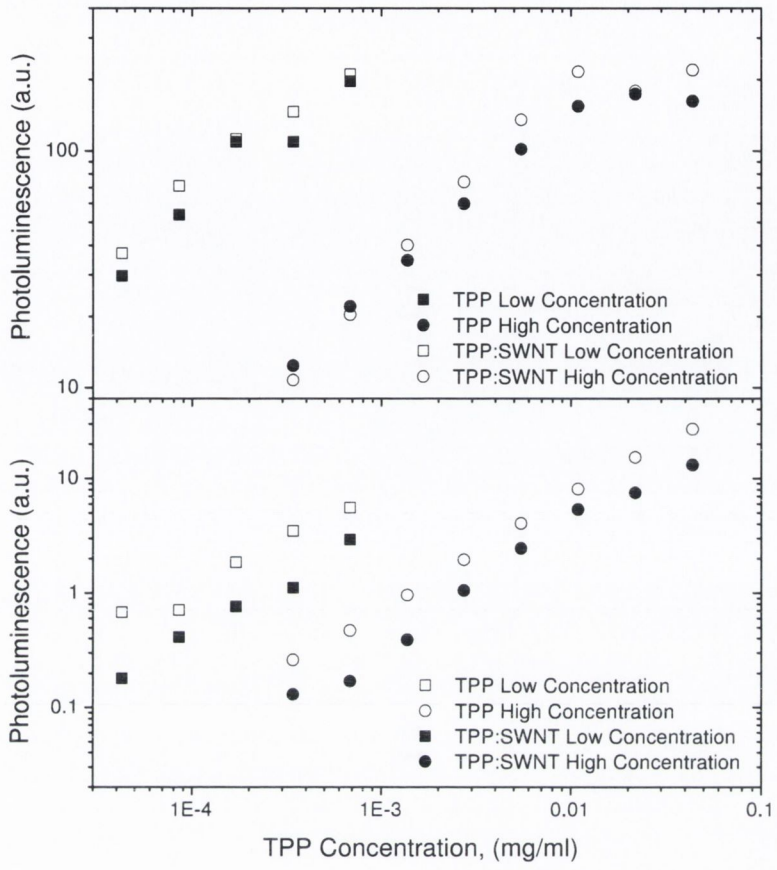

Figure 5.19: PL intensity as a function of concentration for 5:1 porphyrin:SWNT solutions for TPP shows enhanced luminescence for composites. These solutions were photoexcited at the Soret band wavelength of 417 nm (Top) and Q band wavelength of 590 nm (Bottom)

5.4 Sonication-Induced Degradation of Chlorinated Solvents leading to Protonation of Porphyrin-Nanotube Composites.

The possible acquisition of intrinsic porphyrin properties such as luminescence and biocompatibility is a major benefit of using porphyrin molecules to functionalize SWNTs and recent research efforts have focussed on the nature of porphyrin - carbon nanotube inter-

actions.[1,4,16,2,13,3,14,15] In order to create carbon nanotube composite solutions, sonication is a necessary step which breaks up the nanotube bundles and disperses the nanotubes homogeneously throughout the solution. Chloroform is also a very widely used solvent for these nanocomposite systems, and therefore concerns about the effects of sonication on the properties and purity of chloroform are potentially of great importance to the materials science community.[36,37]

In this section, the spectroscopic changes of porphyrin composite solutions in chloroform are investigated, and subsequently attributed to the protonation of the porphyrin core nitrogen atoms upon sonication in chloroform. These changes were first observed when TPP-SWNT composite solutions were prepared in chloroform, with the intention of undertaking a complete linear and nonlinear optical characterization of this system. Due to this degradation of the chloroform upon either sonication or laser irradiation during the z-scan technique, the chloroform solutions characterized in these chapters were of the di-protonated form of the TPP molecule, as opposed to the free base form. The implications of the results presented in this chapter are that extreme care must be taken when working with carbon nanotube composite solutions in chloroform as protonation of acid sensitive molecules may take place, changing their physicochemical properties.[38]

5.4.1 Experimental Section

Purified single walled nanotubes (HiPCO) were purchased from Carbon Nanotechnologies Inc and used as supplied (lot # PO289). Chemicals were purchased from Aldrich and were used as received. Chloroform was purified by passing it through a column of basic alumina (grade I, 10g/14ml). Pure HiPCO SWNTs were added to porphyrin solutions such that the porphyrin : SWNT mass ratio was 1 : 1. Sonication was performed using a high power ultrasonic tip, model GEX600 (120W, 60kHz). Absorption spectra were recorded using a Shimadzu UV3100 UV-Vis-NIR spectrometer. Photoluminescence measurements were carried out using an LS-55 Perkin-Elmer luminescence spectrometer with an excitation wavelength equal to the Soret band of the porphyrin in each case.

5.4.2 Results and Discussion

Sonication and Protonation in Chloroform

Absorption and Emission spectroscopy techniques were used to investigate the effect of sonication and protonation on the optical properties of tetraphenylporphyrin (TPP) and tetraphenylporphyrin zinc (Zn-TPP) composite solutions in chloroform.

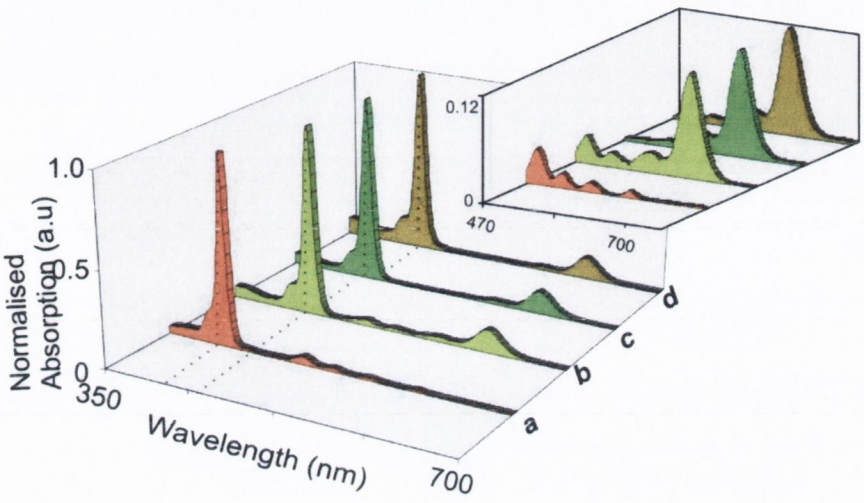

Figure 5.20: Absorption spectra of (a) a solution of TPP before sonication, (b) after sonication for 1 minute (c) after addition of 150 equivalents of HCl and of (d) a composite solution of TPP and SWNTs (4.5 μM, $CHCl_3$, 25^{o}C).

The absorption spectrum of an unsonicated red solution of TPP (Figure 5.20a) in chloroform shows a typical Soret band at 418 nm and four Q-bands at 516, 550, 590 and 646 nm. Upon protonation with HCl, the spectrum is characterized by two strong maxima at 610 and 661 nm, as seen in Figure 5.20c, and the Soret band shifts to 446 nm. The absorption spectrum of the sonicated TPP solution (Figure 5.20b) was found to be indistinguishable from that of the protonated TPP solution. Once the absorption and the concentration were measured, the ground state absorption cross- section σ_g was found from the relation $\alpha_g = N\sigma_g$, where α_g is the ground state absorption coefficient and N is the molecular concentration. The values obtained for σ_g at 532 nm were 6.51 x 10^{-16}

cm^2 for the bi- protonated TPP form and 7.137 x 10^{-16} cm^2 for the de- protonated one at a concentration of 0.0216 kg/m^3. This is in conservative agreement with reported values of 0.8 x 10^{-17} cm^2 and 2.1 x 10^{-17} cm^2 for bi- protonated and de- protonated solutions respectively of the TPP derivative $TPPS_4$. It was found that the absorption spectra of the green TPP : SWNT composite solution (Figure 5.20d) was very different in profile, exhibiting a Soret band at 446 nm and two Q-bands at 610 and 660 nm. Similar spectral changes for a TPP derivative (5-p-hydroxyphenyl-10, 15, 20-tritolylporphyrin) in chloroform have been previously reported by Baskaran et al.[17] In their study, however, these changes in the absorption spectra were attributed to the interaction of residual acid groups on the surface of the carbon nanotubes and the grafted porphyrin molecules. As we see the same behaviour in the absence of nanotubes, the validity of this hypothesis must be called into question.

They also stated that noncovalently adsorbed (or) complexed porphyrins with SWNT do not show a major shift in the Soret band and referred to two other literature papers. These findings are consistent with our results from Chapter 5, which is to be expected as both of these papers also analysed non-covalent interactions of porphyrins with SWNT in DMF. When chloroform was used as the solvent, we also observed a red shift extremely similar to that reported above. It was found that no such spectral shifts were observed for composites prepared in the non-chlorinated solvent dimethylformamide (DMF). In order to explain this spectroscopic behaviour, the effects of sonication and protonation on the optical spectra of the porphyrin molecules were investigated before and after addition of SWNT. The solutions were first examined in the absence of nanotubes. Upon sonication, the porphyrin Soret band was largely shifted to a longer wavelength and the color changed from red to green. Also the characteristic porphyrin Q-bands were converted to two bands at 610 and 660 nm (Figure 5.20b). The red shifted Soret band and the pattern of Q- bands in those sonicated solutions suggest that the porphyrin molecules exist in a protonated form. The formation of di-protonated TPP was deemed evident in both the observed Soret band red shift and in the replacement of the four Q bands caused by D2h symmetry of the TPP molecule with two strong bands characteristic of the D4h symmetry of the diprotonated $TPPH_4^{2+}$.[39]

It is evident that the occurrence of these spectral changes are independent of the presence of carbon nanotubes in solution, and cannot therefore be attributed to the interaction of the porphyrins with the nanotube surface, as proposed by Baskaran and co-workers.[17] Although sonication was not explicitly mentioned in their sample preparation techniques, it is not possible to form a homogeneous nanotube dispersion without sonicating the sample. When the conjugated polymer PPyPV was similarly utilized to solubilize SWNTs in $CHCl_3$,[36] the resultant absorption spectrum indicated a significant degree of protonation compared with the case without SWNTs. It is inevitable in our opinion that this protonation is at least partially caused by sonication during composite preparation, and indicates that many such studies may exist where neglecting the sonication effects on such systems may have resulted in erroneous spectral interpretation. It was instead proposed that these sonication- induced changes in the optical absorption behaviour of the porphyrins were due to the creation of hydrochloric acid by sonodegradation of chloroform[40,41,42,43] and the subsequent protonation of the core nitrogen atoms of the free base porphyrins.

In order to confirm this hypothesis HCl was added to an unsonicated porphyrin solution. Upon protonation, the absorption spectrum (Figure 5.20c) was found to be identical to that observed for the sonicated TPP and composite solutions, with a Soret band at 446 nm and Q bands at 610 and 661 nm. Figure 5.21 shows the typical Soret absorption band at 418 nm and four Q-bands at 516, 550, 590 and 646 nm for a red solution of the deprotonated TPP molecule in chloroform. The solution was titrated by gradual addition of 25 equivalents of HCl from a concentrated stock solution to a 4.5 μM solution of TPP. Upon titration, the Soret band was found to split, with the 418 nm band decreasing in intensity while a second band at 446 nm simultaneously appeared and increased in intensity as the solution was protonated. The Q- bands were also affected, with the appearance of two strong maxima at 610 and 661 nm upon protonation of the TPP solution. Complete protonation of the solution was observed after addition of 150 equivalents of HCl. The equilibrium nature of the protonation mechanism was confirmed by the observation of an isosbestic point at 429 nm during the titration. Addition of a few drops of triethylamine completely reversed the protonation process, shifting the Soret band back to 418 nm. The Lambert- Beer law was observed for both TPP and PPSW solutions throughout the titrations.

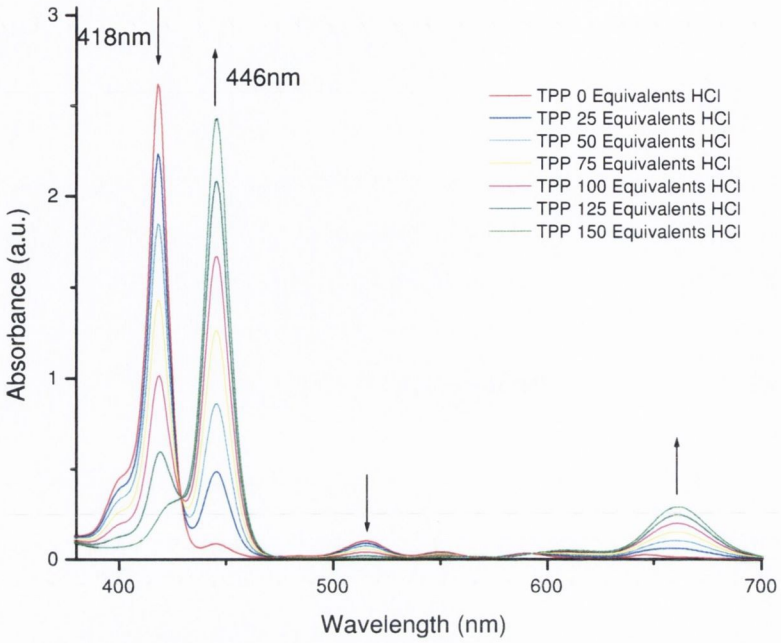

Figure 5.21: Absorption spectra of TPP upon addition of 0, 25, 50, 75, 100, 125, 150 equivalents of HCl (4.5 μM, $CHCl_3$, 25°C) The spectral changes represent protonation equilibrium between two forms of porphyrin.

Further support for this hypothesis came from the protonation of a TPP solution using a different acid. A number of TPP and Zn-TPP solutions were made up in chloroform for a range of concentrations and the resultant solutions were treated with 99% Trifluoroacetic Acid (TFA). To each of the TPP solutions, 1000eq of TFA was added, and the resulting solutions were found to be fully protonated. The absorption spectrum of TPP protonated with TFA showed a 22 nm red shift of the Soret absorption band to 440 nm, and a similar bathochromic shift of the Q bands to 604 nm and 654.5 nm. For the Zn-TPP solutions 5000 equivalents of TFA were added before the absorption spectrum showed the solution to be fully protonated. Jongwan Yu et al reported that the effect of the acid counterion significantly affects the Stokes' shift observed upon protonation, with the chloride ion showing the largest red shift of all the acids studied.[39] This is fully consistent with our findings above, with a red shift of 28 nm observed for the TPP solution protonated

with HCl, and a shift of 22 nm observed for the TFA protonated TPP. These results also confirm that HCl must be the acid responsible for the TPP protonation upon sonication, as a Soret peak at 446 nm and Q band peaks at 610 and 661 nm are characteristic of TPP bi-protonated with HCl in chloroform, due to the involvement of the acid counterion.

Further studies were conducted to confirm the origin of the observed protonation. The chloroform was first purified by passing it though a column of basic alumina (grade I, 10g/14ml) in order to remove all impurities, including the residual traces of HCl always present in this commercially available organic solvent. The origin of the observed protonation was confirmed by using a pH indicator, azopyridine (AZ), which was added to the chloroform and the resultant solution then sonicated for 1 minute. The AZ solution changed colour from yellow to pink indicating that protonation of the AZ molecule had taken place, with acid created during sonication. The changes in the absorption spectra of AZ before and after sonication in chloroform were identical to those previously reported for the switching from AZ to the protonated form AZH upon addition of acid, and the interconversion between the orange AZ solution and the red-purple AZH can be followed by absorption spectroscopy.[44] The absorption spectrum of an orange solution of AZ (Figure 5.22a) shows a strong band at 428 nm. After one minute sonication the absorption band at 428 nm disappears and a new band at 540 nm appears (Figure 5.22b), and the solution turns red-purple. Identical changes were found for the protonated AZH form confirming that AZ is completely protonated upon sonication in chloroform. Sonodegradation of $CHCl_3$ produces HCl as one of the main reaction products. Hence, protonation of porphyrin solutions was caused by HCl created during the sonication process.

This sonication- induced protonation behavior was also observed for Zn-TPP solutions. However, a far greater amount of energy was required for protonation of the metalloporphyrins to take place, which is which is consistent with the fact that each nitrogen atom is already engaged in a coordinate-covalent bond with the central metal ion. Addition of a few drops of triethylamine in fact yielded an absorption spectrum identical to that of the free base TPP, shifting the Soret band back to 418 nm, indicating that the zinc cation is not reintroduced into the cavity of the porphyrin macrocycle.

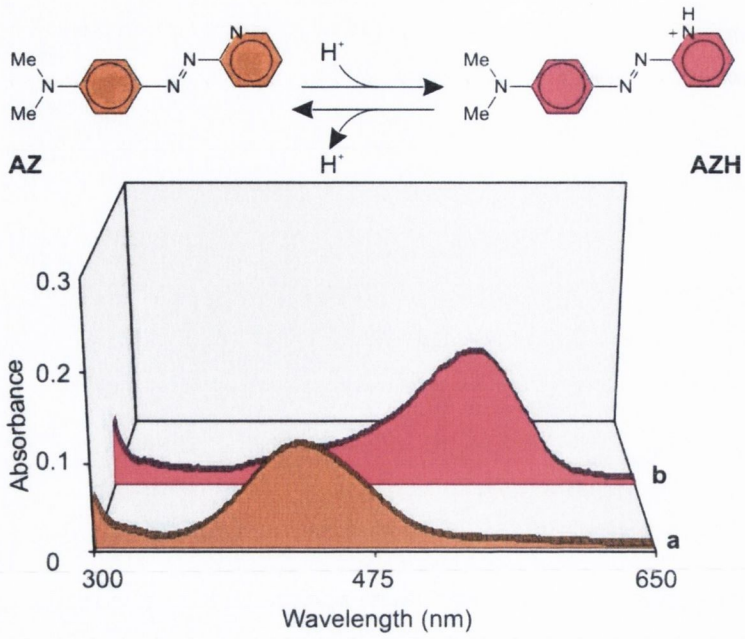

Figure 5.22: Absorption spectra of AZ in $CHCl_3$ (a) before and (b) after sonication for 1 minute.

The fluorescence properties of the sonicated and unsonicated porphyrin and composite solutions were also investigated. Excitation at the Soret band of unsonicated TPP solution results in two emission peaks at 650 and 715 nm, typical for such porphyrin molecules (Figure 5.24a). The emission spectrum of the sonicated porphyrin solution is very different, showing a broad emission band with the maximum located at 685 nm (Figure 5.24b). After addition of acid the emission observed from the di-protonated TPP solution (Figure 5.24c) was indistinguishable from that of the sonicated TPP solution.

In the case of SWNT composite solution (Figure 5.24d), only one emission band was again also observed at 685 nm at all concentrations studied (1 - 200 μM). For the composite, only one emission band was observed at 685 nm at all concentrations studied (1 - 200 μM). In addition, significant quenching was observed only for the composite solution for porphyrin concentrations of 6.5μM and above (Figure 5.23), which is an artefact observed due to the occurrence of the inner filter effect.

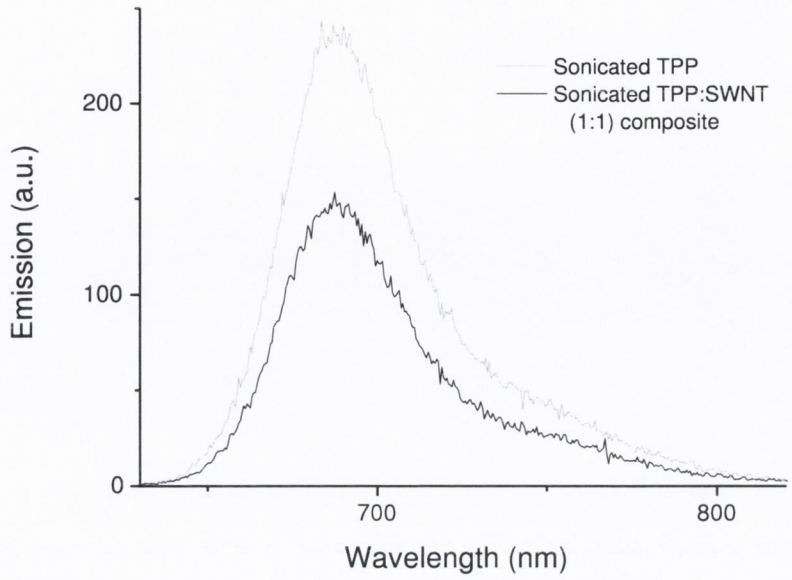

Figure 5.23: Emission spectra of sonicated TPP (a) without SWNT (grey line) and (b) with SWNT (black line) upon excitation at 446 nm μM, $CHCl_3$, 25°C).

Emission spectra for solutions of the Zn-TPP molecule with and without SWNT over the same concentration range displayed a similar red shift of 44.5 nm of the peak emission band from 603.5 nm to 648 nm upon sonication. It should be pointed out that these molecules were not as readily protonated as the free base porphyrins.

Sonication Studies in other Chlorinated Solvents

Following on from these observations, it was anticipated that a similar sonodegradation of other common chlorinated solvents would also lead to porphyrin protonation. In order to investigate this phenomenon, solutions of the same porphyrin molecule, TPP, were investigated with dichloroethane (DCE), dichlorobenzene (DCB), dichloromethane (DCM), N,N-dimethylformamide (DMF), N-methylopyrrolidinone (NMP) and tetrahydrofurane (THF) used as solvents. Sonication experiments were then performed on the resulting solutions. The same spectral shifts were observed upon sonication of TPP in dichloroethane (DCE) and dichlorobenzene (DCB) and complete protonation was found after sonication for 2

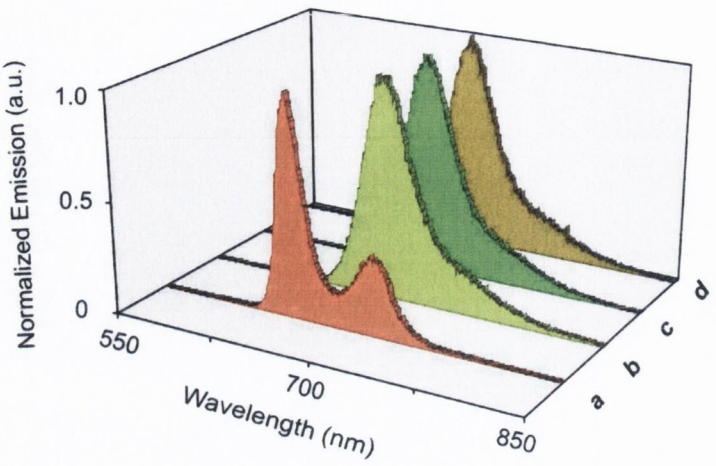

Figure 5.24: Emission spectra of (a) a solution of TPP before sonication, (b) after sonication for 1 minute (c) after addition of 150 equivalents of HCl and of (d) a composite solution of TPP and SWNTs. Excitation at the corresponding Soret band in all cases (6.5 μM, $CHCl_3$, 25°C).

minutes and 30 seconds respectively. These results can be seen in Figure 5.25 and Figure 5.26 below.

No spectral shifts were observed when dichloromethane (DCM), N,N-dimethylformamide (DMF), N-methylopyrrolidinone (NMP) and tetrahydrofurane (THF) were used as solvents.The absorption spectrum of TPP in DCM remained unchanged after up to 90 minutes sonication (Figure 5.27).

After 1 minute sonication of a solution of TPP in DCM, DCB and DCE no protonation, partial and complete protonation was achieved respectively (Figure 5.28). It is unclear why protonation does not take place for TPP in DCM, as this solvent also undergoes degradation when sonicated.

5.4.3 Effect of Carbon Nanotubes on Porphyrin Protonation

Chloroform used as Solvent

The presence of nanotubes was found to greatly affect the extent to which the porphyrin molecules were protonated during the sonication process. TPP solution sonicated for 30

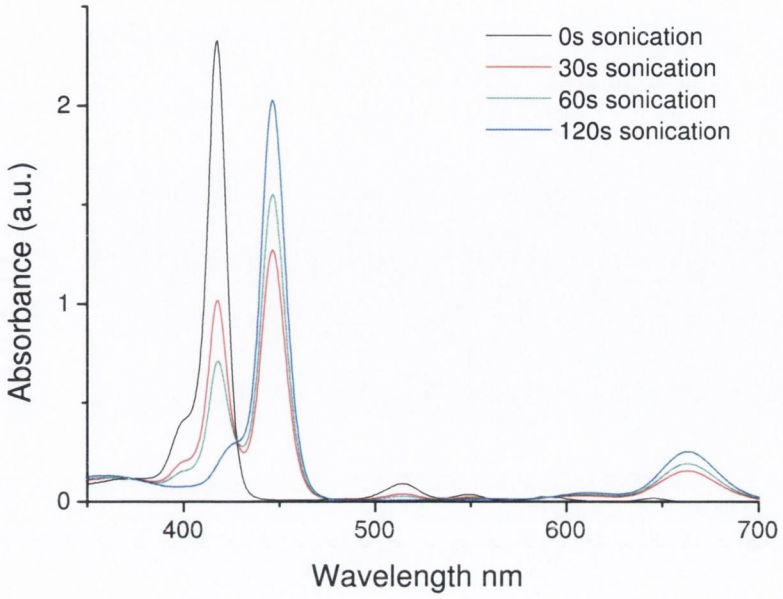

Figure 5.25: Absorption changes of TPP (4.5 μM, CH_2Cl-CH_2Cl, 25^{o}C) before (black line) and after tip sonication for 30 seconds (red line), 1 minute (green line) and 2 minutes (blue line).

seconds shows an initial level of protonation equal to that achieved by 77 equivalents of HCl. It is interesting to note that composite solutions sonicated for 30 seconds do not show a significant initial level of protonation. The absorption spectra of TPP and of the composite solutions which were each sonicated for 30 seconds looked dramatically different to each other, with the composite solutions displaying little sign of protonation (Figure 5.29 grey line)while the porphyrin is almost completely protonated (Figure 5.29 red line). It appears that the sonic energy is absorbed by nanotubes and dissipated through their vibrational manifolds in the composite solutions, whereas in the pure TPP solutions it causes degradation of the chloroform molecules, creating HCl.

In Figure 5.30, the absorbance at 446 nm is plotted against the number of equivalents of acid added during the titration of both TPP and composite solutions. Titration of unsonicated TPP yields a graph that goes through the origin, as the original solution contains no protonated TPP molecules. Complete protonation was achieved after addition

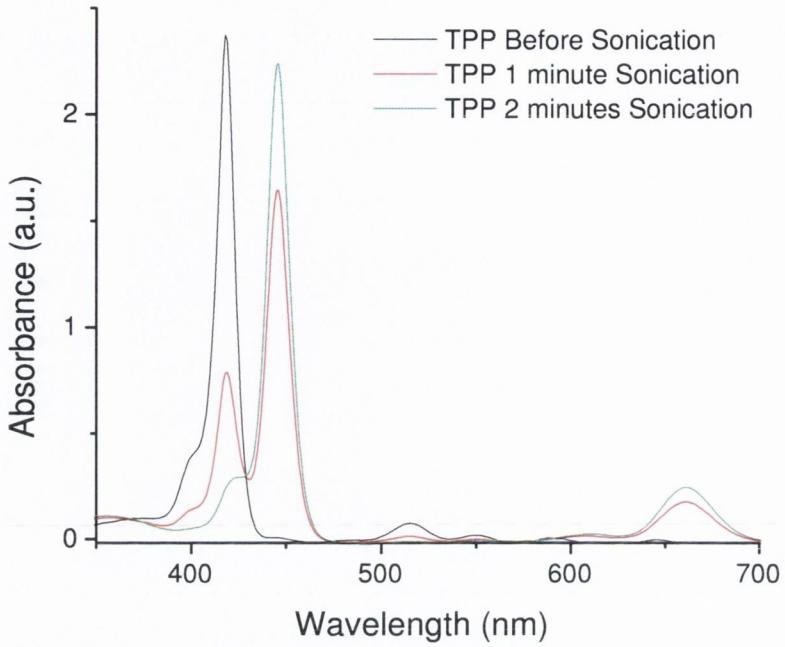

Figure 5.26: Absorption changes of TPP (4.5μM, $C_6H_4Cl_2$, 25^{o}C) before (black line) and after tip sonication for 15 seconds (red line), 30 seconds (green line) and 1 minute (blue line).

of 150, 75 and 40 equivalents of HCl to the unsonicated TPP, sonicated TPP and composite solutions respectively. However, the sonicated and unsonicated TPP solutions are protonated at very similar rates (with slopes of 0.012 and 0.016 respectively) whereas the composite has a much higher slope of 0.046. This indicates that the presence of SWNT accelerates porphyrin protonation. This is consistent with a recent study by Steuerman et al where similar protonation behavior was observed for the basic polymer poly (2, 6-pyridinylenevinylene) - co - [(2, 5-dioctyloxy-p-phenylene) vinylene] upon addition of carbon nanotubes.[36] When PPyPV was utilized to solubilize SWNTs in $CHCl_3$, the resultant absorption spectrum indicated a significant degree of protonation, with a tenfold increase in the protonated form of the polymer, compared with the case without SWNTs. It is inevitable in our opinion that this protonation is at least partially caused by the sonication process during composite preparation. It is not possible to determine the number of

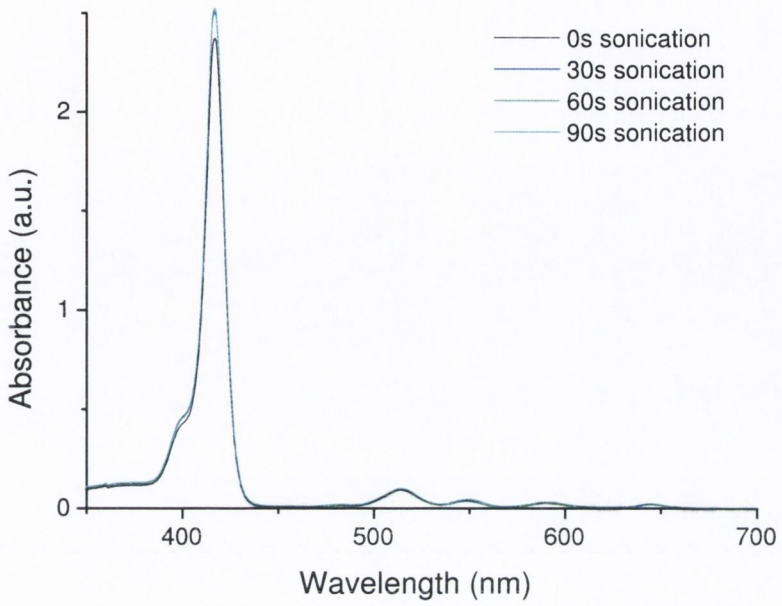

Figure 5.27: Absorption spectra of TPP (4.5μM, CH_2Cl_2, 25^{o}C) before and after tip sonication for 30, 60 and 90 minutes remained unchanged.

equivalents of acid required for completed protonation as we do not know the quantity of polymer being titrated.

DMF used as Solvent

The accelerated rate of porphyrin protonation in the presence of SWNT is indicative of an increase in sensitivity of the TPP molecule to an acidic environment for these chloroform dispersions. These composites therefore show potential as sensitive nanoscale pH sensors. The chlorinated solvents investigated in this chapter have a tendency to degrade upon sonication and laser irradiation and thus contribute to the extent of the porphyrin protonation. Hence, another solvent must be found which would allow for accurate measurement of the quantity of protonated porphyrin present in solution without risk of solvent degradation. For this reason, the solvent DMF was used, as it was investigated and found to be stable upon sonication for prolonged periods of time, and under laser irradiation during the z-scan

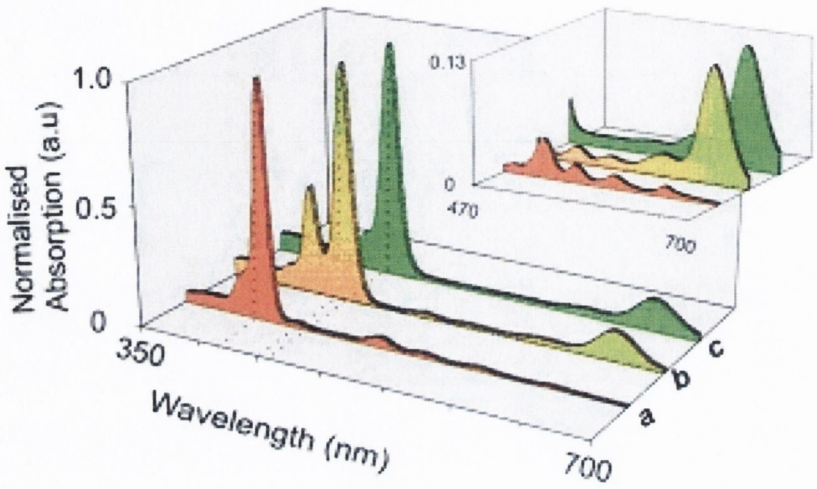

Figure 5.28: Absorption spectra of a solution of TPP after sonication for 1 minute in (a) DCM, (b) DCE (c) DCB (4.5μM, 25^{o}C)

technique (Chapter 6).

As previously observed, addition of aqueous HCl to a TPP solution results in porphyrin protonation in $CHCl_3$ solution. This titration may be easily followed optically as the unique optical signature of the porphyrin diacid is distinctly different to that of the free base porphyrin (Figure 5.21). The titration may be presented as illustrated in Figure 5.30, or by plotting the ratio of the relative intensity of the low-energy (red) absorption feature (i.e. Soret band of the free base porphyrin) to that of the high-energy (blue) absorption feature (i.e. Soret band of the porphyrin diacid) as a function of the volume of acid added. Such plots are commonly used as they are extremely useful for illustrating titrations, accurately conveying the protonation progress and indicating saturation behavior where applicable.[36] This type of plot will be used to describe the protonation behaviour of the different acids investigated in this chapter.

Solutions of TPP and TPP/SWNT were made up using DMF as solvent, and titrated to full protonation by adding acid. The rate of protonation was measured for TPP and its composite in DMF for a range of acids, including HCl. The HCl titration of TPP in DMF proceeded as expected, with an isosbestic point observed at 425.3 nm both with

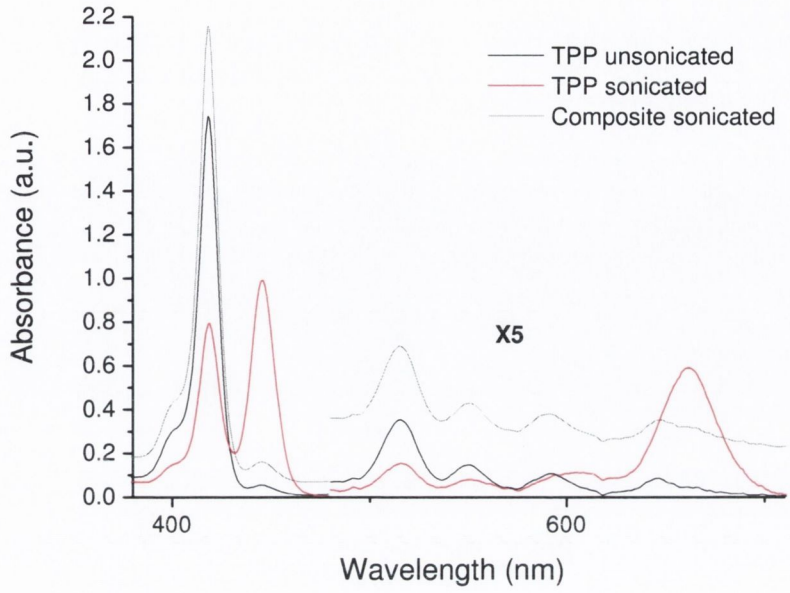

Figure 5.29: Absorption spectra of a solution of TPP before sonication (black line), after sonication for 30 seconds (red line) and of a composite solution of TPP and SWNTs after sonication for 30 seconds (grey line). (4.5 μM, $CHCl_3$, 25^{o}C)

and without nanotubes present. This is shown below in Figures 5.31 and 5.32.

Representative data for this titration is presented in Figure 5.33 for both the TPP and TPP/SWNT solutions. These experiments displayed notable differences in the protonation behaviour of TPP composites in DMF when compared with their behaviour in $CHCl_3$. The amount of HCl required to protonate TPP was not reduced through the addition of SWNTs for the non-chlorinated solvent, and the rate of protonation also remained approximately the same for TPP upon the addition of SWNTs. This was in marked contrast to the experiments performed in chloroform, where the protonation rate was observed to sharply increase for the composites.

Titrations of TPP and TPP/SWNT solutions in DMF were also undertaken using a number of other acids. The acids investigated were Trifluoroacetic acid (TFA) and the naturally occurring water soluble citric and ascorbic acids. Graphs of the ratio of the absorbance maximum of the diacid to that of the free base as functions of added acid for

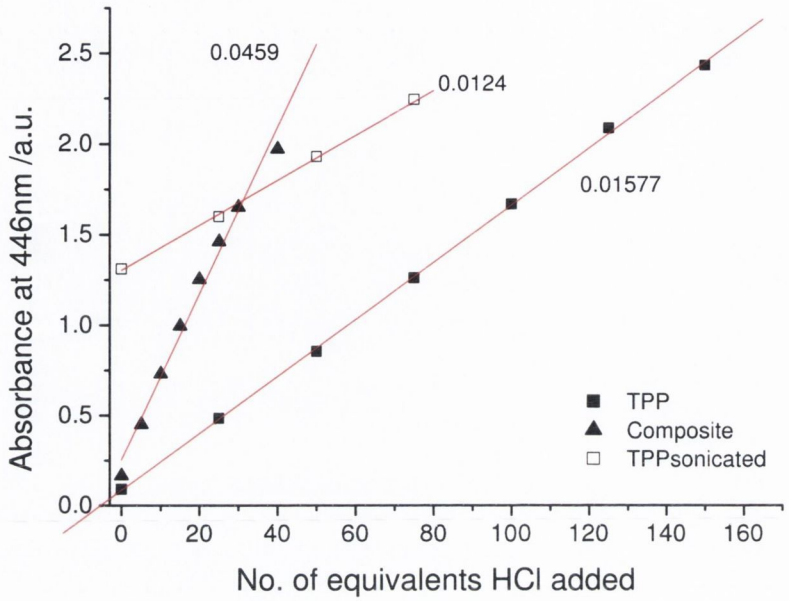

Figure 5.30: Absorbance of protonated TPP upon titration with HCl for (a) porphyrin (filled squares) and (b) composite (empty squares) solutions 4.5 μM, $CHCl_3$, 25^{o}C)

pure porphyrin and porphyrin/SWNT solution were again plotted for each acid and are shown in Figure 5.34, Figure 5.35 and Figure 5.36. The results for these experiments were consistent with those obtained for the HCl titrations performed in DMF, indicating that the solvent used is of great importance in determining the protonation behaviour of the system.

Therefore, the solvent used appears to be of paramount importance in enhancing the sensitivity of tetraphenylporphyrin (TPP) composites to ambient protons in solution. In chloroform, the protonation behaviour of TPP with and without nanotubes present is in agreement with that observed by Steuerman et al.,[36] whereas no such accelerated protonation behaviour is observed for a range of acids in DMF, including HCl. These experimental findings clearly merit further investigation within a different context.

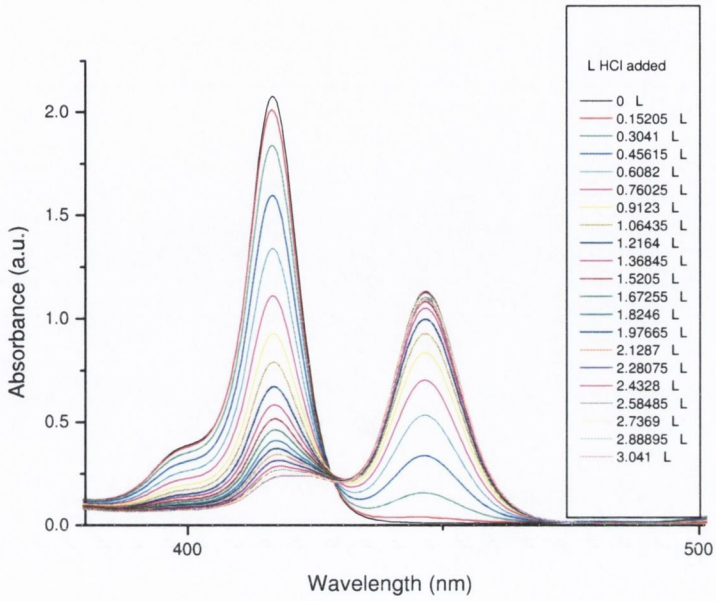

Figure 5.31: Titration of TPP with HCl in DMF shows an isosbestic point at 425.3 nm

5.5 Conclusions

In this chapter, linear optical techniques were utilized in clarifying the existence and extent of non-covalent interaction between a series of aromatic tetraphenylporphyrin derivatives and carbon nanotubes in solution. It is evident from our studies that much of the reported photoluminescence quenching effects previously reported in the literature are in fact artefacts resulting from the manifestation of the well known inner filter phenomenon. In the majority of previous studies, this quenching was attributed to the non-covalent binding of the luminescent porphyrin molecules onto the carbon nanotube surface, and the subsequent non-radiative porphyrin de-excitation through the vibrational manifold of the nanotubes, as seen for non-covalent binding studies using conjugated organic polymers and oligomers in Chapter 4.

A series of tetraphenylporphyrin (TPP) derivatives provided a means of systematically investigating the importance of porphyrin macrocycle conformation on the strength

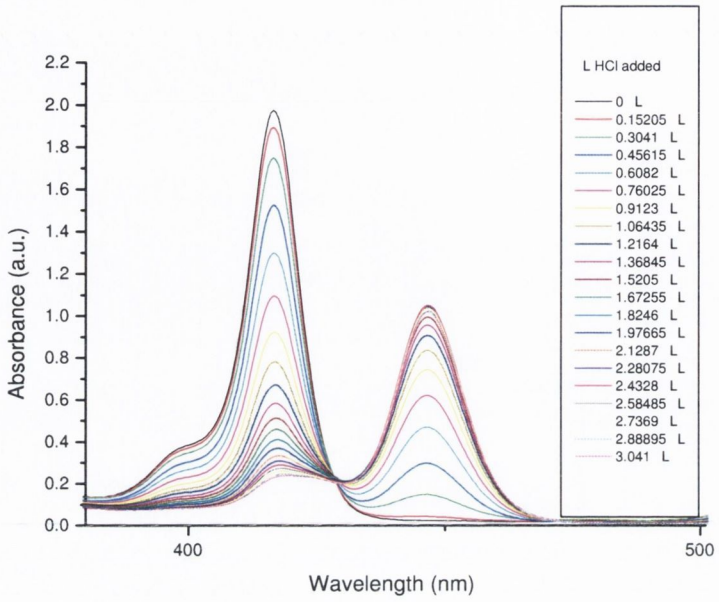

Figure 5.32: Titration of the TPP composite with HCl in DMF also shows an isosbestic point at 425.3 nm

of this non-covalent interaction between these two moities. It would appear, following correction for the inner filter effect, that such quenching does not arise for the tetraphenyl porphyrin derivative molecules upon interaction with the carbon nanotubes, with the exception of tTETPP, where quenching was observed for the 1:1 composites for concentrations where the inner filter effect was not in evidence. Convincing evidence of binding between SWNT and several of these porphyrins was discovered using a number of experimental techniques. Absorption spectroscopy indicated binding of HETPP and OETPP, the two most non-planar porphyrins studied, onto the surface of the SWNT in solution. The evidence for their binding came from shifts in the porphyrin Q-bands and some of the carbon nanotube Van Hove peaks in the absorption spectra measured for these systems. This shift of the Q-bands to lower energies is consistent with literature where evidence of noncovalent binding has been reported. The tTETPP molecule did not show these shifts in the absorption spectra, but was found to exhibit significant photoluminescence quenching for the compos-

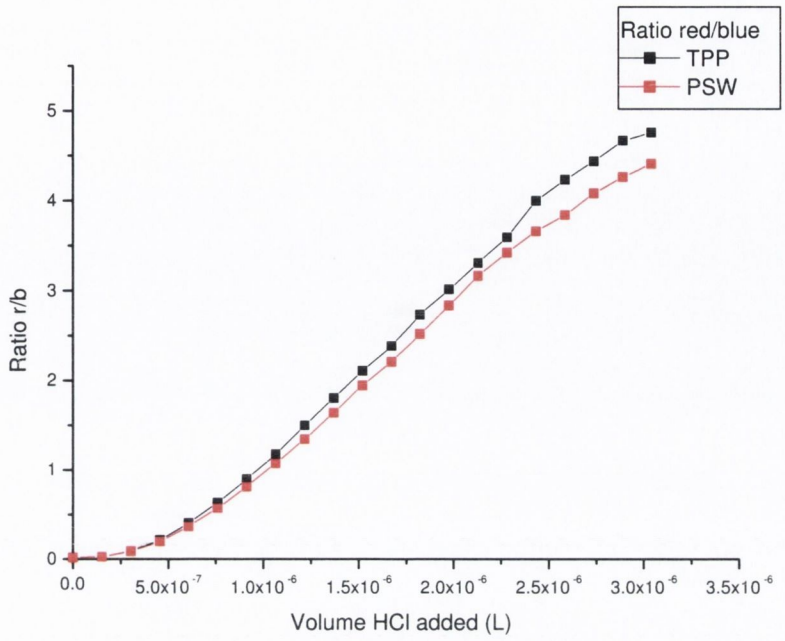

Figure 5.33: Titration of TPP with HCl in DMF

ite solutions, in excellent agreement with the binding model described in Chapter 4. The tTETPP molecule was the only porphyrin found to obey this binding model. DETPP also displayed weak (15%) PL quenching for dilute 1:1 composite solutions. It was not possible to assess the interaction of the most nonplanar molecule OETPP with SWNT using these concentration-dependent PL studies, as this molecule did not emit any measurable fluorescence. The increased solubility of the nanotubes, and the stability of their nanotube composites- as evidenced by their staying in solution over a period of months- was also indicative of binding between the two moities in solution. Furthermore, the prevention of porphyrin self- aggregation upon addition of carbon nanotubes is consistent with the porphryin molecules being more attracted to the nanotubes than they are to each other.

It may thus be concluded that while porphyrins do appear to bind non-covalently onto the nanotube surface, they do not do so in such a way that facilitates energy transfer from the photoexcited porphyrin to the SWNT vibrational manifold. Therefore, in order

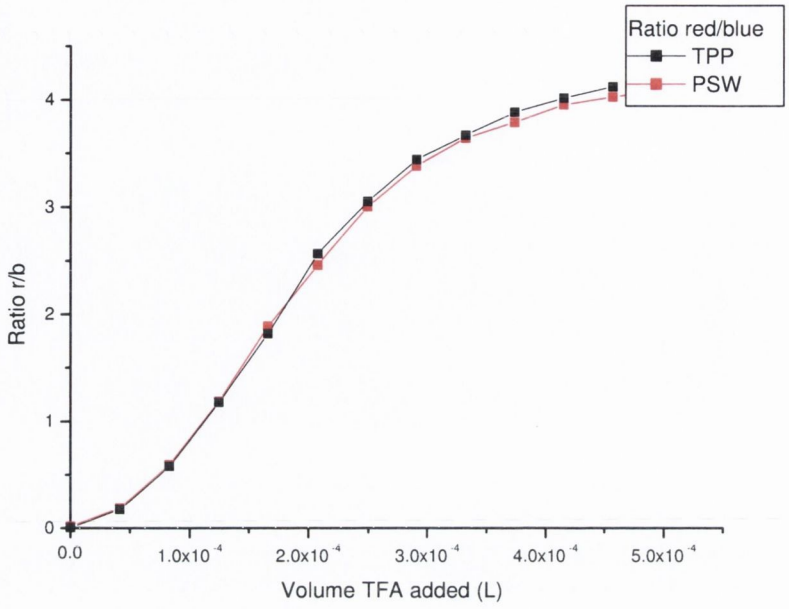

Figure 5.34: Titration of TPP with TFA in DMF

to create efficient electron donor-acceptor systems for photovoltaic applications, another method must be utilized for maximum results. As the porphyrin photoluminescence is not efficiently quenched for the systems studied, it was not possible to use the binding model to determine the extent of nanotube de-bundling in these solutions.

Tetraphenylporphyrin solutions in chloroform were found to change spectroscopically upon addition of nanotubes to form composite solutions. These changes were found to originate from the protonation of the core nitrogen atoms of the porphyrin molecules upon sonication in chloroform. These changes were observed for TPP-SWNT composite solutions prepared in chloroform, but were subsequently found to also take place in the absence of nanotubes. As sonication is a key step in the preparation of homogeneous carbon nanotube dispersions, these changes were always observed for the composite solutions. This degradation of the chloroform molecules was found to occur upon either sonication or laser irradiation during the z-scan technique, giving rise to the di-protonated form of the porphyrin molecule.

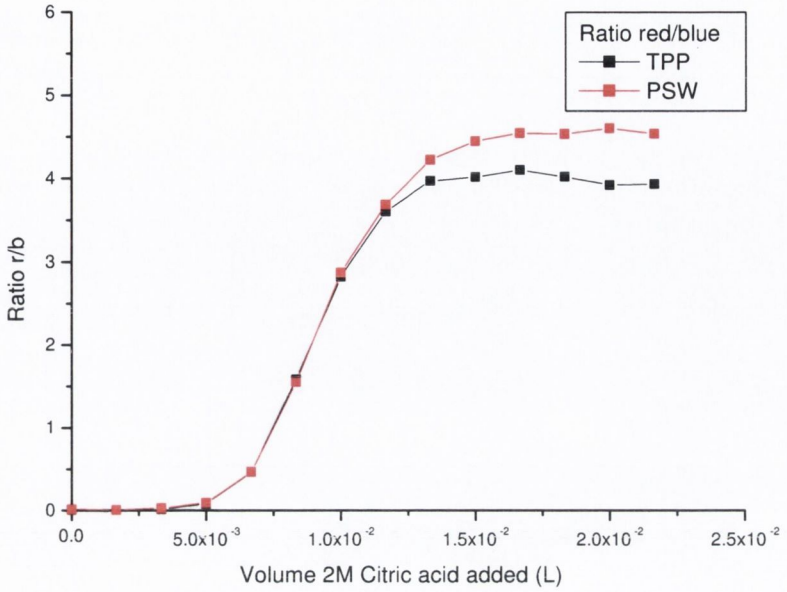

Figure 5.35: Titration of TPP with Citric Acid in DMF

The rate of porphryin protonation in chloroform was found to be strongly affected by the presence of carbon nanotubes. TPP composite solutions were found to be extremely sensitive to the presence of HCl, and might be suitable for use as highly sensitive nanoscale pH probes in particular environments. No heightened sensitivity to HCl or any other acid was observed for the TPP:SWNT composite solutions in DMF. This area clearly merits further investigation within a different context.

A similar sonodegradation of other common chlorinated solvents was also found to lead to porphyrin protonation with the same spectral shifts observed upon sonication of TPP in dichloroethane (DCE) and dichlorobenzene (DCB). The implications of these results are that extreme care must be taken when working with carbon nanotube composite solutions in chlorinated solvents as protonation of acid sensitive molecules may take place, changing their physicochemical properties.

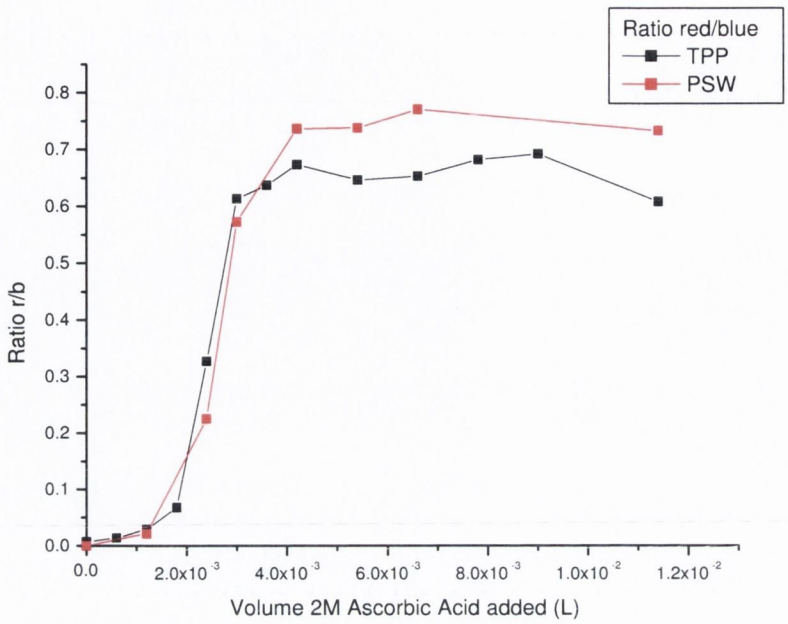

Figure 5.36: Titration of TPP with Ascorbic Acid in DMF

Bibliography

1. Murakami, H., Nomura, T., and Nakashima, N. *Chemical Physics Letters, 378, 481-485* (2003).

2. Chen, J. and Collier, C. P. *Journal of Physical Chemistry B, 109, 7605-7609* (2005).

3. Chichak, K. S., Star, A., Altoe, M. V. P., and Stoddart, J. F. *Small 1(4), 452-461* (2005).

4. Li, H., Zhou, B., Lin, Y., Gu, L., Wang, W., Fernando, K., Kumar, S., Allard, L., and Sun, Y. *Journal of the American Chemical Society, 126, 1014-1015* (2004).

5. Satake, A., Miyajima, Y., and Kobuke, Y. *Chemistry of Materials, 17, 716-724* (2005).

6. Hasobe, T., Fukuzumi, S. ., and Kamat, P. *Journal of the American Chemical Society, 127, 11884-11885* (2005).

7. Cheng, F. and Adronov, A. *Chemistry - A European Journal, 12, 5053 - 5059* (2006).

8. Imahori, H., Hagiwara, K., Aoki, M., Akiyama, T., Taniguchi, S., Okada, T., Shirakawa, M., and Sakata, Y. *Journal of the American Chemical Society, 118, 11771-11782* (1996).

9. Schuster, D., Cheng, P., Jarowski, P., Guldi, D., Luo, C., Echegoyen, L., Pyo, S., Holzwarth, A., Braslavsky, S., Williams, R., and Klihm, G. *Journal of the American Chemical Society, 126, 7257-7270* (2004).

10. Imahori, H., Yamada, H., Guldi, D., Endo, Y., Shimomura, A., Kundu, S., Yamada, K., Okada, T., Sakata, Y., and Fukuzumi, S. *Angewandte Chemie International Edition, 41, 13, 2344-2347* (2002).

11. Luo, C., Guldi, D. M., Imahori, H., Tamaki, K., and Sakata, K. *Journal of the American Chemical Society, 122, 6535* (2000).

12. Hecht, D. S., Ramirez, R. J. A., Briman, M., Artukovic, E., Chichak, K. S., Stoddart, J. F., and Gruner, G. *Nano Letters, 6(9), 2031-2036* (2006).

13. Li, H., Martin, R. B., Harruff, B. A., Carino, R. A., Allard, L. F., and Sun, Y.-P. *Advanced Materials, 16, 11, 896-900* (2004).

14. Alvaro, M., Atienzar, P., de la Cruz, P., Delgado, J., Troiani, V., Garcia, H., Langa, F., Palkar, A., and Echegoyen, L. *Journal of the American Chemical Society, 128, 6626-6635* (2006).

15. Guldi, D., Rahman, G., Jux, N., Tagmatarchis, N., and Prato, M. *Angewandte Chemie International Edition 43, 5526- 5530* (2004).

16. Guldi, D. M., Taieb, H., Rahman, G., Tagmatarchis, N., and Prato, M. *Advanced Materials 17,7, 871-875* (2005).

17. Baskaran, D., Mays, J., Zhang, X., and Bratcher, M. *Journal of the American Chemical Society, 127, 6916-6917* (2005).

18. Cheng, F. and co workers. *Chemistry - A European Journal, 12, 6062 - 6070* (2006).

19. Bonifazi, D., Scholl, M., Song, F., Echegoyen, L., Accorsi, G., Armaroli, N., and Diederich, F. *Angewandte Chemie 115, 5116 -5120* (2003).

20. Bonifazi, D., Scholl, M., Song, F., Echegoyen, L., Accorsi, G., Armaroli, N., and Diederich, F. *Angewandte Chemie International Edition, 42, 4966 - 4970* (2003).

21. Guldi, D. M., Rahman, G. M. A., Ramey, J., Marcaccio, M., Paolucci, D., Paolucci, F., Qin, S., Ford, W. T., Balbinot, D., Jux, N., Tagmatarchis, N., and Prato, M. *Chemical Communications, 2034 - 2035* (2004).

22. Guo, Z., Du, F., Ren, D., Chen, Y., Zheng, J., Liu, Z., and Tian, J. *Journal of Materials Chemistry, 16, 3021-3030* (2006).

23. Guldi, D. M., Rahman, G. M. A., Prato, M., Jux, N., Qin, S., and Ford, W. *Angewandte Chemie International Edition, 44, 2015 -2018* (2005).

24. Guldi, D. M., Rahman, G. M. A., Jux, N., Balbinot, D., Hartnagel, U., Tagmatarchis, N., and Prato, M. *Journal of the American Chemical Society, 127, 9830-9838* (2005).

25. Guldi, D. M., Rahman, G. M. A., Qin, S., Tchoul, M., Ford, W., Marcaccio, M., Paolucci, D., Paolucci, F., Campidelli, S., and Prato, M. *Chemistry - A European Journal, 12, 2152 - 2161* (2006).

26. Rahman, G., Guldi, D., Campidelli, S., and Prato, M. *Journal of Materials Chemistry, 16, 62-65* (2006).

27. Tagmatarchisa, N., Prato, M., and Guldi, D. *Physica E 29, 546-550* (2005).

28. Senge, M. O. and Kalisch, W. W. *Inorganic Chemistry, 36, 6103-6116* (1997).

29. Senge, M. O., Medforth, C., Sparks, L., Shelnutt, J., and Smith, K. *Inorganic Chemistry, 32, 1716* (1993).

30. Senge, M. O., Renner, M. W., Kalisch, W. W., and Fajer, J. *Journal Of The Chemical Society- Dalton Transactions, 381-385.* (2000).

31. Ravikanth, M. and Chandrashekar, T. *Structure and Bonding (Berlin), 82, 105-188* (1995).

32. Maiti, N. and M., R. *Journal Of The Chemical Society- Faraday Transactions, 92, 1095-1100* (1996).

33. Rosa, A., Ricciardi, G., Baerends, E., Romeo, A., and Monsu Scolaro, L. *Journal of Physical Chemistry A, 107, 11468-11482* (2003).

34. Parker, C. and Rees, W. *Analyst, 87, 83* (1962).

35. Coleman, J., Fleming, A., Maier, S., O'Flaherty, S., Minett, A., Ferreira, M., Hutzler, S., and Blau, W. *Journal of Physical Chemistry B 108, 3446-3450* (2004).

36. Steuerman, D. W., Star, A., Narizzano, R., Choi, H., Ries, R., Nicolini, C., Stoddart, J., and Heath, J. *Journal of Physical Chemistry B, 106, 3124-3130* (2002).

37. Star, A., Liu, Y., Grant, K., Ridvan, L., Stoddart, J., Steuerman, D., Diehl, M., Boukai, A., and Heath, J. a. *Macromolecules, 36, 553* (2003).

38. Goncalves, P., De Boni, L., Barbosa Neto, N., Rodrigues, J. J., Zilio, S., and Borissevitch, I. *Chemical Physics Letters, 407, 236- 241* (2005).

39. Yu, J., Yu, B., Cheong, K., Choi, H., and Yu, S. *Bulletin of the Korea Chemical Society, 19(4), 439-443* (1998).

40. Shemer, H. and Narkis, N. *Environmental Science & Technology, 38, 4856-4859* (2004).

41. Castellanos, M., Reyman, D., Calle, P., and Camacho, J. *Ultrasonics Sonochemistry, 5, 107-111* (1998).

42. Colussi, A., Hung, H., and Hoffmann, M. *Journal of Physical Chemistry A, 103, 2696* (1999).

43. Bhatnagart, A. and Cheung, H. *Environmental Science & Technology, 28, 1481* (1994).

44. Giordani, S., Cejas, M., and Raymo, F. *Tetrahedron, 60, 10973* (2004).

Chapter 6

Nonlinear Optical Characterization of Carbon Nanotube:Porphyrin systems

6.1 Introduction to Nonlinear Optical Properties of Porphyrins and their Carbon Nanotube Composites.

Members of the porphyrin family are renowned for the architectural flexibility made possible by their macrocyclic structures and chemical reactivity, which in turn facilitate the tailoring of their physical, chemical and optoelectronic characteristics. Additionally, they are known to have outstanding chemical and thermal stability. The optical properties of the tetrapyrrolic macrocycle of porphyrin molecules combined with the synthetic methodologies now available and the already available theoretical and spectroscopic knowledge on their optical behaviour make porphyrins an ideal target material for the area of nonlinear optics, with much recent research focusing on phthalocyanines and porphyrin derivatives offering potential for nonlinear optical (NLO) applications. For this reason, this field has been reviewed numerous times of late by different research groups.[1,2,3,4,5,6,7,8,9,10,11,12,13,14,15,16,17,18] In this section, we introduce the field of porphyrin third order nonlinear optics as described in the most recent extensive review in this area by Eleni Notaras and co-workers.[19]

An optical limiter is a material which efficiently transmits incident light of low energy whilst suppressing potentially damaging light under conditions of high input intensities through optical extinction. Under low intensity irradiation, an ideal optical limiter has a linear transmittance (i.e. the transmitted light intensity is directly proportional to incident intensity) whereas for incident irradiation above a threshold intensity the transmittance reaches a plateau and remains constant. There exists tremendous interest at present in the development of new NLO materials and devices capable of attenuating intense light bursts for the protection of delicate sensors and/or human eyes. High dissipative optical nonlinearities, fast response times and a broadband spectral response are among the essential characteristics a potential optical limiting material must have. Conjugated tetrapyrrolic molecules such as porphyrins have many of these features with the ground state absorption capable of being tuned through molecular design and engineering. In porphyrins, absorption of a photon of appropriate energy leads to promotion of an electron from the ground state, into a short-lived singlet excited state and then into a longer-lived triplet state through intersystem crossing.

The development of novel NLO materials has been greatly encouraged in the past decade by the development of organic materials such as porphyrins offering the advantage of flexible chemical synthesis.[20,21,22,23] The NLO response of organic materials such as porphyrins and phthalocyanines is extremely rapid because the effects occur primarily through electronic polarization and these materials have thus been studied extensively in recent years. Porphyrins have many characteristics which make them uniquely superior to other compounds as NLO chromophores. It is possible to selectively tune the optical properties of a porphyrin molecule through altering the metal centre,[24,25,26] the type of axial ligands,[15,26] or the substituents at the macrocycle periphery. It is also possible to control various porphyrin properties through use of conformationally designed molecules[27,28,29,30] as conformational distortion of the aromatic porphyrin macrocycle facilitates significant changes in the physicochemical properties of the system.[31] For example, the absorption bands become bathochromically shifted through nonplanar distortion, as seen in Chapter 5 of this thesis.

Blau et al. first reported on the nonlinear optical properties of the symmetric

porphyrin 5,10,15,20-tetraphenylporphyrin (TPP) in 1985[32] and TPP and its derivatives remain the most widely studied porphyrins to this day due to the ease of their synthesis. In this initial paper, the effect of reverse saturable absorption (RSA) in the free base TPP molecule was compared to that observed for metal complexes. Since this report, a large variety of porphyrins have been studied for their NLO behaviour using a number of different techniques in a number of different environments.[33,34,35,36,37,38,39,40,41,42,43,44,45,46,47,48,49,50,51,52,53] During the 22 years which have elapsed since this initial study, the NLO properties of porphyrin molecules have been investigated exhaustively for a number of porphyrin systems. Initial studies featured simple symmetric porphyrin systems such as TPP and its derivatives, but research was subsequently conducted on increasingly complicated systems such as push-pull porphyrins, porphyrin oligomers and porphyrin arrays.

Initially, promising NLO properties were found for the simple symmetric porphyrins, but research efforts gradually moved towards increasingly unsymmetrical porphyrins such as push pull porphyrins as varying substituents on these molecules allowed for sensitive tuning of the porphyrin optical properties. Contemporary research is now focused on push pull porphyrins, especially those with extended π-conjugation systems, due to recent advances in synthetic porphyrin chemistry.[54,55]

Porphyrin excited states may also be altered through macrocyclic conformational design. First studies on the effect of macrocycle distortion with regard to optical applications were reported by Ravikanth and co-workers, where the effect of the porphyrin nonplanarity on the spectral and electrochemical properties of short chain basket-handle porphyrins was investigated.[56,57,58,59] They showed optical limiting RSA under visible picosecond laser pulse excitation and showed that heavy atom substitution enhances the limiting property. It was subsequently postulated that the susceptibility is reduced by the deformation of the macrocycle as it hinders the delocalization of the π-electrons in the molecule. Macrocyclic conformational design may ultimately facilitate molecular engineering of porphyrins, with synthesis of specifically designed macrocyclic systems producing optimal NLO candidates with subsequent optimization of properties through synthetic variations. The combination of porphyrin macrocycle optical properties and advanced synthetic methodologies available in addition to the enormous volume of information already avail-

able both theoretically and spectroscopically on their optical behavior make porphyrins a target of choice for future optical limiting applications.

Since the first reports by Blau et al.[32] of RSA in porphyrins for laser pulses at 532 nm with 80 ps duration for a series of tetraphenylporphyrin derivatives, much work has been carried out on improving the optical limiting properties of porphyrins and metalloporphyrins. Of late, supramolecular functionalization of carbon nanotubes with porphyrins has been increasingly investigated as the aromatic sidewalls of SWNTs are ideal for π-stacking interactions with the planar aromatic porphyrin macrocycles and they exhibit unique photophysical and electrochemical properties.[60,61,62,63,64,65,66] It was originally shown by Nakashima et al that stable nanotube- Zn-protoporphyrins (ZnPP) composite solutions could be created in DMF due to the binding of ZnPP onto the surface of the SWNTs in the presence of excess porphyrin.[61] In subsequent studies, the development of CNT nanoconjugates and nanohybrids has attracted considerable attention, and all literature in this area has been extensively reviewed in Chapter 5 of this thesis.[67,68,69,70,71] The solubilization of SWNT or MWNT with electron donating antennae through the use of functional chromophores such as porphyrins offers outstanding opportunities, lending itself to a range of potential commercial applications such as photovoltaic cells, photodiodes, and light-harvesting systems.[62,68]

It has been shown that SWNTs and MWNTs in suspension excited with high intensity at 532 nm and 1064 nm also behave as optical limiters.[72,73,74] This nonlinear behaviour has been shown to arise from strong nonlinear scattering due to the creation of new scattering centers by ionized carbon microplasmas and solvent microbubbles. Improved optical nonlinear behaviour is therefore to be expected from porphyrin- SWNT composite solutions, with an additional scattering component expected to enhance the nonlinear optical limiting behaviour of the porphyrin macrocycle. Thus, the optical properties of carbon nanotubes functionalized both covalently and non- covalently with porphyrin molecules are of great interest in both the linear and nonlinear regimes.

However, optical limiting properties have hardly been studied for functionalized SWNTs with light harvesting chromophores. In particular, SWNTs functionalized with reverse saturation absorption (RSA) groups, such as porphyrins, have not been studied

in great detail for their optical limiting response. At the time of printing, only two such studies had been published.[71,75] Recent studies by Zhen Guo and co- workers showed that covalently porphyrin-functionalized single-walled carbon nanotubes (SWNTs) suspensions in dimethylformamide, demonstrated superior optical limiting properties compared with both the benchmark material, C_{60}, and the individual components, tetraphenylporphyrin (TPP) and SWNTs. This enhanced optical limiting performance of SWNTs-TPP was ascribed to the charge-separated excited state produced by photoinduced electron transfer from the electron-donating TPP moiety to the electron-accepting SWNTs, based on the donor-acceptor property of this nanohybrid in the excited state.

This was in agreement with the research presented in this chapter on the optical characteristics of SWNTs non- covalently functionalized with both the same porphyrin (TPP) and protoporphyrin IX under the same experimental conditions. The composite solutions were again found to be superior optical limiters for all porphyrin systems studied, including the metalloporphyrin Zn-TPP which does not itself exhibit strong optical limiting behaviour.

6.2 Experimental Section

The purified SWNTs used in this work were prepared by the HiPCO process, supplied by Carbon Nanotechnologies Inc. and used without further treatment, as before. The porphyrin molecules used were purchased from Aldrich. Two identical sets of solutions of each porphyrin were made with concentrations ranging from approximately 1μM-200μM in chloroform and dimethylformamide. Pure HiPCO SWNT was added to one porphyrin solution at each concentration such that the porphyrin- SWNT mass ratio was 1:1.

The open aperture z-scan technique was used for the nonlinear optical experiments. In this experiment which was described in Chapter 3, the sample is scanned through the focus of a Gaussian laser beam. Initially the beam energy density is low and hence negligible nonlinear activity occurs. As the sample approaches the focus the beam diameter decreases and thus the energy density increases exciting the nonlinear activity within the sample medium. After the focus, the optical activity tends toward the linear regime again as

the beam diameter increases with a corresponding energy density decrease. The measured beam transmittance as a function of position from the focus constitutes the open aperture z-scan spectra from which the nonlinear extinction coefficient can be extracted. Effective absorption coefficients were calculated by fitting theory previously reported. All experiments described in this study were performed using 6ns Gaussian pulses from a Q-switched Nd:YAG laser with energies of approximately 0.2-0.3 mJ per pulse. The beam was spatially filtered to remove the higher order modes and tightly focused. The laser was operated at its second harmonic, 532nm, with a pulse repetition rate of 10 Hz. All linear and nonlinear optical measurements were performed in 1 cm path length quartz cells.

6.2.1 Results and Discussion

Planar Porphyrins

The open aperture of a Z-scan experiment was used to measure the total transmittance through the samples.[76] Effective absorption coefficients were calculated by fitting theory previously reported.[77] Normalized transmittance as a function of position z, $T_{Norm}(z)$, was given by

$$T_{Norm}(z) = \frac{ln[1 + q_0(z)]}{q_0(z)} \tag{6.1}$$

where $q_0(z) = \frac{q_{00}}{1+(z/z_0)^2}$, z_0 is the diffraction length of the beam, and $q_{00} = \beta_{eff} I_0 L_{eff}$, where $L_{eff} = 1 - exp(-\alpha_0 L)/\alpha_0$.

β_{eff} is the effective intensity-dependent nonlinear absorption coefficient, and I_0 is the intensity of the light at focus. L_{eff} is known as the effective length of the sample defined in terms of the linear absorption coefficient, α_0, and the true optical path length through the sample, L. The imaginary third-order optical susceptibility $Im\chi^{(3)}$, is directly related to the intensity-dependent absorption coefficient β_I and is expressed as $Im\chi^{(3)} = n_0^2 \epsilon_0 c \lambda \beta_I / 2\pi$ where n_0 is the linear refractive index, ϵ_0 is the permittivity of free space, c is the speed of light, and λ is the wavelength of the incident light. All experiments described in this study were performed using 6ns Gaussian pulses from a Q-switched Nd:YAG laser with energies of approximately 0.2-0.3 mJ per pulse.

Typical normalized energy transmission without an aperture (i.e. open aperture)

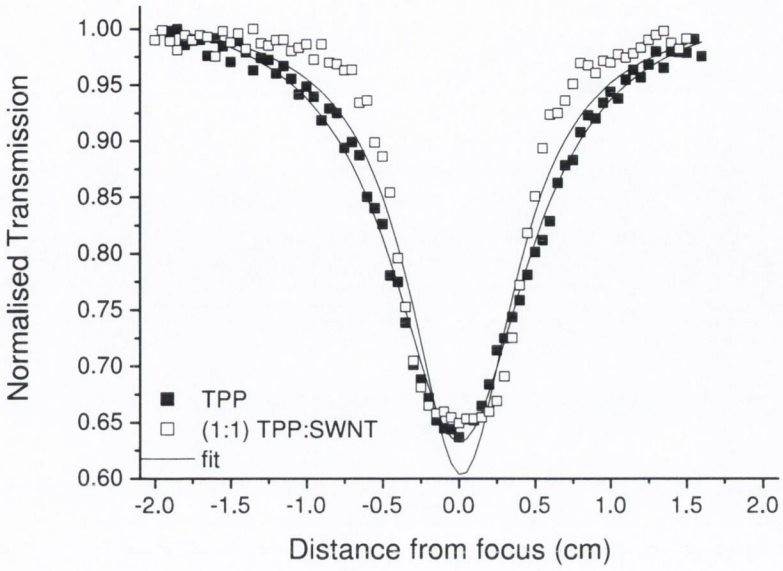

Figure 6.1: Plot of normalised transmission vs. distance from focus for TPP and composite solutions at low concentration and low energy. Concentrations were 21 μM for the TPP solution and 2.7 μM for the composite solution with on-focus intensities of 0.138 and 0.194 GW/cm^2 for the TPP and composite solutions respectively

are shown in Figure 6.1 for a range of input energies. Both tetraphenylporphyrin (TPP) and the metalloporphyrin zinc- tetraphenylporphyrin (Zn- TPP) were studied over the concentration range 2.8 μM -162.7 μM along with their single wall nanotube composite solutions, with linear transmission in the region of 50-80%. These solutions were prepared and studied in both chloroform and dimethylformamide (DMF). All Z-scans performed in this study exhibited a reduction in transmittance about the focus (see Figures 6.1-6.4). This is typical of nonlinear absorption of incident light being induced in the sample. Figures 6.1-6.4 summarize the nonlinear behaviour observed with plots of normalised transmission as a function of distance from the focus shown for TPP solutions at low and high concentrations, with and without nanotubes present, at low and high irradiation energy.

At higher incident intensities (> approx. 0.3GW/cm^2) the transmission of the porphyrin solutions about the focus deviated from ideal RSA behaviour, as illustrated in Figure 6.2. This was probably caused by porphyrin degradation due to local heating effects in the

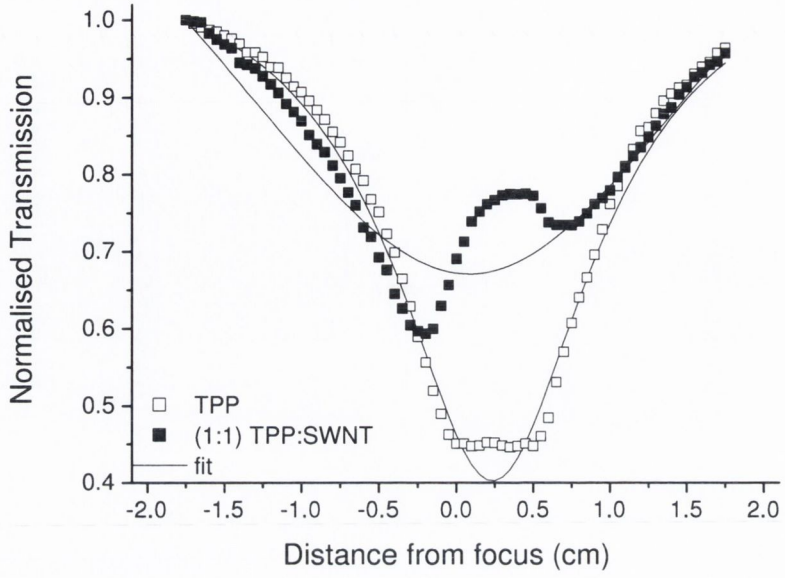

Figure 6.2: Plot of normalised transmission vs. distance from focus for TPP and composite solutions at low concentration and high energy. Concentrations were 21 μM for the TPP solution and 2.7 μM for the composite solution with on-focus intensities of 1.23 and 1.80 GW/cm^2 for the TPP and composite solutions respectively. Thermal degradation of the TPP sample is evident at these intensities, although conditions were chosen to minimize this effect.

solution, and was minimised during experiments by shaking the sample between scans. Introduction of carbon nanotubes into the system completely prevented this degradation at all irradiances. Carbon nanotubes are known to be excellent thermal conductors, and prevent local heating in these solutions by conducting heat away from areas of higher temperature.

The nonlinear absorption coefficient, β_I, experienced by the incident pulses was determined from these spectra as a function of the on- focus intensity. The values of β_I as a function of the on- focus intensity for (A) TPP, (B) TPP:SWNT, (C) ZnTPP and (D) ZnTPP:SWNT solutions in chloroform and (E) TPP and (F) TPP:SWNT solutions in DMF are plotted in Figure 6.5.

It can be clearly seen that as I_0 increases, β_I, decreases in magnitude. The interpolated values of β_I, for (A)- (F) under 0.4 GW cm^{-2} irradiation were found to be 5.2x10^{-10},

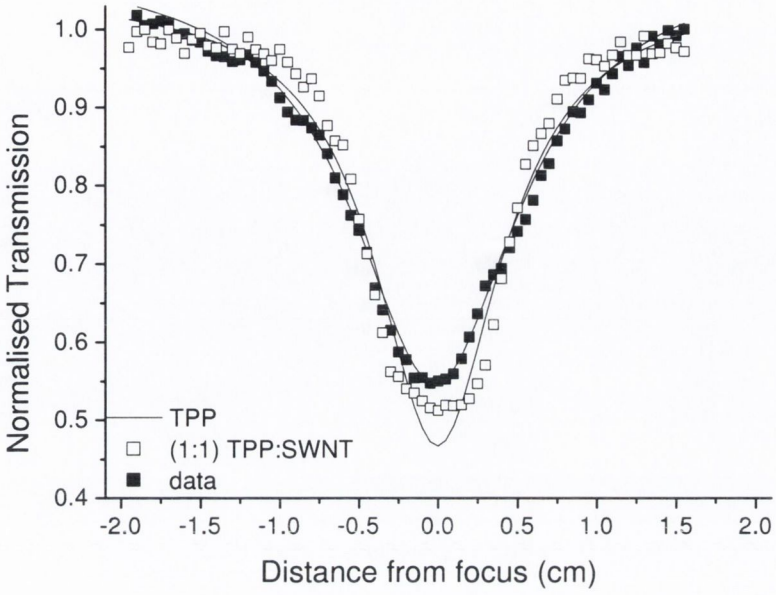

Figure 6.3: Plot of normalised transmission vs. distance from focus for TPP and composite solutions at high concentration and low energy. Concentrations were 98 μM for the TPP solution and 7.6 μM for the composite solution with on-focus intensities of 0.136 and 0.188 GW/cm^2 for TPP and composite solutions respectively

9.57x10^{-9}, 2.81x10^{-9} and 1.72x10^{-8} cm GW^{-1} respectively for solutions in chloroform and 2.78x10^{-9} and 8.95x10^{-9} cm GW^{-1} respectively for the solutions in DMF. The concentration of solutions (A)-(D) was approximately 12 μM and (E) and (F) were at the higher concentration of 21.5 μM. It is clear from the graph above that introduction of the carbon nanotubes into the porphyrin solutions consistently led to a significant increase of the effective nonlinear absorption coefficient, β_I- by almost an order of magnitude in some cases.

The nonlinear behaviour of protoporphyrin IX solutions in DMF was also measured, in the presence and absence of nanotubes. The interpolated values of β_I for PPIX and its composite respectively under 0.4 GWcm^{-2} irradiation were found to be 3.1x10^{-10} and 6.6x10^{-9} cm GW^{-1} respectively at a concentration of 7.8 μM. Introduction of the carbon nanotubes into the porphyrin solutions again led to a significant increase of the effective nonlinear absorption coefficient at all concentrations β_I of the protoporphyrin solutions. It

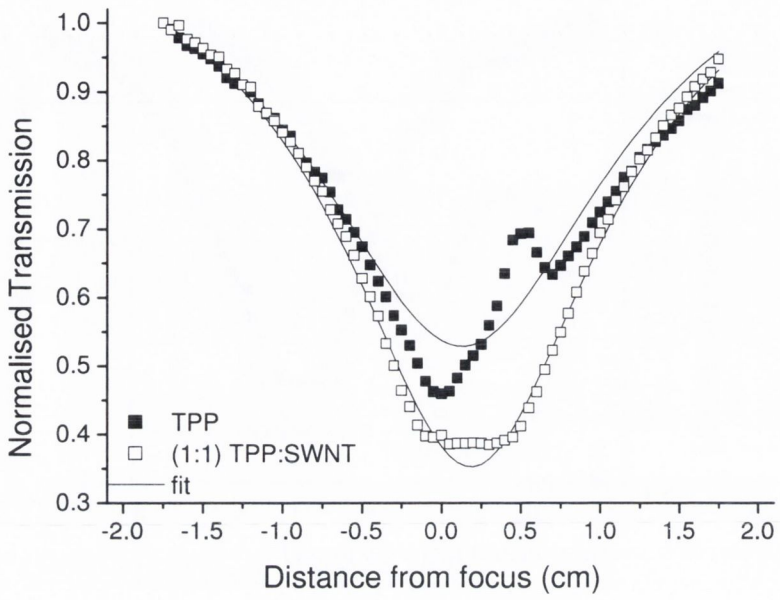

Figure 6.4: Plot of normalised transmission vs. distance from focus for TPP and composite solutions at high concentration and high energy. Concentrations were 98 μM for the TPP solution and 7.6 μM for the composite solution with on-focus intensities of 1.16 and 1.58 GW/cm^2 for TPP and composite solutions respectively

was found to remain fairly constant as a function of concentration over the range studied whereas it increased linearly with concentration for the composite solutions. The nonlinear absorption coefficient, β_I, again decreased in magnitude as I_0 increased.

β_I was found to be non- stationary with respect to the on-focus intensity in all cases, both with and without nanotubes present. This is clearly to seen in Figure 6.5. Each data point on the plot represents an independent open aperture z-scan of the compound in question and the solid lines are sketched merely as guides to the eye. It is clear that the nonlinear absorption coefficient β_I reduces in magnitude with increasing focal intensity I_0. Assuming very low irradiation intensities where I << I_{sat} , then the intensity dependent absorption coefficient may be written as

$$\alpha_{(I,I_{sat},\kappa,)} \approx \alpha_0(1 + (\kappa - 1)I/I_{sat}) \tag{6.2}$$

which is the equation for a straight line of slope (κ-1). However for a reverse saturable

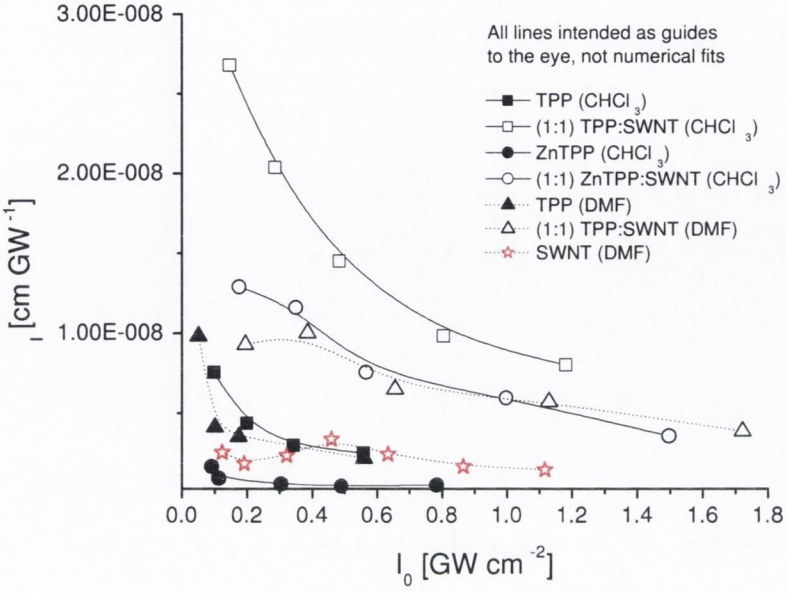

Figure 6.5: Plots of effective β_I against the on- focus beam intensity I_0 for TPP (Black Square), TPP:SWNT (Open Square), ZnTPP (Black Circle), ZnTPP:SWNT (Open Circle) solutions (12.7 μM, TPP (Black Triangle), TPP:SWNT (Open Triangle) solutions (21.5 μM) and a 0.01mg/ml SWNT suspension (Red Star). Solid lines indicate $CHCl_3$ solutions and dotted lines indicate DMF solutions.

absorber, κ by definition and so where I<< I_{sat} one would expect the nonlinear absorption coefficient to increase as a function of I_0. This is not in agreement with the behaviour of β_I as a function of I_0, which was measured here and so these materials are not behaving as effective third order nonlinear absorbers. The reduction in the nonlinear absorption coefficient could be due to some sort of saturation of the accessible energy levels under high intensity pumping. Despite this, effective third order nonlinear absorption coefficients β_I were estimated by suitably interpolating data such as that above for all compounds at on-focus intensities of 0.4 GW cm^{-2} (arbitrarily chosen) where possible.

Table 6.1: Optical Coefficients measured for the Planar Porphyrin systems studied.

Sample	**Conc.** μM	**Solvent**	α_0 cm^{-1}	β_I cm W^{-1}	$\mathbf{Im}\chi^{(3)}_{eff}$ e.s.u.	$\mathbf{I}_0$ GW cm^{-2}	$\mathbf{F}_{sat}$ J cm^{-2}	κ σ_{ex}/σ_0
TPP	12.7	$CHCl_3$	0.07	$4.37x10^{-9}$	$1.53x10^{-12}$	0.20	2.58±0.14	11.20±0.36
TPP+SWNT	12.7	$CHCl_3$	0.29	$2.18x10^{-8}$	$7.65x10^{-12}$	0.24	8.14±0.87	14.99±1.19
Zn-TPP	11.5	$CHCl_3$	0.82	$2.80x10^{-10}$	$9.79x10^{-14}$	0.27	15.3±11.0	1.26±0.16
Zn-TPP+SWNT	11.5	$CHCl_3$	0.29	$9.80x10^{-9}$	$3.44x10^{-12}$	0.41	5.36±2.11	7.46±1.84
TPP	21.5	DMF	0.11	$2.84x10^{-9}$	$9.74x10^{-13}$	0.13	2.14±0.22	4.38±0.24
TPP+SWNT	21.5	DMF	0.42	$6.22x10^{-9}$	$2.14x10^{-12}$	0.19	4.14±0.31	3.62±0.15
PP(ix)	21.5	DMF	0.22	$4.45x10^{-10}$	$1.53x10^{-13}$	0.31	1.15±0.16	1.35±0.02
PP(ix)+SWNT	21.5	DMF	0.72	$6.65x10^{-9}$	$2.28x10^{-12}$	0.21	16.3±8.7	5.18±2.04
SWNT	0.01g/L	DMF	0.29	$1.87x10^{-9}$	$6.41x10^{-13}$	0.19	5.28±2.18	2.72±0.56

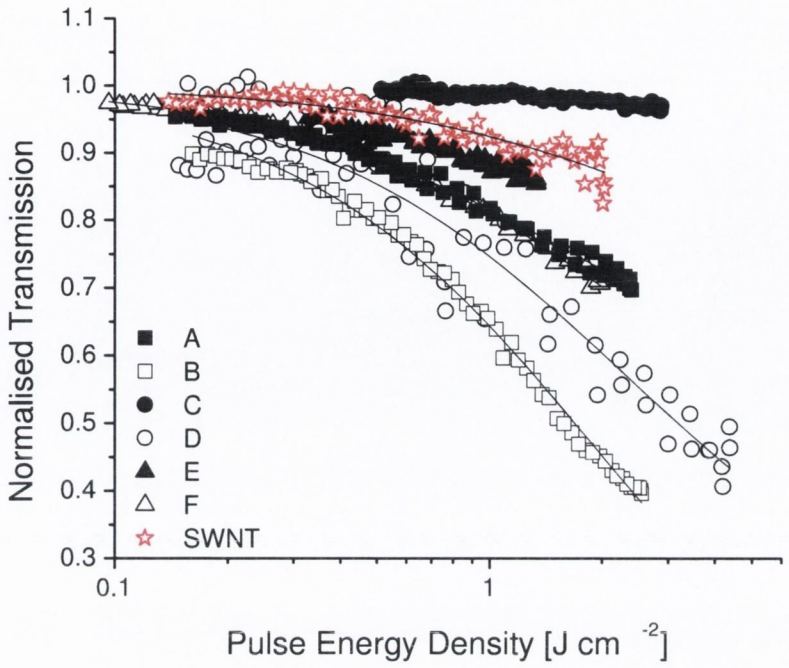

Figure 6.6: Plots of normalized transmission against pulse energy density for solutions A-F. Symbols used are as described in Figure 6.5. The composite solutions (open symbols) were found to be much better optical limiters than both the porphyrin solutions (filled symbols) and SWNT alone (Red star).

The optical limiting curves are shown in Figure 6.6. Normalized transmission (T_{norm}) was plotted as a function of incident pulse energy density (J cm^{-2}). The nonlinear absorption coefficient $\alpha(F, F_{sat}, \kappa)$ was used to fit the normalized transmission as a function of this energy density to the data sets of all open aperture z-scans performed for each compound over a concentration range. Here, $\alpha(F, F_{sat}, \kappa)$ is derived from laser rate equations for the steady state and is defined as $\alpha(F, F_{\rm sat}, \kappa) \approx \alpha_0(1 + F/F_{\rm sat})^{-1}(1 + \kappa F/F_{\rm sat})$. In this expression F represents the energy density, F_{sat} the saturation energy density, and κ the ratio of the excited to ground state absorption cross sections σ_{ex}/σ_0. The parameters κ and $F_{\rm sat}$ were treated as free constants in the fitting algorithm. The plots of normalized transmission against pulse energy density for all solutions where the solid lines are theoretical fits to the experimental data are shown in Figures 6.6 and 6.7. The α_0,κ and F_{sat}

values for each compound are presented in tabular form in Appendix A of this thesis. Our results for tetraphenylporphyrin were found to compare favourably with reported values for the benchmark molecule chloroindium phthalocyanine with the absorption cross section κ calculated as being (30 $\pm$ 6) and β_I approximately equal to 4.5x10^{-8} cm/W at an irradiation of 0.4 GW/cm^2.[78]

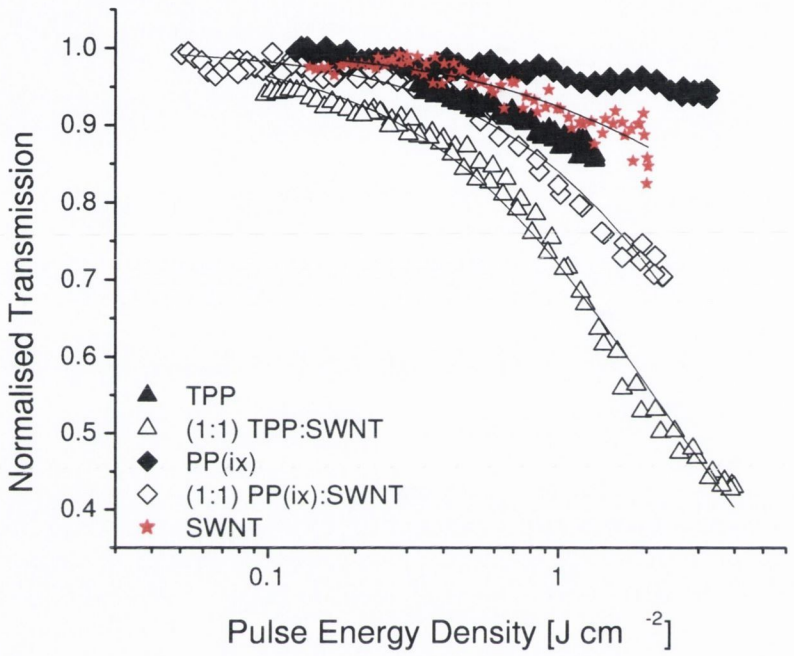

Figure 6.7: Plots of normalized transmission against pulse energy density for TPP (Black Triangle), TPP:SWNT (Open Triangle), PP(ix) (Black Diamond), PP(ix):SWNT (Open Diamond) solutions (21.5 μM, DMF, 25^{o}C) and a 0.01mg/ml SWNT suspension (Red Star). All plots shown were observed at an on- focus beam intensity, I0, of approximately 0.2 GW cm^{-2}

For comparison purposes, a full optical study was conducted on protoporphyrin (IX) solutions for a range of concentrations. The normalised transmission plotted against incident pulse energy density is shown in Figure 6.7 for both porphyrin molecules in DMF, with and without nanotubes present. The composite solutions (open symbols) were found to be much better optical limiters than the porphyrin solutions alone (filled symbols) for

all solutions examined. A 0.01mg/ml SWNT dispersion in DMF is also included in both Figures 6.6 and 6.7 for comparison purposes. It can be clearly seen that porphyrin composite solutions are far superior optical limiters to SWNT alone, for all porphyrins studied. Thus, these solutions of carbon nanotube composites, noncovalently-functionalized with planar porphyrin molecules have enormous industrial potential for optical limiting applications.

Nonplanar Porphyrins

As previously mentioned in the introductions to this chapter and to Chapter 5, natural co- factors are often found to be tetrapyrroles due to the high versatility of these organic structures. The functional variety afforded by this class of compound is related to the flexibility of their molecular conformations, as the physicochemical properties of such molecules may be tuned through manipulation of the macrocycle planarity. Through functionalization with porphyrins, it is hoped that the superior physicochemical properties of the porphyrin moiety may be achieved by SWNT (single walled carbon nanotubes). The studies with the porphyrins TPP (tetraphenylporphyrin),ZnTPP (Zinc tetraphenylporphyrin) and PP(ix) (Protoporphyrin IX) above showed that the solubility and optical limiting performance of carbon nanotubes is enhanced upon interaction with these relatively planar porphyrin molecules in solution. Non-covalent interactions between SWNT and nonplanar porphyrins are therefore of great importance in determining what correlation, if any, exists between the degree of macrocycle nonplanarity and the consequent effects on the binding between the two moities in solution and the nonlinear optical characteristics of the resultant nanotube composites. One of the ultimate goals of the study of such nanohybrids is the discovery of superior materials for optical limiting applications.

A series of SWNT composite solutions were thus obtained using the series of six ethyl- substituted tetraphenylporphyrins with intermediate graded degrees of distortion due to β-ethyl- substituted pyrrole rings ranging from that of tetraphenylporphyrin (H_2TPP) to the standard nonplanar porphyrin 2,3,7,8,12,13,17,18-octaethyl-5,10,15,20-tetraphenylporphyrin (H_2OETPP) previously described in Chapter 5. The interactions between SWNT and these sterically crowded, nonplanar porphyrins was expected to give rise to interesting optical nonlinear behaviour for these composite solutions.

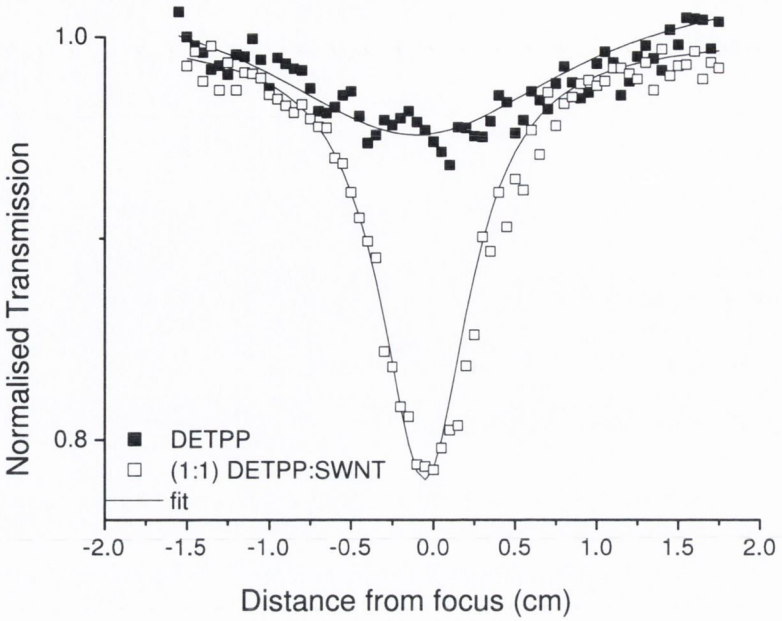

Figure 6.8: Normalised transmission vs. distance from focus for porphyrin and composite solutions at low energies for DETPP. Porphyrin and composite solutions were at concentrations of 0.01 mg/ml, with on-focus intensities of 0.12 GW/cm^2 for porphyrin solutions and 0.25 GW/cm^2 for composite solutions

Normalized open aperture energy transmission spectra (i.e. without an aperture) are shown in Figures 6.8-6.13 for a range of input energies at low on-focus intensities. All tetraphenylporphyrin derivatives were studied at the concentration 0.01 mg/ml along with their single wall nanotube composite solutions, with linear transmission in the region of 50-80%. These solutions were prepared and studied in dimethylformamide (DMF). All Z-scans performed in this study exhibited a reduction in transmittance about the focus at low intensities (e.g. see Figure 6.8). This is typical of nonlinear absorption of incident light being induced in the sample. For higher incident intensities ($I_0 > \approx 0.2 GWcm^{-2}$), all of the nonplanar porphyrins were found to completely degrade, the transmission of the porphyrin solutions about the focus displaying apparent saturable absorption (SA). Confirmation that this was a degradation effect as opposed to genuine SA taking place came from examination of the z-scan traces obtained. For an open aperture scan, the transmission as a function of

distance from the focus typically changes symmetrically. More importantly, the initial and final transmission should be the same for a given scan (i.e. 100% after normalisation of these plots). It can be clearly seen that this is not the case for the nonplanar porphyrin scans, an example of which is shown in Figure 6.13. For each case, the transmittance after the scan is much higher than the initial transmittance, indicating the destruction of materials present in the solution.

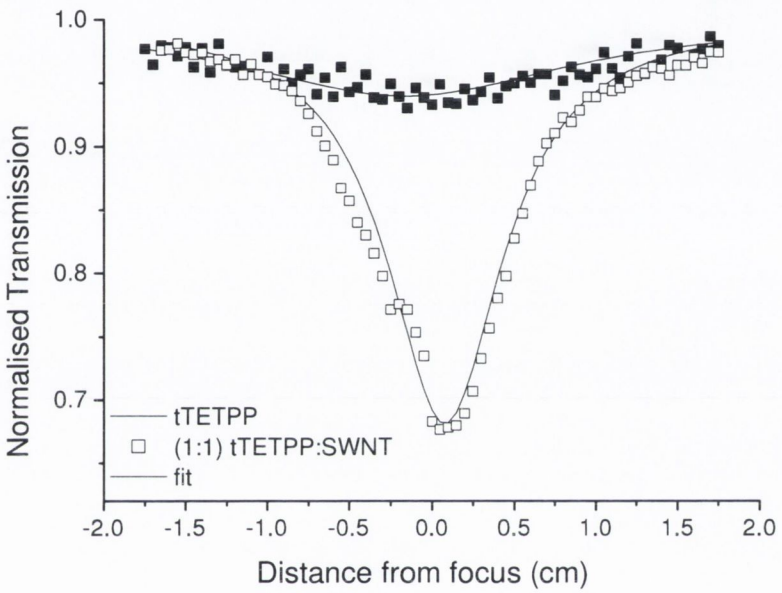

Figure 6.9: Normalised transmission vs. distance from focus for porphyrin and composite solutions at low energies for tTETPP. Porphyrin and composite solutions were at concentrations of 0.01 mg/ml, with on-focus intensities of 0.13 GW/cm^2 for porphyrin solutions and 0.16 GW/cm^2 for composite solutions

All composite Z-scans performed in this study exhibited a reduction in transmittance about the focus. This is typical of nonlinear absorption of incident light being induced in the sample. As previously reported for TPP composites, introduction of carbon nanotubes into the system completely prevented this degradation at all irradiances, most likely due to the remarkable thermal conduction properties of carbon nanotubes preventing local heating in these solutions.

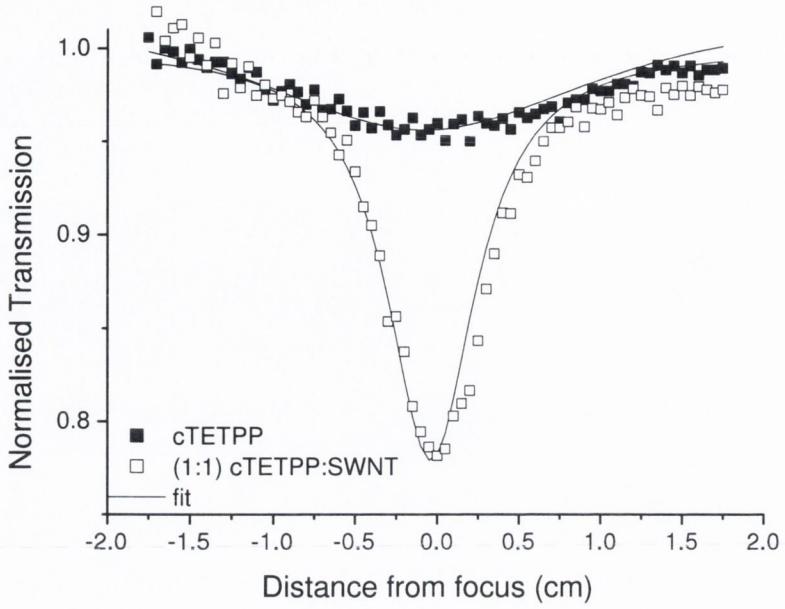

Figure 6.10: Normalised transmission vs. distance from focus for porphyrin and composite solutions at low energies for cTETPP. Porphyrin and composite solutions were at concentrations of 0.01 mg/ml, with on-focus intensities of 0.14 GW/cm^2 for porphyrin solutions and 0.24 GW/cm^2 for composite solutions

The nonlinear absorption coefficient, β_I, experienced by the incident pulses was determined from these spectra as a function of the on- focus intensity. The values of β_I and $\mathrm{Im}\chi^{(3)}_{eff}$ as a function of the on- focus intensity for all molecules in DMF are plotted in Figures 6.14 and 6.15.

It can be clearly seen that as the non planarity increases, β_I and $\mathrm{Im}\chi^{(3)}$ decrease in magnitude. This means that deteriorating optical limiting behaviour is observed as molecules become more nonplanar without nanotubes present. No definite trend was observed in the value of $\mathrm{Im}\chi^{(3)}$ for the composite solutions. The composites were found to be better optical limiters than porphyrin molecules alone. The same was also found for the TPP molecules. All nonplanar porphyrins were worse optical limiters than TPP. SWNT alone were found to be better optical limiters than all porphyrins studied (except TPP and DETPP) and worse optical limiters than all composite solutions.

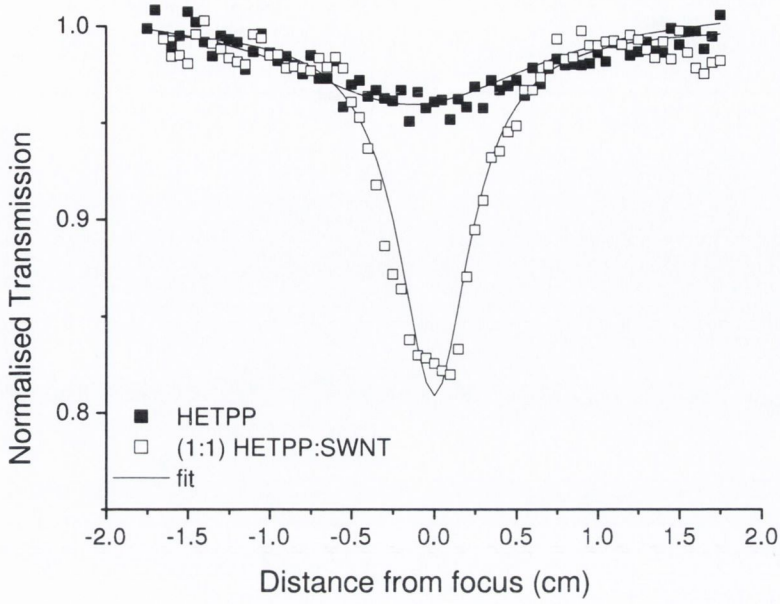

Figure 6.11: Normalised transmission vs. distance from focus for porphyrin and composite solutions at low energies for HETPP. Porphyrin and composite solutions were at concentrations of 0.01 mg/ml, with on-focus intensities of 0.25 GW/cm^2 for porphyrin solutions and 0.23 GW/cm^2 for composite solutions

In the case of three of the nonplanar molecules- tTETPP, HETPP and OETPP- the optical limiting characteristics of the composites were found to be superior to the combination of the composite components. This was determined by comparing the product of the % transmittance of the constituent porphyrin and SWNT with the % transmittance of the composite at the same concentration for a range of energies. If the superior OL behaviour of a composite was simply due to an addition of its two optical limiting components, then the transmission shown by the composite should be equal to the product of the transmittance spectra of its porphyrin and nanotube parts. This was found to be the case for DETPP and cTETPP, indicating negligible interaction between these porphyrins and the carbon nanotubes in solution.

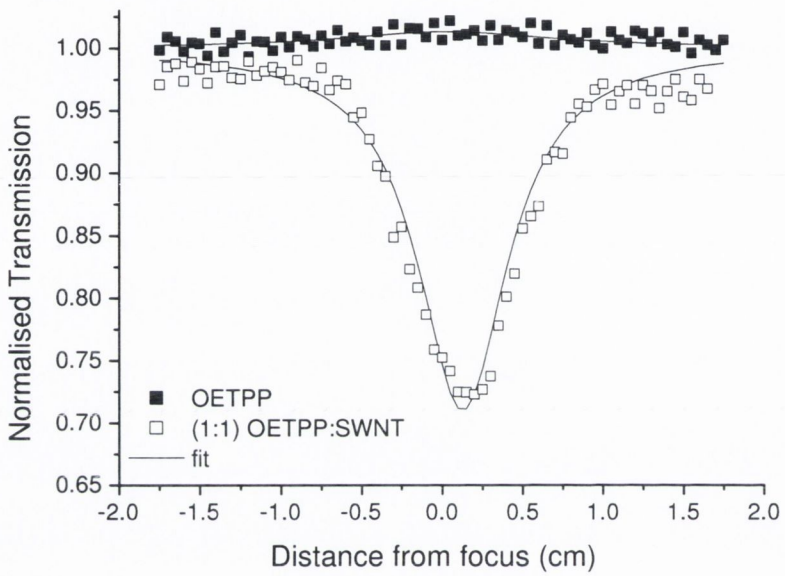

Figure 6.12: Normalised transmission vs. distance from focus for porphyrin and composite solutions at low energies for OETPP. Porphyrin and composite solutions were at concentrations of 0.01 mg/ml, with on-focus intensities of 0.23 GW/cm^2 for porphyrin solutions and 0.19 GW/cm^2 for composite solutions

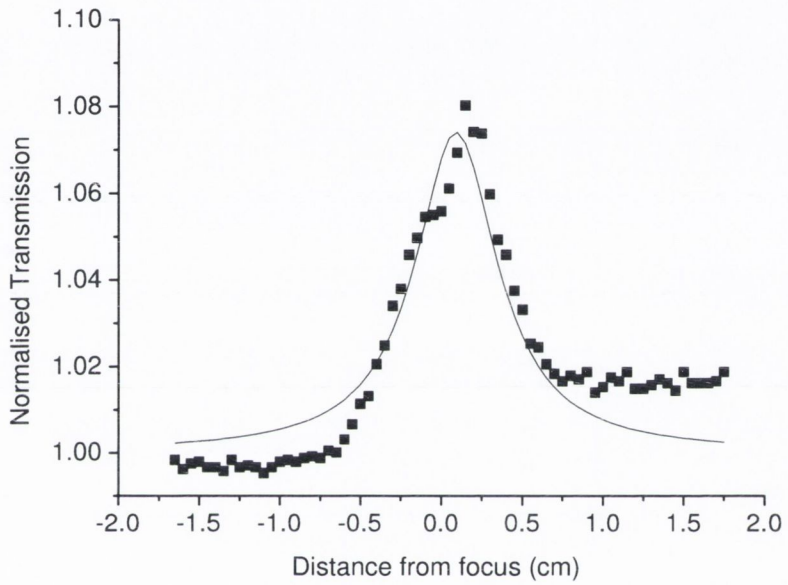

Figure 6.13: The higher final transmittance compared with the initial transmittance indicates the destruction of molecules present in the solution. Porphyrin and composite solutions were at concentrations of 0.01mg/ml, with on-focus intensities of 1.63575 GW/cm^2 for porphyrin solutions and 0.19 GW/cm^2 for composite solutions.

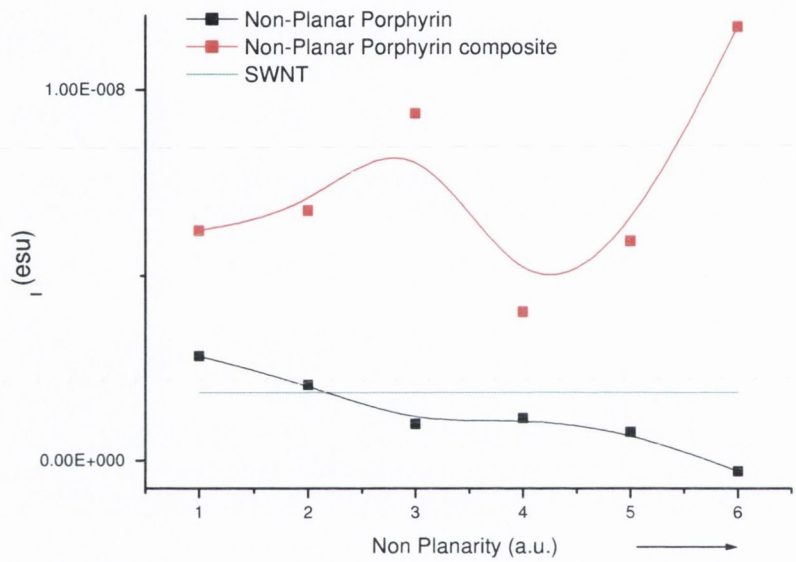

Figure 6.14: Plots of the nonlinear absorption coefficient, β_I at an on- focus beam intensity I_0 of 0.2 GW /cm^2 in DMF as a function of Non planarity. With 1=TPP, 2=DETPP, 3= tTETPP, 4= cTETPP, 5= HETPP and 6= OETPP.

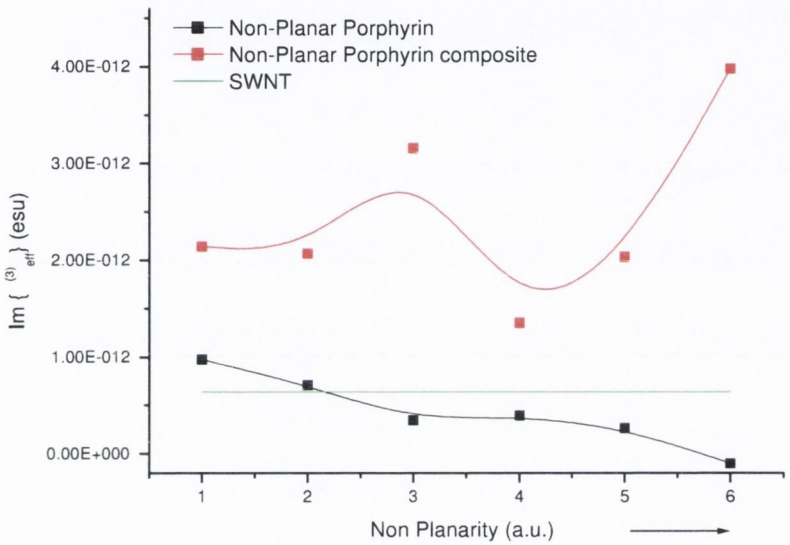

Figure 6.15: Plots of the effective $\mathrm{Im}\chi^{(3)}$ at an on- focus beam intensity I_0 of 0.2 GW /cm^2 in DMF as a function of Non planarity. With 1=TPP, 2=DETPP, 3= tTETPP, 4= cTETPP, 5= HETPP and 6= OETPP.

Table 6.2: Optical Coefficients measured for the Nonplanar Porphyrin systems studied

Sample	**Conc.** μM	**Solvent**	α_0 cm^{-1}	β_I cm W^{-1}	$\mathbf{Im}\chi^{(3)}_{eff}$ e.s.u.	$\mathbf{I}_0$ GW cm^{-2}	$\mathbf{F}_{sat}$ J cm^{-2}	κ σ_{ex}/σ_0
TPP	21.5	DMF	0.11	$2.84x10^{-9}$	$9.74x10^{-13}$	0.13	2.14±0.22	4.38±0.24
TPP+SWNT	21.5	DMF	0.42	$6.22x10^{-9}$	$2.14x10^{-12}$	0.19	4.14±0.31	3.62±0.15
DETPP	c.16.0	DMF	0.25	$2.63x10^{-9}$	$9.03x10^{-13}$	0.12	0.2±0.01	1.57±0.01
DETPP+SWNT	c.16.0	DMF	0.55	$5.49x10^{-9}$	$1.89x10^{-12}$	0.25	17.86±7.02	5.30±1.54
tTETPP	c.16.0	DMF	0.24	$1.17x10^{-9}$	$4.03x10^{-13}$	0.13	0.09±0.01	1.28±0.01
tTETPP+SWNT	c. 16.0	DMF	0.57	$1.06x10^{-8}$	$3.65x10^{-12}$	0.16	14.30±3.42	5.27±0.90
cTETPP	c.16.0	DMF	0.42	$1.33x10^{-9}$	$4.57x10^{-13}$	0.14	0.07±0.004	1.18±0.003
cTETPP+SWNT	c.16.0	DMF	0.69	$3.35x10^{-9}$	$1.15x10^{-12}$	0.24	18.42±8.6	3.81±1.19
HETPP	c.16.0	DMF	0.20	$5.6x10^{-10}$	$1.92x10^{-13}$	0.25	0.26±0.02	1.33±0.01
HETPP+SWNT	c.16.0	DMF	0.65	$5.84x10^{-9}$	$2.01x10^{-12}$	0.23	6.74±1.20	3.11±0.30
OETPP	c.16.0	DMF	0.20	$-2.82x10^{-10}$	$-9.68x10^{-14}$	0.23	-3.79±0.21	1.08±0.01
OETPP+SWNT	c.16.0	DMF	0.73	$1.18x10^{-8}$	$4.07x10^{-12}$	0.19	3726±10	1247±33
SWNT	0.01g/L	DMF	0.29	$1.87x10^{-9}$	$6.41x10^{-13}$	0.19	5.28±2.18	2.72±0.56

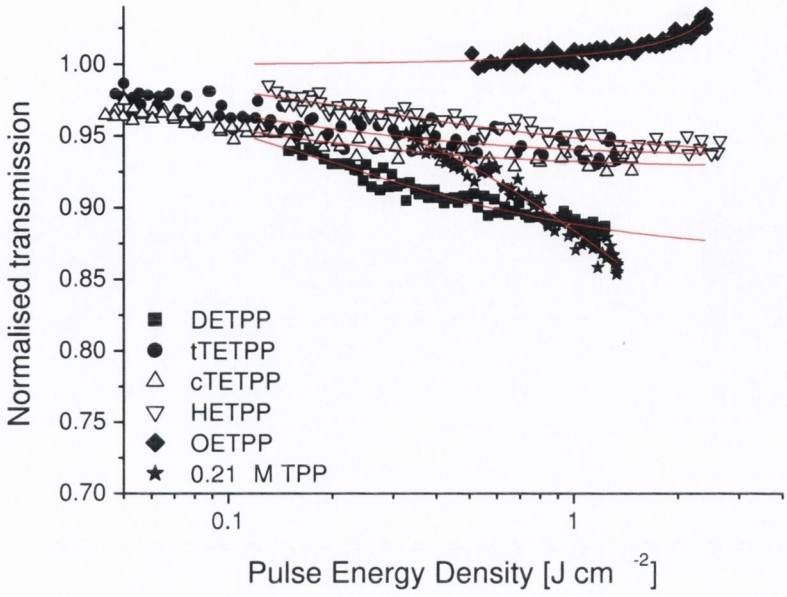

Figure 6.16: Optical limiting behaviour of porphyrin solutions is shown in these plots of normalised transmission vs pulse energy density. All plots are for on- focus beam intensity I_0 of approximately 0.2 GW /cm^2.

The optical limiting curves are shown in Figures 6.16 and 6.17 for the porphyrin and composite solutions respectively. Normalized transmission (T_{norm}) was plotted as a function of incident pulse energy density (J cm^{-2}). The nonlinear absorption coefficient $\alpha(F, F_{sat}, \kappa)$ was used to fit the normalized transmission as a function of this energy density to the data sets of all open aperture z-scans performed for each compound over a concentration range. Here, $\alpha(F, F_{sat}, \kappa)$ is derived from laser rate equations for the steady state and is defined as $\alpha(F, F_{sat}, \kappa) \approx \alpha_0(1 + F/F_{sat})^{-1}(1 + \kappa F/F_{sat})$, where F represents the energy density, F_{sat} the saturation energy density, and κ the ratio of the excited to ground state absorption cross sections, as previously described.[76] The optical limiting curves (plots of normalized transmission against pulse energy density) for all solutions are shown in Figures 6.16 and 6.17 where the solid lines are theoretical fits to the experimental data. All values of α_0, κ and F_{sat} calculated for each compound are presented in tabular form in Appendix B of this thesis.

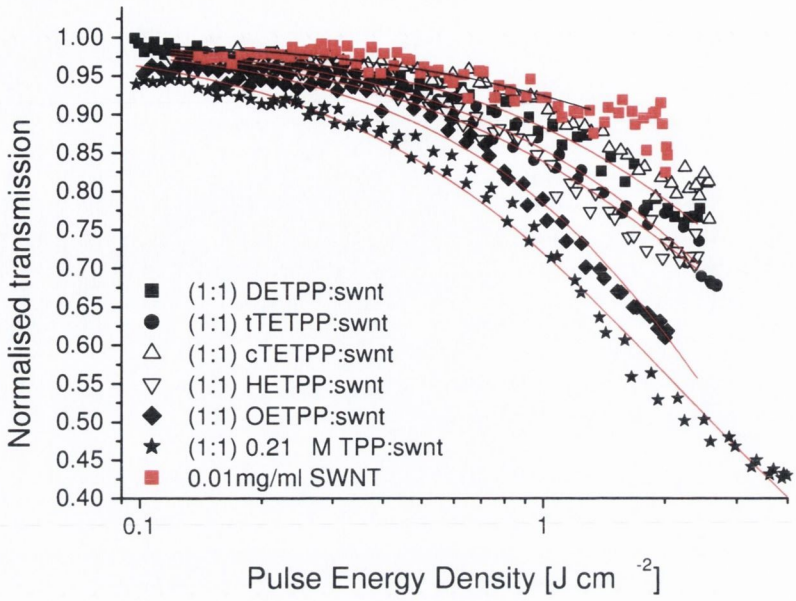

Figure 6.17: Superior optical limiting behaviour of porphyrin composites is clearly to be seen by comparing these plots of normalised transmission vs pulse energy density to those in Figure 6.16. All plots are for on- focus beam intensity I_0 of approximately 0.2 GW /cm^2.

Reported values calculate an absorption cross section κ of (30 ± 6) and β_I of approximately 4.5x10^{-8} cm/W at an irradiation of 0.4 GW/cm^2 for the benchmark molecule chloroindium phthalocyanine.[78]

6.3 Molecular Simulation

Due to the interesting properties observed experimentally for such systems, a molecular dynamics simulation (NVT ensemble) was carried out on these planar and nonplanar porphyrin composite systems in solution by Dr. Donal Mac Kernan in Trinity College Dublin. The experimentally determined linear and nonlinear optical characteristics presented in Chapters 5 and 6 of this thesis for the tetraphenylporphyrin derivatives were also compared with the results of this simulation, and the tendency exhibited by these porphyrin molecules to aggregate close to a nanotube surface in the same solvent (DMF) was investigated.

6.3.1 Simulation Setup

The molecular simulation was undertaken on the planar molecule tetraphenylporphyrin (TPP) and the series of nonplanar TPP derivatives in the presence of a 7-7 SWNT in the solvent DMF. A 7-7 SWNT has a radius close to that of HiPCO SWNT. This computational work utilized a molecular dynamics simulation (NVT ensemble) to investigate whether the TPP derivatives exhibited enhanced tendencies to aggregate onto the surface of a SWNT in the presence of DMF solvent molecules at standard density (0.944 g/cm^3) and temperature (298 Kelvin). Each system was simulated in a periodic box of size roughly 65 X 65 X 41.81 $Angsrom^3$, with small differences made to take into account small differences in effective volume of different porphyrin derivatives. The initial conditions in all cases consisted of three layers. The left and right layers each consisted of ten porphyrin molecules in a solvent of 500 DMF molecules, while the middle layer consisted of an uncapped 7-7 SWNT of length 41 Angstroms. These conditions are illustrated in Figure 6.18. Each system thus consisted of 20 TPP derivative molecules, 1000 DMF molecules and a single SWNT. Each system was equilibrated for at least 1 ns, and statistics were subsequently collected for a further 0.2 ns. The COMPASS Force field was used, and Coulombic and Van der Waals contributions to the forces were computed using a fast- cell multipole technique due to rapid convergence and high precision. The NVT ensemble was then sampled using Anderson thermostated molecular dynamics, and an integrating time step of 1 femtosecond.

6.3.2 Results and Discussion

It was found through molecular simulation of these porphyrin composite systems that some porphyrin molecules -DETPP and tTETPP in particular- did exhibit a pronounced tendency to aggregate onto the SWNT surface, or at closest remove within 4-5 angstroms of the SWNT with no DMF solvation layer present. However, other porphyrins- TPP and cTETPP in particular- exhibited no tendency to aggregate onto the SWNT in these studies. All porphyrin molecules studied exhibited a tendency to self-aggregate. These observations are summarised in Table 6.3, where N denotes the number of porphyrin molecules in contact with the SWNT, and M denotes the largest porphyrin derivative self-aggregate. The

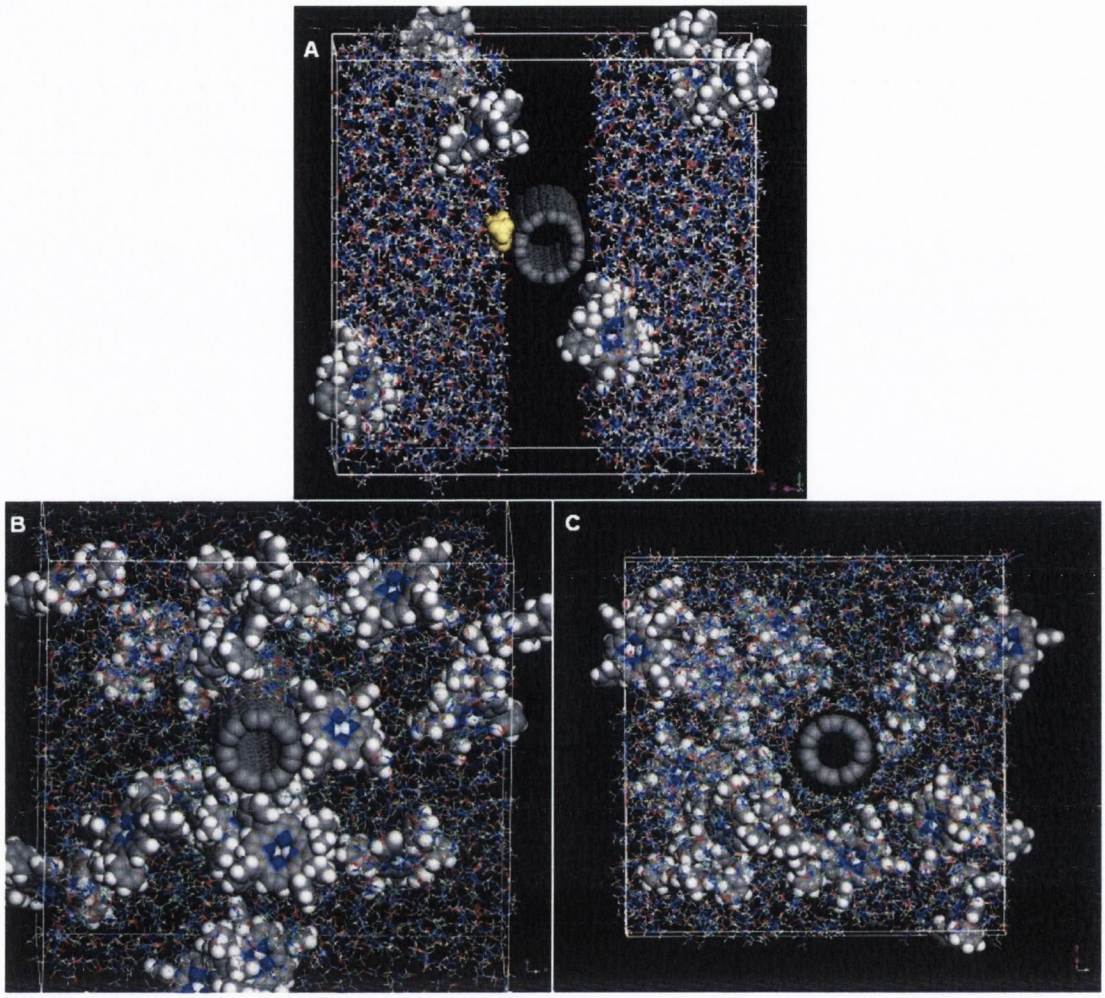

Figure 6.18: (A) Simulation initial conditions are shown for the HETPP-SWNT-DMF system. While there are 20 HETPP molecules, only 4 HETPP molecules, a single DMF (yellow) molecule and the SWNT are actually rendered using effective Van der Waals diameters. The box is infact repeated in all directions periodically, to simulate a bulk solvent, and an infinitely long SWNT (B) The DETPP- SWNT- DMF solvent system. The prounced tendencies of DETPP to aggregate on, and close to the SWNT is evident (C) The TPP-CNT-dmf solvent system. There is no tendency for TPP to aggregate on or close to the CNT.

observations were made over a 0.2 ns interval subsequent to the 1 ns equilibration period, by which time the values of N and M did not fluctuate appreciably. The two extreme

cases, DETPP and TPP, are presented in Figure 6.18, along with the starting conditions

Table 6.3: Summary of porphyrin aggregation behaviour. N denotes the number of porphyrin molecules in contact with the SWNT, and M denotes the largest porphyrin derivative self-aggregate

Sample	N	M
TPP	0-1	3
DETPP	5-6	5
tTETPP	5-6	3
cTETPP	0-1	3
HETPP	2	3
OETPP	2	5

for the simulations. The simulations revealed the tendency of certain porphyrin molecules to have enhanced aggregation abilities onto the CNT, roughly in line with experiment. All porphryin-derivative molecules additionally exhibited a tendency to self-aggregate. This tendency was confirmed by running simulations for the porphyrin molecules alone both in pure DMF solvent and in vacuum in the absence of SWNT. A more extensive study is being prepared to compute the relative free energies of these systems as functions of appropriate order parameters and effective reaction co-ordinates.

6.4 Conclusions

The nonlinear optical characteristics of a range of porphyrin- carbon nanotube composite solutions were investigated in this chapter. Both planar porphyrin systems (tetraphenylporphyrin and protoporphyrin IX) and nonplanar porphryins (tetraphenylporphyrin derivatives) were utilized in these studies over a wide concentration range.

All Z-scans performed in the study of the planar porphyrins exhibited a reduction in transmittance about the focus, typical of nonlinear absorption of incident light being induced in the sample. The porphyrin solutions deviated from ideal RSA behaviour at high incident intensities, due to thermal degradation. Introduction of carbon nanotubes into the system completely prevented this degradation at all irradiances, yielding a more thermally stable optical limiting material.

The nonlinear absorption coefficient, β_I, of the planar porphyrins and their composites was found to decrease with increasing on- focus beam intensity (I_0). Introduction of

the carbon nanotubes into the porphyrin solutions consistently led to a significant increase of the effective nonlinear absorption coefficient, β_I, resulting in superior optical extinction properties. It was found that these materials are not behaving as effective third order nonlinear absorbers, possibly due to a saturation of the accessible energy levels under intense irradiation. All planar systems studied were found to exhibit optical limiting with the composite solutions found to be greatly superior optical limiters to both the porphyrin solutions and SWNT alone. The formation of composites therefore yielded materials with superior optical limiting properties.

A series of SWNT composite solutions was also obtained using the series of six nonplanar ethyl- substituted tetraphenylporphyrins with intermediate graded degrees of distortion due to β-ethyl- substituted pyrrole rings previously introduced in Chapter 5 of this thesis. Again, all Z-scans performed exhibited typical nonlinear absorption behaviour with the exception of the most nonplanar porphyrin OETPP, which was almost completely optically inactive in the nonlinear regime. The nonplanar porphyrins were all found to be highly sensitive to thermal degradation effects, with evidence of porphyrin destruction present upon irradiation at even extremely low incident energies. Deteriorating optical limiting behaviour was observed with increasing porphyrin macrocycle nonplanarity, and all nonplanar porphyrins were found to be inferior optical limiters to the planar porphyrin TPP.

No thermal degradation was evident upon irradiation of the nonplanar composite solutions. All porphyrins studied, with the exception of the two most planar porphyrins TPP and DETPP, were found to display inferior optical limiting properties to SWNT alone, and all composite solutions were found to be superior optical limiters to their constituent porphyrins. In the case of three of the nonplanar molecules- tTETPP, HETPP and OETPP- the optical limiting characteristics of the composites were found to be superior to the combination of the composite components, confirming an interaction between these porphyrins and carbon nanotubes in solution.

No evidence of interaction was found experimentally using NLO techniques for the molecules TPP, DETPP and cTETPP. However, linear optical techniques implied some interaction between DETPP and SWNT in DMF. In general, while it was found that the

more nonplanar porphyrin molecules have a higher likelihood of non-covalent binding onto nanotubes, it is clear that this is not the only factor determining the noncovalent interaction between them. Complementary molecular dynamics studies performed by a colleague in- house were in striking agreement with these experimental observations. It should be noted that DMF is a very polar solvent, and other solvents may exhibit different properties. Therefore it may also be of interest to examine other solvents and their effects on these systems. In summary, it was found that non-covalent interactions were found to exist between carbon nanotubes and some nonplanar porphyrin molecules. Such carbon nanotube composites noncovalently functionalized with both planar and nonplanar porphyrin molecules have enormous industrial potential for optical limiting applications due to their superior optical limiting performance and enhanced thermal stability.

Bibliography

1. De la Torre, G., Claessens, C. G., and Torres, T. *European Journal of Organic Chemistry, 2821* (2000).

2. de la Torre, G., Vazquez, P., Agullo-Lopez, F., and Torres, T. *Journal of Materials Chemistry, 8, 1671* (1998).

3. Chen, Y., El-Khaty, M. E., Doyle, J. J., Notaras, E., Blau, W., and O'Flaherty, S. *Update this later* (2006).

4. Claessens, C., Blau, W. J., Cook, M., Hanack, M., Nolte, R. J. M., Torres, T., and Wohrle, D. *Monatshefte Fur Chemie, 132, 3* (2001).

5. De La Torre, G. and Torres, T. *Journal of Porphyrins and Phthalocyanines, 1, 221* (1997).

6. De la Torre, G., Torres, T., and Agullo-Lopez, F. *Advanced Materials, 9, 265* .

7. de la Torre, G., Vazquez, P., Agullo-Lopez, F., and Torres, T. *Chemical Reviews, 104, 3723* (2004).

8. Dini, D. and Hanack, M. *Journal of Porphyrins and Phthalocyanines, 8, 915* (2004).

9. Dini, D., Yang, G. Y., and Hanack, M. *Targets in Heterocyclic Systems, 8, 1* (2004).

10. Ercolani, C. *Journal of Porphyrins and Phthalocyanines, 4, 340* (2000).

11. Hanack, M., Dini, D., Barthel, M., and Vagin, S. *The Chemical Record, 2, 129* (2002).

12. Hanack, M., Dini, D., Barthel, M., and Vagin, S. *Advanced Colour Science & Technology, 6, 47* (2003).

13. Hanack, M., Schneider, T., Barthel, M., Shirk, J. S., Flom, S. R., and Pong, R. G. S. *Coordination Chemistry Reviews, 219-221, 235* (2001).

14. Nagamura, T. *Springer Series in Photonics, 2, 376* (1999).

15. O'Flaherty, S. M., Hold, S. V., Cook, M. J., Torres, T., Chen, Hanack, M., and Blau, W. J. *Advanced Materials, 15, 19* (2003).

16. Schultz, H., Lehmann, H., Rein, M., and Hanack, M. *Structure and Bonding, 74, 41* (1991).

17. Seto, J. e., Tamura, S.-i., Asai, N., Kishii, N., Kijima, Y., and Magsuzawa, N. *Pure and Applied Chemistry, 68, 1429* (1996).

18. Shirk, J. S. *Phthalocyanines, 4, 79* (1996).

19. Notaras, E. G. A., Fazekas, M., Ni Mhuircheartaigh, E., Senge, M., and Blau, W. *Advanced Materials (In Press)* (Submitted 2006).

20. Ashwell, G. J. and Bloor, D. *"Organic Materials for Nonlinear Optics III", Royal Society of Chemistry, Boston.* (1993).

21. Chemla, D. S. and Zyss, J. *Nonlinear Optical Properties of Organic Molecules and Crystals, Vol. I-II, Academic Press, Orlando* (1987).

22. Hann, R. A. and Bloor, D. *Organic Materials for Nonlinear Optics II, Royal Society of Chemistry, London.* (1991).

23. Zyss, J. *Molecular Nonlinear Optics: Materials, Physics and Devices, Academic Press, Boston.* (1994).

24. Mishra, S. R., Rawat, H. S., and Laghate, M. *Journal Of Optical Communications, 147, 328* (1998).

25. Sakaguchi, T., Shimizu, Y., Miya, M., Fukumi, T., Ohta, K., and Nagata, A. *Chemistry Letters, 281* (1992).

26. Kandasamy, K., Shetty, S. J., Puntambekar, P. N., Srivastava, T. S., Kundu, T., and Singh, B. P. *Journal of Porphyrins and Phthalocyanines, 3, 81* (1999).

27. Kadish, K. M., Smith, K. M., and Guilard, R. E. *The Porphyrin Handbook, Vol. 1, Academic Press, New York.* (2000).

28. Vicente, M. G. H. and Smith, K. M. *Current Organic Chemistry, 4, 139* (2000).

29. Ravikanth, M. and Chandrashekar, T. K. *Structure and Bonding, 82, 105* (1995).

30. Senge, M. O. *Chemical Communications, 243* (2006).

31. Senge, M. O. *Journal of Photochemistry and Photobiology B, 16, 3* (1992).

32. Blau, W., Byrne, H., Dennis, W. M., and Kelly, J. *Journal Of Optical Communications, 56, 25* (1985).

33. Humphrey, J. and Kuciauskas, D. *Journal of Physical Chemistry B, 108, 12016.* (2004).

34. Jiang, H., Su, W., Hazel, J., Grant, J. T., Tsukruk, V. V., Cooper, T. M., and Bunning, T. J. *Thin Solid Films, 372, 85* (2000).

35. Jiang, L., Lu, F., Li, H., Chang, Q., Li, Y., Liu, H., Wang, S., Song, Y., Cui, G., Wang, N., He, X., and Zhu, D. *Journal of Physical Chemistry B, 109, 6311* (2005).

36. Collini, E., Ferrante, C., Bozio, R., Lodi, A., and Ponterini, G. *Journal of Materials Chemistry, 16, 1573* (2006).

37. Kano, H. and Kobayashi, T. *Journal Of Optical Communications, 178, 133* (2000).

38. Misawa, K. and Kobayashi, T. *Journal of Chemical Physics, 110, 5844* (1999).

39. Bezerra, A. G., Borissevitch, I. E., de Araujo, R. E., Gomes, A. S. L., and de Araujo, C. B. *Chemical Physics Letters, 318, 511* (2000).

40. Borissevitch, I. E., Bezerra Jr., A. G., Gomes, A. S. L., De Araujo, R. E., De Araujo, C. B., Oliveira, K. M. T., and Trsic, M. *Journal of Porphyrins and Phthalocyanines, 5, 51* (2001).

41. Kandasamy, K., Shetty, S. J., Puntambekar, P. N., Srivastava, T. S., Kundu, T., and Singh, B. P. *Chemical Communications, 1159* (1997).

42. Martin, R. B., Li, H., Gu, L., Kumar, S., Sanders, C. M., and Sun, Y.-P. *Optical Materials, 27, 1340* (2005).

43. McEwan, K. J., Bourhill, G., Robertson, J. M., and Anderson, H. L. *Journal of Nonlinear Optical Physics and Materials, 9, 451* (2000).

44. Tian, H.-J., Mao, H.-F., Zhou, Q.-F., Xu, H.-J., Si, J.-H., Wang, Y., Yang, Q., and Ye, P.-X. *Chemical Physics Letters, 263, 471* (1996).

45. Kandasamy, K., Shetty, S. J., Puntambekar, P. N., Srivastava, T. S., Kundu, T., and Singh, B. P. *Chemical Communications, 1159* (1997).

46. Borissevitch, I. E., Rakov, N., Maciel, G. S., and de Araujo, C. B. *Applied Optics, 39, 4431.* (2000).

47. De Araujo, C. B., Gomes, A. S. L., and Borissevitch, I. E. *MCLC S & T, Section B: Nonlinear Optics, 378, 113* (2002).

48. Fujiwara, K., Monjushiro, H., and Watarai, H. *Chemical Physics Letters, 394, 349* (2004).

49. Kuznetsova, R. T., Kopylova, T. N., Mayer, G. V., Samsonova, L. G., Svetlichnyi, V. A., Vasil'ev, A. V., Filinov, D. N., Tel'minov, E. N., Kabotaeva, N. S., Svarovskaya, N. V., Podgaetskii, V. M., and Reznichenko, A. V. *IEEE Journal of Quantum Electronics, 34, 139* (2004).

50. Maciel, G. S., Rakov, N., and de Araujo, C. B. *Optics Letters, 27, 740* (2002).

51. Nagatani, H., Piron, A., Brevet, P.-F., Fermin, D. J., and Girault, H. H. *Langmuir, 18, 6647* (2002).

52. Sendhil, K., Vijayan, C., and Kothiyal, M. P. *Optics and Laser Technology, 38, 512* (2006).

53. Kandasamy, K., Divakar Rao, K., Deshpande, R., Puntambekar, P. N., Singh, B. P., Shetty, S. J., and Srivastava, T. S. *Applied Physics B-Lasers And Optics, 64, 479* (1997).

54. Hatscher, S. and Senge, M. O. *Tetrahedron Letters, 44, 157* (2002).

55. Zaidi, S. H. H., Fico Jr., R. M., and Lindsey, J. S. *Organic Process Research & Development, 10, 118* (2006).

56. Ravikanth, M., Reddy, D., Misra, A., and Chandrashekar, T. K. *Journal Of The Chemical Society-Dalton Transactions, 1137* (1993).

57. Kumar, G. R., Ravikanth, M., Banerjee, S., and Sevian, A. *Journal Of Optical Communications, 144, 245* (1997).

58. Reddy, D., Ravikanth, M., and Chandrashekar, T. K. *Journal Of The Chemical Society-Dalton Transactions, 3575* (1993).

59. Sevian, A., Ravikanth, M., and Kumar, G. R. *Chemical Physics Letters, 263, 241* (1996).

60. Satake, A., Miyajima, Y., and Kobuke, Y. *Chemistry of Materials, 17, 716-724* (2005).

61. Murakami, H., Nomura, T., and Nakashima, N. *Chemical Physics Letters, 378, 481-485* (2003).

62. Li, H., Zhou, B., Lin, Y., Gu, L., Wang, W., Fernando, K., Kumar, S., Allard, L., and Sun, Y. *Journal of the American Chemical Society, 126, 1014-1015* (2004).

63. Chen, J. and Collier, C. P. *Journal of Physical Chemistry B, 109, 7605-7609* (2005).

64. Hasobe, T., Fukuzumi, S. ., and Kamat, P. *Journal of the American Chemical Society, 127, 11884-11885* (2005).

65. Cheng, F. and Adronov, A. *Chemistry - A European Journal, 12, 5053 - 5059* (2006).

66. Guldi, D. M., Taieb, H., Rahman, G., Tagmatarchis, N., and Prato, M. *Advanced Materials 17,7, 871-875* (2005).

67. Li, H., Martin, R. B., Harruff, B. A., Carino, R. A., Allard, L. F., and Sun, Y.-P. *Advanced Materials, 16, 11, 896-900* (2004).

68. Baskaran, D., Mays, J., Zhang, X., and Bratcher, M. *Journal of the American Chemical Society, 127, 6916-6917* (2005).

69. Guldi, D. M., Rahman, G. M. A., Ramey, J., Marcaccio, M., Paolucci, D., Paolucci, F., Qin, S., Ford, W. T., Balbinot, D., Jux, N., Tagmatarchis, N., and Prato, M. *Chemical Communications, 2034 - 2035* (2004).

70. Tanaka, H., Yajima, T., Kawao, M., and T., O. *Journal of Nanoscience and Nanotechnology, 6, 1644-1648* (2006).

71. Guo, Z., Du, F., Ren, D., Chen, Y., Zheng, J., Liu, Z., and Tian, J. *Journal of Materials Chemistry, 16, 3021-3030* (2006).

72. Vivien, L., Anglaret, E., Riehl, D., Hache, F., Bacou, F., Andrieux, M., Lafonta, F., Journet, C., Goze, C., Brunet, M., and Bernier, P. *Journal Of Optical Communications, 174, 271-275* (2000).

73. Mishra, S., Rawat, H., Mehendale, S., Rustagi, K., Sood, A., Bandyopadhyay, R., Govindaraj, A., and Rao, C. *Chemical Physics Letters, 317, 510-514* (2000).

74. Riggs, J., Walker, D., Carroll, D., and Sun, Y. *Journal of Physical Chemistry B, 104(30), 7071-7076* (2000).

75. Ni Mhuircheartaigh, E., Giordani, S., and Blau, W. *Journal of Physical Chemistry B, 110, 23136-23141* (2006).

76. Sheik-Bahae, M., Said, A., Wei, T., Hagan, D., and Van Stryland, E. *IEEE Journal of Quantum Electronics. 26(4), 760* (1990).

77. O'Flaherty, S., Hold, S., Cook, M., Torres, T., Chen, Y., Hanack, M., and Blau, W. *Advanced Materials, 15(1), 19-32* (2003).

78. Perry, J., Mansour, K., Lee, I., Wu, X., Bedworth, P., Chen, C., Ng, D., Marder, S., Miles, P., Wada, T., Tian, M., and Sasabe, H. *Science 273, 1533-1536* (1996).

Chapter 7

Conclusions

As they exist in rope-like bundles, single-walled carbon nanotubes (SWNT) are severely restricted in their applications. Nanotube bundle dissociation in low concentration SWNT-polymer composites may be monitored using a spectroscopic method developed by J. Coleman.[1] This study utilized luminescent spectroscopy to monitor the surface area of nanotube bundles in solution. The existence of isolated individual SWNT in low concentration dispersions was clearly shown for a conjugated polymer.

This thesis aims to gain a better understanding of the physics behind SWNT interactions with a variety of conjugated organic molecules, with a view to ultimately aiding the development and optimization of a technique for isolating individual SWNT in solution. An understanding of the binding scheme, and the magnitude of the binding energy between these molecules and SWNT is necessary. Recent research in Trinity College has thus focussed on broadening the understanding of the physical processes governing SWNT de-bundling, and a wide range of suitable polymers and short-chain molecules have been used to examine the importance of the molecular structure of the dispersant.[2,3,4]

In this thesis, a complete linear and nonlinear optical characterization of carbon nanotube interactions with a number of conjugated organic molecules is undertaken. The properties of carbon nanotube composites formed with conjugated polymers and molecules are first described. A number of different carbon nanotube composite systems were characterized using a simple adsorption/desorption equilibrium model which facilitates mea-

surement of the carbon nanotube dispersion capability of these conjugated organic systems. Firstly, the interaction between carbon nanotubes and the conjugated polymers PmPV (poly[metaphenylenevinylene-co-2,5-dioctyloxy-para-phenylenevinylene]) and PFO (poly[9,9-di-n-octylfluorenyl-2,7'-diyl]). PmPV/SWNT composites were found to behave in excellent agreement with the binding model as a function of concentration, whereas PFO did not. Therefore, molecules related structurally to PmPV were also predicted to follow a similar noncovalent binding behaviour. Thus the molecule pDSB (2,5- dioctyloxy-1,4- distyrylbenzene) which is a short-chain analogue of the well known polymer Poly(p-phenylenevinylene) was investigated. Successful dispersion of SWNTs in chloroform was achieved upon formation of composites with pDSB, and luminescence quenching behaviour indicated that the pDSB molecule- nanotube binding energy is in fact higher than the PmPV- nanotube binding energy. Following on from these successful PL binding studies with PmPV and pDSB, Cuniffe et al[5] extended the PL studies to investigate nanotube dispersions with two other short molecules structually similar to PmPV- pDNB and PVB- as well as some fractions of varying lengths of the crude PmPV polymer. PVB was found to be unsuitable for use in monitoring SWNT dispersion using the photoluminescence quenching technique described, as self aggregation was evident. The PL work undertaken by Cuniffe indicated a strong interaction between carbon nanotubes and all of the other molecules and PmPV fractions studied, with superior nanotube dispersion achieved using shorter molecules.

It was confirmed using centrifugation and absorption spectroscopy techniques that non-covalent binding did exist between SWNT and selected PmPV fractions with 7, 18 and 51 repeat units. The same absorption study was conducted on the PVB molecule, which is extremely similar structurally to the shortest PmPV (n=5) fraction studied by Cuniffe et al. but contains para linkages instead of the meta linkages found for the polymer. Interestingly, this molecule was found to bind to the nanotubes. Similarly, pDNB was also found to bind non-covalently to carbon nanotubes in chloroform. It has therefore been shown that molecules which are similar in structure to the polymer PmPV bind noncovalently to SWNT in solution, irrespective of whether they contain para linkages or meta linkages. The nanotube composites formed are stable following mild centrifugation, with the presence of

nanotubes in solution confirmed post- centrifugation by absorption spectroscopy. A detailed picture of non-covalent interaction between carbon nanotubes and organic molecules was therefore built up using centrifugation to remove any large nanotube aggregates formed at higher concentrations and confirm the existence of non-covalent binding between them at lower concentrations. Absorption spectroscopy also proved a complementary technique for providing evidence of the nanotube de-bundling implied by PL studies for the PmPV polymer. A technique developed by Giordani et al.[6] was employed to monitor composites of the mid-length PmPV fraction with 18 repeating units as a function of concentration. The increase in the pre-centrifugation SWNT absorption coefficient at low concentration was found to be consistent with debundling of the SWNT in solution, and may be associated with the increased presence of small bundles and individual nanotubes as opposed to larger bundles at higher concentrations.[6]

The linear optical properties of other non- covalent carbon nanotube composite systems were then investigated. Due to their high degree of conjugation, it was expected that molecules from the porphyrin family would interact strongly with carbon nanotubes through Van der Waals interactions. Porphyrins are an enormously important family of functional dyes with a variety of unique photophysical, chemical and biological properties. Recent reports in literature have indicated that metalloporphyrins can indeed dissolve SWNTs in aqueous solutions and in organic solvents ranging from dimethylformamide to chloroform. Carbon nanotubes non-covalently functionalized with porphyrin molecules were therefore studied optically, as these composite systems were predicted to follow the photoluminescence- based binding model which proved so useful in the monitoring of the PmPV/SWNT system. It was found that much of the photoluminescence quenching effects previously reported in the literature may in fact be artefacts resulting from the manifestation of the well known inner filter phenomenon. In the majority of previous studies, this quenching was attributed to the non-covalent binding of the luminescent porphyrin molecules onto the carbon nanotube surface, and the subsequent non-radiative porphyrin de-excitation through the vibrational manifold of the nanotubes, as seen for non-covalent binding studies using conjugated organic polymers and molecules in Chapter 4 of this thesis. Following correction for the inner filter effect, photoluminescence quenching does not

arise for the tetraphenyl porphyrin derivative molecules upon interaction with the carbon nanotubes, with the exception of tTETPP, where fairly strong quenching was observed for the 1:1 composites at concentrations where the inner filter effect was not in evidence.

However, this does not mean that no interaction is taking place between these two moities in solution. Absorption spectra show a red- shifting of the porphyrin Q-bands to lower energies upon interaction with nanotubes for 1:1 SWNT:non-planar porphryin solutions. This is consistent with literature where convincing evidence of noncovalent binding has been reported. No such absorption shifts were observed for the planar porphyrin tetraphenyl pophyrin. Additionally, the increased solubility of the nanotubes, and the stability of their nanotube composites- as evidenced by their staying in solution over a period of months- is indicative of binding between the nanotubes and the porphyrin molecules in solution. Prevention of porphyrin self- aggregation upon addition of carbon nanotubes is consistent with the porphryin molecules being more attracted to the nanotubes than they are to each other. It may thus be concluded that while porphyrins do appear to bind noncovalently onto the nanotube surface, they do not do so in such a way that facilitates energy transfer from the photoexcited porphyrin to the SWNT vibrational manifold. Therefore, in order to create efficient electron donor-acceptor systems for photovoltaic applications, another method must be utilized for maximum results. As the porphyrin photoluminescence is not efficiently quenched in these systems studied, it was not possible to use the binding model to determine the extent of nanotube de-bundling in these solutions.

All of the above porphyrin/SWNT studies were conducted in the solvent DMF because porphyrin solutions in chloroform appeared to change spectroscopically upon addition of nanotubes to form composite solutions. These changes were found to originate from the protonation of the core nitrogen atoms of the porphyrin molecules upon sonication in chloroform, and were in fact independent of the presence of carbon nanotubes in solution. These changes were observed for TPP/SWNT composite solutions prepared in chloroform, but were subsequently found to also take place in the absence of nanotubes. As sonication is a key step in the preparation of homogeneous carbon nanotube dispersions, these changes were always observed for the composite solutions. This degradation of the chloroform molecules was found to occur upon either sonication or laser irradiation during the

z-scan technique, giving rise to the di-protonated form of the porphyrin molecule. The rate of porphryin protonation in chloroform was found to be strongly affected by the presence of carbon nanotubes. TPP composite solutions were found to be extremely sensitive to the presence of HCl, and might be suitable for use as highly sensitive nanoscale pH probes in particular environments. No heightened sensitivity to HCl or any other acid was observed for the TPP/SWNT composite solutions in DMF. A similar sonodegradation of other common chlorinated solvents was also found to lead to porphyrin protonation with the same spectral shifts observed upon sonication of TPP in dichloroethane (DCE) and dichlorobenzene (DCB). This area clearly merits further investigation within a different context. The implications of these results are that extreme care must be taken when working with carbon nanotube composite solutions in chlorinated solvents as protonation of acid sensitive molecules may take place, changing their physicochemical properties.

The nonlinear optical characteristics of a range of porphyrin- carbon nanotube composite solutions were therefore investigated for these porphyrin systems. Both planar porphyrin systems (tetraphenylporphyrin and protoporphyrin IX) and nonplanar porphryins (tetraphenylporphyrin derivatives) were utilized in these studies over a wide concentration range. All Z-scans performed in the study of the planar porphyrins exhibited a reduction in transmittance about the focus, typical of nonlinear absorption of incident light being induced in the sample. The porphyrin solutions deviated from ideal RSA behaviour at high incident intensities, due to thermal degradation. Introduction of carbon nanotubes into the system completely prevented this degradation at all irradiances, yielding a more thermally stable optical limiting material. The nonlinear absorption coefficient, β_I, of the planar porphyrins and their composites was found to decrease with increasing on- focus beam intensity (I_0). Introduction of the carbon nanotubes into the porphyrin solutions consistently led to a significant increase of the effective nonlinear absorption coefficient, β_I, resulting in superior optical extinction properties. It was found that these materials are not behaving as effective third order nonlinear absorbers, possibly due to a saturation of the accessible energy levels under intense irradiation. All planar systems studied were found to exhibit optical limiting with the composite solutions found to be greatly superior optical limiters to both the porphyrin solutions and SWNT alone. The formation of composites

therefore yielded materials with superior optical limiting properties.

A series of SWNT composite solutions was also obtained using the series of six nonplanar ethyl- substituted tetraphenylporphyrins with intermediate graded degrees of distortion due to β-ethyl- substituted pyrrole rings previously introduced in Chapter 5 of this thesis. Again, all Z-scans performed exhibited typical nonlinear absorption behaviour with the exception of the most nonplanar porphyrin OETPP, which was almost completely optically inactive in the nonlinear regime. The nonplanar porphyrins were all found to be highly sensitive to thermal degradation effects, with evidence of porphyrin destruction present upon irradiation at even extremely low incident energies. Deteriorating optical limiting behaviour was observed with increasing porphyrin macrocycle nonplanarity, and all nonplanar porphyrins were found to be inferior optical limiters to the planar porphyrin TPP.

No thermal degradation was evident upon irradiation of the nonplanar composite solutions. All porphyrins studied, with the exception of the two most planar porphyrins TPP and DETPP, were found to display inferior optical limiting properties to SWNT alone, and all composite solutions were found to be superior optical limiters to their constituent porphyrins. In the case of three of the nonplanar molecules- tTETPP, HETPP and OETPP- the optical limiting characteristics of the composites were found to be superior to the combination of the composite components, providing further confirmation of the existence of an interaction between these porphyrins and carbon nanotubes in solution.

A complementary molecular dynamics simulation was carried out by colleagues in Trinity College Dublin on the series of tetraphenylporphyrin derivatives studied in this thesis. The tendency to aggregate close to a nanotube surface exhibited by these molecules in the same solvent was investigated. The results of these complementary molecular dynamics studies were found to be in striking agreement with the linear and nonlinear experimental observations for the porphyrin molecules studied.

It is likely that the future of information and communications data processing may be reliant on the successful development and implementation of photonics technologies. If this is the case, protection of delicate optical sensors such as the human eye from intense laser irradiation will be enormously relevant. Therefore the field of optical limit-

ing will become increasingly important. The work presented in this thesis indicates that porphyrin/carbon nanotube composite systems are potentially of enormous use for such applications. Carbon nanotube composites noncovalently functionalized with both planar and nonplanar porphyrin molecules therefore appear to have enormous industrial potential for optical limiting applications due to their superior optical limiting performance and enhanced thermal stability.

Bibliography

1. Coleman, J., Fleming, A., Maier, S., O'Flaherty, S., Minett, A., Ferreira, M., Hutzler, S., and Blau, W. *Journal of Physical Chemistry B 108, 3446-3450* (2004).

2. Giordani, S., Bergin, S., Drury, A., Mhuircheartaigh, E., Coleman, J., and Blau, W. *NATO Science Series: II Mathematics, Physics and Chemistry (Kluwer Acad. Publ.), Carbon Nanotubes: From Basic Research To Nanotechnology 222, 211-212* (2006).

3. Giordani, S., Bergin, S., Drury, A., Mhuircheartaigh, E., Coleman, J., and Blau, W. *Proceedings SPIE, Vol. 5842, p. 42-49* (2005).

4. Giordani, S., Bergin, S., Drury, A., Ní Mhuircheartaigh, E., Coleman, J., and Blau, W. *AIP Conference Proceedings, Volume 786, pp. 232-235* (2005).

5. Cuniffe, G. *Undergraduate Final Year Thesis, Trinity College Dublin* (2006).

6. Giordani, S., Bergin, S., Nicolosi, V., Lebedkin, S., Kappes, M., Blau, W., and Coleman, J. *Journal of Physical Chemistry B, 110(32), 15708-15718* (2006).

List of Publications

1. "Molecular Engineering of Nonplanar Porphyrin and Carbon Nanotube Assemblies- a Linear and Nonlinear Spectroscopic and Modelling Study"

Ní Mhuircheartaigh, E.M., Giordani, S., MacKernan, D., King, S.M., Rickard, D., Val Verde, L.M., Senge, M.O. and Blau, W.J.

Physical Review B (Submitted) ***2007***

2. "Optical Properties of Porphyrin- Carbon Nanotube Composites (Review)"

Ní Mhuircheartaigh, E.M., King, S.M., Giordani, S. and Blau, W.J.

Journal of Nanoscience and Nanotechnology (Submitted) ***2007***

3. "Sonication-induced Degradation of Chlorinated Solvents Leading to Protonation of Porphyrin- Nanotube Composites"

Ní Mhuircheartaigh, E.M., Giordani, S. and Blau, W.J.

Chemical Communications (Submitted) ***2007***

4. "Nonlinear Optical Properties of Porphyrins and Phthalocyanines"

Notaras, E.G.A., Fazekasa, M., **Ní Mhuircheartaigh, E.M.**, Senge, M.O. and Blau,W.J.

Advanced Materials (Submitted) ***2006***

5. "Strained Silicon Quantum Wells: A spectroscopical Analysis"

Mc Carthy, J., **Ní Mhuircheartaigh, E.M.**, Lyutovitch, K., Perova, T.S., Moore, R.A., and Blau, W.J.

European Physical Journal- Applied Physics (Submitted) ***2006***

6. "Linear and Nonlinear Optical Characterization of a Tetraphenylporphyrin-Carbon Nanotube Composite System"

Ní Mhuircheartaigh, E.M., Giordani, S., and Blau, W.J.

Journal of Physical Chemistry B ***2006****, 110, 23136-23141*

7. "Effect of Solvent and Dispersant on the Bundle Dissociation of Single-Wall Carbon Nanotube"

Giordani, S., Bergin, S., Drury, A., **Ní Mhuircheartaigh, E.M.**, Coleman, J.N. and Blau, W.

NATO Science Series: II Mathematics, Physics and Chemistry (Kluwer Acad. Publ.), Carbon Nanotubes: From Basic Research To Nanotechnology 222: 211-212, ***2006***

8. "Composition and Stress analysis in Strained Silicon"

McCarthy, J., Bhattacharya, S., **Ní Mhuircheartaigh, E.M.**, Perova, T.S., Moore, R.A., Gamble, H., and Armstrong B.M.

Journal of Postgraduate Research, Trinity College Dublin, ***2006****, p156-159*

9. "Strain induced photoluminescence from silicon and germanium nanowire arrays"

Audoit, G., **Ní Mhuircheartaigh, E.M.**, Lipson, S.M., Morris, M.A., Blau W.J. and Holmes,J.D.

Journal of Materials Chemistry, ***2005****, 15, 4809-4815*

10. "Spectroscopical analysis of strained silicon quantum wells"

McCarthy, J., **Ní Mhuircheartaigh, E.M.**, Lyutovich, K., Oehme, M., Perova, T.S., Moore, R.A. and Blau, W.

Proceedings of the SPIE - The International Society for Optical Engineering, 5824, 1, ***2005****, p 174-181*

11. "Effect of Solvents and Dispersants on the Bundle Dissociation of Single-Wall Carbon Nanotube"

Giordani, S.,Bergin, S., Drury, A., **Ní Mhuircheartaigh, E.M.**, Coleman, J.N. and Blau, W. *Proceedings SPIE, Vol. 5842, p. 42-49, June* ***2005***

12. "Effect of Solvents and Dispersants on the Bundle Dissociation of Single-Wall Carbon Nanotube"

Giordani, S., Bergin, S., Drury, A., **Ní Mhuircheartaigh, E.M.**, Coleman, J.N. and Blau, W.J.

AIP Conference Proceedings, Volume 786, pp. 232-235, ***2005***